

An experimental determination of the turbulent Prandtl number in a developing temperature boundary layer

Citation for published version (APA):

Blom, J. (1970). *An experimental determination of the turbulent Prandtl number in a developing temperature boundary layer*. [Phd Thesis 1 (Research TU/e / Graduation TU/e), Applied Physics and Science Education]. Technische Hogeschool Eindhoven. <https://doi.org/10.6100/IR51512>

DOI:

[10.6100/IR51512](https://doi.org/10.6100/IR51512)

Document status and date:

Published: 01/01/1970

Document Version:

Publisher's PDF, also known as Version of Record (includes final page, issue and volume numbers)

Please check the document version of this publication:

- A submitted manuscript is the version of the article upon submission and before peer-review. There can be important differences between the submitted version and the official published version of record. People interested in the research are advised to contact the author for the final version of the publication, or visit the DOI to the publisher's website.
- The final author version and the galley proof are versions of the publication after peer review.
- The final published version features the final layout of the paper including the volume, issue and page numbers.

[Link to publication](#)

General rights

Copyright and moral rights for the publications made accessible in the public portal are retained by the authors and/or other copyright owners and it is a condition of accessing publications that users recognise and abide by the legal requirements associated with these rights.

- Users may download and print one copy of any publication from the public portal for the purpose of private study or research.
- You may not further distribute the material or use it for any profit-making activity or commercial gain
- You may freely distribute the URL identifying the publication in the public portal.

If the publication is distributed under the terms of Article 25fa of the Dutch Copyright Act, indicated by the "Taverne" license above, please follow below link for the End User Agreement:

www.tue.nl/taverne

Take down policy

If you believe that this document breaches copyright please contact us at:

openaccess@tue.nl

providing details and we will investigate your claim.

AN EXPERIMENTAL DETERMINATION
OF THE TURBULENT PRANDTL NUMBER
IN A DEVELOPING TEMPERATURE BOUNDARY LAYER

J. BLOM

DC, 7003 ~~6003~~
BmA

AN EXPERIMENTAL DETERMINATION
OF THE TURBULENT PRANDTL NUMBER
IN A DEVELOPING TEMPERATURE BOUNDARY LAYER

PROEFSCHRIFT

TER VERKRIJGING VAN DE GRAAD VAN DOCTOR
IN DE TECHNISCHE WETENSCHAPPEN AAN DE
TECHNISCHE HOGESCHOOL TE EINDHOVEN,
OP GEZAG VAN DE RECTOR MAGNIFICUS,
DR IR A.A.Th.M. VAN TRIER, HOGLERAAR IN DE
AFDELING DER ELEKTROTECHNIEK VOOR EEN
COMMISSIE UIT DE SENAAT TE VERDEDIGEN OP
DINSDAG 12 MEI 1970, DES NAMIDDAGS OM 4 UUR

DOOR

JOHANNES BLOM

Geboren te 's-Hertogenbosch

**DIT PROEFSCHRIFT IS GOEDGEDEURD DOOR DE PROMOTOR
PROF. Dr. D. A. DE VRIES**

aan mijn moeder en Sigrid

I. INTRODUCTION AND DESCRIPTION OF THE PROBLEM INVESTIGATED

A. Introduction

Since the introduction of the hot-wire anemometer as a tool for measuring mean and fluctuating velocities a vast number of experiments have been carried out to determine the characteristics of turbulent boundary layers under all kinds of conditions. These investigations have greatly increased our knowledge of the nature of turbulent flow and have led to generally accepted laws, describing the distribution of important quantities of a turbulent boundary layer, such as velocity, shear stress and skin friction.

However, since the general turbulence problem is still unsolved, all these laws have a more or less empirical character and much work, both theoretical and experimental, remains to be done to obtain a detailed understanding of the physical mechanism involved.

The above argument holds even more forcibly for other turbulent transport processes, such as turbulent heat transfer, since no theoretical predictions of these processes can be made without a basic knowledge of the turbulent flow situation. Apart from the many determinations of heat transfer coefficients under varying conditions, the number of measurements of mean temperature profiles is restricted and measurements of temperature fluctuations are even scarce.

More recent theories of turbulent heat transfer [1-10] try to give exact solutions of the energy equation, assuming a known velocity distribution. However, the energy equation can only be solved if one makes an assumption concerning the unknown turbulent heat transfer it contains. Since the study of fluid flow was antecedent to that of heat transfer, it is a logical sequence of events that such an assumption is mostly based on some kind of analogy between heat and momentum transfer.

Describing the transport of heat and momentum by means of eddy diffusivities, we can introduce a turbulent Prandtl number, Pr_t , equal to the ratio of the eddy diffusivities of momentum and heat. At a known velocity distribution the eddy diffusivity of momentum is a known quantity, so that an assumption about Pr_t is equivalent to one about the turbulent heat transfer term.

Up to now the energy equation has been solved only by making ad hoc assumptions as to the value of Pr_t . Usually it is assumed that $Pr_t = 1$ (Reynolds' analogy) or Pr_t is a constant (about 0.8). Since the nature of the turbulent transport is not sufficiently understood to permit a theoretical evaluation of Pr_t , relevant information can only be obtained from direct measurements of quantities such as the eddy diffusivities.

In Figure 1.1 we have presented a survey of the experimental values of Pr_t in boundary layers, derived from the data published by various authors [11-20]. A more detailed discussion of this figure will be found in Chapter III. Here we only call attention to the fact that this figure gives a clear demonstration of the wide scatter in the experimental results of Pr_t , even for the same value of Pr , which leaves the general behaviour of Pr_t an unsolved problem. The obvious need for more accurate determinations of Pr_t has led to the investigations reported here.

It must be noted that the above-mentioned remarks concerning turbulent heat transfer also apply for turbulent mass transfer, if one introduces the eddy diffusivity of mass and the turbulent Schmidt number.

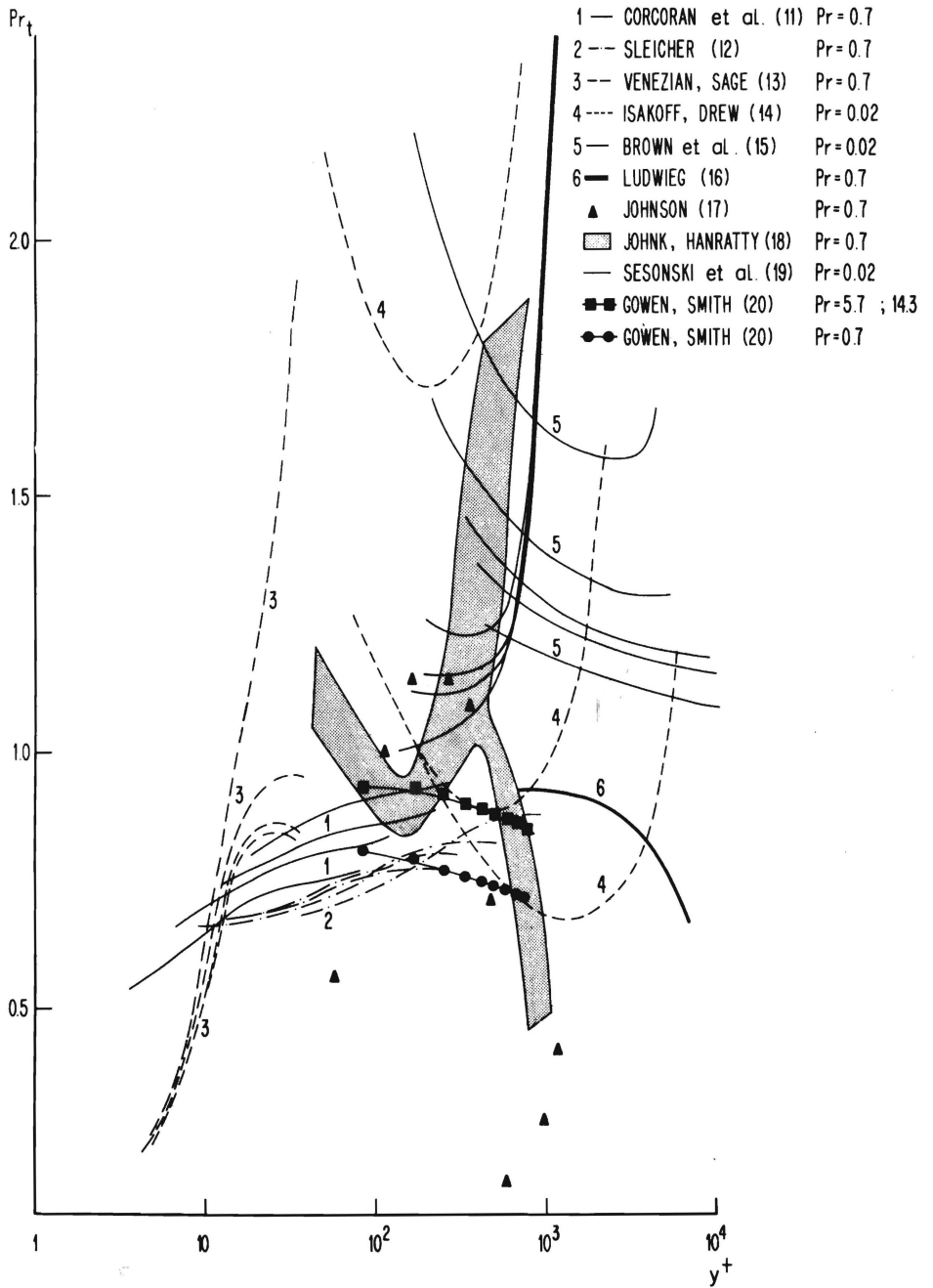


FIGURE 1.1
REVIEW OF PUBLISHED Pr_t VALUES

B. Problem Investigated

For the experimental study of heat transfer in a turbulent boundary layer we have chosen the fundamental problem of the heat transfer from a flat plate with a stepwise discontinuity in wall temperature. This problem is a fundamental one because its solution - the energy equation with constant fluid parameters being linear in the temperature - can be used for the computation of the heat transfer from a flat plate with an arbitrary wall temperature distribution by means of well-known superposition techniques.

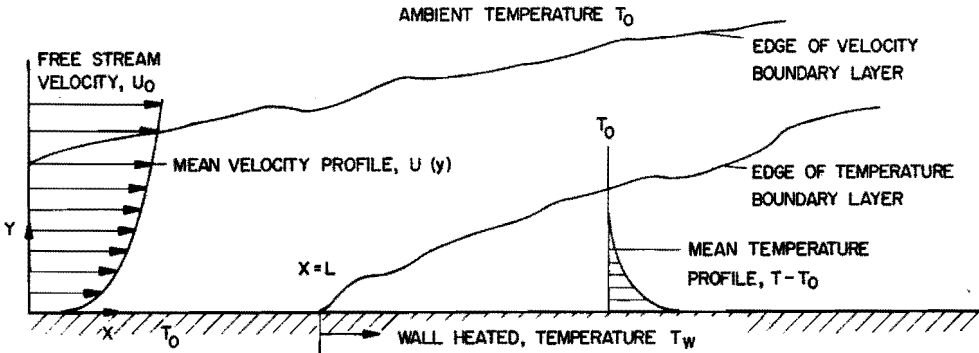


FIGURE 1.2 SKETCH OF PROBLEM INVESTIGATED

A sketch of the velocity and temperature fields of the problem investigated is presented in Figure 1.2. At $x \geq L$ the wall temperature is equal to $T_w > T_0$ and there is a growth of a temperature boundary layer in an already fully developed velocity boundary layer. The mean velocity and temperature fields are described by the following equations:

momentum equation:

$$U \frac{\partial U}{\partial x} + V \frac{\partial U}{\partial y} = - \frac{1}{\rho} \frac{\partial p}{\partial x} + \frac{1}{\rho} \frac{\partial \tau}{\partial y}; \quad (1.1)$$

continuity equation:

$$\frac{\partial U}{\partial x} + \frac{\partial V}{\partial y} = 0; \quad (1.2)$$

energy equation:

$$U \frac{\partial T}{\partial x} + V \frac{\partial T}{\partial y} = - \frac{1}{\rho c_p} \frac{\partial q}{\partial y}. \quad (1.3)$$

These equations are subject to the boundary conditions:

$$\begin{aligned} y = 0 & : U = V = 0 \\ y = 0, x \geq L & : T = T_w \\ y > 0, x = L & : T = T_0 \\ y = \infty & : U = U_0, T = T_0 \end{aligned} \quad (1.4)$$

In deriving the above-mentioned equations we use the customary boundary layer approximations. These equations are valid for a stationary, two-dimensional, incompressible flow with negligible viscous dissipation. In addition, we assume $T_w - T_0$ to be so small that the fluid parameters may be taken as constants and buoyancy forces are negligible. A rough approximation of the buoyancy effects can be made by applying the analysis of Sparrow and Minkowycz [21], who showed the buoyancy effects to depend on $Gr_x Re_x^{-5/2}$. In our experiments the maximum value of this parameter was about $1.5 \cdot 10^{-5}$, hence small enough to justify the neglect of the buoyancy forces.

The equations given above differ in form from the corresponding ones for the laminar boundary layer by the fact that both the shear stress and the heat flux density contain an additional term involving the turbulent transport of momentum and heat, respectively. This is expressed by the equations

$$\tau = \eta \frac{\partial \bar{U}}{\partial y} - \rho \overline{uv} \quad (1.5)$$

and

$$q = -\lambda \partial T / \partial y + \rho c_p \overline{v\theta} . \quad (1.6)$$

Introducing the concept of eddy diffusivities, we may write for the turbulent contributions of the momentum and heat transfer:

$$-\overline{uv} = \nu_t \partial U / \partial y \quad (1.7)$$

and

$$-\overline{v\theta} = a_t \partial T / \partial y . \quad (1.8)$$

By analogy with the molecular Prandtl number a turbulent Prandtl number can now be defined:

$$Pr_t = \nu_t / a_t . \quad (1.9)$$

With the help of Eqs. (1.5) - (1.9) the energy equation can be written as

$$U \frac{\partial T}{\partial x} + V \frac{\partial T}{\partial y} = \frac{\partial}{\partial y} \left[\left(a + \frac{\nu_t}{Pr_t} \right) \frac{\partial T}{\partial y} \right] . \quad (1.10)$$

Equation (1.10) clearly demonstrates that for a given velocity distribution the energy equation can only be solved if Pr_t is known.

From the equations given above it can be deduced that there are two possibilities of determining ν_t and a_t :

- (a) Directly from the measured values of \overline{uv} , $\overline{v\theta}$, $U(y)$ and $T(y)$, applying Eqs. (1.7) and (1.8). As far as we know, Johnson [17] has been the only one to carry out direct measurements of $\overline{v\theta}$ in wind-tunnel experiments, which illustrates the difficulty of this kind of measurement.
- (b) From the measured values of q_w , τ_w , $U(y)$ and $T(y)$ at different stations along the plate. From these measurements the distributions of $\tau(y)$ and $q(y)$ can be calculated by integration of Eqs. (1.1) and (1.3), respectively, after which ν_t and a_t can be determined from Eqs. (1.5) and (1.6). Except for the values of Johnson [17], all other values of Pr_t presented in Fig. 1.1 have been obtained in this way.

The present investigation is the first in which both methods are used in order to gain an impression of the accuracy and reproducibility of our measured Pr_t values.

To be able to compare our measuring results with existing theories of turbulent heat transfer, we shall first go further into the features of these theories. Since the turbulent heat transfer problem can only be solved with a knowledge of the velocity field, we will start with a discussion of turbulent boundary layer theories.

The separate discussion of the turbulent boundary layer is justified in our case, because the constancy of the fluid parameters and the absence of buoyancy forces give rise to a velocity field that is independent of the temperature field.

II. THE TURBULENT BOUNDARY LAYER

We shall mainly discuss those features of the turbulent boundary layer which are of direct importance for the calculation of turbulent heat transfer. This means that we shall concentrate on the distributions of mean velocity, shear stress and skin friction, from which we can calculate the distribution of the eddy diffusivity of momentum within the boundary layer.

For more detailed information about other aspects of turbulent flow, the reader is referred to the textbooks of Hinze [22], Townsend [23], Batchelor [24], Schlichting [25], Lumley and Panofsky [26] and Rotta [27]. These textbooks, however, do not deal with the large number of methods for the calculation of developing turbulent boundary layers, which have appeared in the literature during the last decade. We must, of course, bear in mind that most of these methods became possible only as a result of the fast development and application of high-speed computers. A critical review of the methods is presented below.

A. Review of Recent Calculation Methods

Our review will be confined to the case of a stationary, incompressible, two-dimensional boundary layer, developing along a smooth, solid wall under the influence of a given, arbitrary pressure gradient. With the usual boundary layer approximations, the distribution of the mean quantities of such a boundary layer is described by the momentum equation

$$U \frac{\partial U}{\partial x} + V \frac{\partial U}{\partial y} = -\frac{1}{\rho} \frac{dp}{dx} + \nu \frac{\partial^2 U}{\partial y^2} + \frac{\partial}{\partial y} (-\overline{uv}), \quad (2.1)$$

and the continuity equation,

$$\frac{\partial U}{\partial x} + \frac{\partial V}{\partial y} = 0, \quad (2.2)$$

together with appropriate boundary conditions. Equations (2.1) and (2.2) immediately demonstrate the fundamental problem of turbulent boundary layer theories: the appearance of the kinematic Reynolds shear stress, $-\overline{uv}$, results in an indeterminate system of equations, the number of equations being one less than the number of unknown quantities.

In order to make the system of equations determinate, one has to find an expression for $-\overline{uv}$ in terms of the other mean quantities or deduce further relations between the unknown quantities. The solution of this problem has been the main aim of all turbulent boundary layer theories and the resulting calculation methods differ only in the means by which these further relations - usually called the auxiliary equations - are deduced.

Up to now the mechanism of turbulence has not been completely understood, which means that a generally valid relation between the shear stress and the velocity profile is still missing. Therefore all calculation methods must inevitably rely on empiricism and in every method the postulated auxiliary equations are based partly or wholly on experimental observations. Among these observations certain basic types of boundary layer development can be distinguished, namely, boundary layers developing under zero, positive or negative pressure gradients, equilibrium, non-equilibrium and reattaching boundary layers.

If a calculation method pretends to be of universal validity, it must be able to give a good prediction of all types of boundary layer development. Every proposed calculation method should therefore be tested against as many experimental boundary layers as possible and should be discarded if it only predicts a restricted number of boundary layer developments.

Obviously, great interest attaches to accurate measurements of turbulent boundary layers, developing under all types of pressure conditions. These experiments not only provide test cases for the existing calculation methods, but may also be used to improve the empirical part of the auxiliary equations belonging to those methods.

If we compare the predictions of the many different existing methods with modern empirical data of boundary layers developing under severe pressure gradients, it becomes clear that there are only a few recent ones which meet the requirement of universal validity. It is these methods which will be treated in more detail.

We distinguish between two main classes, namely the integral and the differential methods.

All integral methods make use of the von Kármán momentum-integral equation, which can be obtained by integration of Eq. (2.1) across the boundary layer. It expresses the rate of change of momentum defect in terms of the pressure gradient and the wall shear stress:

$$\frac{d}{dx} (\rho U_0^2 \delta_2) = \delta_1 \frac{dp}{dx} + \tau_w. \quad (2.3)$$

Equation (2.3) contains three unknown quantities, the momentum thickness δ_2 , the displacement thickness δ_1 , and the local wall shear stress τ_w . In order to solve Eq. (2.3) two further equations involving these quantities are required. This usually leads to a system of coupled ordinary differential equations, together with some algebraic equations. These algebraic relations arise, for example, from the auxiliary equations or from assumptions concerning the mean velocity profile.

The differential methods start from Eqs. (2.1) and (2.2) and lead, via assumptions by which $-\overline{uv}$ is expressed in terms of the mean velocity field or in other quantities of the turbulent boundary layer, to a system of coupled partial differential equations together with some algebraic equations.

In the following we will discuss the two classes of methods separately.

1. Differential Methods

The oldest assumptions concerning the behaviour of $-\overline{uv}$ are the mixing-length or eddy-viscosity hypotheses, originated by Prandtl [28], Taylor [29] and von Kármán [30]. In these hypotheses the Reynolds stress is related to the local gradient of the mean velocity, which for the mixing-length concept can be expressed in the form:

$$-\overline{uv} = \ell^2 \left| \frac{\partial U}{\partial y} \right| \frac{\partial U}{\partial y} \quad (2.4)$$

and for the eddy-viscosity concept by

$$-\overline{uv} = \nu_t \frac{\partial U}{\partial y}, \quad (2.5)$$

both concepts being connected by the relation

$$\nu_t = \ell^2 \left| \frac{\partial U}{\partial y} \right|. \quad (2.6)$$

In order to obtain velocity profiles an assumption is required concerning the dependence of ℓ or ν_t on the position in the boundary layer and on the flow conditions.

In most discussions the turbulent boundary layer is divided into an inner and an outer region, each having its own characteristics. The inner region may be regarded as the region where the turbulent motion is greatly affected by the presence of the wall, whereas in the outer region the flow pattern closely resembles that of a wake. Analytically both regions are usually treated separately, and an overlap or intermediate region is introduced in which the solutions of both regions are simultaneously valid. In this way one can obtain continuous functions for the entire velocity and shear-stress profiles. Illustrative examples of this procedure are given by Mellor [31] and Stevenson [32].

Originally it was assumed that, with increasing distance from the wall, the inner region (thickness about 0.15δ) could be divided into three main parts:

- (a) A very thin layer, adjacent to the wall, which is fully laminar; hence within this layer $\nu_t = \ell = 0$, resulting into $u^+ = y^+$.
- (b) A transition region, in which the total shear stress is composed of both turbulent and laminar contributions.
- (c) A fully turbulent part, where the turbulent shear stress predominates over the viscous shear stress, so that $\tau = -\rho u \bar{v}$. It was assumed that in this region $\ell = ky$, in which k is the universal von Kármán constant, $k \approx 0.4$. Together with the assumption of a constant shear stress, $\tau = \tau_w$, this leads to the well-known logarithmic velocity distribution:

$$u^+ = k^{-1} \ell n y^+ + B. \quad (2.7)$$

In the outer part of the boundary layer, the velocity profiles can be correlated reasonably well by the assumption of a constant eddy viscosity. For instance, Clauser [33] has shown that the formula

$$\nu_t = 0.018 U_0 \delta_1 \quad (2.8)$$

gives a good representation for equilibrium layers in zero and variable pressure gradients. In fact, this assumption of a constant value of ν_t is not more than a rough approximation for boundary layers in arbitrary pressure gradients, as has been pointed out by Rotta [27] and Bradshaw [35].

Extensive hot-wire measurements of Klebanoff [36] and Laufer [37] showed that turbulent velocity fluctuations are present up to the wall, thereby disproving the concept of a purely laminar layer adjacent to the wall. Accordingly, this layer is now called the viscous sublayer, in which ν_t is assumed to be different from zero. The same conclusion was reached by Reichardt [38] and Deissler [39] who discovered that the assumption of $\nu_t = 0$ in the viscous sublayer was contradictory to experimental data on heat transfer at large Prandtl numbers.

The introduction of the viscous sublayer has led to a large number of modifications of the mixing-length theory in which distributions of v_t for the entire boundary layer have been proposed. These modifications are reviewed in detail by Rotta [27], Hinze [22] and Townsend [23]. Some recent modifications, dealing in particular with boundary layers under variable pressure gradients, are given by Townsend [40, 41], Mellor and Gibson [42], Mellor [31], Perry, Bell and Joubert [43], Perry [44] and McDonald [45]. They all meet the requirement that the proposed distribution of v_t must result in a velocity profile which agrees with the experimentally verified law of the wall, stating that u^+ is a universal function of y^+ .

Brand and Persen [46] followed the reverse order of solution and started with the law of the wall in a form proposed by Spalding [47], considering it as an experimentally established stress-strain rate relation, valid for turbulent motions. By substituting the law of the wall into Eqs. (2.1) and (2.2) they arrived at a differential equation for u_x , which was solved numerically. Of course, this kind of reasoning can only have approximate validity, since the law of the wall does not correctly represent the existing velocity profile in the outer parts of the boundary layer.

Much has been written about the defects of the mixing-length hypothesis, particularly concerning the crudity of the assumed mixing process (Hinze [22], Rotta [27]). A more fundamental objection to the use of mixing-length formulas for boundary layers in arbitrary pressure gradients is the fact that $-\overline{uv}$ is only related to local mean quantities, the effect of the past history of the boundary layer being ignored.

This fundamental objection has induced Bradshaw, Ferriss and Atwell [48] to introduce an entirely new hypothesis. In their theory $-\overline{uv}$ is closely related to the turbulent kinetic energy, $\frac{1}{2}\overline{\rho q^2}$, which quantity, being governed by the turbulent kinetic energy equation, is certainly not determined uniquely by the local mean flow conditions. In this way the turbulent quantity $-\overline{uv}$ is related to other turbulent properties, which obviously seems to be a better hypothesis than relating a turbulent property to the properties of the mean velocity field. Since their predictions of boundary layer development compare favourably with the results of most other methods, the method of Bradshaw et al. [48] will be treated in more detail here.

Their work was, in fact, initiated by Townsend [40, 49]. Also starting from the turbulent kinetic energy equations, he showed that the mixing-length hypothesis is valid in the inner, fully turbulent part of the boundary layer, where to a good approximation the production and dissipation of turbulent kinetic energy are in equilibrium, so that the balance of turbulent kinetic energy is unaffected by the nature of the flow in adjacent regions.

With the usual boundary layer approximations for stationary flow, the turbulent kinetic energy equation can be written as (Townsend [23])

$$U \frac{\partial (\overline{\frac{1}{2}\rho q^2})}{\partial x} + v \frac{\partial (\overline{\frac{1}{2}\rho q^2})}{\partial y} = -\rho \overline{uv} \frac{\partial U}{\partial y} - \frac{\partial}{\partial y} (\overline{\frac{1}{2}\rho q^2 v} + \overline{p'v}) - \epsilon \rho. \quad (2.9)$$

In this equation the terms on the left represent the rate of change of turbulent kinetic energy along a streamline of the mean flow, sometimes called the advection of turbulent kinetic energy by the mean flow. The first term on the right stands for the production of turbulent kinetic energy from the mean flow, the second term for the diffusion of it in the y -direction, and the last term for its dissipation into heat by viscous forces. The experiments of Klebanoff [50] and Laufer [37] have shown that except near the outer edge of the boundary layer, say $y/\delta > 0.7$, and very close to the wall the production and the dissipation term are the largest terms in Eq. (2.9); the advection and diffusion are usually smaller though not negligible.

By introducing the quantities

$$a_1 = \frac{\tau}{\rho q^2} \quad (2.10^a)$$

$$L = \frac{(\tau/\rho)^{\frac{3}{2}}}{\varepsilon} \quad (2.10^b)$$

$$\text{and } G_1 = \frac{\overline{p'v}/\rho + \frac{1}{2} \overline{q^2 v}}{\left(\frac{\tau_{\max}}{\rho}\right)^{\frac{1}{2}} \cdot \frac{\tau}{\rho}} \quad (2.10^c)$$

Bradshaw et al. converted Eq. (2.9) into an equation for the rate of change of τ along a mean streamline, which has the form:

$$U \frac{\partial}{\partial x} \left(\frac{\tau}{2a_1 \rho} \right) + V \frac{\partial}{\partial y} \left(\frac{\tau}{2a_1 \rho} \right) - \frac{\tau}{\rho} \frac{\partial U}{\partial y} + \left(\frac{\tau_{\max}}{\rho} \right)^{\frac{1}{2}} \frac{\partial}{\partial y} \left(G_1 \frac{\tau}{\rho} \right) + \frac{(\tau/\rho)^{\frac{3}{2}}}{L} = 0 \quad (2.11)$$

In view of their assumption that $-\rho \overline{uv} = \tau$, this equation is only valid outside the viscous sublayer and the transition layer, say for $y^+ > 30$.

If adequate assumptions can be made for expressing a_1 , L and G_1 in the independent variables, then Eq. (2.11) together with the Eqs. (2.1) and (2.2) form a set of three in the three unknowns U , V and τ and can be solved numerically. Bradshaw et al. have used the experimental results of Klebanoff [50] in a zero-pressure-gradient boundary layer to find the best choices for a_1 , L and G_1 . It turns out that with the extremely simple assumptions

$$a_1 = 0.15, \quad \frac{L}{\delta} = f_1 \left(\frac{y}{\delta} \right), \quad G_1 = \left(\frac{\tau_{\max}}{U^2} \right)^{\frac{1}{2}} \cdot f_2 \left(\frac{y}{\delta} \right), \quad (2.12)$$

where $f_1(y/\delta)$ and $f_2(y/\delta)$ are numerically specified, the calculations accurately predict turbulent boundary layer developments in all kinds of pressure gradients. Fig. 2.1 shows the functions used.

Bradshaw et al. have extensively discussed the implications of the Eqs. (2.10^a) - (2.10^c). In a subsequent article Bradshaw [51] has published a number of experimental results regarding the distributions of a_1 , L and G_1 in boundary layers with non-zero pressure gradients. These last results indicate that the assumptions of Eq. (2.12) are quite universally valid.

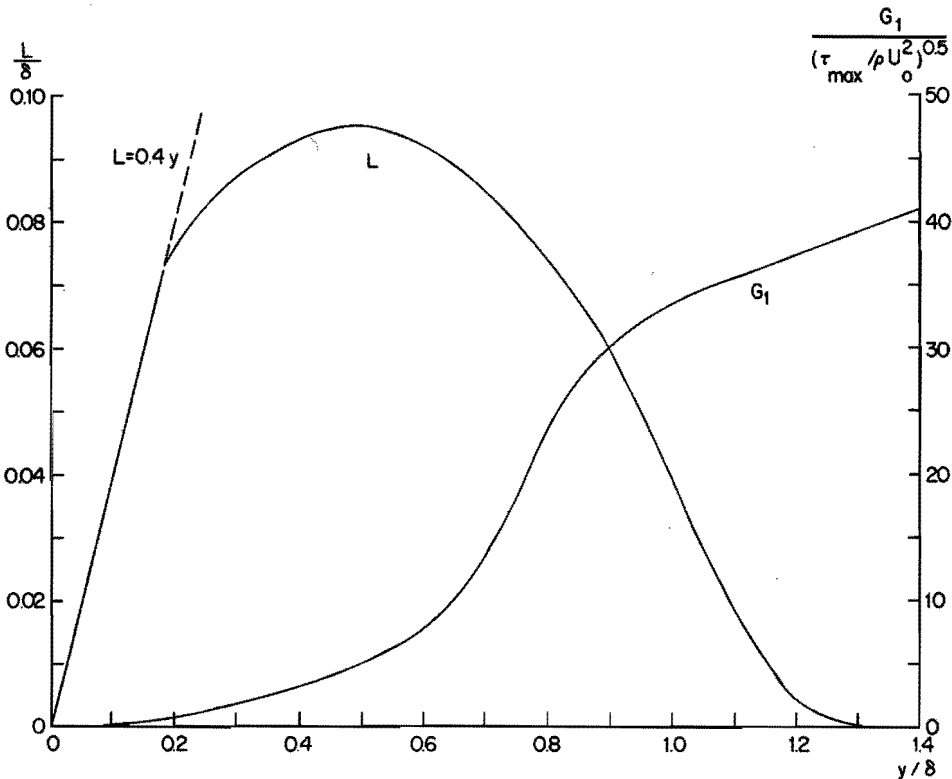


FIG. 2.1 THE EMPIRICAL FUNCTIONS L AND G_1 USED IN THE CALCULATION METHOD OF BRADSHAW ET AL. [48]

It can easily be proved that the calculation method of Bradshaw et al. reduces to the mixing-length theory in those regions of the turbulent boundary layer in which that theory might be expected to be valid. Within the fully turbulent part of the boundary layer the advection and diffusion of turbulent kinetic energy may be neglected, so that one finds from Eq. (2.11)

$$\frac{\tau}{\rho} \frac{\partial U}{\partial y} = \frac{(\tau/\rho)^{\frac{3}{2}}}{L} \quad \text{or} \quad \frac{\partial U}{\partial y} = \frac{(\tau/\rho)^{\frac{1}{2}}}{L} \quad (2.13)$$

Hence, under these circumstances the dissipation length parameter L is identical with the mixing length ℓ .

The above derivation was given by Townsend [40] to justify the use of the mixing-length hypothesis. Bradshaw et al. have availed themselves of the mixing-length hypothesis to derive the boundary conditions at $y^+ = 30$ for their numerical solution. Making some additional assumptions, Bradshaw [52] has indicated how this calculation method can easily be extended to include cases of compressible boundary layers, heat transfer and transpired boundary layers. Quite recently Nash [53] has extended Bradshaw's method to the calculation of three-dimensional boundary layers.

Since Bradshaw's method is capable of incorporating the behaviour of various turbulent parameters, it may be refined in the future if more knowledge about this behaviour becomes available, for instance from experimental data on pressure fluctuations within the turbulent boundary layers.

2. Integral Methods

The integral methods try to find a solution of the von Kármán momentum integral equation, usually expressed in the form:

$$\frac{d\delta_2}{dx} + \frac{\delta_2(2+H)}{U_0} \frac{dU_0}{dx} = \frac{c_f}{2} \quad (2.14)$$

Being an ordinary differential equation, it represents the simplest mathematical description of the turbulent boundary layer. The momentum thickness δ_2 , the displacement thickness δ_1 , the shape parameter H and the local skin friction coefficient c_f in this equation are defined by the following relations:

$$\delta_1 = U_0^{-1} \int_0^{\infty} (U_0 - U) dy, \quad (2.15)$$

$$\delta_2 = U_0^{-2} \int_0^{\infty} U(U_0 - U) dy, \quad (2.16)$$

$$H = \delta_1 / \delta_2, \quad (2.17)$$

$$c_f = 2\tau_w / \rho U_0^2. \quad (2.18)$$

As in the momentum equation (2.1), we have neglected in Eq. (2.14) the term due to the normal Reynolds stresses, $U_0^{-2} \int_0^{\infty} (u^2 - \bar{v}^2) dy$. This seems to be justified on the basis of the experiments of Newman [54], Sandborn and Slogar [55] and Schubauer and Klebanoff [56], provided the boundary layer is not too close to separation (see also Ross [57] and Rotta [27].).

If $U_0(x)$ is given, Eq. (2.14) still contains three unknowns δ_2 , H and c_f ; thus a solution of Eq. (2.14) is only possible if two further equations involving these quantities are deduced. Using the conventional nomenclature, these equations are referred to as the "skin friction equation" and "the auxiliary equation" or "shape parameter equation".

The skin friction equation usually relates the local skin friction coefficient to a Reynolds number, based on some length scale of the boundary layer, and to a shape parameter of the velocity profile, such as H . An example of such a skin friction equation is the empirical relation of Ludwig and Tillmann [58]:

$$c_f = 0.246 \cdot 10^{-0.678 H} (U_0 \delta_2 / \nu)^{-0.268}, \quad (2.19)$$

which is frequently used in integral methods.

The auxiliary equation essentially describes the effect of pressure gradients on the shape of the mean velocity profile. Because of our incomplete knowledge of the turbulent flow mechanism, the auxiliary equations are basically correlations of experimental data, no matter whether or not some physical concept has been suggested as the basis of the correlation. Consequently much depends on the range of types of boundary layer development which has been examined in obtaining the correlation.

In the past various attempts have been made to derive a satisfactory form of the auxiliary equation. A detailed discussion has been given by Rotta [27] and Thompson [59]. Rotta [27] has reviewed known shape parameter equations, all rearranged to fit an equation of the form:

$$L\delta_2 \frac{dH}{dx} = -M \frac{\delta_2}{U_0} \frac{dU_0}{dx} + N, \quad (2.20)$$

in which L has the value 1 or 0. The symbols M and N denote functions of H and Re_2 ($\equiv \delta_2 U_0/\nu$). If $L = 0$, any historical effect on the development of the profile shape is neglected, which is very unrealistic (see Nash [60]). The other methods, with $L = 1$, are based on the idea that a sudden change in dU_0/dx will produce a change in dH/dx rather than in H itself.

Rotta presented the resulting functions M and N for 14 methods, ranging in chronological order from Buri [61] to Spence [62]. The diversity of the proposed M and N functions was confusing, and a comparison of Clauser's [63] measurements with the shape parameter predictions of the various methods showed that agreement was poor, not only between theory and experiment, but also between the various methods mutually. This finding was substantiated by the review of Thompson [59] in which a selection of the better-known auxiliary equations was used to predict H and δ_2 for 11 experiments on boundary layers. With the exception of the method of Head [64], which was not included in Rotta's review, agreement between measurements and calculations was poor.

The reasons for the inadequacy of the older methods are not difficult to detect. Most auxiliary equations had been deduced from a limited number and range of experiments on boundary layers and were consequently of restricted validity. Thompson [59] observed that some calculation methods, such as those of Spence [62] and Maskell [65], have passed into textbooks, for example that of Duncan, Thom and Young [66], on the basis of very few comparisons with experiments and even fewer comparisons with observed boundary layers other than those used in the derivation of the particular auxiliary equation. In addition, Thompson has shown that there are three-dimensional effects present in most of the measured boundary layers, which influence the auxiliary equations [67, 68].

The method of Head [64] is usually called the entrainment method, because his calculation procedure is based on a universal relation he has postulated for the entrainment velocity. By entrainment we denote the process by which at the outer edge of the boundary layer the turbulence spreads with distance due to the turbulent mixing. The original entrainment equation was derived by making the assumption that the entrainment velocity, V_e , was a universal function of the velocity defect in the outer layer. The latter quantity could be specified by a shape parameter, such as H, and the free stream velocity, U_0 .

The quantity of flow in the boundary layer, Q, can be expressed as

$$Q = \int_0^{\delta} U \, dy = \int_0^{\delta} U_0 \, dy - \int_0^{\delta} U_0 \left(1 - \frac{U}{U_0}\right) dy = U_0(\delta - \delta_1), \quad (2.21)$$

so

$$V_e = \frac{dQ}{dx} = \frac{d}{dx} [U_o(\delta - \delta_1)] . \quad (2.22)$$

From the above assumption it then follows that

$$\frac{V_e}{U_o} = \frac{1}{U_o} \frac{d}{dx} [U_o(\delta - \delta_1)] = f(H) . \quad (2.23)$$

Instead of the usual shape parameter H, Head considered it rather more convenient to use the alternative form parameter

$$H_{\delta-\delta_1} \equiv \frac{\delta - \delta_1}{\delta_2} ,$$

which can be simply related to H, assuming a one-parameter family of velocity profiles. Hence the auxiliary equations of Head take the form:

$$\frac{1}{U_o} \frac{d}{dx} [U_o(\delta - \delta_1)] = F(H_{\delta-\delta_1})$$

and

(2.24)

$$H_{\delta-\delta_1} = G_2(H) .$$

The functions F and G_2 were found by analysing the boundary layer developments measured by Newman [54] and Schubauer and Klebanoff [56]. They are presented in Fig. 2.2. These curves can be approximated very satisfactorily by the expressions:

$$F = 0.0306 (H_{\delta-\delta_1} - 3.0)^{-0.653}$$

and

(2.25)

$$G_2 = 1.535 (H - 0.7)^{-2.715} + 3.3 .$$

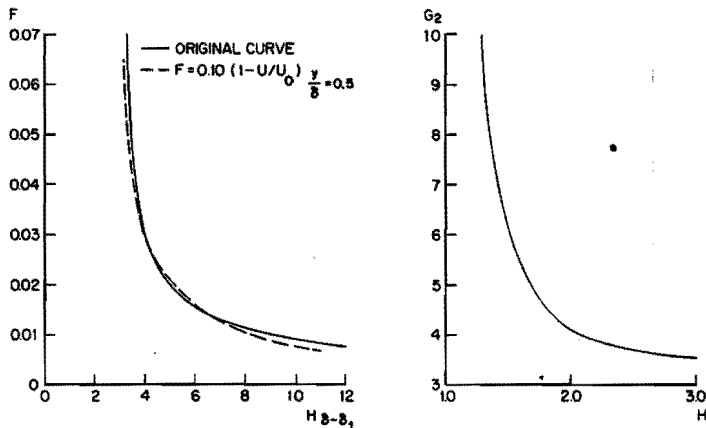


FIG. 2.2 THE FUNCTIONS F AND G OF HEAD'S ENTRAINMENT APPROACH

When the method was first proposed reasonably extensive comparisons with experiment were made, which showed a very fair agreement between predicted and measured H developments. At that stage, however, it was not recognized that Head's method had a much wider applicability than the existing ones. This aspect has been clearly brought out by Thompson [59] in making his extensive comparisons between the different methods for a wider range of measured developments.

Thompson [59] also showed that the agreement of Head's theory with experiments was still unsatisfactory in some cases, especially for equilibrium boundary layers. He therefore revised the whole basis of the entrainment equation and introduced an additional term which represented the rate of change of the form parameter (see also Head [69]).

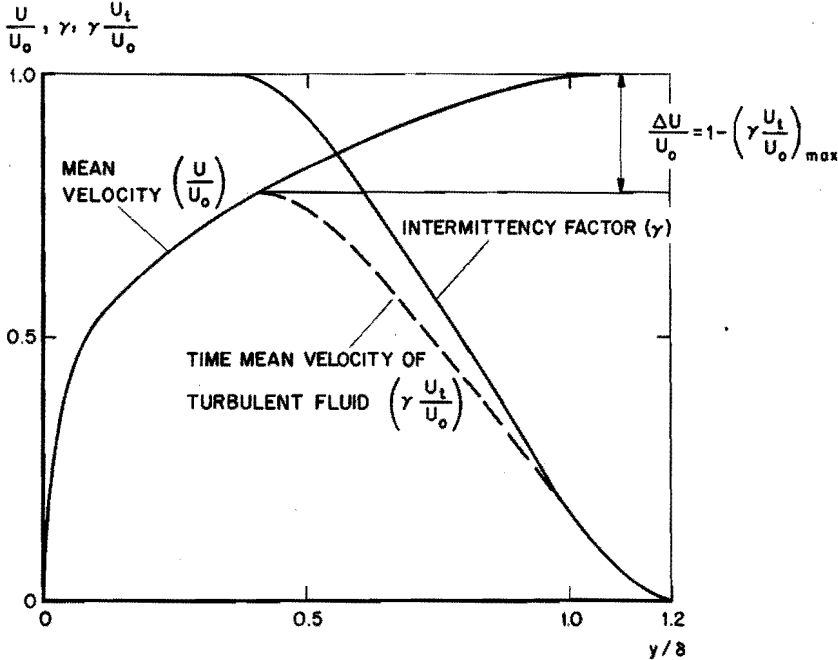


FIG. 2. 3 EXPLANATION OF TERMS USED IN THOMPSON'S ENTRAINMENT APPROACH

For the mean velocity U in the boundary layer Thompson [68] wrote (see Fig. 2.3)

$$U = \gamma U_t + (1 - \gamma) U_p, \tag{2.26}$$

in which U_t is the average velocity of the turbulent flow, taken over "time turbulent", U_p is the average velocity of the irrotational flow over "time potential" and γ is the fraction of the time during which the flow is turbulent at a particular position, also called the intermittency factor. Assuming the mean flux of turbulent fluid, Q_t , to be a better-defined physical quantity than the total quantity of flow in the boundary layer (Head's Q), Thompson introduced an entrainment velocity $V_{e,t}$, equal to the rate of change of Q_t , hence with

$$Q_t = \int_0^{\infty} \gamma U_t dy = U_o L_t, \quad (2.27)$$

$$V_{e,t} = \frac{d}{dx} (Q_t) = \frac{d}{dx} (U_o L_t), \quad (2.28)$$

where L_t is a so-called turbulent flux thickness. The remaining problem is to make a plausible hypothesis for the entrainment velocity $V_{e,t}$.

On physical grounds it was inferred that a proper velocity scale for $V_{e,t}$ is the velocity defect in the intermittency region, which can be expressed by the defect in turbulent flux profile (see Fig. 2.3.). Thompson used a velocity scale ΔU , defined as

$$\frac{\Delta U}{U_o} = 1 - \left[\gamma \frac{U_t}{U_o} \right]_{\max} \quad (2.29)$$

To start with, by assuming an overall similarity of the flow as in equilibrium layers, he took $V_{e,t}$ to be proportional to ΔU . In consequence, the entrainment equation became

$$\frac{1}{U_o} \frac{d}{dx} [U_o L_t] = \frac{V_{e,t}}{U_o} = \alpha_e \frac{\Delta U}{U_o}, \quad (2.30)$$

in which the entrainment coefficient α_e was assumed to be a universal constant.

In the absence of more detailed measurements it was further assumed that (a) $U_p = U_o$ and (b) γ is a universal function of y/δ given by the measurements of Klebanoff [50]. Rewriting Eqs. (2.14) and (2.30), one obtains the following equations to be solved:

$$\frac{dR_2}{dx} = \frac{c_f}{2} \frac{U_o}{v} - (H + 2) \frac{R_2}{U_o} \frac{dU_o}{dx} \quad (2.14^a)$$

and

$$\frac{d[R_2 \cdot L_t / \delta_2]}{dx} = \alpha_e \frac{\Delta U}{U_o} \cdot \frac{U_o}{v} \quad (2.30^a)$$

Using a new two-parameter velocity profile family (see the next section), Thompson constructed three charts, giving L_t/δ_2 , $\Delta U/U_o$ and c_f as functions of H and R_2 . With the aid of these charts the Eqs.(2.14^a) and (2.30^a) were solved simultaneously by a stepwise procedure.

Now Thompson found that with a value of $\alpha_e = 0.09$, Eq. (2.30^a) produced results that agreed closely with the equilibrium layers measured by Clauser and the flat plate boundary layer, but which showed poor agreement with layers that were proceeding more or less rapidly towards separation. He therefore introduced a dependency upon the rate of change of the form parameter, L_t/δ_2 , by assuming

$$\alpha_e = \alpha + \beta \delta \frac{d(L_t/\delta_2)}{dx} \quad (2.31)$$

(For equilibrium boundary layers $d/dx[L_t/\delta_2] = 0$.) The entrainment equation (2.30^a) could then be written as follows:

$$\frac{d(L_t/\delta_2)}{dx} = \frac{\alpha \frac{U_o}{v} \frac{\Delta U}{U_o} - \frac{L_t}{\delta_2} \frac{dR_2}{dx}}{R_2(1 - \beta \frac{\Delta U}{U_o})} \quad (2.32)$$

With $\alpha = 0.09$ and $\beta = 1.0$ this equation was found to provide data agreeing satisfactorily with boundary layers measured on flat surfaces, even better agreement being obtained if β was increased to 2.0 for $\delta_2 d(L_t/\delta_2)/dx > 0.003$.

Thompson has further given corrections of Eq. (2.32) for the effects of surface curvature and has extended the entrainment method to cases of three-dimensional boundary layers and boundary layers with suction or injection. These cases and the extensions of the entrainment method to compressible boundary layers with heat transfer are treated in detail in a later review by Head [69]. Escudier and Nicoll [70] have also given recommendations for entrainment functions for both boundary layers and wall jets.

Nash [60] has reviewed the principle governing the various general types of auxiliary equation, such as Eq. (2.20). Being a differential equation of the first order in H , it requires the specification of an initial value of H . In this way the upstream history of the boundary layer is taken into account, in so far as it affects the velocity profile. However, no provision is made for the possible effects of the initial shear stress distribution, which is related through the equation of motion to the derivatives of the velocities in the x -direction and may be characterized by the specification of an initial value of dH/dx . In general, therefore, the shape parameter equation must be a second-order differential equation in H .

In the derivation of his shape parameter equation, Nash considered the equilibrium boundary layer to be the basic form of boundary layer development. Such a layer is characterized by a streamwise pressure distribution for which

$$P \equiv \frac{\delta_1}{\tau_w} \frac{dp}{dx} = \text{constant} \quad (2.33)$$

It can then be shown that, to a good approximation (cf. Clauser [33]), the velocity-defect profiles in that layer are similar, i. e. the velocity-defect profile has a given shape irrespective of the streamwise position:

$$\frac{U_o - U}{u_\tau} = f\left(\frac{y}{\delta}\right) \quad (2.34)$$

As a convenient shape factor for this velocity-defect profile Nash used the parameter G , related to H by

$$G = \left(\frac{2}{c_f}\right)^{0.5} (1 - H^{-1}) \quad (2.35)$$

Thus for equilibrium boundary layers G is a unique function of P . The functions $G(P)$ as indicated by the theories of Townsend [40, 71] and Mellor and Gibson [42] together with some relevant experimental data [33, 35, 58, 72, 73] are presented in Fig. 2.4. For the purpose of his calculation method, Nash has drawn a curve, shown in Fig. 2.4, representing a synthesis of experiment and theory and given by the relation:

$$G = 6.1 (P + 1.81)^{0.5} - 1.7 \quad (2.36)$$

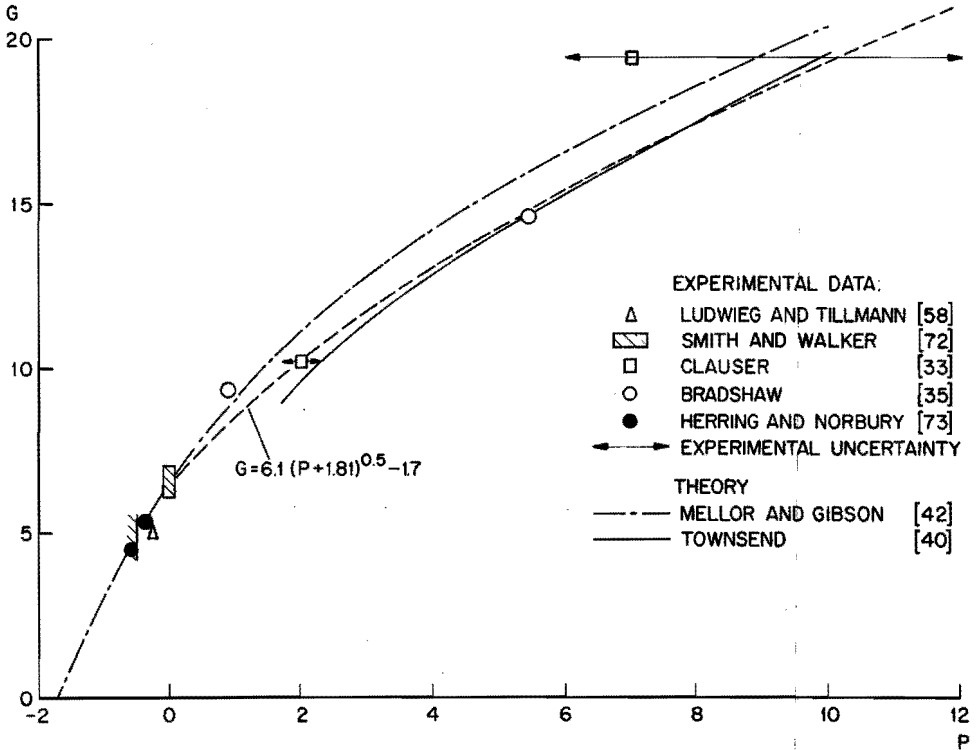


FIG. 2.4 THE FUNCTION G (P) FOR EQUILIBRIUM BOUNDARY LAYERS

For a boundary layer with an arbitrary pressure distribution, the parameters P and G will in general be functions of x. Now Nash has postulated that every developing boundary layer has a tendency to reach a "local equilibrium" state, which means that the function G(x) has the tendency to approach the local equilibrium distribution, $G_e(x)$, which is obtained by substitution of the given P(x) into Eq. (2.36). Following this hypothesis, Nash derived the following shape parameter equation:

$$\frac{d^2G}{d\bar{x}^2} = \lambda \left\{ \frac{d}{d\bar{x}} (G - G_e) \right\}^\alpha (G - G_e)^\beta, \quad (2.37)$$

in which \bar{x} is a non-dimensional distance parameter, given by

$$\bar{x} = \int_{x_0}^x \delta_1^{-1} dx \quad (2.38)$$

and x_0 is an initial position in the boundary layer, forming the starting point from which the development is calculated.

A comparison with experiments showed that in general two possibilities must be distinguished, according to whether $dP/dx > 0$ or $dP/dx < 0$. For the former case G(x) proved to remain close to $G_e(x)$, while for the latter case G(x) departed markedly from $G_e(x)$.

By trial and error the values of the parameters λ , α and β in Eq. (2.37) have been assessed to give satisfactory agreement with two or more sets of boundary layer data for both $dP/dx > 0$ and $dP/dx < 0$. In this way Nash obtained the following provisional values:

$$\left. \begin{aligned} \frac{d}{dx} (G - G_e) > 0 : \lambda = -0.25, \quad \alpha = 3, \quad \beta = -2 \\ \frac{d}{dx} (G - G_e) < 0 : \lambda = 5, \quad \alpha = 2, \quad \beta = -2. \end{aligned} \right\} (2.39)$$

Nash compared the results of his calculation method with a number of experimental boundary layer data, which showed a very satisfactory agreement. However, further experimental evidence is needed to ascertain the general applicability of his method, which will probably require some adjustment of the constants in the auxiliary equation to maintain the best overall agreement.

The shape parameter equations of the integral methods discussed above are all based on some physical concept concerning the behaviour of the turbulent boundary layer. Another large class of integral methods can be distinguished for which the shape parameter equation is derived from integral forms of the equations of motion other than the integral momentum equation. These integral forms can be derived in a quite general manner by multiplying each term of the equation of motion by $U^m y^\ell$ and then integrating over y . The integral equations which have found application in existing calculation methods are:

the integral kinetic energy equation ($m = 1, \ell = 0$):

$$\frac{1}{2} \frac{d}{dx} (U_0^3 \delta_3) = \frac{1}{\rho} \int_0^{\infty} \tau \frac{\partial U}{\partial y} dy, \quad (2.40)$$

in which the kinetic energy thickness, δ_3 , is given by

$$\delta_3 = \frac{1}{U_0^3} \int_0^{\infty} U(U_0^2 - U^2) dy, \quad (2.41)$$

and the integral moment-of-momentum equation ($m = 0, \ell = 1$):

$$\int_0^{\infty} \left[y \frac{\partial}{\partial x} (U^2) - y \frac{\partial}{\partial y} \left(U \int_0^{\infty} \frac{\partial U}{\partial x} dy_1 \right) \right] dy = \frac{\delta^2}{2} U_0 \frac{dU_0}{dx} - \frac{1}{\rho} \int_0^{\infty} \tau dy. \quad (2.42)$$

In both equations (2.40) and (2.42) the contribution of the normal Reynolds stresses has been neglected.

To transform Eqs. (2.40) and (2.42) into shape parameter equations we need, besides the usual assumptions about the shape of the velocity profile, additional relations concerning the shear-stress distribution. The shape of the velocity profile presents little difficulty in practice, because the velocity profiles can be satisfactorily regarded as belonging to a single- or two-parameter family (see next section). However, a central problem for the application of Eq. (2.40) is an assumption concerning the shear-stress integral:

$$\int_0^{\infty} \tau \frac{\partial U}{\partial y} dy, \quad (2.43)$$

usually called the dissipation integral. It can be expressed with the aid of a non-dimensional dissipation coefficient, c_D , by

$$\int_0^{\infty} \tau \frac{\partial U}{\partial y} dy = \frac{c_D \rho U_o^3}{2}. \quad (2.44)$$

In the early 1950s several authors such as Rotta [74], Truckenbrodt [75], Tetervin and Lin [76] and Rubert and Persh [77] proposed calculation methods based on a relation for c_D . Through Schlichting's textbook [25], Truckenbrodt's method has become widely known. In it c_D is given by

$$c_D = 0.0112 Re_2^{-1/6}. \quad (2.45)$$

Spalding [78], reviewing the existing theoretical and experimental information concerning c_D , has shown that the shortcomings of the calculation methods mentioned above, which have been clearly indicated in Thompson's review [59], are due to the inadequacies of the c_D -relations used. By combining Eq. (2.14), (2.22) and (2.40) together with the assumption that the quantities c_D , V_e and c_f depend only on the velocity profile and Re_2 , Spalding derived the following relation between c_D and V_e :

$$c_D \frac{H+1}{H_3} - \frac{H-1}{H_{\delta-\delta_1}} \frac{V_e}{U_o} - c_f = 0. \quad (2.46)$$

In it H_3 is defined by

$$H_3 = \delta_3 / \delta_2. \quad (2.47)$$

Equation (2.46) permits the dissipation coefficient to be calculated if the velocity-profile family and the entrainment velocity are known.

Assuming a velocity-profile family with two parameters z_e and l' [79] (see next section):

$$\frac{U}{U_o} = z_e \left\{ 1 + \frac{\ln(y/\delta)}{l'} \right\} + \frac{1}{2}(1 - z_e) \left(1 - \cos \pi \frac{y}{\delta} \right) \quad (2.48)$$

and V_e expressed by

$$\left. \begin{aligned} z_e \leq 1 : V_e / U_o &= 0.06 - 0.05 z_e \\ z_e \geq 1 : V_e / U_o &= 0.03 z_e - 0.02 \end{aligned} \right\} (2.49)$$

Spalding arrived at an improved expression for c_D (z_e , l'), to be recommended for boundary layer calculations, presented in Figure 2.5. Although this expression agrees more closely with experimental data than previous ones, further research will be needed to verify and improve the recommendation for c_D . Spalding has already given some suggestions for extension of his c_D relations to cases of greater complexity.

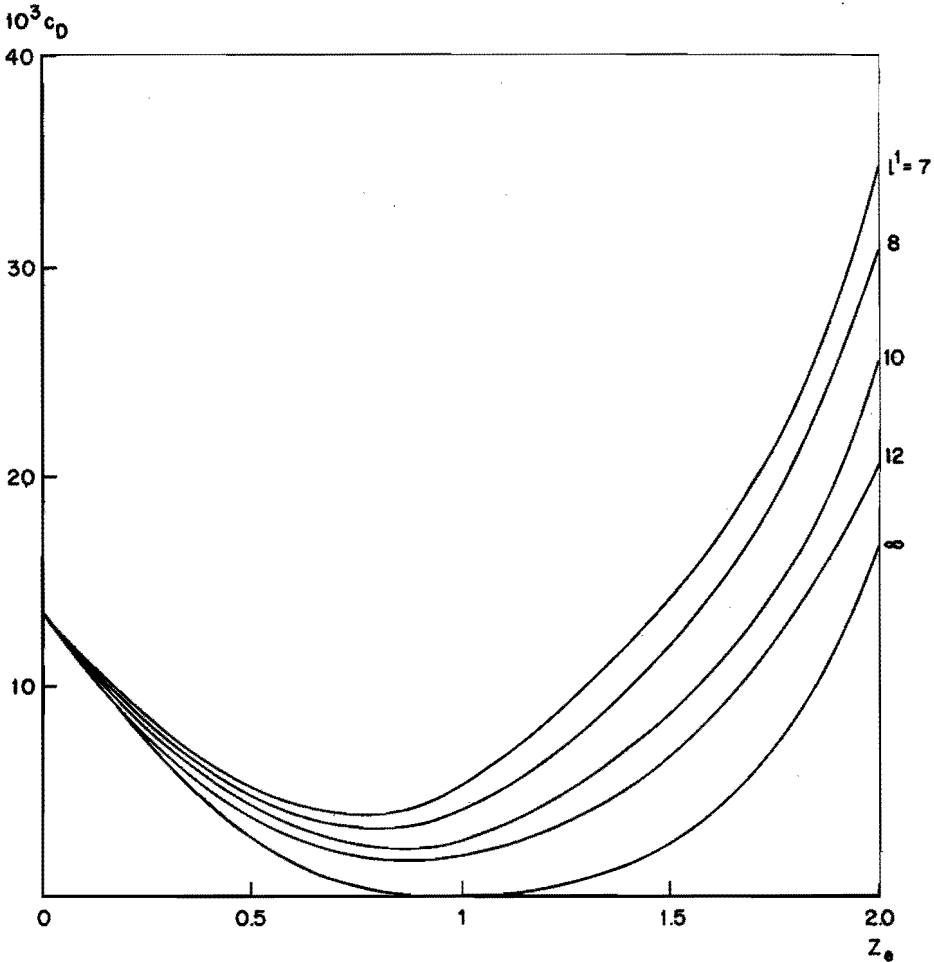


FIG. 2. 5 THE $c_D(Z_0, l')$ FUNCTION DEDUCED FROM EQ. (2.46) AND THE ENTRAINMENT LAW OF EQ. (2.49)

The calculation method of McDonald and Stoddart [80] is the only one - to the author's knowledge - which uses the integral moment-of-momentum equation (2.42) in arriving at a shape parameter equation. The central problem in this method is the evaluation of the integral of the shear stress across the boundary layer, non-dimensionally expressed by

$$I = \int \frac{2\tau}{\rho U_0^2} d\left(\frac{Y}{\delta}\right). \quad (2.50)$$

McDonald and Stoddart started their evaluation of I with considerations concerning a representative shear-stress distribution for a boundary layer developing in an adverse pressure gradient; see Fig. 2.6.

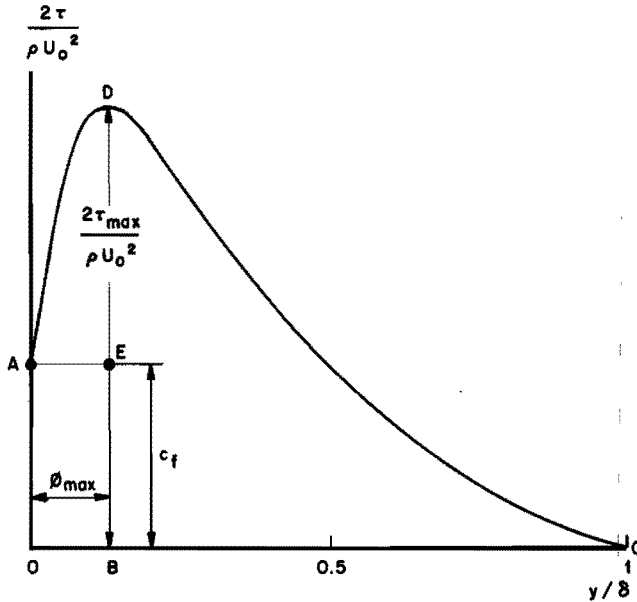


FIG. 2.6 REPRESENTATIVE SHEAR STRESS DISTRIBUTION FOR A BOUNDARY LAYER IN AN ADVERSE PRESSURE GRADIENT

The part BCD was considered similar to the shear-stress distribution at constant pressure with an apparent wall shear stress τ_{\max} and boundary layer thickness $(1 - \varphi_{\max})\delta$, where τ_{\max} is the maximum shear stress at a dimensionless distance $\varphi_{\max} = y_{\max}/\delta$ from the wall. Since for a developing flow at constant pressure

$$I = 0.58 c_f \quad (2.51)$$

is a good approximation of the experimental results, we may write

$$I_{BCD} = 0.58 \frac{2\tau_{\max}}{\rho U_0^2} (1 - \varphi_{\max}) .$$

By similar arguments for AED:

$$I_{AED} = \frac{0.58 \cdot 2}{\rho U_0^2} (\tau_{\max} - \tau_w) \varphi_{\max} ,$$

which finally results in

$$I = \frac{2}{\rho U_0^2} (0.58 \tau_{\max} + 0.42 \varphi_{\max} \tau_w) . \quad (2.52)$$

Equation (2.52) was considered to be a crude representation and was compared with hot-wire anemometer measurements of shear-stress distributions conducted by Schubauer and Klebanoff [56], Newman [54], Klebanoff [50], Mueller and Robertson [81] and Liebmam and Laufer [82]. These experiments showed that, despite the considerable experimental scatter at high values of φ_{\max} , a simple correlation exists between τ_{\max}/τ_w and φ_{\max} , which suggests that approximately

$$I = c_f f(\varphi_{\max}) . \quad (2.53)$$

Hence φ_{\max} may be regarded as a shape parameter for the shear-stress profile, and a fair fit to most of the data is provided by

$$I = c_f (1.75 - 5\varphi_{\max} - 3.44 \varphi_{\max}^2)^{-1} . \quad (2.54)$$

In this way the problem of calculating I has been reduced to the calculation of φ_{\max} .

From comparisons with experiments McDonald and Stoddart proposed the following simple relations:

$$\varphi_{\max} > 0.075 : \frac{d}{dx} \frac{U_{y=y_{\max}}}{U_o} = 0 \quad (2.55)$$

and

$$\varphi_{\max} < 0.075 : \frac{dy_{\max}}{dx} = \frac{P^{2/3}}{107} . \quad (2.56)$$

They used Coles' universal velocity profile through which by means of Eqs. (2.55) and (2.56) φ_{\max} can be expressed in the shape parameters of the velocity profile. The shear stress integral term which appears in Eq. (2.42) may then be evaluated in terms of the shape parameters via Eq. (2.54).

The above-mentioned hypotheses are certainly of a tentative nature and can only be refined if further shear-stress measurements become available. McDonald and Stoddart have compared more than two dozen measured boundary layers, developing under various conditions, with the predictions of their method. The close agreement between predictions and measurements clearly shows that their integral method is admirably suitable for the calculation of the incompressible two-dimensional turbulent boundary layer.

As we concluded our survey of calculation methods, we came across a paper by Kline, Moffatt and Morkovin [83], reporting on the AFOSR-IFP-Stanford conference on the computation of turbulent boundary layers. This conference had as its prime objective a comparison of the many existing calculation methods, particularly in terms of their accuracy, computational speed and adaptability to widely varying conditions. To this end, tabulated data defining 33 standard flows of various types were sent to various authors, who were invited to predict the development of R_2 , H and c_f for the flows, each according to his own method. Twenty-one integral methods and nine differential methods were employed. The predicted results were replotted in a manner that facilitated comparison and studied by a special evaluation committee, leading to the indication of the best dozen of these methods.

B. The Distribution of Mean Quantities in a Turbulent Boundary Layer

In this section we shall concentrate on those quantities of the turbulent boundary layer which are of direct importance for the calculation of turbulent heat transfer. Particular attention will be paid to the distributions of mean velocity and eddy viscosity.

1. The Mean Velocity Profile

As mentioned in Section A.1, the turbulent boundary layer is often divided into an inner and an outer layer, each having its own characteristics. This division has led to a number of proposed velocity profiles which are only valid in either the inner or the outer region. Very few formulae can be found in the literature which give an acceptable description of the entire velocity profile.

In the following we shall only discuss the main characteristics of the mean velocity profile with special reference to the formulae proposed in recent years. For a more comprehensive review of this subject the reader may be referred to the textbooks of Hinze [22] and Rotta [27].

(a) The Inner Region

As mentioned in Section A.1, the inner layer may, with increasing distance from the wall, be divided into a viscous sublayer, a transition region and a fully turbulent region. The first of these is a very thin layer adjacent to the wall in which the Reynolds shear stress can be neglected in comparison with the viscous contribution to the shear stress, so that

$$\tau = \eta \frac{\partial U}{\partial y} \quad (2.57)$$

For a boundary layer with zero pressure gradient and for sufficiently small values of y , the shear stress τ is independent of y and

$$\tau = \tau_w \quad (2.58)$$

Equation (2.58) can easily be derived from an integration of the equation of motion (2.1) in which for small values of y the acceleration term $U \partial U / \partial x + V \partial U / \partial y$ is neglected.

From Eqs. (2.57) and (2.58) the velocity distribution within the viscous sublayer can be expressed as

$$U = \frac{\tau_w}{\eta} y \quad (2.58)$$

or

$$u^+ = y^+ \quad (2.59)$$

For $y^+ \leq 5$ Eq. (2.58) has been experimentally verified by Deissler [84], Laufer [37] and Klebanoff [36] and more recently, with the application of new measuring techniques, by Popovich and Hummel [85], Kline et al. [86], Sherwood et al. [87], Lindgren and Chao [88] and by Clark [89].

In the past it was generally accepted that the viscous sublayer was fully laminar, which implied $\nu_t = \ell = 0$. The experiments of Klebanoff [36] and Laufer [37], however, clearly showed that this assumption was incorrect, because they observed turbulent velocity fluctuations up to the wall. In addition, they found that very close to the wall (at y^+ about 11.5) the production and dissipation of

turbulent kinetic energy show a maximum, while both quantities decrease rapidly with increasing y^+ . Evidently, about half of the turbulent kinetic energy is produced within the wall region, i.e. the region $0 \leq y^+ \leq 30$ which must be interpreted as a combination of the viscous sublayer and the transition region, whereas the outer region of the boundary layer (thickness $\approx 0.8 \delta$) contributes only about 20% of the energy produced.

Since then it was generally recognized that a more complete understanding of the flow characteristics of the wall region is of special importance for a closer insight into the mechanism of a turbulent shear flow. This has led to a number of experimental investigations of the flow behaviour in the wall region, of which we only mention the more recent ones by Nedderman [90], Reiss and Hanratty [91], Mitchell and Hanratty [92], Rundstadler et al. [93], Kline et al. [86], Armistead and Keyes [94] and Corino and Brodkey [95]. According to their experiments the observed flow phenomena change in character with distance from the wall. Within the viscous sublayer, $y^+ \leq 5$, the flow is not laminar but continuously disturbed by small-scale velocity fluctuations and frequently disturbed by fluid elements which penetrate into this layer from positions further removed from the wall. A thin region, $5 \leq y^+ \leq 15$, adjacent to the sublayer forms the origin of fluid elements which are periodically ejected. In the region $7 \leq y^+ \leq 30$ the ejected elements interact with the main flow, thereby creating intense, chaotic velocity fluctuations.

The ejections and the resulting velocity fluctuations are the most important features of the wall region. They are three-dimensional disturbances which occur locally and randomly with respect to time and streamwise position and have a well-defined character which is independent of the mean flow parameters. However, their intensity and frequency of occurrence are a measurable function of these parameters. It is believed that the action of these ejected elements creates turbulence.

In the region beyond $y^+ > 30$ the intensity of the velocity fluctuations gradually decreases and the scale of turbulence gradually increases.

Further details of the flow phenomena close to the wall can be found in the really magnificent flow visualization studies of Kline et al. [86] and of Corino and Brodkey [95]. The observed phenomena have led Danckwerts [96], Einstein and Li [97], Hanratty [98] and Black [99] to the introduction of a flow model for the viscous sublayer, featuring a periodical growth and disintegration of a viscous boundary layer close to the wall. The disintegration was assumed to be caused by the hydrodynamic instability of the growing viscous layer once it had reached a certain critical thickness. Obviously, in view of the observed complex nature of the flow phenomena, such a model cannot be but a simplification of the real flow pattern. However, the resulting velocity profile (Hanratty [98]):

$$u^+ = 13.5 \int_0^1 \operatorname{erf} \left(\frac{y^+ \sqrt{\pi}}{54 \sqrt{\tau}} \right) d\tau \quad (2.60)$$

shows a reasonable agreement with the measured velocity profiles within the wall region. In Eq. (2.60) τ is the fraction of time in which the viscous layer is growing.

Sternberg [100, 101] has suggested a linearized model of the viscous sublayer where the flow fluctuations are controlled by pressure fluctuations imposed from outside. The predictions of his theory seem to be incorrect, since they are at variance with the measurements of Mitchell and Hanratty [92].

From the considerations given above it is obvious that $\nu_t = 0$ is only correct for $y = 0$ and Eq. (2.59) is only valid if $\nu_t \ll \nu$. Hence, instead of Eq. (2.57) we have in the wall region

$$\frac{\tau}{\rho} = (\nu + \nu_t) \frac{\partial U}{\partial y} \quad (2.61)$$

or in dimensionless form, with $\tau = \tau_w$,

$$1 = \left(1 + \frac{\nu_t}{\nu}\right) \frac{\partial u^+}{\partial y^+} \quad (2.62)$$

For the variation of ν_t within the wall region a number of formulae have been proposed, which can all be written in the form:

$$\frac{\nu_t}{\nu} = g(y^+) \quad (2.63)$$

If the function $g(y^+)$ is known, the velocity profile can be obtained by integration of (2.62), which results in

$$u^+ = y^+ - \int_0^{y^+} \frac{g(y')}{1 + g(y')} dy' \quad (2.64)$$

All proposed distributions of ν_t are subject to the requirement that the resulting velocity profile must agree with $u^+ = y^+$ for y^+ approaching zero and with the logarithmic velocity distribution (see further on) for y^+ values within the fully turbulent region. In addition, the resulting velocity profile has to fit the available experimental data at intermediate y^+ values.

Most of the distributions of ν_t proposed earlier are reviewed in detail by Hinze [22], Rotta [27] and Townsend [23]; they will be treated in a subsequent section. Some of the resulting velocity distributions are:

Von Kármán [102]:

$$\begin{aligned} 0 \leq y^+ < 5 & : u^+ = y^+ \\ 5 \leq y^+ < 30 & : u^+ = 5 \ln y^+ - 3.05 \\ y^+ \geq 30 & : u^+ = 2.5 \ln y^+ + 5.5 \end{aligned} \quad (2.65)$$

Reichardt [103]:

$$\begin{aligned} y^+ \geq 0 & : \\ u^+ = 2.5 \ln(1 + 0.4 y^+) + 7.8 & \left\{ 1 - e^{-y^+/11} - \frac{y^+}{11} e^{-0.33 y^+} \right\} \end{aligned} \quad (2.66)$$

Deissler [39]:

$$0 \leq y^+ < 26 :$$

$$u^+ = \int_0^{y^+} \frac{dy^+}{1 + n^2 u^+ y^+ (1 - e^{-n^2 u^+ y^+})} \quad \text{with } n = 0.124 \quad (2.67)$$

$$y^+ \geq 26 : u^+ = 2.78 \ln y^+ + 3.8$$

van Driest [104]:

$$u^+ = \int_0^{y^+} \frac{2 dy^+}{1 + \left\{ 1 + 0.64 (y^+)^2 \left[1 - \exp \left(-\frac{y^+}{26} \right) \right]^2 \right\}^{\frac{1}{2}}} \quad (2.68)$$

and

Rannie [105]:

$$0 \leq y^+ < 27.5 : u^+ = 14.53 \tanh (0.0688 y^+) \quad (2.69)$$

$$y^+ \geq 27.5 : u^+ = 2.5 \ln y^+ + 5.5$$

They are presented in Fig. 2.7 together with some proposed more recently, which were not included in the reviews of Hinze, Rotta and Townsend, viz.:

Spalding [47]:

$$y^+ \geq 0 : u^+ = u^+ + 0.1108 \left\{ e^{0.4 u^+} - 1 - (0.4 u^+) - \frac{(0.4 u^+)^2}{2!} - \frac{(0.4 u^+)^3}{3!} \right\} \quad (2.70)$$

Burton [106]:

$$y^+ \leq 100 : y^+ = u^+ + \left(\frac{u^+}{8.74} \right)^7 \quad (2.71)$$

and

Sherwood et al. [87]:

$$y^+ \geq 0 : y^+ = u^+ + 5.32 \cdot 10^{-2} (u^+)^2 - 7.68 \cdot 10^{-3} (u^+)^3 + 2.19 \cdot 10^{-4} (u^+)^4 + 1.64 \cdot 10^{-4} (u^+)^5 - 2.16 \cdot 10^{-5} (u^+)^6 + 9.12 \cdot 10^{-7} (u^+)^7 \quad (2.72)$$

Also included in Fig. 2.7 are the experimental data from references 36, 37 and 84 - 89.

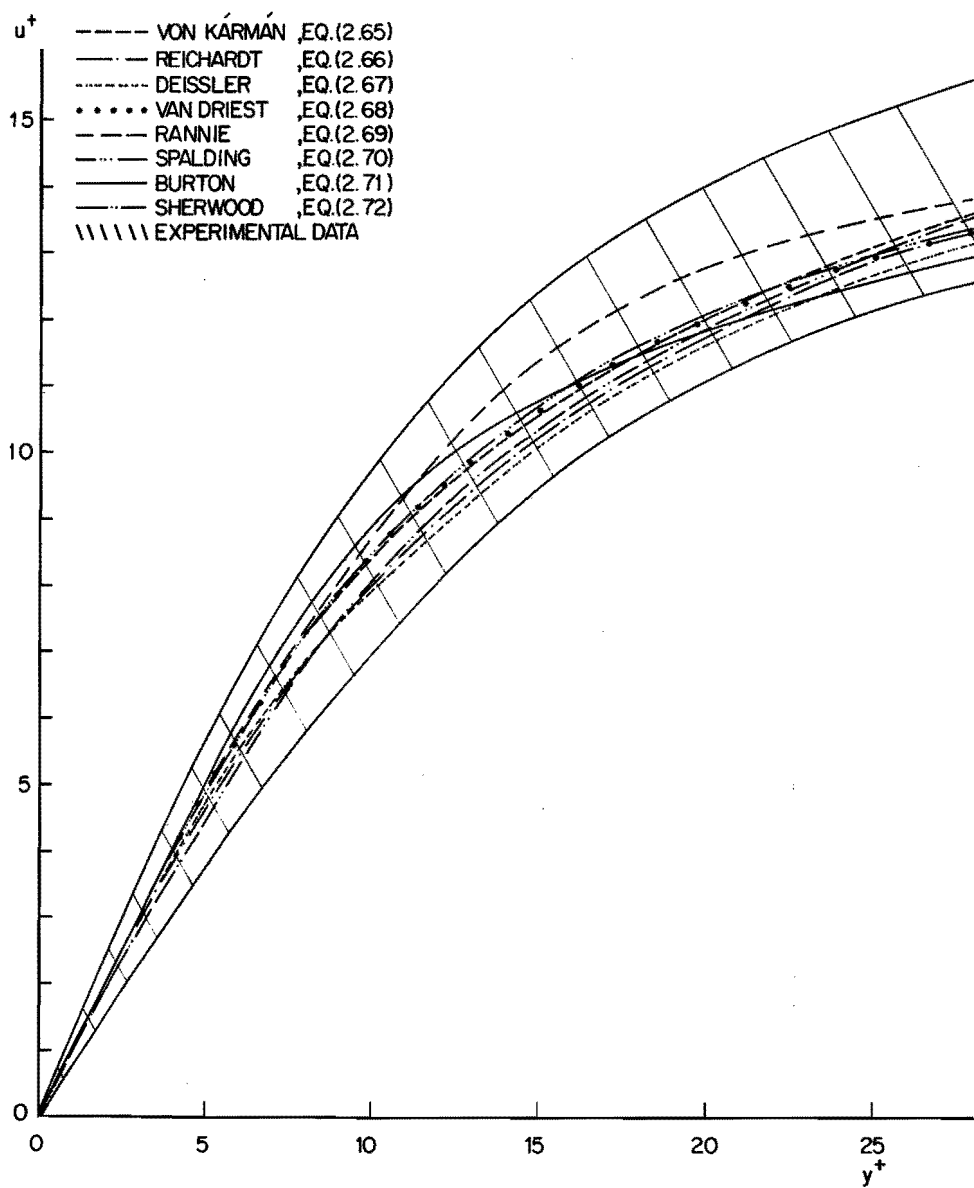


FIGURE 2.7 COMPARISON BETWEEN VARIOUS PROPOSED $u^+(y^+)$ RELATIONS AND EXPERIMENTAL DATA CLOSE TO THE WALL

The discrepancies between the various proposed velocity distributions prove to be even smaller than the scatter in the experimental data, which means that all the formulae afford a good representation of the velocity profile in the wall region. However, by studying the behaviour of the velocity fluctuations in the immediate vicinity of the wall, Townsend [23], Elrod [107] and Rotta [27] have shown that the variation of ν_t with y^+ , when y^+ approaches zero, must be at least cubic. For the velocity profiles this implies

$$y^+ \rightarrow 0 \quad u^+ \rightarrow y^+ + k_1(y^+)^4 + \dots, \quad (2.73)$$

a condition which is only fulfilled by the formulae of Spalding [47] and Burton [106]. Spalding's formulation is undoubtedly to be preferred, also because it presents a single analytically smooth expression for the whole inner region, including the fully turbulent part.

In the fully turbulent region (say, for $y^+ \geq 30$) the laminar contribution to the shear stress may be neglected. Equation (2.61) then reduces to

$$\frac{\tau}{\rho} = \nu_t \frac{\partial U}{\partial y} \quad (2.74)$$

or in dimensionless form, again with the assumption $\tau = \tau_w$,

$$1 = \frac{\nu_t}{\nu} \frac{\partial u^+}{\partial y^+}. \quad (2.75)$$

It is now well established that in the turbulent region the eddy viscosity can be represented by

$$\frac{\nu_t}{\nu} = k^2(y^+)^2 \frac{\partial u^+}{\partial y^+}, \quad (2.76)$$

which can be derived either from the mixing-length hypothesis $l = ky$ or from dimensional arguments. Substitution of Eq. (2.76) into Eq. (2.75) gives upon integration

$$u^+ = k^{-1} \ln y^+ + B, \quad (2.77)$$

in which B is a constant of integration. Equation (2.77) is the well-known logarithmic velocity distribution, which has been verified by a large number of experiments. These experiments have yielded different values for the empirical coefficients k and B, ranging between 0.35 and 0.44 and between 3.8 and 6.0, respectively [33, 37, 47, 56, 62, 84, 88, 102-104, 108-110]. However, $k = 0.40$ and $B = 5.5$ seem to be the most representative values, which have also been found in the present investigation.

In the above analysis we have assumed $\tau = \tau_w$, which is only approximately valid in the inner region of a boundary layer at zero pressure gradient. Within the outer region of such a boundary layer the condition $\tau = \tau_w$ is no longer fulfilled, since τ has to approach zero towards the outer edge of the boundary layer. The velocity distribution in the outer region will be treated in the next section. Here we only remark that in many cases the logarithmic velocity distribution gives a reasonably good approximation of the velocity profile in quite a large part of the outer region as well.

The condition $\tau = \tau_w$ is not fulfilled either in the inner region of a boundary layer with a non-zero pressure gradient in the direction of flow. If we assume the acceleration term in the equation of motion to be negligible within the inner region, we find for this case by integration of Eq. (2.1):

$$\tau = \tau_w + \frac{dp}{dx} y, \quad (2.78)$$

or in dimensionless form:

$$\frac{\tau}{\rho u_\tau^2} = 1 + P_1 y^+, \quad (2.79)$$

with

$$P_1 \equiv \frac{\nu}{\rho} \frac{dp}{dx} \frac{1}{u_\tau^3} \quad (2.80)$$

which is often used as a pressure gradient parameter.

Experiments did show that the neglect of the acceleration term is only justified in the wall region ($y^+ \leq 30$). On the basis of Schubauer and Klebanoff's [56] experiments, however, Townsend [40, 41] has suggested that in the fully turbulent part of the boundary layer the shear stress gradient is indeed constant, but not equal to the streamwise pressure gradient. This suggestion has been supported by the experiments of Newman [54], Sandborn and Slogar [55], Bradshaw [51] and Spangenberg et al. [111]. Hence, for the fully turbulent part of the boundary layer we can write

$$\tau = \tau_w + \alpha y \quad (2.81)$$

or

$$\frac{\tau_w}{\rho u_\tau^2} = 1 + \frac{\nu \alpha}{\rho u_\tau^3} y^+. \quad (2.82)$$

In all papers dealing with the influence of a pressure gradient on the law of the wall, $u^+ = f(y^+)$, it is assumed that the distribution of the eddy viscosity, expressed as a function of a similarity coordinate normal to the wall (for instance y^+) is unaffected by the presence of a pressure gradient. Within the fully turbulent part therefore the relation (2.76) remains valid. Combination of (2.82) with (2.74) and (2.76) yields

$$1 + Zy^+ = k^2 (y^+)^2 \left(\frac{du^+}{dy^+} \right)^2, \quad (2.83)$$

with

$$Z \equiv \frac{\nu \alpha}{\rho u_\tau^3}. \quad (2.84)$$

Integration of Eq. (2.83) leads to

$$u^+ = \frac{1}{k} \left[\ln \left| \frac{\sqrt{1+Zy^+} - 1}{\sqrt{1+Zy^+} + 1} \right| + 2\sqrt{1+Zy^+} \right] + B_1, \quad (2.85)$$

in which the constant of integration B_1 depends upon conditions in the wall region.

Townsend [40] has determined B_1 by assuming the velocity profile in the wall region, $y^+ \leq 30$, to be independent of the pressure gradient. This assumption is only valid when the fractional change of the shear stress across the wall region is small, which is expressed by the condition $Z \ll 1/30$. In that case the velocity distribution given by Eq. (2.85) has to be identical with the logarithmic velocity profile, Eq. (2.77), for small values of Zy^+ . For these values of Zy^+ Eq. (2.85) may be written as

$$u^+ = \frac{1}{k} \left(\ell n \left| \frac{Zy^+}{4} \right| + 2 \right) + B_1 \quad , \quad (2.86)$$

which must be identical with

$$u^+ = \frac{1}{k} \ell n y^+ + B \quad . \quad (2.77)$$

This yields for B_1 :

$$B_1 = B - \frac{1}{k} \left(\ell n \left| \frac{Z}{4} \right| + 2 \right) \quad . \quad (2.87)$$

Substitution of Eq. (2.87) into Eq. (2.85) results in

$$u^+ = \frac{1}{k} \left[\ell n \left| \frac{4}{Z} \frac{\sqrt{1+Zy^+} - 1}{\sqrt{1+Zy^+} + 1} \right| + 2\sqrt{1+Zy^+} - 2 \right] + B \quad . \quad (2.88)$$

For boundary layers in very strong adverse pressure gradients Zy^+ is much larger than 1 and Eq. (2.88) can be approximated by

$$U = \frac{2}{k} \left(\frac{\alpha y}{\rho} \right)^{\frac{1}{2}} + \frac{u_T}{k} \left(\ell n \frac{4}{Z} - 2 + Bk \right) \quad . \quad (2.89)$$

This relation between the velocity and the square root of the distance normal to the wall (the so-called half-power law) has been verified experimentally by Stratford [112] and Perry et al. [44].

Mellor [113] has improved the analysis of Townsend [40] by estimating the effect of a pressure gradient on the velocity distribution within the wall region. Instead of y^+ he suggested using a new similarity coordinate $\zeta \equiv \nu^{-1} k^2 y^2 \left| \partial U / \partial y \right|$. The eddy viscosity distribution across the wall region was subsequently derived from velocity profile measurements in a constant-pressure boundary layer and expressed as a function of ζ . The resulting distribution of eddy viscosity was further assumed to be universally valid. With the help of Eq. (2.79) the velocity distribution within the wall region could then be derived. For the velocity profile within the fully turbulent part, Mellor [113] also arrived at Eq. (2.88), with a constant B that proved to be a function of Z. Unfortunately, Mellor has equated Z to P_1 throughout the entire inner region. Because this is not in general valid within the fully turbulent part, some doubt must be felt about using Mellor's $B(Z)$.

Quite recently, an improved treatment has been applied by McDonald [45] in his detailed analysis of the effect of a pressure gradient on the law of the wall.

(b) The Outer Region

The velocity distribution in the outer region has not received so much attention as that in the inner region and no equally appropriate theories have been developed. This is in part due to the fact that for the description of the transfer of momentum, heat or mass from the wall to the fluid medium the flow phenomena in the inner region play a dominant role. Besides, the inner region is nearly always in some state of equilibrium (see Section A.1), whereas the outer region is greatly influenced by upstream flow conditions. This means that in the outer region velocity profiles of almost arbitrary shape can be obtained by a proper sequential application of positive and negative pressure gradients.

There is, however, experimental evidence that if the boundary layer is not subject to pressure gradients changing rapidly in the direction of flow, the velocity distribution in the outer region also shows some similarity if proper velocity and length scales are chosen. In the following we shall mainly restrict ourselves to boundary layers with zero or moderately small pressure gradients, for which the inner-region velocity profiles can be well represented by the universal law of the wall, $u^+ = f(y^+)$, for instance Eq. (2.70).

The oldest and simplest representation of the velocity profile makes use of the power law:

$$\frac{U}{U_0} = \left(\frac{y}{\delta}\right)^n, \quad 0 \leq y \leq \delta. \quad (2.90)$$

The essential defect of this law is its poor agreement with the actual velocity distribution close to the wall. It was originally assumed that n was a universal constant, being equal to $1/7$, but later experiments indicated that n must be regarded as a parameter with values between $1/10$ and $1/3$, dependent on Re_δ (Clauser [33]). Neglecting the departure of Eq. (2.90) from the velocity distribution close to the wall, we can derive from Eq. (2.90) and the definitions of δ_1 , δ_2 and H :

$$\left. \begin{aligned} \frac{\delta_1}{\delta} &= \frac{n}{n+1} = \frac{H-1}{H+1}, \\ \frac{\delta_2}{\delta} &= \frac{n}{(n+1)(2n+1)} = \frac{H-1}{H(H+1)}, \end{aligned} \right\} (2.91)$$

and

$$H = 2n+1.$$

Introducing H as a shape parameter instead of n and the length scale δ_2 instead of the ill-defined quantity δ , we can derive from Eqs. (2.90) and (2.91):

$$\frac{U}{U_0} = \left[\left(\frac{y}{\delta_2}\right) \frac{H-1}{H(H+1)} \right]^{(H-1)/2}. \quad (2.92)$$

Equation (2.92) is in close agreement with a large number of experimental data (see Clauser [33], von Doenhoff and Tetervin [114], Spence [62] and Rotta [27]).

Nowadays the velocity profile in the outer region is usually expressed in terms of the velocity defect $U_0 - U$. From a dimensional analysis Rotta [27] derived that the velocity in the outer region can be written without loss of generality as

$$\frac{U_0 - U}{u_\tau} = F\left(\frac{y}{\delta}, \frac{u_\tau}{U_0}\right). \quad (2.93)$$

Within the fully turbulent region the velocity distribution of Eq. (2.93) must obey Eq. (2.76), so that upon integration we obtain for $y \leq 0.15 \delta$:

$$\frac{U_0 - U}{u_\tau} = -\frac{1}{k} \ln \frac{y}{\delta} + K, \quad (2.94)$$

where K is a constant of integration, depending on u_τ/U_0 . The fully turbulent region may thus be regarded as the overlap region of the velocity profiles of the inner and the outer region. Within the fully turbulent region one has

$$\frac{U}{u_\tau} = \frac{1}{k} \ln \frac{y u_\tau}{\nu} + B. \quad (2.77)$$

Elimination of U/u_τ from Eqs. (2.94) and (2.77) yields a skin friction law which in fact interconnects the parameters of both regions:

$$\sqrt{\frac{2}{c_f}} = \frac{1}{k} \ln \left(\text{Re}_\delta \sqrt{\frac{c_f}{2}} \right) + B + K. \quad (2.95)$$

Hama [115] has proposed the following empirical formula for the velocity distribution in the region $y \geq 0.15 \delta$:

$$\frac{U_0 - U}{u_\tau} = 9.6 \left(1 - \frac{y}{\delta} \right)^2, \quad (2.96)$$

which agrees satisfactorily with the experimental data collected by Clauser [33]. These data also indicated that the dependence of K on u_τ/U_0 is only a weak one. Hinze even proposed a constant value, viz. $K = 2.5$.

Since δ is an ill-defined quantity, Rotta [27] introduced the dimensionless wall distance $y u_\tau / \delta_1 U_0$ instead of y/δ . From the definition of δ_1 one finds

$$\int_0^\infty \frac{U_0 - U}{u_\tau} d \left(\frac{y u_\tau}{\delta_1 U_0} \right) = 1. \quad (2.97)$$

Equation (2.94) may now be written as

$$\frac{U_0 - U}{u_\tau} = -\frac{1}{k} \ln \left(\frac{y u_\tau}{\delta_1 U_0} \right) + K', \quad (2.94^a)$$

while for the skin friction factor the following relation is obtained:

$$\sqrt{\frac{2}{c_f}} = \frac{1}{k} \ln \frac{U_0 \delta_1}{\nu} + B + K'. \quad (2.98)$$

Here K' is another integration constant depending on u_τ/U_0 .

From comparisons with experiments, Rotta [27] also found that K' is nearly constant, which leads to

$$\sqrt{\frac{2}{c_f}} \equiv \frac{U_0}{u_\tau} = 5.75 \ln \frac{U_0 \delta_1}{\nu} + 3.7. \quad (2.99)$$

This relation agrees within a few percent with the available experimental data.

Quite another approach of the velocity distribution in the outer region was presented by Clauser [33]. He showed that the velocity defect profile can be derived from the equation of motion, Eq. (2.1), with $dp/dx = 0$, if v_t has a constant value, given by

$$v_t = 0.018 U_0 \delta_1 . \quad (2.100)$$

He also found, assuming $v_t = c U_0 \delta_1$, that for an equilibrium boundary layer, characterized by $P = \text{constant}$, the velocity distribution in the outer region can be represented by a universal velocity defect profile, its shape being determined by the pressure gradient parameter P (see also Section A. 2.). Comparison with experiments revealed that Eq. (2.100) remains valid for an equilibrium boundary layer, i. e. $c = 0.018$. Recently, this work has been extended by Mellor and Gibson [42, 113], who calculated a continuous and analytically precise family of defect profiles for the entire range $-0.5 \leq P \leq \infty$.

We conclude this discussion of the velocity distribution in a turbulent boundary layer with a presentation of a few proposed formulae which describe the entire velocity profile, i. e. for $0 \leq y \leq \delta$. After an extensive review of boundary layer data Coles [116] put forward the following velocity profile:

$$u^+ = \frac{1}{k} \ell_n y^+ + B + \frac{\Pi}{k} w(y/\delta) , \quad (2.101)$$

in which he assumed $w(y/\delta)$ to be a universal function for all two-dimensional turbulent boundary layers and Π is a profile parameter. The quantities k and B may be regarded as universal constants. The function $w(y/\delta)$ described the departure of the velocity profile from the universal law of the wall and was called the "law of the wake". The wake function is subject to the following normalizing and boundary conditions:

$$\int_0^1 w \, d(y/\delta) = 1, \quad w(0) = 0, \quad w(1) = 2 . \quad (2.102)$$

Coles expressed his recommendation for $w(y/\delta)$ in tabular form. Hinze [22] showed that the wake function is nearly identical with

$$w(y/\delta) = 1 - \cos(\pi y/\delta) . \quad (2.103)$$

Except for the very thin wall region, Eq. (2.101) gives a representation of the velocity profile for the entire boundary layer. For the zero-pressure-gradient boundary layer, Coles proposed the value $\Pi = 0.55$.

Equation (2.101) may be regarded as a two-parameter velocity profile with parameters $\sqrt{c_f/2}$ and Π . This is clearly demonstrated if we write Eq. (2.101) together with Eq. (2.103) in the form:

$$\frac{U}{U_0} = \sqrt{\frac{c_f}{2}} \frac{1}{k} \left\{ \ell_n \left(\frac{y}{\delta} \text{Re}_\delta \sqrt{\frac{c_f}{2}} \right) + B + \frac{\Pi}{k} \left[1 - \cos \left(\pi \frac{y}{\delta} \right) \right] \right\} , \quad (2.104)$$

which indeed contains only two parameters $\sqrt{c_f/2}$ and Π , since the quantity Re_δ can be expressed in terms of these parameters by means of the skin friction relation:

$$\sqrt{\frac{2}{c_f}} = \frac{1}{k} \ln(\text{Re}_\delta \sqrt{\frac{c_f}{2}}) + B + \frac{2\Pi}{k}, \quad (2.105)$$

by substitution of the boundary condition $U = U_0$ for $y = \delta$. With the use of Eq. (2.104) the quantities δ_1/δ , δ_2/δ and H can be expressed in terms of the velocity profile parameters $\sqrt{c_f/2}$ and Π . These expressions together with Eq. (2.105) result in a skin friction relation of the form $c_f = c_f(\text{Re}_\delta, H)$. The skin friction relations, which are implied by the existence of a two-parameter velocity profile, may be used instead of Eq. (2.19) in the application of an integral method (see also McDonald and Stoddard [80], Thompson [59] and Spalding [78]).

Spalding [78] also proposed a profile holding for $0 \leq y \leq \delta$, resembling Eq. (2.101). Instead of Π Spalding introduced a parameter z_e given by

$$\frac{U_0}{u_\tau}(1 - z_e) = \frac{2\Pi}{k}, \quad (2.106)$$

while he expressed the law of the wall in the form:

$$\frac{1}{k} \ln y^+ + B = \frac{1}{k} \ln E y^+, \quad (2.107)$$

$E = 9.02$ corresponding with $B = 5.5$. Substitution of Eqs. (2.106) and (2.107) into Eq. (2.101) yields:

$$u^+ = \frac{1}{k} \ln(E y^+) + \frac{1-z_e}{2} \left[1 - \cos\left(\pi \frac{y}{\delta}\right) \right] \frac{U_0}{u_\tau}. \quad (2.108)$$

The parameter z_e can be interpreted physically as the ratio of the law-of-the-wall velocity at $y = \delta$ to the main stream velocity. For normal boundary layers $0 < z_e < 1$, while wall-jet velocity profiles can be described by $z_e < 0$. The skin friction law resulting from Eq. (2.108) is:

$$z_e = \sqrt{\frac{c_f}{2}} \frac{1}{k} \ln\left(E \text{Re}_\delta \sqrt{\frac{c_f}{2}}\right). \quad (2.109)$$

By introduction of a parameter ℓ' , defined by

$$\ell' = \ln\left(E \text{Re}_\delta \sqrt{\frac{c_f}{2}}\right), \quad (2.110)$$

Eq. (2.109) can be written as

$$\frac{c_f}{2} = \left(\frac{k z_e}{\ell'}\right)^2. \quad (2.111)$$

Eliminating $\sqrt{\frac{c_f}{2}}$ from Eq. (2.108) by means of Eq. (2.111) finally results in Spalding's profile:

$$\frac{U}{U_0} = z_e \left\{ 1 + \frac{\ln(y/\delta)}{\ell'} \right\} + \frac{(1-z_e)}{2} \left[1 - \cos\left(\pi \frac{y}{\delta}\right) \right]. \quad (2.48)$$

Escudier and Nicoll [70] found Eq. (2.48) to be in good agreement with a large number of measured velocity profiles of boundary layers with positive and negative pressure gradients. The skin friction law, Eq. (2.11), likewise proved to be in close agreement with experimental data.

The velocity profiles of Coles and Spalding have the disadvantage that, at the edge of the boundary layer, $y = \delta$, the velocity profiles have a finite slope which is equal to that obtained when the law of the wall is extended to $y = \delta$. This difficulty is avoided in the velocity profile proposed by Sarnecki [117] and described in detail by Thompson [59] and Head [69]. Instead of a wake function a weighting function γ_s is introduced, given by

$$U = \gamma_s u_\tau \left(\frac{1}{k} \ln y^+ + B \right) + (1 - \gamma_s) U_0 . \quad (2.112)$$

In fact, γ_s determines to what extent the actual velocity at a given point depends upon that given by the law of the wall and upon the free stream velocity. From the analysis of a large number of velocity profiles Sarnecki found that γ_s is a universal function of y/δ , for which he gave an experimental curve. We note that his experimental curve can be very well approximated by the expression

$$\gamma_s = \frac{1}{2} \left[1 + \cos \left(\pi \frac{y}{\delta} \right) \right] . \quad (2.113)$$

From Eq. (2.112), following the same procedure as used for the velocity profiles of Coles and Spalding, one can also derive a skin friction relation. Thompson [59] compared Eq. (2.112) with a large number of measured velocity profiles. He found that the agreement was almost universally satisfactory even for profiles very close to separation. He also constructed three charts giving y/δ_2 , U/U_0 and c_f as functions of H and Re_2 . Using these charts a velocity profile for given values of Re_2 and H can be constructed very rapidly. This is very convenient if one wants to apply integral methods.

2. The Distribution of the Eddy Viscosity

We have seen that a solution of the equation of motion of a turbulent boundary layer is possible only when the distribution of $-\overline{uv}$ is known. Usually this quantity is expressed in terms of the local mean velocity gradient by the introduction of an eddy viscosity, ν_t , or a mixing length ℓ :

$$-\overline{uv} = \nu_t \frac{\partial U}{\partial y} \quad (2.5)$$

or

$$-\overline{uv} = \ell^2 \left| \frac{\partial U}{\partial y} \right| \frac{\partial U}{\partial y} .$$

However, as can easily be seen from Eqs. (2.1) and (2.11), the turbulent shear stress is not only determined by local flow conditions but depends also on the past history of the boundary layer (represented by the appearance of streamwise gradients in these equations). This means that an eddy viscosity or mixing length concept is physically significant only in those regions of the boundary layer where the influence of the upstream flow conditions is negligible. In general this is only the case in the inner region of the turbulent boundary layer: in the wall region because the inertia terms in the equation of motion can be neglected, and in the fully turbulent part because of the local equilibrium of the turbulent kinetic energy (see Townsend [40] and Eq. (2.13)).

In the outer region of the turbulent boundary layer the flow field, and hence ν_t , is greatly influenced by upstream flow conditions. This implies that no universal distribution of ν_t can be expected. In this region the eddy viscosity must simply be regarded as a parameter relating the gradient of the mean velocity to the turbulent shear stress. When the mean velocity distribution $U(x, y)$ is known, the shear stress $\tau(x, y)$ can be obtained by integration of Eq. (2.1). The eddy viscosity can then be calculated by means of Eq. (2.61).

Some authors, for instance Clauser [33] and Mellor and Gibson [42], have introduced the concept of a constant value of the eddy viscosity in the outer region, given by

$$\nu_t = 0.018 U_o \delta_1 \quad (2.8)$$

This relation, however, must be regarded as a rough approximation for equilibrium and zero-pressure-gradient boundary layers. We will in the following concentrate on the distribution of the eddy viscosity within the inner region of the turbulent boundary layer.

It is now generally accepted that in the fully turbulent region the mixing length relation

$$\ell = ky \quad (2.114)$$

is universally valid, irrespective of the value of the pressure gradient. This implies that the eddy viscosity is given by

$$\nu_t = k^2 y^2 \left| \frac{\partial U}{\partial y} \right| \quad (2.115)$$

or, in dimensionless form,

$$\frac{\nu_t}{\nu} = k^2 (y^+)^2 \frac{du^+}{dy^+} \quad (2.76)$$

Substitution of Eq. (2.76) into

$$\frac{\tau}{\rho} = (\nu + \nu_t) \frac{\partial U}{\partial y} \quad (2.61)$$

leads to

$$\left(1 + k^2 y^{+2} \frac{du^+}{dy^+} \right) \frac{du^+}{dy^+} = \frac{\tau}{\tau_w} \quad (2.116)$$

from which du^+/dy^+ can be obtained if τ/τ_w is a known quantity.

For a zero-pressure-gradient boundary layer $\tau \simeq \tau_w$, resulting in

$$\frac{du^+}{dy^+} = (ky^+)^{-1} \sqrt{1 + (2ky^+)^{-2}} - \frac{(ky^+)^{-2}}{2} \quad (2.117)$$

and

$$\frac{\nu_t}{\nu} = ky^+ \sqrt{1 + (2ky^+)^{-2}} - \frac{1}{2} \quad (2.118)$$

Usually it is assumed that within the fully turbulent region $v_t \gg v$, in which case Eq. (2.116) simplifies to

$$\left(ky^+ \frac{du^+}{dy^+} \right)^2 = \frac{\tau}{\tau_w} . \quad (2.119)$$

Instead of Eqs. (2.117) and (2.118) we then obtain

$$\frac{du^+}{dy^+} = \frac{1}{ky^+} \quad (2.120)$$

and

$$\frac{v_t}{v} = ky^+ . \quad (2.121)$$

The results of Eqs. (2.118) and (2.121) agree within one percent for $ky^+ > 50$ or $y^+ > 125$. If the boundary layer is subject to a pressure gradient, we have

$$\frac{\tau}{\tau_w} = 1 + Zy^+ , \quad (2.82)$$

which, substituted into Eq. (2.116), results in

$$\frac{du^+}{dy^+} = (ky^+)^{-1} \left[1 + (Zy^+ + 1) (2ky^+)^{-2} \right]^{\frac{1}{2}} - \frac{(ky^+)^{-2}}{2} \quad (2.122)$$

and

$$\frac{v_t}{v} = ky^+ \left[1 + (Zy^+ + 1) (2ky^+)^{-2} \right]^{\frac{1}{2}} - \frac{1}{2} . \quad (2.123)$$

Again, on the assumption that $v_t \gg v$ the above equations become

$$\frac{du^+}{dy^+} = \frac{\sqrt{1+Zy^+}}{ky^+} \quad (2.124)$$

and

$$\frac{v_t}{v} = ky^+ \sqrt{1+Zy^+} . \quad (2.125)$$

It should be borne in mind that the velocity profiles given in the preceding section, Eqs. (2.77) and (2.85), are derived from Eqs. (2.120) and (2.124), respectively, and therefore are valid only when the condition $v_t \gg v$ is fulfilled.

For the wall region ($y^+ \leq 30$) no universal relation like Eq. (2.76) can be given and various distributions of $v_t(y^+)/v$ have been proposed. Detailed reviews of these proposals are given by Hinze [22], Rotta [27] and Jayatilke [118]. For a zero-pressure-gradient boundary layer $v_t(y^+)/v$ can be calculated from Eq. (2.62):

$$\frac{v_t}{v} = \left(\frac{du^+}{dy^+} \right)^{-1} - 1 \quad (2.62)$$

is du^+/dy^+ is known. The gradient du^+/dy^+ can be obtained either by differentiation of a measured velocity distribution or by employing one of the $u^+(y^+)$ relations given by Eqs. (2.65) to (2.72). For instance, using Spalding's velocity profile, Eq. (2.70), we arrive at

$$\frac{v_t}{\nu} = 0.04432 e^{0.4 u^+} - 1 - 0.4 u^+ - \frac{(0.4 u^+)^2}{2} \quad (2.126)$$

or for $y^+ \rightarrow 0$

$$\frac{v_t}{\nu} = 0.04432 \cdot \frac{(0.4 u^+)^3}{3!} = 4.74 \cdot 10^{-4} (y^+)^3 \quad (2.127)$$

For boundary layers with an arbitrary pressure gradient the eddy viscosity distribution in the wall region can be calculated from the analyses of Mellor [113] and McDonald [45]. Both authors, with the help of dimensional arguments, introduced a new similarity coordinate normal to the wall. The eddy viscosity distribution across the wall region was subsequently derived from velocity profile measurements in a constant pressure flow and expressed as a function of the new similarity coordinate only. In this way Mellor arrived at

$$\frac{v_t}{\nu} = \varphi(\zeta) \quad (2.128)$$

while McDonald gave

$$\frac{v_t}{\nu} = \bar{\varphi}(Y) \quad (2.129)$$

with

$$\zeta = k^2 (y^+)^2 du^+/dy^+ \quad (2.130)$$

and

$$Y = y^+ (du^+/dy^+)^{\frac{1}{2}} \quad (2.131)$$

The functions $\varphi(\zeta)$ and $\bar{\varphi}(Y)$ were presented in graphical form and supposed to be independent of pressure gradients. In this context we remark that the functions $\varphi(\zeta)$ or $\bar{\varphi}(Y)$ can also be derived from Eqs. (2.70) and (2.126).

When the distribution of the shear stress in the wall region is known - often given to a good approximation by Eq. (2.78) - the functions φ and $\bar{\varphi}$ can be used to calculate the velocity profile in the wall region of a boundary layer with an arbitrary pressure gradient.

The distribution of v_t/ν in the viscous sublayer can also be determined from turbulent heat and mass transfer measurements at very high Prandtl and Schmidt numbers, respectively. For very high Prandtl and Schmidt numbers the temperature and concentration boundary layers lie fully within the viscous sublayer. Assuming

$$\frac{v_t}{\nu} = b (y^+)^n \quad (2.132)$$

one can then derive (see [119]) that for fully developed heat transfer

$$Pr \gg 1 : Nu = \frac{n}{\pi} b^{1/n} \left(\sin \frac{\pi}{n} \right) Re \sqrt{\frac{C_f}{2}} \cdot Pr^{1/n} \quad (2.133)$$

and for fully developed mass transfer

$$Sc \gg 1 : Sh = \frac{n}{\pi} b^{1/n} \left(\sin \frac{\pi}{n} \right) Re \sqrt{\frac{C_f}{2}} \cdot Sc^{1/n} . \quad (2.134)$$

From Eq. (2.134) and on the basis of mass transfer data obtained by various investigators with Schmidt numbers ranging from 400 to 2400, Son and Hanratty [119] arrived at

$$\frac{v_t}{\nu} = 0.00032 (y^+)^4 . \quad (2.135)$$

However, recent mass transfer data at much larger values of Sc indicate that the exponent n in (2.132) has the value 3, in accordance with Eq. (2.127). The data of Hamilton and Hamott [120] concerning turbulent mass transfer at Schmidt numbers of 430 to 10^5 correlate with an average deviation of 5.4 percent with

$$Sh = 0.0096 Re^{0.913} Sc^{0.346} . \quad (2.136)$$

From these data for $Sc > 5000$ Hughmark [121] derived

$$\frac{v_t}{\nu} = 0.00096 (y^+)^3 . \quad (2.137)$$

Very recently Gukhman and Kader [122] have presented turbulent mass transfer data for Schmidt numbers up to 10^6 . They actually found $Sh \propto \sqrt{\frac{C_f}{2}}$ and gave as a final result

$$Sh = 0.0188 Re^{0.845} Sc^{0.341} . \quad (2.137)$$

From the data of Dukhman and Kader we derived, using Eq. (2.134),

$$\frac{v_t}{\nu} = 0.00131 (y^+)^3 . \quad (2.138)$$

In this connexion it should be emphasized that owing to the normally observed wide scatter of experimental data, it is difficult to distinguish between $Sc^{1/3}$ and $Sc^{1/4}$ and hence between $n = 3$ and $n = 4$. Besides, Eqs. (2.133) and (2.134) have been derived on the assumption that $Pr_t = 1$ and $Sc_t = 1$. If we assume Pr_t and Sc_t to be functions of y^+ and of Pr and Sc , respectively, which seems to be justified by experiments (see Fig. 1.1), different values of n are obtained from the heat and mass transfer data at high Pr and Sc numbers.

III. TURBULENT HEAT TRANSFER

If we wish to calculate the heat transfer from a flat plate on which a stationary, incompressible, two-dimensional turbulent boundary layer has formed, we must find a solution of the energy equation:

$$U \frac{\partial T}{\partial x} + v \frac{\partial T}{\partial y} = \frac{\partial}{\partial y} \left[\left(a + \frac{v_t}{Pr_t} \right) \frac{\partial T}{\partial y} \right] \quad (1.10)$$

together with appropriate boundary conditions. The distributions of U , v and v_t can be obtained by the application of one of the methods presented in Chapter II. This means that Eq. (1.10) can be solved if we make assumptions concerning the distribution of Pr_t , which in fact forms one of the basic problems of turbulent heat transfer.

However, up to now, the nature of the turbulent transport is not sufficiently understood to permit a theoretical evaluation of Pr_t . Hence, further information on this quantity can only be obtained from direct or indirect measurements of the eddy diffusivities for momentum and heat. Therefore, we shall present a review of the published experimental data of Pr_t . This review will be preceded by a discussion on the calculation of turbulent heat transfer and a presentation of calculated and measured mean temperature profiles within the turbulent temperature boundary layer.

A. The Calculation of Turbulent Heat Transfer

The earliest theories concern the heat transfer from a flat plate of uniform surface temperature. They do not give a solution of Eq. (1.10), but calculate the turbulent heat transfer on the basis of some assumed analogy between heat and momentum transfer, the local heat transfer coefficient being related to the local skin friction coefficient. They start from the definitions of v_t and a_t :

$$\frac{\tau}{\rho} = (v + v_t) \frac{\partial U}{\partial y} \equiv v_e \frac{\partial U}{\partial y} \quad (3.1)$$

and

$$\frac{q}{\rho c_p} = (a + a_t) \frac{\partial T}{\partial y} \equiv a_e \frac{\partial U}{\partial y} \quad (3.2)$$

in which v_e and a_e are the effective viscosity and the effective conductivity, respectively. With the introduction of the friction velocity u_τ and the friction temperature T_τ given by

$$u_\tau = \sqrt{\tau_w / \rho}, \quad T_\tau = q_w / (\rho c_p u_\tau) \quad (3.3)$$

Eqs. (3.1) and (3.2) can be written in dimensionless form:

$$\frac{\tau}{\tau_w} = \frac{v_e}{v} \frac{\partial u^+}{\partial y^+} \quad (3.4)$$

and

$$\frac{q}{q_w} = \frac{a_e}{v} \frac{\partial T^+}{\partial y^+} \equiv \frac{v_e}{v} \frac{1}{Pr_e} \frac{\partial T^+}{\partial y^+} \quad (3.5)$$

in which $T^+ = (T_w - T)/T_\tau$, T_w is the temperature at the wall and $Pr_e = \nu_e/a_e$ is the effective Prandtl number. The quantity ν_e/ν can be eliminated from Eqs. (3.4) and (3.5) to give a relation between T^+ and u^+ :

$$\frac{\partial T^+}{\partial y^+} = \frac{q}{q_w} \frac{\tau_w}{\tau} Pr_e \frac{\partial u^+}{\partial y^+} \quad (3.6)$$

Assuming that there will be a universal relationship between u^+ and y^+ and that $q/q_w = \tau/\tau_w = 1$, we find from Eq. (3.6)

$$T^+ = \int_0^{u^+} Pr_e du^+ \quad (3.7)$$

For Pr_e we can write

$$Pr_e = \frac{1 + (\nu_t/\nu)}{Pr^{-1} + Pr_t^{-1} (\nu_t/\nu)} \quad (3.8)$$

or, assuming $\tau = \tau_w$ and $u^+ = u^+(y^+)$,

$$Pr_e = \frac{dy^+/du^+}{Pr^{-1} + Pr_t^{-1} [(dy^+/du^+) - 1]} \quad (3.9)$$

Hence, in general, Pr_e is a function of Pr , Pr_t and u^+ (or y^+) and for the calculation of $T^+(y^+, Pr, Pr_t)$ assumptions must be made concerning $u^+(y^+)$ and Pr_t .

From the definitions of the Stanton number and c_f we derive from Eq. (3.3)

$$St = \frac{\sqrt{c_f/2}}{T_o^+} \quad (3.10)$$

Hence, to obtain a relation between the local Stanton number and the local skin friction coefficient, we only need to express T_o^+ in terms of c_f . This can be done by integration of Eq. (3.7) across the whole velocity boundary layer:

$$T_o^+ = \int_0^{u_o^+} Pr_e du^+ \quad (3.11)$$

As $Pr_e = Pr_e(u^+, Pr, Pr_t)$ the quantity T_o^+ will be a function of u_o^+ , Pr and Pr_t , or, since $u_o^+ = \sqrt{2/c_f}$, we have $T_o^+ = T_o^+(\sqrt{2/c_f}, Pr, Pr_t)$. This means that

in general St will be a function of $\sqrt{c_f/2}$, Pr and Pr_t . In fact, Eq. (3.11) is only correct, if $\delta_T = \delta$, but it also offers a good approximation for the case where the Prandtl number is not much less than unity.

Equation (3.11) may be rewritten as

$$T_o^+ = \int_0^{u_o^+} Pr_t du^+ + \int_0^{u_o^+} (Pr_e - Pr_t) du^+ ,$$

or, assuming a constant Pr_t ,

$$T_o^+ = Pr_t (u_o^+ + P_s) , \quad (3.12)$$

in which

$$P_s = \int_0^{u_o^+} \left[(Pr_e - Pr_t / Pr_t) \right] du^+ . \quad (3.13)$$

From Eqs. (3.10) and (3.12) we now obtain

$$St = \frac{\sqrt{\frac{c_f}{2}}}{Pr_t \sqrt{\frac{2}{c_f}} + Pr_t \cdot P_s} . \quad (3.14)$$

As in the fully turbulent part of the boundary layer $v_t \gg v$ and $a_t \gg a$, which is equivalent to $Pr_e = Pr_t$, the only contribution to P_s comes from the wall region (say $y^+ \leq 30$). Therefore, considering Eq. (3.14), the term $Pr_t \cdot P_s$ represents the extra resistance to heat transfer offered by the wall region on account of the effective Prandtl number in it being different from that in the fully turbulent region. A further consequence of this fact is that the upper limit of the integral in Eq. (3.13) can be extended to infinity without the value of the integral being affected. By means of Eq. (3.8) we transform Eq. (3.13) into

$$P_s = \left(\frac{Pr}{Pr_t} - 1 \right) \int_0^{\infty} \left(1 + \frac{Pr}{Pr_t} \frac{v_t}{v} \right)^{-1} du^+ , \quad (3.15)$$

which is a convenient expression for the calculation of P_s (Pr , Pr_t), because v_t/v can be found as a function of u^+ when the velocity profile $u^+(y^+)$ is given. Reynolds [123] assumed $Pr_e = Pr_t = 1$ throughout the boundary layer. From Eq. (3.13) this results in $P_s = 0$. Then it follows from Eqs. (3.12) and (3.10) that

$$St = \frac{1}{2} c_f . \quad (3.16)$$

This relation is known as the Reynolds analogy. Prandtl [124] and Taylor [125] have improved the Reynolds analogy by the introduction of a laminar viscous sublayer adjacent to the wall. In this sublayer, $y^+ \leq 11$, it was assumed that $v_t = 0$, which, again with the assumption $Pr_t = 1$, yields for P_s :

$$P_s = 11 (Pr - 1) \quad (3.17)$$

or, substituted into Eq. (3.14)

$$St = \frac{c_f/2}{1 + 11 \sqrt{\frac{c_f}{2}} (Pr - 1)} . \quad (3.18)$$

Experimental evidence did show that Eq. (3.18) holds for relatively small values of Pr only, perhaps up to Pr = 2, while for larger values of Pr there is a discrepancy between Eq. (3.18) and the experimental results, increasing with increasing Pr. It is evident that this is caused by the unrealistic sharp boundary between a turbulent region and a laminar region at $y^+ = 11$. Therefore, Von Kármán [102] improved Eq. (3.18) by introducing a transition region between the viscous sublayer and the fully turbulent region. For $y^+ \leq 5$ the layer was assumed to be fully laminar, while for $5 \leq y^+ \leq 30$ both ν_t and ν were taken into account. For $y^+ \geq 30$ the boundary layer was assumed to be fully turbulent, hence $Pr_t = Pr_e$. For $5 \leq y^+ \leq 30$ the velocity profile $u^+ = 5 \ln y^+ - 3.05$ was proposed. This, together with the additional assumption of $Pr_t = 1$, gives for P_s :

$$P_s = 5(Pr - 1) + \ln\left(\frac{5}{6} Pr + \frac{1}{8}\right) \quad (3.19)$$

or from Eq. (3.14)

$$St = \frac{c_f/2}{1 + 5\sqrt{\frac{c_f}{2}} \left[Pr - 1 + \ln\left(\frac{5}{6} Pr + \frac{1}{8}\right)\right]} \quad (3.20)$$

It is noted that both Eq. (3.18) and (3.20) become identical with (3.16) for Pr = 1, because for $Pr_t = Pr = 1$ also $Pr_e = 1$ throughout the boundary layer, hence $P_s = 0$. As pointed out by Von Kármán the accordance between Eq. (3.20) and the experimental results is very satisfactory for Pr up to 20.

As we know from modern turbulent boundary layer theories, a fundamental objection can be raised against Von Kármán's assumption that ν_t is zero in the viscous sublayer. At high Pr numbers, for which the thermal boundary layer lies fully within the viscous sublayer, it leads to a Nu number independent of Pr (for $Pr_t = 1$ and $Pr \rightarrow \infty$, $T_o^+ \rightarrow Pr$ hence $Nu \rightarrow \frac{1}{2} c_f Re$), which is contradictory to the experimental evidence. Therefore Reichardt [38], Deissler [39] and Rannie [105] assumed a non-zero value of ν_t within the sublayer, for which relations of ν_t/ν as a function of y^+ were presented. These relations led to the improved velocity profiles $u^+(y^+)$, given by Eqs. (2.66), (2.67) and (2.69) and, substituted into Eq. (3.15) with the additional assumption of $Pr_t = 1$, to improved expressions for $P_s(Pr)$. The resulting heat transfer relations, unlike Eq. (3.20), are in good agreement with the experimental results for much higher values of Pr than 20.

Since then many authors, for instance Kutateladze [126], Wasan and Wilke [127] and Kropholler and Carr [128], have presented improvements of the Von Kármán analysis by assuming a particular distribution of $\nu_t(y^+)/\nu$ in the wall region. In fact any of the equations (2.66) to (2.72) can be used for this purpose.

Very recently Jayatilke [118] has given an extensive review of the various proposed distributions of $\nu_t(y^+)/\nu$ and the corresponding expressions for P_s . On the basis of a large number of published heat transfer measurements with Prandtl numbers between 0.6 and 3,000, he recommended

$$P_s = \frac{A_1}{Pr_t} \left[\left(\frac{Pr}{Pr_t} \right)^{3/4} - 1 \right] \left[1 + 0.28 \exp\left(-0.007 \frac{Pr}{Pr_t}\right) \right] \quad (3.21)$$

with $A_1 = 8.32$ for $Pr_t = 0.9$ and $A_1 = 9.00$ for $Pr_t = 1$.

The second factor in square brackets on the right-hand side of Eq. (3.21) is a correction factor introduced to obtain a better fit at moderate Pr than can be obtained with the simpler form

$$P_s = \frac{A_1}{Pr_t} \left[\left(\frac{Pr}{Pr_t} \right)^{3/4} - 1 \right], \quad (3.22)$$

which gives a good fit at high Pr numbers.

For large values of Pr the asymptotic expression for P_s can easily be derived. In this case the eddy viscosity distribution within the thermal boundary layer is given by

$$\nu_t/\nu = b(y^+)^n \approx b(u^+)^n, \quad (2.132)$$

which, substituted into Eq. (3.15), leads to

$$P_s \approx \left(\frac{Pr}{Pr_t} - 1 \right) \int_0^\infty \left[1 + \frac{Pr}{Pr_t} b(u^+)^n \right]^{-1} du^+. \quad (3.23)$$

For $\frac{Pr}{Pr_t} \rightarrow \infty$ this leads to

$$P_s \rightarrow \left(\frac{Pr}{Pr_t} \right)^{\frac{n-1}{n}} \cdot \frac{n}{\pi} (b)^{-1/n} \sin(\pi/n). \quad (3.24)$$

On substitution of Eq. (3.24) into Eq. (3.14) and taking $Pr_t = 1$, Eq. (2.133) is obtained. It should be noted that the form recommended by Jayatilke, Eq. (3.22), implies $n = 4$, which does not agree with mass transfer measurements at high Sc numbers, Eqs. (2.136) and (2.137), which imply $n = 3$.

The formulae given above were derived for the heat transfer from flat plate with a uniform temperature T_w . Various approximate solutions have been given for the problem of heat transfer from a flat plate with a stepwise discontinuity in wall temperature (unheated starting length L). Reynolds et al. [129] reviewed some of these analyses, in particular those of Rubesin [130], Scesa [131] and Klein and Tribus [132], and found that the results can in general be represented by an equation of the form

$$\frac{St}{St_T} = \left[1 - \left(\frac{L}{x} \right)^a \right]^b, \quad (3.25)$$

where St_T is the local Stanton number for the case of a flat plate at uniform temperature and a and b are constants. Assuming velocity and temperature profiles according to power laws with exponent $1/m$, they derived from the energy integral equation for the exponents a and b in Eq. (3.25):

$$a = \frac{4(m+2)}{5(m+1)}, \quad b = -\frac{1}{m+2}. \quad (3.26)$$

Taking $m = 7$, Eqs. (3.25) and (3.26) result in

$$\frac{St}{St_T} = \left[1 - \left(\frac{L}{x} \right)^{9/10} \right]^{-1/9}, \quad (3.27)$$

which was in excellent agreement with their own measurements and was recommended as the best approximate formula. Equation (3.27) is in fair agreement with the empirical relations of Klein and Tribus [132]:

$$\frac{St}{St_T} = \left[1 - \left(\frac{L}{x} \right)^{0.8} \right]^{-0.11} \quad (3.28)$$

and of Jacob and Dow [133]:

$$\frac{St}{St_T} = 0.8 + 0.2 \left(\frac{L}{x} \right) - 0.78 \left(\frac{L}{x} \right)^{2.75} + 1.18 \left(\frac{L}{x} \right)^{3.75} \quad (3.29)$$

More fundamental and preferable to any of the analyses mentioned previously are the methods involving the use of Eq. (1.10) for the solution of turbulent heat transfer. It has the advantage that no assumption concerning the variation of $q(y)$ needs to be made and it permits the solution of transfer problems for various boundary conditions. However, it should be kept in mind that Eq. (1.10) can only be solved by making an assumption concerning the distribution of Pr_t . Up to now solutions of Eq. (1.10) have only been given by making ad hoc assumptions as to the value of Pr_t . Usually it is assumed that $Pr_t = 1$ or Pr_t is a constant (about 0.8). As a consequence, a solution of Eq. (1.10) can only be exact in a mathematical sense, also because assumptions concerning the turbulent boundary layer must be incorporated, which, from a physical point of view, usually have a restricted validity. Mathematically exact solution methods have been initiated by the work of Spalding [1], discussed in detail by Kestin and Richardson [134]. Assuming a universal relationship between u^+ and y^+ and introducing the independent variables u^+ and x^+ , with

$$x^+ = \int_L^x (u \tau / \nu) dx \quad , \quad (3.30)$$

he transformed Eq. (1.10) into a parabolic differential equation:

$$\frac{\partial \Theta}{\partial x^+} = \frac{1}{u^+} \frac{du^+}{dy^+} \frac{\partial}{\partial u^+} \left\{ \frac{1}{Pr_e} \frac{\tau}{\tau_w} \frac{\partial \Theta}{\partial u^+} \right\} \quad (3.31)$$

Here Θ is defined as

$$\Theta = (T - T_o) / (T_w - T_o) \quad (3.32)$$

For the case of a stepwise discontinuity in wall temperature at $x = L$, Eq. (3.31) is subject to the boundary conditions:

$$\left. \begin{array}{l} x^+ = 0, \quad u^+ \geq 0 \\ \text{all } x^+, \quad u^+ \rightarrow \infty \\ x^+ > 0, \quad u^+ = 0 \end{array} \right\} : \Theta = 0 \quad (3.31^a)$$

$$: \Theta = 1$$

Spalding further assumed $\tau = \tau_w$, hence Eq. (3.9) can be used to express Pr_e in u^+ , Pr and Pr_t , writing for short:

$$f(u^+) \equiv u^+ (dy^+/du^+) \text{ and } Pr_e^{-1} \equiv \varphi(u^+, Pr, Pr_t) \quad (3.33)$$

Equation (3.31) takes the form:

$$\frac{\partial \Theta}{\partial x^+} = \frac{1}{f(u^+)} \frac{\partial}{\partial u^+} \left[\varphi(u^+, Pr, Pr_t) \frac{\partial \Theta}{\partial u^+} \right] \quad (3.34)$$

In this equation the functions $f(u^+)$ and $\varphi(u^+, Pr, Pr_t)$ can be calculated from a given law of the wall, $u^+(y^+)$, which, for practical reasons, was inverted by Spalding [47] into

$$y^+ = u^+ + A \left\{ e^{ku^+} - 1 - ku^+ - \frac{(ku^+)^2}{2!} - \frac{(ku^+)^3}{3!} - \frac{(ku^+)^4}{4!} \right\} \quad (3.35)$$

so that

$$\frac{v+v_t}{v} = 1 + kA \left\{ e^{ku^+} - 1 - ku^+ - \frac{(ku^+)^2}{2!} - \frac{(ku^+)^3}{3!} \right\} \quad (3.36)$$

and

$$\frac{a+a_t}{v} = Pr^{-1} + Pr_t^{-1} kA \left\{ e^{ku^+} - 1 - ku^+ - \frac{(ku^+)^2}{2!} - \frac{(ku^+)^3}{3!} \right\} \quad (3.37)$$

In these equations $k = 0.4$ and A is a constant with a proposed value of 0.1108.

Equation (3.34) forms the basis of many heat transfer analyses and its solution can in general be expressed as a function $\Theta(x^+, u^+, Pr, Pr_t)$. For the calculation of the heat transfer coefficient we only need to obtain the so-called Spalding function:

$$Sp(x^+, Pr, Pr_t) = - \left(\frac{\partial \Theta}{\partial u^+} \right)_{u^+=0} \quad (3.38)$$

The Spalding function contains Pr and Pr_t as parameters and is easily shown to be related to the local Stanton number by the equation

$$St = Sp \sqrt{\frac{c_f}{2}} \frac{1}{Pr} \quad (3.39)$$

Comparing this relation with Eq. (3.10), we see that the quantity $Pr Sp^{-1}$ can be interpreted as a resistance to heat transfer. As can be inferred from Chapter II, Spalding's assumptions concerning the velocity boundary layer are only valid for the inner region of a boundary layer with zero or moderately small pressure gradients. Hence the heat transfer analysis, treated above, will only give correct results if the thermal boundary layer is appreciably thinner than the velocity boundary layer. This condition can be expressed as [135]

$$St Pr \gg c_f/2 \quad (3.40)$$

This holds, for example, when the position on the wall from which the thermal boundary layer originates is located far downstream of the point of origin of the velocity boundary layer and for cases of not too small Pr numbers.

For the case of $Pr = 1$ and with the additional assumption $Pr_t = 1$, we have from Eq. (3.9) $Pr_e = 1$, and in this particular case Eq. (3.34) simplifies to

$$\frac{\partial \Theta}{\partial x^+} = \frac{1}{f(u^+)} \frac{\partial^2 \Theta}{\partial u^{+2}} \quad (3.41)$$

Spalding [1] has given an approximate solution for $Sp(x^+, 1, 1)$ by the use of the energy integral equation, while Murali Dharan [136] obtained $Sp(x^+, 1, 1)$ by means of an analog computer. Kestin and Persen [137] presented a numerically exact solution for $Sp(x^+, 1, 1)$, solving Eq. (3.41) by means of a digital computer. To start their calculation from the singular point at $x^+ = 0$, they used an analytical solution for $\Theta(u^+, x^+)$ valid for $x^+ \rightarrow 0$:

$$\Theta(u^+, x^+) = 1 - \frac{\gamma(1/3, \eta_1)}{\Gamma(1/3)} \quad (3.42)$$

where $\gamma(1/3, \eta_1)$ is the incomplete gamma function of order $1/3$ and of the similarity parameter:

$$\eta_1 = (y^+)^3 Pr / 9 x^+ \quad (3.43)$$

in which y^+ can be expressed in terms of u^+ by the use of Eq. (3.35). Equation (3.42) also implies that for very small values of x^+ the Spalding function $Sp(x^+, Pr, 1)$ is given by

$$x^+ \rightarrow 0 \quad Sp(x^+, Pr, 1) = \frac{3^{1/3}}{\Gamma(1/3)} \left(\frac{x^+}{Pr} \right)^{-1/3} = 0.53835 \left(\frac{x^+}{Pr} \right)^{-1/3} \quad (3.44)$$

A detailed derivation of Eq. (3.42) can be found in reference [138] (see also Baker [6]).

Gardner and Kestin [139] extended the calculations of Kestin and Persen [137] to Prandtl numbers different from unity, again with the assumption $Pr_t = 1$. To obtain an equation similar to Eq. (3.41) they introduced the new independent variable

$$\xi = \int_0^{u^+} Pr_e du^+ \quad (3.45)$$

which in the case of a uniform temperature of the flat plate is equivalent to T^+ (see Eq. 3.7). With Eq. (3.9) and the assumption $Pr_t = 1$, Eq. (3.34) now transforms into

$$\frac{\partial \Theta}{\partial x^+} = \frac{1}{u^+ [Pr^{-1} - 1 + dy^+/du^+]} \frac{\partial^2 \Theta}{\partial \xi^2} \quad (3.46)$$

with

$$\xi = \frac{du^+}{(du^+/dy^+)(Pr^{-1} - 1) + 1} \quad (3.47)$$

Equation (3.46) was solved for $Pr = 0.71, 1, 7, 30, 100$ and 1000 and the corresponding Spalding functions were tabulated. The results are presented in Fig. 3.1.

Smith and Shah [2, 140] obtained digital-computer solutions of Eq. (3.34) for another fundamental heat transfer problem, namely for the situation in which $q_w = 0$ upstream of the plane $x^+ = 0$ but has a uniform value downstream of this plane. For this case the corresponding boundary conditions, instead of (3.31^a), are

$$\left. \begin{aligned} x^+ = 0, u^+ \geq 0 \\ \text{all } x^+, u^+ \rightarrow \infty \end{aligned} \right\} : \Theta = 0$$

$$x^+ > 0, u^+ = 0 : \left(\frac{\partial \Theta}{\partial u^+} \right)_{u^+=0} = \text{constant} \quad (3.34^a)$$

Solution of this problem yields $\Theta(x^+, y^+)$ and therefore the wall temperature T_w as a function of x^+ . Smith and Shah also assumed $Pr_t = 1$ and gave solutions for $Pr = 0.7, 1$ and 10 .

In a later publication Spalding [3] showed that certain regularities exist in the solutions published by Gardner and Kestin [139] and Smith and Shah [2], from which he developed some explicit approximate formulae for $Sp(x^+, Pr, 1)$. At low values of x^+ , the Spalding function has the asymptotic form [137]

$$Sp(x^+, Pr, 1) \rightarrow 0.53835 (x^+/Pr)^{-1/3} \quad \text{for } x^+ \rightarrow 0 \quad (3.44)$$

Obviously for large values of x^+ the solution to the problem with a stepwise change of wall temperature will approach that for the case of a uniform surface temperature. Hence for large values of x^+ and Pr we have

$$Sp(x^+, Pr, 1) \rightarrow \frac{\pi}{4} \sin\left(\frac{\pi}{4}\right) \frac{k^{5/4} A^{1/4}}{(4!)^{1/4}} Pr^{1/4} \quad (3.48)$$

This relation can easily be derived from the Eqs. (3.14), (3.24) and (3.38) by taking $Pr_t = 1$ and keeping in mind that for Spalding's velocity profile we have according to Eq. (3.36)

$$u^+ \rightarrow 0 \quad \frac{v_t}{v} \rightarrow \frac{k^5 A}{4!} (u^+)^4 \quad (3.49)$$

With $A = 0.1108$ and $k = 0.4$, Eq. (3.48) becomes

$$Sp(x^+, Pr, 1) \rightarrow 0.0746 Pr^{1/4} \quad (3.48^a)$$

These asymptotic values of $Sp(x^+, Pr, 1)$ are presented in Fig. 3.1 as broken lines.

Spalding also calculated the quantity P_2 :

$$P_2 = \frac{Pr}{Sp(x^+, Pr, 1)} - \frac{1}{Sp(x^+, 1, 1)} \quad (3.50)$$

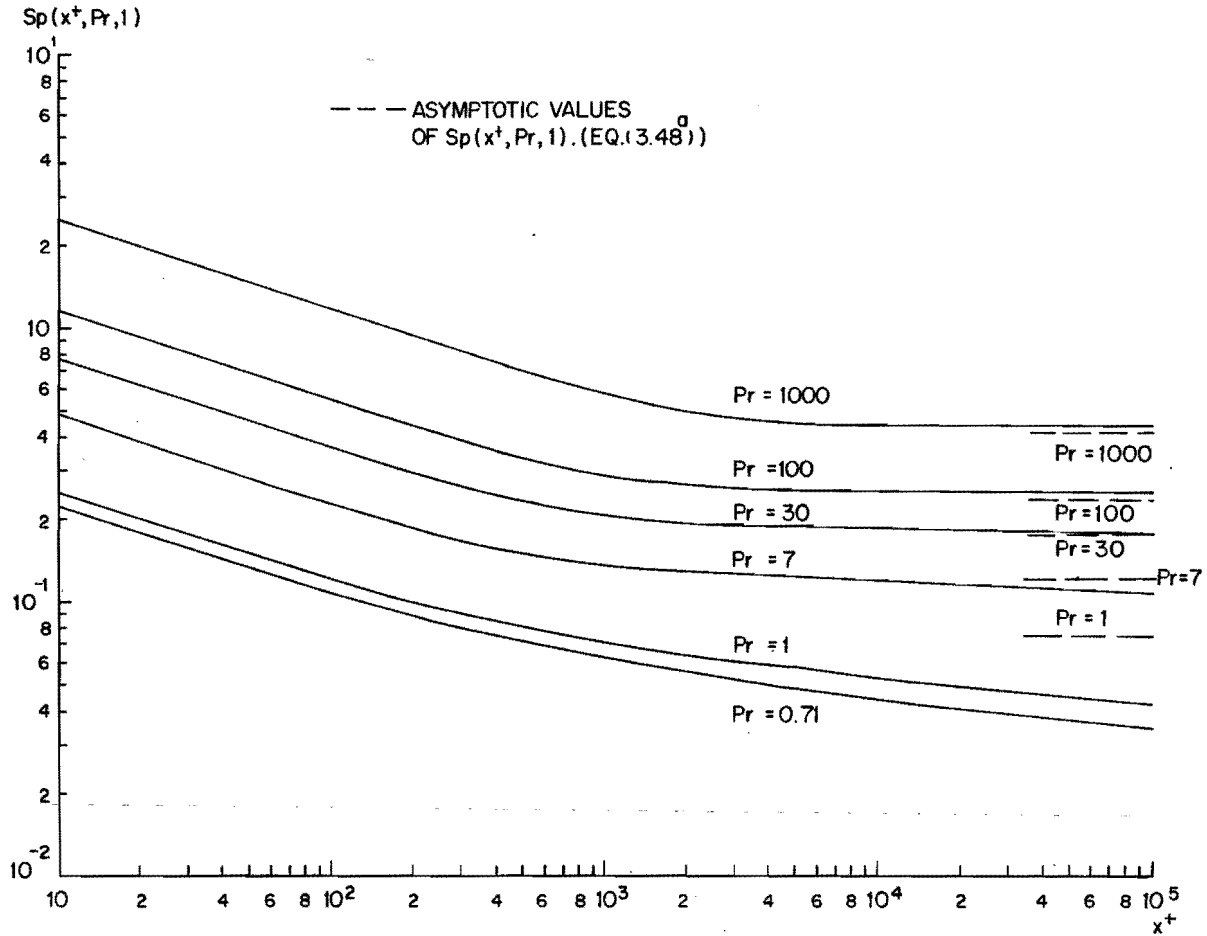


FIGURE 3.1 VALUES OF $Sp(x^+, Pr, 1)$ CALCULATED BY GARDNER AND KESTIN [139]

which for $x^+ \geq 10^4$ proved to be a function of Pr only, for which he recommended

$$P_2 = 13.4 (\text{Pr}^{3/4} - 1) . \quad (3.51)$$

This result, however, is not very surprising, because for these large values of x^+ the solution of the uniform temperature case must be approached and with Eqs. (3.14) and (3.38) it is a simple matter to derive that $P_2 = P_8(\text{Pr}, \text{Pr}_t)$. This also means that with the use of Eq. (3.21) we can give an improved expression for P_2 for the case $\text{Pr}_t = 1$:

$$P_2 = 9 \left[\text{Pr}^{3/4} - 1 \right] \left[1 + 0.28 \exp(-0.007 \text{Pr}) \right] . \quad (3.51^a)$$

With the help of the function P_2 and Eq. (3.50) it is now possible to present an approximate explicit formula for the calculation of $\text{Sp}(x^+, \text{Pr}, 1)$, if such a formula is given for $\text{Sp}(x^+, 1, 1)$. Spalding has given an analytical solution of Eq. (3.34) with the assumption of a power law velocity profile, $a(u^+)^b = y^+$, which results in

$$\text{Sp}(x^+, \text{Pr}, 1) = \frac{[a b / (2+b)^2]^{1/(b+2)} \left(\frac{\text{Pr}}{x^+} \right)^{1/(2+b)}}{\Gamma[(b+3)/(b+2)]} . \quad (3.52)$$

Suitable values are: $a = 2.412 \cdot 10^{-7}$, $b = 7$ ($u^+ = 8.8 (y^+)^{1/7}$). Insertion into Eq. (3.52) yields

$$\text{Sp}(x^+, 1, 1) = 0.1479 (x^+)^{-1/9} . \quad (3.53)$$

Combining Eqs. (3.53) and (3.50) we now find

$$x^+ \geq 10^4: \text{Sp}(x^+, \text{Pr}, 1) = \text{Pr} \left[6.76 (x^+)^{1/9} + P_2 \right]^{-1} . \quad (3.54)$$

For the whole range of x^+ values Spalding proposed a combination of Eqs. (3.54) and (3.44) of the form:

$$\text{Sp}(x^+, \text{Pr}, 1) = \left\{ \left[\frac{\text{Pr}}{6.76 (x^+)^{1/9} + P_2} \right]^4 + \left[0.53835 \left(\frac{x^+}{\text{Pr}} \right)^{-1/3} \right]^4 \right\}^{1/4} . \quad (3.55)$$

With P_2 inserted from Eq. (3.51) this gave a good agreement with the calculations of Gardner and Kestin. Finally, Spalding has generalized the solutions so as to hold for cases in which Pr_t is a constant differing from unity. Using Eq. (3.9) we can write for Eq. (3.34):

$$\frac{\partial \Theta}{\partial x^+} = \frac{1}{f(u^+)} \frac{\partial}{\partial u^+} \left[\frac{\text{Pr}^{-1} + \text{Pr}_t^{-1} (dy^+/du^+ - 1)}{dy^+/du^+} \frac{\partial \Theta}{\partial u^+} \right] . \quad (3.34^a)$$

With $\text{Pr}_t = \text{constant}$ this equation can be rearranged as follows:

$$\frac{\partial \Theta}{\partial (x^+/\text{Pr}_t)} = \frac{1}{f(u^+)} \frac{\partial}{\partial u^+} \left[\frac{(\text{Pr}/\text{Pr}_t)^{-1} + (dy^+/du^+ - 1)}{dy^+/du^+} \frac{\partial \Theta}{\partial u^+} \right] . \quad (3.34^b)$$

Now, Gardner and Kestin [139] solved Eq. (3.34^a) with $Pr_t = 1$:

$$\frac{\partial \theta}{\partial x^+} = \frac{1}{f(u^+)} \frac{\partial}{\partial u^+} \left[\frac{Pr^{-1} + (dy^+/du^+ - 1)}{dy^+/du^+} \frac{\partial \theta}{\partial u^+} \right]. \quad (3.34^c)$$

From Eqs. (3.34^b) and (3.34^c) it follows that the solutions of Gardner and Kestin are still valid when Pr_t is a constant differing from unity, provided that x^+ is replaced by x^+/Pr_t and Pr by Pr/Pr_t . Hence

$$Sp \left(\frac{x^+}{Pr_t}, \frac{Pr}{Pr_t}, Pr_t \right) = Sp(x^+, Pr, 1). \quad (3.56)$$

Because in the literature we could not find any comparison between experiments and the heat transfer analyses given above, which we will call the Spalding Method, we have presented such a comparison in Fig. 3.2. The experimental data of Reynolds et al. [129] were used for this purpose. These investigators measured the heat transfer from a flat plate with a zero pressure gradient and a stepwise discontinuity of the surface temperature, the position of the latter being varied. For this comparison we have taken $Pr_t = 1$ and as can be seen from Fig. 3.2, the agreement between theory and experiment is very satisfactory.

We have already mentioned that the Spalding Method will only give correct heat transfer predictions if the thermal boundary layer lies fully within the region in which the assumptions concerning the velocity field, i.e. $\tau = \tau_w$ and $u^+ = u^+(y^+)$, are valid. This implies, for instance, that the Spalding Method is in general not applicable when considerable pressure gradients are present, as demonstrated by Back and Seban [5]. However, this defect can be removed by solving Eq. (1.10) with the use of more generally valid velocity and shear stress distributions, which can be obtained by the application of one of the more recent turbulent boundary layer theories, presented in Chapter II.

A first improvement has been made by Hatton [4], who extended the Spalding Method to cases where Pr is much smaller than unity. With a boundary layer analysis similar to that given by Brand and Persen [46] (see also Chapter II), he calculated the distribution $\tau(y^+)/\tau_w$ and the corresponding $v_t(y^+)/v$ profiles. These results were substituted into Eq. (3.31) which was solved numerically for the boundary conditions given by Eq. (3.31^a) for Prandtl numbers of 0.01, 0.1, 0.7, 1.0 and 10, with the additional assumption that $Pr_t = 1$. For Prandtl numbers larger than 0.7 his results were in close agreement with those of Gardner and Kestin [139]. Slightly different curves were obtained, particularly at the lower Prandtl numbers, for different unheated starting lengths, due to the fact that the distributions of $\tau(y^+)$ and $v_t(y^+)$ at the origin of the thermal boundary layer are different for different unheated starting lengths. Similar analyses, based on the assumption of other velocity profiles than $u^+(y^+)$, are given by Strunk and Tao [141] and Haberstroh and Baldwin [10], again for $Pr_t = 1$.

Dvorak and Head [9] have presented a heat transfer analysis based on an integral method for the calculation of the turbulent boundary layer. They used the following procedure: the development of the turbulent boundary layer was calculated by means of the entrainment method [69] (see Chapter II), resulting in known distributions of $\delta_2(x)$ and $H(x)$, from which the velocity profiles $U(x, y)$ were computed by the use of Thompson's two-parameter family (Eq. (2.112)). With the velocity distribution in the boundary layer completely determined, they obtained shear stress profiles by applying the equation of motion, and from the profiles of shear stress and mean velocity calculated corresponding profiles of eddy viscosity. In this way, together with an assumption for Pr_t , Eq. (1.10) was solved directly by a digital computer. Solutions were presented for the case with a step in the wall temperature, for boundary layers in zero and adverse pressure gradients. At a zero pressure gradient the calculated heat transfer for $Pr_t = 1$

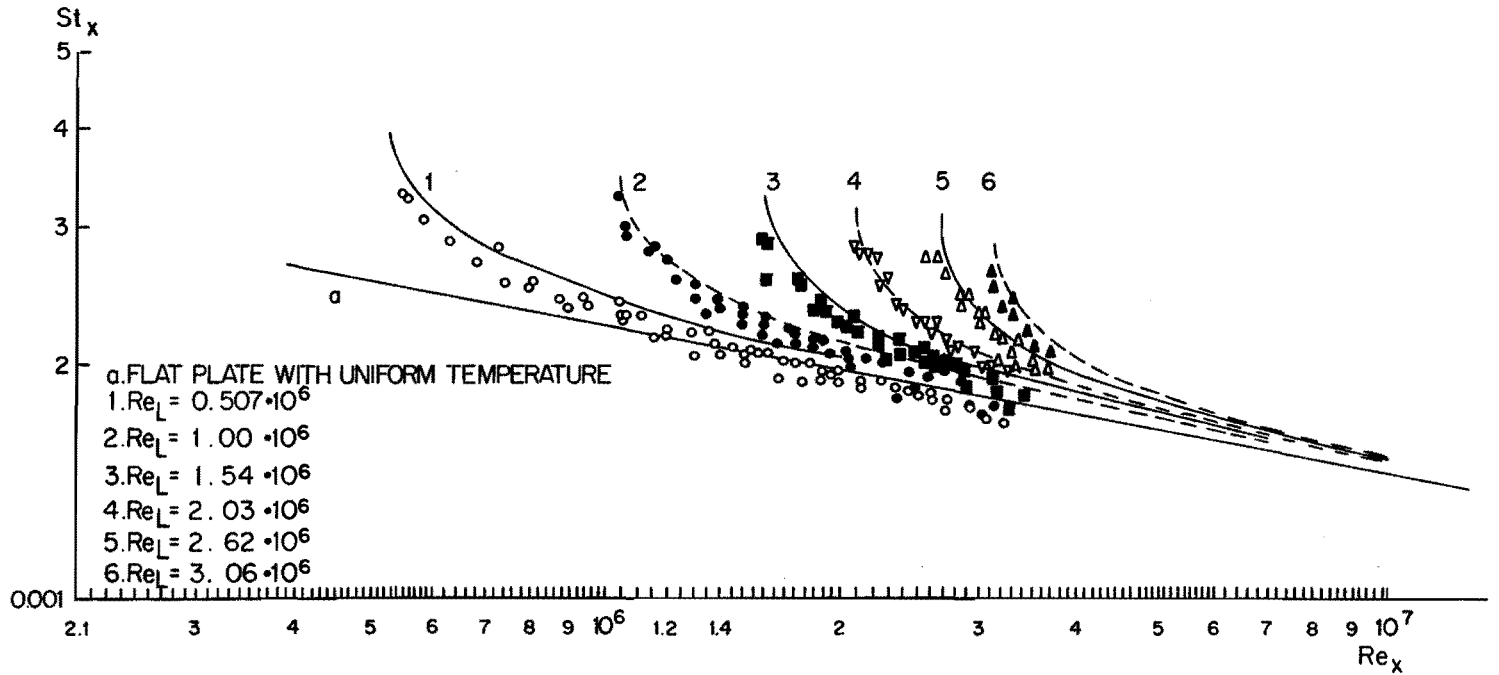


FIGURE 3.2 COMPARISON OF THE SPALDING METHOD WITH EXPERIMENTS OF REYNOLDS ET AL. [129]

and $Pr = 0.7$ was in good agreement with the results of Hatton [4]. They were in disagreement for the case of an adverse pressure gradient. However, Hatton's results are almost certainly in error, since his assumption of a universal velocity profile $u^+(y^+)$ but poorly represents the velocity profiles encountered in adverse-pressure-gradient boundary layers (see also Chapter II). Following the same procedure as applied by Dvorak and Head any of the integral methods presented in Chapter II can be used as a basis for a heat transfer analysis.

Essentially different from the heat transfer analysis treated above are those of Persen [142] and Bradshaw [52]. These authors also try to solve the energy equation, Eq. (1.10), but instead of making an assumption concerning the value of Pr_t , they postulate some independent hypothesis for the characteristics of the thermal boundary layer. Persen [143] has solved the energy equation by assuming not only a universal velocity profile $u^+(y^+)$, but also a universal temperature profile. He assumed that the non-dimensional temperature Θ was a universal function of the non-dimensional distance to the wall

$$\eta^+ = \frac{q_w}{\lambda(T_w - T_o)} y .$$

The function $\Theta(\eta^+)$ was chosen so as to make the development of the thermal boundary layer at its origin conform with the solution

$$\Theta = \Theta(\eta_1^+) = 1 - \frac{\gamma(1/3, \eta_1^+)}{\Gamma(1/3)} , \quad (3.42)$$

which is known to be valid for x^+ approaching zero. Equation (3.42) gives

$$q_w = \frac{3^{1/3}}{\Gamma(1/3)} \frac{u_\tau \lambda(T_w - T_o) Pr^{1/3}}{v (x^+)^{1/3}} \quad (3.57)$$

and this reveals that η_1^+ may be expressed as

$$\eta_1^+ = \left[\frac{1}{3} \Gamma(1/3) \right]^3 (\eta^+)^3 . \quad (3.58)$$

This led Persen to postulate the following universal temperature profile:

$$\Theta(\eta^+) = 1 - \frac{\gamma\left(\frac{1}{3}, \left[\frac{1}{3} \Gamma\left(\frac{1}{3}\right) \eta^+\right]^3\right)}{\Gamma(1/3)} . \quad (3.59)$$

Using the velocity profile $\Theta(\eta^+)$ Persen numerically solved the energy equation by means of a digital computer. He has calculated the local Stanton number as a function of the local Reynolds number for different positions of the discontinuity in wall temperature and for Prandtl numbers of 0.1, 0.5, 1, 2 and 10. To his knowledge there were no experimental results available which allowed a direct comparison with the results of his theory.

Bradshaw [52] has proposed a heat transfer theory analogous to his turbulent boundary layer theory, treated in Chapter II. He started from the following equation, which is similar to the turbulent kinetic energy equation:

$$U \frac{\partial(\frac{1}{2} \overline{\theta^2})}{\partial x} + V \frac{\partial(\frac{1}{2} \overline{\theta^2})}{\partial y} = - \overline{\theta v} \frac{\partial T}{\partial y} - \frac{\partial}{\partial y} \left(\frac{1}{2} \overline{\theta^2 v} \right) - a \left[\frac{\partial^2(\frac{1}{2} \overline{\theta^2})}{\partial y^2} - \overline{\left(\frac{\partial \theta}{\partial x}\right)^2} - \overline{\left(\frac{\partial \theta}{\partial y}\right)^2} \right] \quad (3.60)$$

In this equation the terms on the left represent the rate of change of $\overline{\theta^2}$ along a streamline of the mean flow. On the right, the first term represents the production of turbulent thermal energy from the mean temperature field; the second term represents the diffusion of turbulent energy and the last term represents the effects of molecular transport, analogous to the dissipation term in Eq. (2.9). Therefore this last term is sometimes called the thermal dissipation and denoted by ϵ_θ . By introducing, in the same way as in Eq. (2.10), the quantities

$$L_\theta = \frac{\overline{(\theta v)^2}}{\epsilon_\theta \tau^{\frac{1}{2}}}, \quad (3.61^a)$$

$$G_{1,\theta} = \frac{\frac{1}{2} \overline{\theta^2 v}}{\overline{\theta^2} \tau^{\frac{1}{2}}_{\max}} \quad (3.61^b)$$

and

$$a_{1,\theta} = \frac{\overline{\theta v}}{(\overline{\theta^2} \cdot \tau)^{\frac{1}{2}}}, \quad (3.61^c)$$

Bradshaw converted Eq. (3.60) into an equation for the rate of change of $\overline{\theta v}$ along a mean streamline, which for the calculation of heat transfer must be solved together with the boundary layer equations, Eqs. (2.11), (2.1) and (2.2). However, Bradshaw did not present any heat transfer calculations since there are, up to now, no experimental data available which allow the determination of the functions L_θ , $G_{1,\theta}$ and $a_{1,\theta}$. This would be an interesting object for future experimental research.

In concluding this discussion on heat transfer theories we wish to mention the calculation methods proposed quite recently by Patankar [8] and Patankar and Spalding [7]. Both methods use two integral forms of the energy equation, which can be obtained by integration of Eq. (1.10) across the thermal boundary layer, after multiplication by unity and T , respectively, as weighting functions. With the assumption of a two-parameter temperature profile, these integral equations can be transformed into two ordinary differential equations for the two temperature profile parameters. If the velocity distribution is known and an assumption is made concerning Pr_t , these ordinary differential equations can be solved numerically. Patankar [8] used the Spalding velocity profile, Eq. (3.35), and thus calculated the Spalding functions $Sp(x^+, Pr, 1)$ for Pr numbers of 0.71, 1.0, 7, 30, 100 and 1000. His calculations are in good agreement (within 2 per cent) with those of Gardner and Kestin [140]. Patankar and Spalding [7] used an integral method to calculate the velocity distribution prior to the solution of the two integral energy equations (see also reference [78]). Comparison of their calculations with measurements of heat transfer through turbulent boundary layers in positive and negative pressure gradients [5, 143, 144, 145, 146, 147] showed a reasonable agreement.

B. The Mean Temperature Profile

In the discussion of mean temperature profiles we must distinguish between the profiles in a fully developed thermal boundary layer and those in a thermal entrance region. For the former we may, following Reichardt [38] and Deissler [39], assume that to a good approximation $(q\tau_w)/q_w T$ equals unity, so we have from section A:

$$T^+ = \int_0^{u^+} \text{Pr}_e \, du^+ , \quad (3.7)$$

with

$$\text{Pr}_e = \frac{1 + (\nu_t/\nu)}{\text{Pr}^{-1} + \text{Pr}_t^{-1}(\nu_t/\nu)} . \quad (3.8)$$

For a boundary layer at a zero or moderately small pressure gradient within the inner region $\tau \simeq \tau_w$ and $u^+ = u^+(y^+)$, which results in

$$\text{Pr}_e = \frac{dy^+/du^+}{\text{Pr}^{-1} + \text{Pr}_t^{-1}(dy^+/du^+ - 1)} . \quad (3.9)$$

Hence, with any of the $u^+(y^+)$ relations given in Chapter II, the function $\text{Pr}_e(\text{Pr}, \text{Pr}_t, u^+)$ can be calculated, which, substituted into Eq. (3.7), results in a temperature profile $T^+ = T^+(y^+, \text{Pr}, \text{Pr}_t)$. For the calculation of the temperature profile in the wall region ($y^+ \leq 30$) one of the Eqs. (2.65) to (2.72) can be used. With the simplest possible assumption, viz. that of a constant turbulent Prandtl number, the temperature profile in the wall region corresponding with the von Kármán velocity profile, Eq. (2.65), becomes

$$\begin{aligned} 0 \leq y^+ \leq 5 & : T^+ = \text{Pr} y^+ \\ 5 \leq y^+ \leq 30 & : T^+ = 5 \text{Pr}_t \ln \left[1 + \frac{\text{Pr}}{\text{Pr}_t} \left(\frac{y^+}{5} - 1 \right) \right] + 5 \text{Pr} . \end{aligned} \quad (3.62)$$

For the temperature profiles corresponding with the velocity profiles of Eqs. (2.66) to (2.72) no analytical expressions can be given, since for these velocity profiles Eq. (3.7) can only be solved numerically.

In the fully turbulent region ($y^+ > 30$) the molecular contributions to the heat and momentum transport may be neglected in comparison with the turbulent ones; hence $\text{Pr}_e = \text{Pr}_t$ and assuming a constant turbulent Prandtl number we can derive from Eqs. (3.7) and (3.12):

$$T^+ = \text{Pr}_t(u^+ + P_s) , \quad (3.63)$$

in which P_s is defined by Eq. (3.13) or (3.15). As in the fully turbulent region the logarithmic law of the wall holds:

$$u^+ = 2.5 \ln y^+ + 5.5 , \quad (2.77)$$

the temperature distribution can be expressed as

$$T^+ = \text{Pr}_t(2.5 \ln y^+ + 5.5 + P_s) . \quad (3.64)$$

It must be emphasized that the logarithmic temperature distribution of Eq. (3.64) does not hold for either very small or very large Prandtl numbers. This is caused by the fact that for very large Pr the thermal boundary layer lies fully within the wall region, while for very small Pr the condition $a_t \gg a$ is not fulfilled.

The characteristics of the function $P_S(\text{Pr}, \text{Pr}_t)$ have already been discussed in Section A, in which we recommended the P_S function, Eq. (3.21), very recently put forward by Jayatilke [118]. For the velocity profile given by von Kármán, Eq. (2.65), we find from Eq. (3.15)

$$P_S = 5 \ln \left(1 + 5 \frac{\text{Pr}}{\text{Pr}_t} \right) + 5 \frac{\text{Pr}}{\text{Pr}_t} - 2.5 \ln 30 - 5.5, \quad (3.65)$$

while Spalding's velocity profile, Eq. (2.70), yields

$$P_S = 13.4 \left[\left(\frac{\text{Pr}}{\text{Pr}_t} \right)^{3/4} - 1 \right]. \quad (3.66)$$

For air ($\text{Pr} = 0.71$) and assuming $\text{Pr}_t = 1$, these various proposed P_S functions lead to nearly the same results: Eq. (3.65): $P_S = -2.89$; Eq. (3.66): $P_S = -3.01$ and Eq. (3.21): $P_S = -2.61$. However, irrespective of the precise value of P_S , Eq. (3.64) yields a simple way by which Pr_t within the fully turbulent region can be measured, viz. by the determination of the slope of the curve obtained by plotting T^+ versus $\ln y^+$.

In the outer region of the thermal boundary layer the assumption $q = q_w$ is no longer correct and usually a temperature defect law similar to the velocity defect law is proposed:

$$T_o^+ - T^+ = \frac{T - T_o}{T_\tau} = F_T \left(\frac{y}{\delta_T} \right). \quad (3.67)$$

Equation (3.64) implies that in the overlap region of Eqs. (3.67) and (3.64) the temperature defect law must approach to

$$\frac{T - T_o}{T_\tau} = -2.5 \text{Pr}_t \ln \frac{y}{\delta_T} + C_T, \quad (3.68)$$

in which C_T takes account of the difference between the actual value of T_o/T_τ and the value according to Eq. (3.64). In general C_T will be a function of Pr and Pr_t . For a detailed discussion of the temperature defect profile the reader should refer to a publication by Rotta [148], who has also calculated the influence of various distributions of Pr_t on the temperature profile in the outer region of the thermal boundary layer.

If one wants to make a comparison between the formulae given above and measured temperature profiles, one must bear in mind that only a very limited number of experiments have been published in the literature. Most of these have been carried out on the fully developed temperature profile in a pipe or a square duct with air as the flowing medium, while only a few have been performed for the turbulent heat transfer from a flat plate at uniform temperature. We have collected a number of measured temperature profiles in the fully turbulent region, recently published by Reynolds et al. [129], Johnk and Hanratty [18], Kokorev and Ryapov [149], Beckwith and Fahien [150], Gowen and Smith [151], Taccocci [152], Brundrett [153] and Che Pen Chen [154]. We have represented all these profiles by an equation of the form:

$$T^+ = A_T \ln y^+ + B_T .$$

With the help of Eq. (3.64) we have calculated the values of Pr_t corresponding to the measured values of A_T . With these Pr_t -values and the known values of Pr we have also determined the values of B_T given by Eqs. (3.64) and (3.65), (3.66) and (3.21), respectively. The results are presented in Table 3.1 together with some formulae which represent the measured temperature profiles in the outer region of the thermal boundary layer.

Table 3.1.

Experimental values of A_T and the corresponding Pr_t -values;
measured and predicted values of B_T

Reference No.	Situation studied	Measured			Calculated				Temperature profile in outer region
		Pr	A_T	B_T	Pr_t (3.64)	B_T (3.65)	B_T (3.66)	B_T (3.21)	
129	flat plate	0.71	2.07	3.85	0.83	3.3	3.6	3.7	$1-\theta = (y/\delta_T)^{1/5.6}$
18	pipe	0.705	2.2	3.8	0.88	3.3	3.0	3.2	$T_o^+ - T^+ = -7.2 [(\delta_T - y)/\delta_T]^2$
149	pipe	0.026	2.04	-7.25	0.82	-6.3	-5.7	-4.5	-
150	pipe	6.0	2.55	28.0	1.02	38.4	42.7	38.7	$T_o^+ - T^+ = -2.55 \ln(y/\delta_T) - 0.4$
151	pipe	0.7	2.18	3.0	0.87	3.1	3.0	3.3	$T_o^+ - T^+ = -2.18 \ln(y/\delta_T) - 0.4$
151	pipe	5.7	2.58	34.5	1.03	37.0	41.5	36.9	$T_o^+ - T^+ = -2.58 \ln(y/\delta_T) - 0.4$
151	pipe	14.3	2.52	76.3	1.01	84.7	91.5	79.8	$T_o^+ - T^+ = -2.52 \ln(y/\delta_T) - 0.7$
152	pipe	0.005	2.46	-13.6	0.98	-8.2	-7.5	-6.0	-
153	square duct	0.71	1.96	3.8	0.78	3.6	3.6	3.7	-
154	pipe	7.5	2.11	4.7	0.84	46.3	51.5	45.5	-

In considering the results of Table 3.1, one must bear in mind that experimental uncertainties as high as 10 per cent in the measured values of A_T and B_T are quite normal. From this table we see that for air ($Pr = 0.7$) the turbulent Prandtl number has a mean value of about 0.85, while the higher Pr values lead to a mean Pr_t of about 0.97. The calculated values of Pr_t and B_T for the cases where Pr is much smaller than unity must be regarded as rough approximations, because for these cases Eq. (3.64) is, strictly speaking, no longer valid. A comparison between the measured and calculated B_T values shows that the agreement is quite satisfactory, the best agreement being obtained with the use of Jayatilke's expression for P_g .

For the temperature profiles close to the origin of a thermal boundary developing in an existent and fully developed velocity boundary layer, Eq. (3.7) is no longer valid, because neither is $(q_{Tw})/(q_w \tau)$ equal to unity nor can the terms on the left-hand side of the energy equation (1.3) be neglected. In general no explicit formulae can be given for these temperature profiles. They can be calculated by solving Eq. (3.31) with either Eq. (3.31^a) or Eq. (3.34^a) as boundary conditions. Such solutions have already been dealt with in Section A, and temperature profiles calculated in this way have been published by Gardner and Kestin [139]. An analytical solution of Eq. (3.31) has been published only

for very small x^+ values, for which the thermal boundary layer lies fully within the viscous sublayer, viz. [138]

$$\theta(u^+, x^+) = 1 - \frac{\gamma(1/3, \eta_1)}{\Gamma(1/3)} \quad (3.42)$$

In the literature we have found only three studies where temperature profiles were measured in a developing thermal boundary layer. Johnk and Hanratty [18] have done so for turbulent flow of air in a pipe downstream of the position at which a constant heat flux at the wall was applied. They measured two sets of temperature profiles at Reynolds numbers, $U_m D/\nu$, of 24,900 and 35,000 (U_m = average velocity over pipe cross-section, D = diameter of the pipe). The profiles were determined at 15 distances from the origin of the thermal boundary layer, ranging from 7.5 to 300 cm. Close to the wall there was a region in which the temperature profile coincides with the fully developed one, while the thickness of this region increases with increasing distance downstream of the origin of the thermal boundary layer. At a distance of about $20 D \approx 150$ cm, the temperature profile was fully developed. The resulting distributions of Pr_t will be discussed in Section C.

Reynolds et al. [129] have determined some temperature profiles for the case of the turbulent heat transfer from a flat plate with a stepwise discontinuity in wall temperature at $x = L$. At $U_o = 12.3$ m/s and 27.8 m/s they measured two sets of profiles at three different distances from the discontinuity in wall temperature, $x/L = 1.20, 1.60$ and 1.94 , respectively. The temperature difference $T_w - T_o$ was about 14 °C. By plotting their temperature profiles as T^+ versus $\ln y^+$, we found that there was a close agreement with the fully developed temperature profile given by Eq. (3.64) even for the lowest value of x . However, in interpreting these results one must bear in mind that there is a large discrepancy between their measured q_w value and the one which can be determined from the slope of the temperature profile at the wall.

Johnson [155] has also determined a number of temperature profiles for an experimental situation similar to that studied by Reynolds et al. [129]. At $U_o = 7.5$ m/s he measured nine temperature profiles at distances ranging from 1.3 to 150 cm from the origin of the thermal boundary layer. As these distances increased the profiles showed a gradual adaptation to the fully developed profile, which was completed at a distance of about 50 cm. However, the fully developed temperature and velocity profiles at a distance of 100 cm behind the origin deviate widely from those generally accepted. Johnson found

$$U^+ = 1.98 \ln y^+ + 7.62$$

and

$$T^+ = 1.49 \ln y^+ + 4.96 .$$

In view of the very few experimental data available we have also measured a number of temperature profiles for a developing thermal boundary layer, using an experimental situation similar to those of Reynolds et al. and Johnson. Our experimental results are presented in Chapter V.

C. The Distribution of the Turbulent Prandtl Number

In the preceding sections we have seen that the turbulent Prandtl number is an important parameter for the calculation of turbulent heat transfer and for the prediction of temperature profiles in a thermal boundary layer. Most of the theories presented assume either Pr_t equal to unity or another constant value. However, from the considerations in section A we must expect that in general Pr_t will be a function of y^+ and the molecular Prandtl number. As the turbulent transfer mechanism is still incompletely understood no generally valid theories concerning the distribution of the turbulent Prandtl number exist. Reliable information regarding Pr_t can therefore only be obtained from experiments. We have made a compilation of the Pr_t values published. In addition, we deduced Pr_t values from a number of suitable investigations. Figure 1.1 shows these Pr_t values plotted against the dimensionless coordinate y^+ . Most of them were already presented in a paper by the author and de Vries [156], but Fig. 1.1 incorporates some additional results published recently. In the following we shall give a short description of the way in which the data of Fig. 1.1 have been obtained.

1. Isakoff and Drew [14]

These investigators measured the temperature and velocity profiles in a vertical cylindrical pipe ($D = 38$ mm) with mercury as the fluid ($Pr = 0.024$). The Reynolds number ($U_m D/\nu$) varied from $3.7 \cdot 10^4$ to $3.7 \cdot 10^5$.

The heat flux at the wall, q_w , and the skin friction, τ_w , were deduced from the velocity and temperature profiles close to the wall. The distributions of $\tau(y)$ and $q(y)$ were calculated from

$$\tau(y)/\tau_w = r/R$$

and

$$q(y)/q_w = \frac{2\pi \rho R}{\varphi_m r} \int_0^r U r dr$$

Here R is the radius of the pipe, r the radial distance to its centre $r = 1-y$, and φ_m the fluid mass flowing through the pipe per unit time. Then a_t and v_t can be calculated with the aid of method (a) described in Chapter I, Section B.

2. Corcoran, Page, Schlinger and Sage [11]

These investigators measured temperature and velocity profiles in a duct with a rectangular cross-section (305×175 mm) at an average velocity ranging from 4.5 to 27 m/s. The medium was air. The distribution of $\tau(y)$ was derived from the measured pressure drop, while $q(y)$ was measured at the wall and assumed to be independent of y .

3. Ludwig [16]

Ludwig carried out measurements of air flow in a cylindrical pipe ($D = 30$ mm) with heat-insulated walls at Mach numbers varying from 0.63 to 0.87 and Re between $3.23 \cdot 10^5$ and $3.74 \cdot 10^5$. He showed that Pr_t could be calculated from the distribution of the total temperature. For his calculations of Pr_t Ludwig used the results of Laufer [37] for the distribution of vq^2 .

4. Brown, Amstead and Short [15]

The flow of mercury in a cylindrical pipe ($D = 41$ mm) was studied at Reynolds values between $2.5 \cdot 10^5$ and $8 \cdot 10^5$. The velocity and temperature profiles were measured, together with the pressure gradient in the direction of flow. From these results we have calculated the distribution of Pr_t by means of method (b) mentioned in Chapter I, Section B.

5. Sleicher [12]

Sleicher studied air flow in a cylindrical pipe ($D = 37.5$ mm) with a uniform wall temperature at Re values between $1.1 \cdot 10^4$ and $5 \cdot 10^4$. The flow velocity and temperature profiles were measured, together with q_w .

6. Johnson [17,155]

Johnson studied the flow of air along a horizontal flat plate. This plate had a stepwise discontinuity of surface temperature and measurements were made at a distance of 118 cm from the discontinuity. At this distance the Reynolds number $(U_0 x / \nu)$ was $3.7 \cdot 10^6$. He measured not only $T(y)$ and $U(y)$ but also $\overline{\theta v}$ and uv . Now a_t and v_t can be found using method (a) of Chapter I, Section B.

Johnson observed intermittency in the turbulent temperature fluctuations in a part of the boundary layer where the velocity is still fully turbulent. This is an indication that the turbulent velocity and temperature fields need not be similar, an assumption which is usually introduced to support the postulate $Pr_t = 1$.

7. Venezian and Sage [13]

These authors applied a correction to the results of Corcoran et al. [11] by taking the viscous energy dissipation into account. This implies that $q(y)$ cannot be considered constant in the y -direction.

8. Johnk and Hanratty [18]

These investigators carried out measurements for fully developed turbulent flow of air in a pipe ($D = 7.7$ cm) using small wall-heat fluxes. Measurements were presented of fully developed temperature and velocity profiles at Reynolds numbers between 18,000 and 71,000. The quantities q_w and τ_w were determined from the electrical heat input and from the measured pressure drop, respectively.

We have calculated Pr_t in a way similar to the procedure followed for the measurements of Brown et al. [15]. Eddy diffusivities of heat were also presented for developing temperature profiles, described in Section B. At the lower y^+ values the Pr_t values for fully developed and developing temperature profiles agree reasonably well. For increasing y^+ values, however, those of the developing profiles increase, whereas those of the developed profiles decrease. This is represented by the two separating bands in Fig. 1.1.

9. Sesonski, Schrock and Buyco [19]

Measurements of fully developed temperature profiles were made at Reynolds numbers between 54,000 and 96,000 for mercury flowing in a pipe. Von Kármán's velocity profile, Eq. (2.65), was used to evaluate the velocity distribution, while q_w and τ_w were measured directly.

10. Gowen and Smith [20]

These investigators measured temperature profiles and heat transfer coefficients for the turbulent flow of air and aqueous ethylene glycol ($Pr = 14.3$) in a smooth tube ($D = 5.15$ cm) at Reynolds numbers ranging from 10,000 to 50,000. They also carried out measurements of the velocity profile and τ_w . Of the two curves shown in Fig. 1.1 the upper one is for $Pr = 5.7$ and 14.3 , while the lower one holds for $Pr = 0.7$.

Measurements of the turbulent Prandtl number for liquid metals have also been conducted by Subbotin et al. [157] and Buhr et al. [158]. Their results show distributions of Pr_t similar to those presented in Fig. 1.1 for liquid metals.

In the lower layers of the atmosphere various investigators have measured Pr_t under different stability conditions. These values showed a clear dependence on the Richardson number (see Priestly [159]). They ranged from 0.25 under highly unstable conditions to 1.9 for stable air layers. Near neutrality the average value was about 1.3. The results of a wind-tunnel test simulating a stratified shear flow have recently been presented by Chuang and Renda [160]. They found Pr_t values between 0.7 and 2.7 for thermally stable flows and Pr_t values between 0.2 and 1.2 for thermally unstable flows.

Quarmby and Amand [161,162] and Goldman and Marchello [163] have recently published some experimental results for the turbulent Schmidt number.

Theoretically some attempts have been made to modify the Reynolds analogy to include the influence of the physical properties of the fluid. Jenkins [164] and Azer and Chao [165] have used a modification of Prandtl's mixing length to relate Pr_t to the molecular Prandtl number and the eddy viscosity. Recently, Tyldesley and Silver [166,167] have calculated the distribution of Pr_t on the basis of a new model for turbulent flow. However, the numerical predictions of the various flow models differ greatly and objections can be raised against all of them. It is obvious that a generally valid theory for turbulent transport phenomena is still lacking.

In interpreting the experimental data in Fig. 1.1 one must bear in mind that

- (a) it is very difficult to perform measurements of this kind accurately. Experimental uncertainties in the quantities measured directly as high as 10-20 per cent are quite normal;
- (b) in most cases experimental curves had to be differentiated to arrive at v_t and a_t , leading to much greater relative errors in these quantities;
- (c) in all investigations mentioned, except those of Johnson [155], no direct determinations of $\overline{\theta v}$ and \overline{uv} were made.

From Fig. 1.1 it is clear that there is a need for more accurate determinations of Pr_t , which has been the main aim of the present investigation. Our experimental values of Pr_t are presented in Chapter V.

IV. EXPERIMENTAL EQUIPMENT AND MEASURING TECHNIQUES

A. Experimental Equipment

1. Wind Tunnel

The experiments were carried out in a "low-turbulence" closed-circuit wind tunnel specially constructed for the present investigations. A photograph is shown in Fig. 4.1, while a sketch of the design is given in Fig. 4.2.

The wind tunnel was built up mainly from sheets of plywood, attached to a framework of steel and wooden beams resting on the floor. The section which accommodated the ventilators was made of steel. The rectangular test section had a length of 2.5 m and a constant cross-sectional area of $0.4 \times 0.5 \text{ m}^2$, causing a small negative pressure gradient. The lower side of this test section was made of plywood; the upper side consisted of a number of boards with a width of 5 cm, joined together with a "tooth-groove" connection. By replacing one of these boards by a narrower one (width 4 cm), we obtained a slot right across the test section through which a probe holder could be inserted (see Fig. 4.3.). The back of the test section was formed by an aluminium plate, through which all connections to the heated plate and the static pressure taps were led. The front consisted of a lucite plate mounted on a carriage, which could be removed, allowing an easy access to the test section. This transparent plate permitted observation of the probes during the measurements.

Two rows of corner blades could be cooled by passing water through them. This made it possible to keep the temperature of the air in the wind tunnel constant within $0.2 \text{ }^\circ\text{C}$ during the test runs. In the test section a main stream velocity between 0.5 and 16 m/s could be established with a turbulence level in the order of 0.02 percent. This low turbulence level was achieved by a combination of four fine screens in the setting chamber and a contraction of suitable design.

2. Traversing Mechanism

The traversing mechanism used to insert the measuring probes into the turbulent boundary layer of the test plate is shown in Fig. 4.3. Its design made it possible to traverse the probes in an accurate way in the y-direction at every desired place. It consisted essentially of two carriages and a support to which the probe holder was attached. The larger carriage, spanning the whole width of the test section, could move on a pair of rails mounted on the top of the U-shaped supporting beams at the upper side of the test section. This made a displacement in the x-direction possible. On this carriage another pair of rails was mounted on which a smaller carriage could move in the z-direction. The smaller carriage was provided with a tolerance-free support to which the probe holder was attached. The carriage wheels were fitted with ball bearings and could be blocked by a kind of brake.

The support could be moved in the y-direction by means of a micrometer device having a total range of movement of 5 cm with a positioning accuracy of 0.002 mm. The support was kept pressed against the micrometer shaft by a counterweight, movable on a pulley. The probe holder consisted of an invar tube, locked in a brass bush which could be rotated about its own axis by means of axial ball bearings. The lower end of the invar tube was provided with a brass bush in which the probes could be fixed, the leads of the probes being passed through the tube. Invar was used to minimize the thermal dilatation of the tube, when placed into the thermal boundary layer.

To permit rotation of the probes in the x-y plane, which was necessary to calibrate the hot wires for the velocity fluctuations in the y-direction, small plates of known thickness were placed under the wheels at one side of the larger carriage.

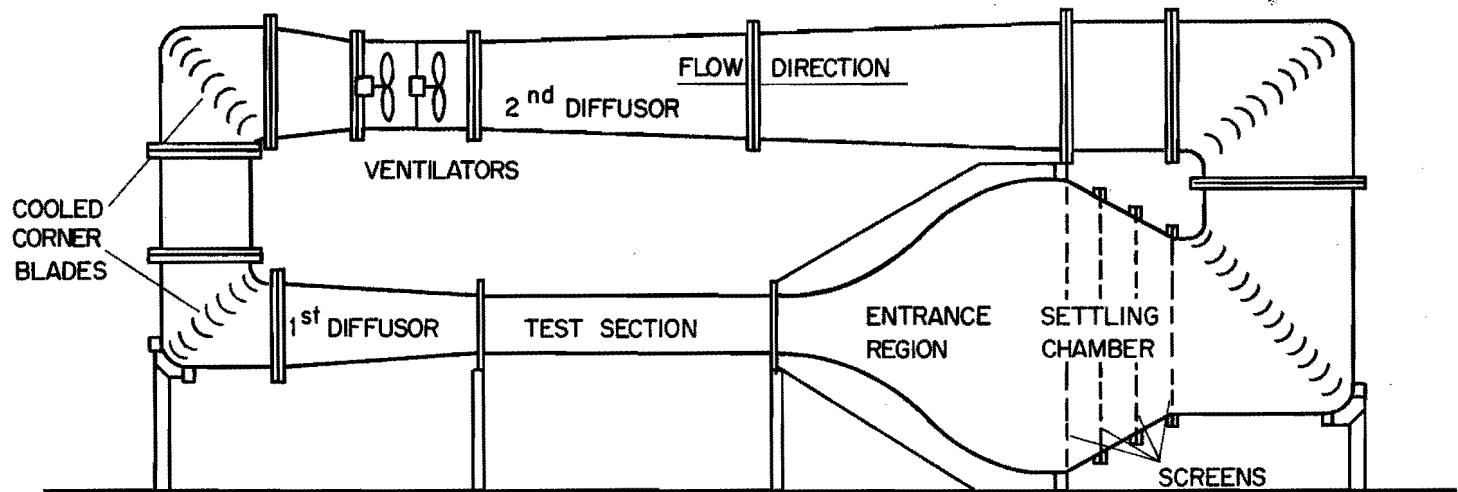


FIGURE 4.2 DIAGRAMMATIC REPRESENTATION OF THE WIND TUNNEL

The zero reading of any traverse, being the position of the upper side of the test plate, was obtained in either of the following ways:

- (a) By measuring the electrical resistance between probe and flat plate. In tests where the heated part of the plate consisted of aluminium a small stainless-steel block with an accurately known thickness was placed between probe and plate.
- (b) By watching the distance between the probe and its reflection in the plate through a telescope and traversing until both images touched each other. The estimated accuracy of this zero reading was 0.002 mm. Zero settings were generally made with the tunnel in operation.

3. Test Plate

(a) Construction

The test plate used was a hydrodynamically smooth, flat plate consisting of three parts: an unheated part with a length of 1 m, a part which could be heated with a length of nearly 80 cm and another unheated part which was 50 cm long. The front end of the plate was an elliptical nose with a length of 5 cm, after which a "trip-cylinder" with a diameter of 3 mm was mounted in order to promote and localize the transition from a laminar boundary layer into a turbulent one. A detailed description of this transition promotion is given by Preston [168].

The width of the plate was 40 cm, hence equal to the width of the test section. The plate was placed parallel to the upper side of the test section with its nose nearly 20 cm away from the entrance. It rested on a number of supporting rods, fitted to the bottom of the test section, by means of which the height could be adjusted. A diagrammatic view is presented in Fig. 4.4.

The unheated parts were made of aluminium with a thickness of 1 cm, with a thin brass covering to allow zero reading of the probes by means of the resistance method. To measure the pressure gradient along the plate, the unheated parts were provided with a number of static pressure holes at several stations along the plate, as indicated in Fig. 4.4. At each station there were two static holes, 5 cm on either side of the centre line of the plate. These holes were made in a set of brass plugs which were mounted flush with the upper surface of the plate. The diameter of the holes was 0.5 mm and they were constructed on similar lines to those used by Ascough [169], who carried out measurements on static pressure corrections due to hole size. In our case these corrections were negligible (at most about 0.01 N/m²).

The static pressures were measured with a Betz micromanometer, manufactured by van Essen N.V., the Netherlands. The accuracy of this micromanometer was about 0.2 N/m².

The heated part of the plate was designed in such a way that it was possible to adjust a uniform temperature at its surface. Because the heat transfer coefficient changes with distance along the plate, the heat supplied must also change with distance to satisfy this demand. Accordingly, the heated plate consisted of 15 individually heated units with a width of 5 cm, which were thermally insulated from each other. Each unit was composed of three, also individually heated elements: a main element, 30 cm long, with on either side a smaller element, 5 cm long, to compensate for the heat loss of the main element to the sides. All elements were made of aluminium, which has the highest thermal conductivity.



Figure 4.1 Photograph of wind tunnel used

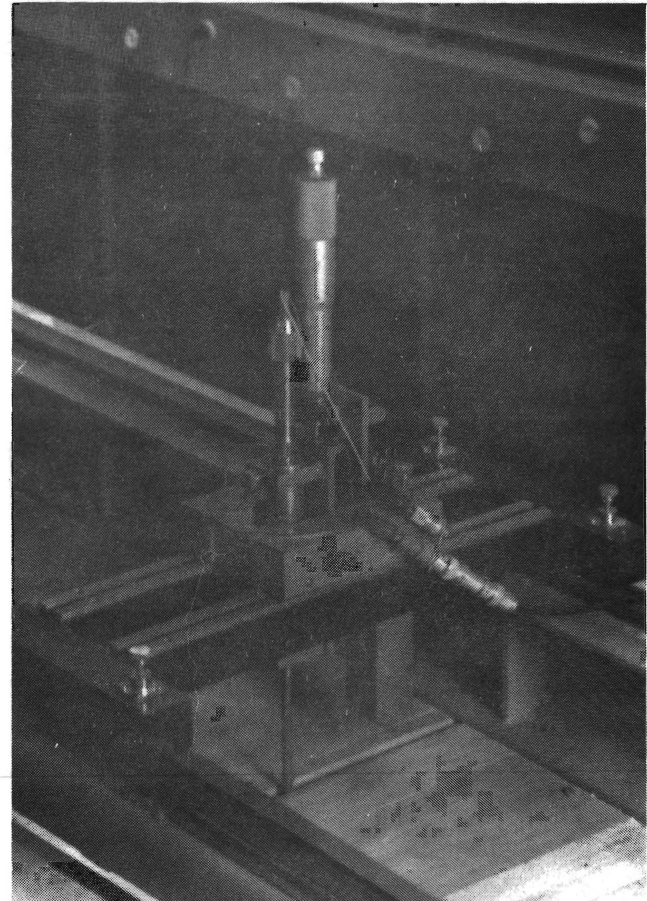


Figure 4.3 The traversing mechanism

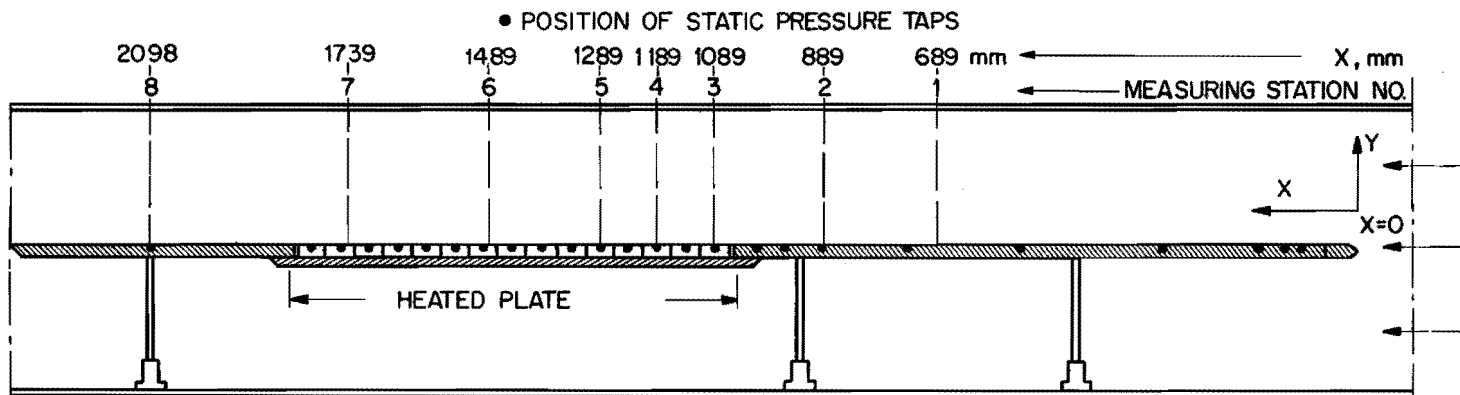


FIGURE 4.4 POSITION OF PLATE AND MEASURING STATIONS IN TEST SECTION

Essentially, each element consisted of a rectangular, flat box in which a heating coil was placed between two sheets of asbestos. The heating coil was made by winding nickel-chromium resistance wire on a mica sheet with grooves at the sides. The box could be closed by screwing a cover against its bottom, giving the element a total thickness of 1.4 cm. The various parts of a heating unit are clearly shown in Fig. 4.5.

Grooves were milled in all inner sides of the elements, in which thermocouples were mounted, while the leads of the heating coils were also passed through them. A number of thermocouples were placed in small holes, drilled into these grooves, to measure the temperature at the inner sides of the elements. Other thermocouples were placed in much deeper holes, situated 0.5 mm under the element surface and extending to the centre line of the main element. These thermocouples were used to measure the surface temperature of the main elements.

To ensure electrical insulation between thermocouples and elements, all elements were anodized before the thermocouples and heating coils were mounted. This treatment provided a strong, thin layer of insulating alumina. The thermocouples were stuck to their places with an Araldite epoxy resin (supplied by Ciba, Basel, Switzerland). The same resin was used to stick the small elements to the main element. The resin layer between the elements was about 2 mm thick. Figure 4.6 gives a photograph of a heating unit before and after assembly.

All thermocouples were made of commercially available insulated copper and constantan wires with a diameter of 0.2 mm. The junctions were formed by melting bare ends together in a hot argon jet. To be sure that the thermocouples had the same sensitivity, they were all made from the same coil of thermocouple wire. To check their sensitivity, five thermocouples with a length of 10 m were made and calibrated in an accurately controlled thermostat. After calibration, one of the long thermocouples was divided into 20 shorter ones which were also calibrated. All calibrations gave the same results within the measuring accuracy, which is sufficient evidence for assuming equal sensitivities for all thermocouples. The sensitivity was found to be $43.1 (\pm 0.4) \mu\text{V}/^\circ\text{C}$.

All heating units were stuck together on a 1-cm-thick Sindanyo plate acting as thermal insulation of the lower side of the heated plate. Again there was a resin layer about 2 mm thick between each two units. To measure the thermal leakage through the lower side, thermocouples were placed in grooves on either side of the Sindanyo plate right below the centre of each heating unit. During the first measurements with the heated plate, it was noticed that this thermal insulation of the lower side was insufficient. It was greatly improved by placing another plate of insulating material under the Sindanyo plate, leaving a 4-mm-thick air gap between both plates.

Figure 4.7 shows the position of all thermocouples in the heated plate. This configuration of thermocouples was chosen after some preliminary tests with a heated plate consisting of three heating units of the construction described above, but each containing a much larger number of thermocouples.

Each heating unit had 12 thermocouples except the two bordering on the unheated parts of the test plate. These two units had 21 thermocouples each, to permit a calculation of the heat loss to the unheated parts. Together with the 30 thermocouples of the Sindanyo plate and the leads of the heating coils, this gave 546 leads leaving the lower side of the heated plate.

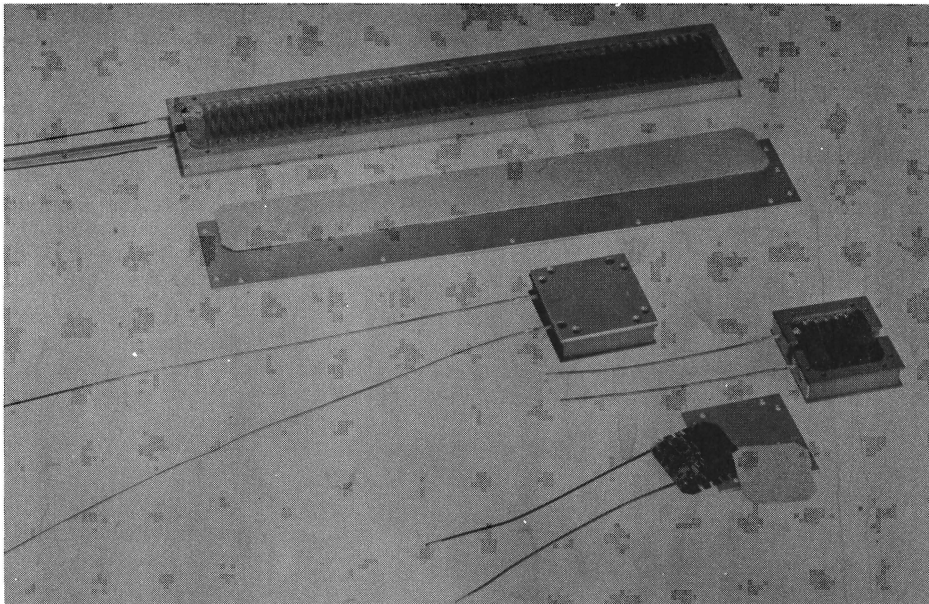


Figure 4.5 The various parts of a heating unit

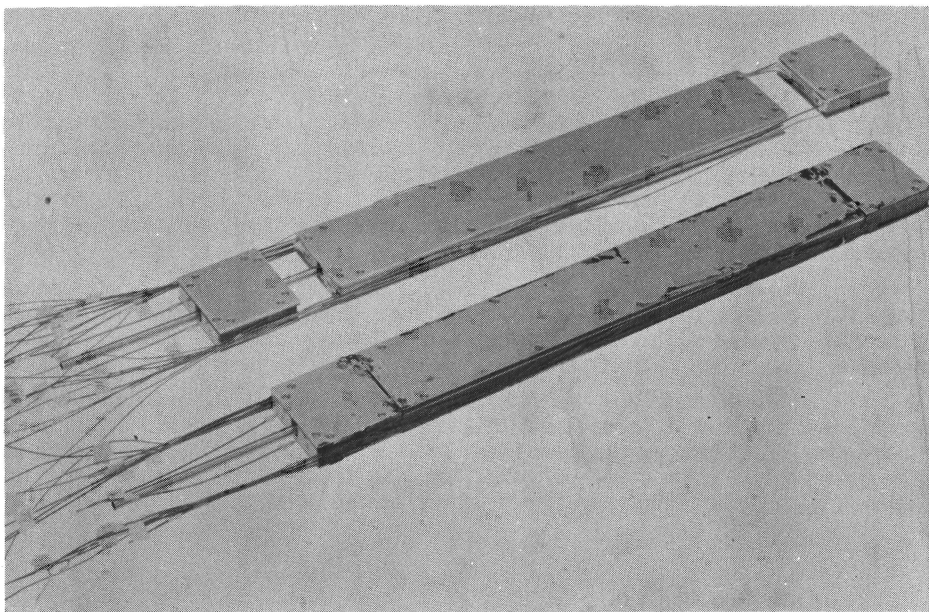


Figure 4.6 Heating unit before and after assembly

- THERMOCOUPLE JUST BELOW THE SURFACE
- THERMOCOUPLE AT THE SIDE OF AN ELEMENT
- X POSITION OF STATIC PRESSURE HOLE

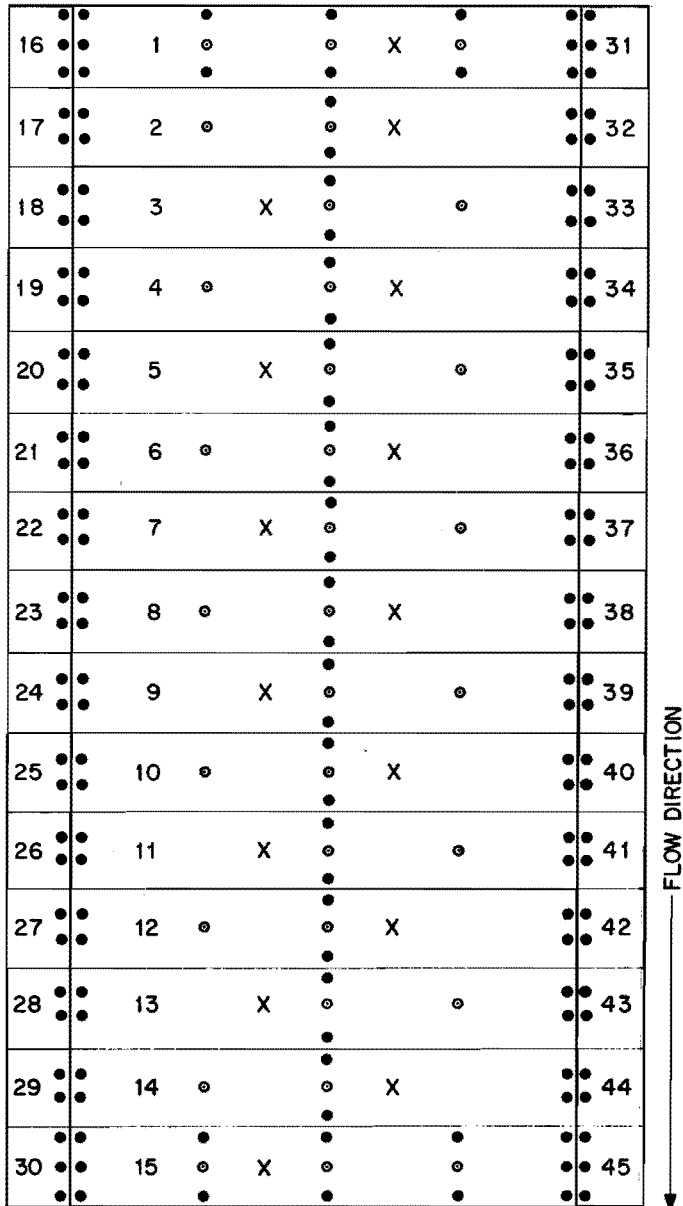


FIGURE 4.7 POSITION OF THERMOCOUPLES IN HEATED PLATE

For convenient handling of this large number of leads, they were all connected to a connector, 90 cm long and 5 cm wide, fastened to the back of the heated plate. This connector was made of insulating material provided with 550 holes with alternately copper and constantan pins pressed into them. The pins extended from both sides of the insulating material. All leads from the heated plate were soft-soldered to the lower ends of these pins. The connector stuck out of the test section through a slot milled into the back.

Every main element of a heating unit also had a static pressure hole with the same dimensions as described earlier. The connecting tubes of these static holes, clearly visible in Fig. 4.6, passed through the connector.

The heated plate was designed to attain temperatures of about 150 °C above gas temperatures. In this investigation only pure forced convection was studied and a temperature difference of about 10 °C adopted. Figure 4.8 shows the heated plate placed into the test section.

(b) Power Supply

The D.C. power input of the heated plate was delivered by seven carefully stabilized Delta power supplies (50 V - 10 A). A diagram of the electrical circuit for the power supply of the main elements 1, 2 and 3 is shown in Fig. 4.9. The power supply to the other main elements followed the same pattern except that these elements were placed parallel to the power supplies in groups of four.

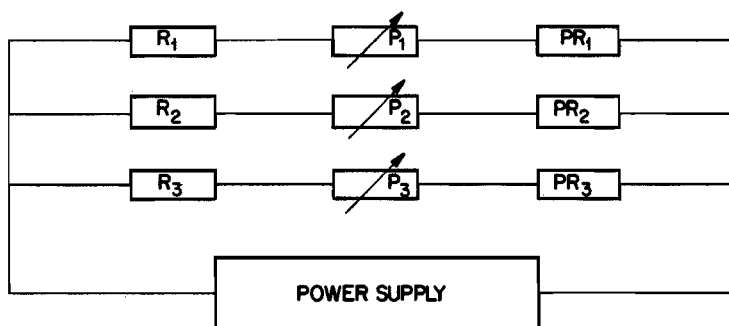


FIG. 4.9 POWER SUPPLY OF THE MAIN ELEMENTS

R_1 , R_2 and R_3 are the resistances of the heating coils of the main elements 1, 2 and 3, respectively. P_1 , P_2 and P_3 are potentiometers controlling the power input of the elements belonging to them. PR_1 , PR_2 and PR_3 are precision resistors.

The power input to each main element was obtained from measurements of the voltage drop across the heating coil and the precision resistor placed in series with it. The voltages were measured with a John Fluke D.C. voltmeter, giving an accuracy of the measured power inputs of 0.1 percent.

An outline of the electrical circuit for the power supply of the smaller elements is given in Fig. 4.10. R_{16} and R_{31} are the resistances of the heating coils of the small elements 16 and 31, respectively. These two small elements belong to the same main element. The position of the potentiometer P_1 now determines in which proportion the power input, adjusted by the potentiometer P_2 , is divided over R_{16} and R_{31} .

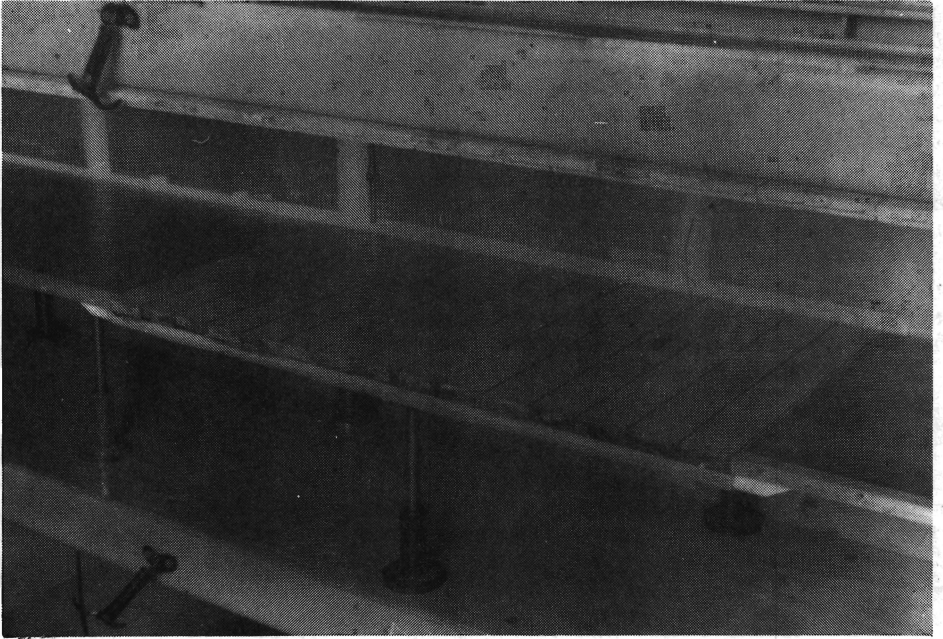


Figure 4.8 Heated plate, placed into test section

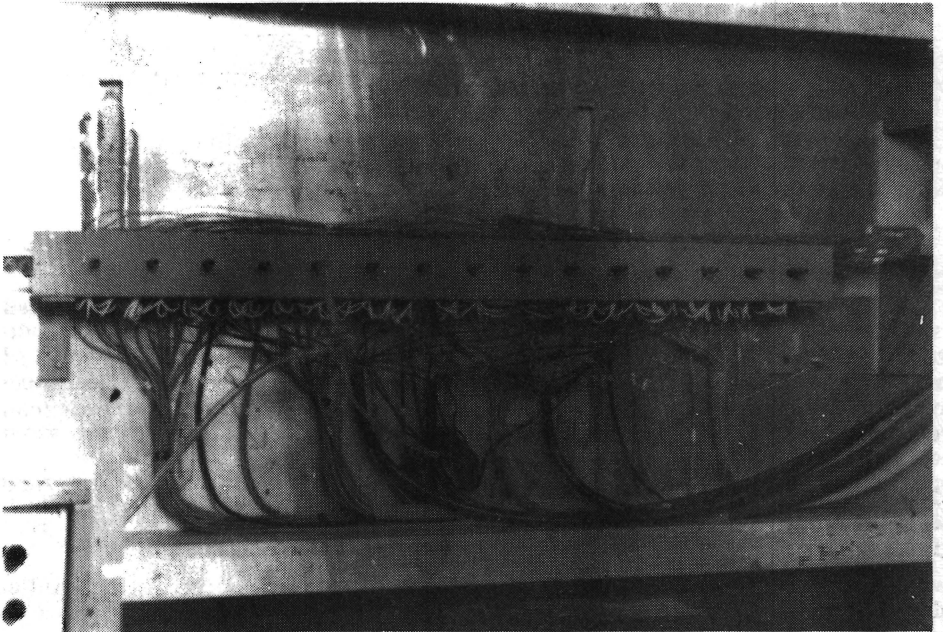


Figure 4.12 Back of test section, showing connecting leads to heated plate

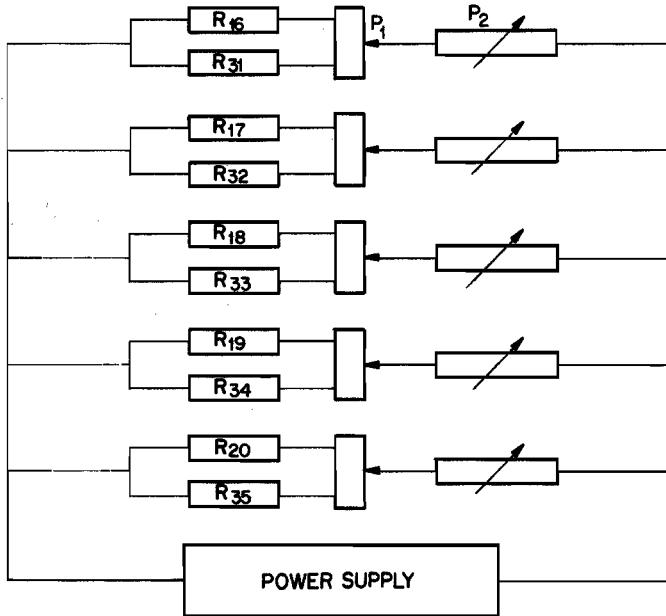


FIG. 4.10 POWER SUPPLY OF THE SMALL ELEMENTS

The remaining small elements are heated in the same manner as explained above.

The whole power supply control system was built into a separate chassis with the 45 controlling potentiometers conveniently grouped on the front panel.

(c) Temperature Measurement

The method designed for measuring differences between thermocouples is schematically shown in Fig. 4.11. All thermocouples leaving the heated plate were lengthened by soldering copper and constantan wires to the upper ends of the copper and constantan pins of the connector. The 228 constantan wires were wrapped round the pins of two multiple connectors with 140 and 100 connections, respectively. The copper block and the connectors were installed into the same cabinet, fastened to the test section wall. The same was done with the constantan and copper wires of a reference thermocouple placed in the entrance of the test section, indicating the temperature of the undisturbed flow.

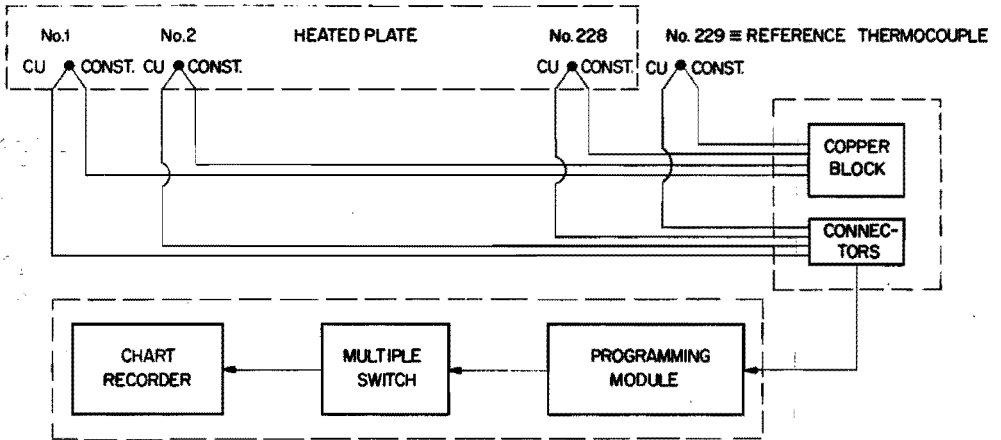


FIG. 4.11 ELECTRICAL CIRCUIT FOR THERMOCOUPLE MEASUREMENTS

With the help of two cables with 140 and 100 normal copper wires these connectors were linked with similar connectors on a "programming module".

The programming module had a large number of sockets on the front panel, divided into two groups. Those of the first group were connected with the contact points of the two connectors; in fact, therefore, these sockets corresponded with the copper wires of the thermocouples. Those of the second group were connected with the 2 x 102 contacts of a double-deck multiple switch with 102 positions, which could be rotated with a motor. By connecting the sockets of both groups by means of short cables, any special thermocouple measuring programme could be put on the multiple switch. The latter was connected to a Philips millivolt recorder of which the -0.5 mV to +0.5 mV range was used.

A microswitch was mounted on the multiple switch; when the latter went from one position to the following this microswitch was closed for a short time. It operated the pen-lifting mechanism of the recorder so that when it was closed, the pen was lifted from the paper. In this way a successive row of short lines was recorded, each line corresponding to one position of the switch.

An impression of the multitude of connecting leads of the heated plate can be gained from Fig. 4.12. The cables leaving the lower side of the cabinet built round the connector of the heated plate are those running to the power supply cabinet. The large number of smaller cables at the upper side are the thermocouple wires leading to the multiple connectors and the copper block, installed in the metal cabinet visible on the right-hand side of the photograph.

The procedure for setting a uniform surface temperature of the heated plate is given in Appendix I.

B. Measuring Techniques

Much attention was given to the accurate determination of the mean and fluctuating quantities of the turbulent velocity and temperature boundary layer, necessary for the calculation of the turbulent Prandtl number. The reliability and accuracy of the measuring results were checked by determining some of these quantities in two or more independent ways. Below we shall give a review of the most important measuring techniques used.

1. Measurement of the Skin Friction

The local turbulent skin friction was determined in two ways.

(a) Application of Preston Tubes

A simple method of determining turbulent skin friction on a smooth surface, which utilizes a round pitot tube resting on the surface, was developed by Preston [170]. The method depends upon the assumption of a universal law of the wall for the velocity distribution in turbulent boundary layers. This leads to a non-dimensional relation for the difference between the total pressure recorded by the tube and the static pressure at the wall, Δp_p , and the skin friction. The relation can be presented in the form:

$$\frac{\tau_w d^2}{4\rho v^2} = F\left(\frac{\Delta p_p d^2}{4\rho v^2}\right), \quad (4.1)$$

in which d is the outside diameter of the Preston tube. The function F has been determined by a number of investigators, using Preston tubes of different diameter in various turbulent flows. A review of these measurements is given by Patel [171], who also calibrated Preston tubes in turbulent pipe flow and indicated the limitations of their use in boundary layers with a streamwise pressure gradient.

We have used Patel's calibration curve which for $1.5 < y^* < 3.5$ is represented by the empirical relation:

$$y^* = 0.8287 - 0.1381 x^* + 0.1437 x^{*2} - 0.0060 x^{*3}. \quad (4.2)$$

In this relation

$$x^* = 10 \log\left(\frac{\tau_w d^2}{4\rho v^2}\right) \text{ and } y^* = 10 \log\left(\frac{\Delta p_p d^2}{4\rho v^2}\right). \quad (4.3)$$

Equation (4.2) is accurate to within 1.5 percent of τ_w .

Figure 4.13 gives a photograph of the Preston tubes used. They had outside diameters of 0.504, 1.019 and 2.005 mm and were constructed from stainless-steel capillary tubing. By means of the traversing mechanism the tubes were placed into the boundary layer at the centre line of the flat plate at the same x -position as a static pressure hole. As the angle between the stem and the forward facing part of the tube was slightly larger than 90° , the forward part could be accurately placed parallel to the wall by gently pushing it against the flat plate.

The τ_w -values, calculated from preliminary measurements with tubes of different diameter, agreed within the experimental accuracy, providing a check for the validity of the calibration curve. As the Preston tube with the diameter of 2.005 mm gives the highest p_p -value at the same τ_w -value, most of the measurements were carried out with this Preston tube.

The pressure difference was measured with a Betz micromanometer.

(b) Application of the von Kármán Momentum Integral Equation

The momentum integral equation of von Kármán can be written in the form:

$$\tau_w = \rho U_o^2 \frac{d\delta_2}{dx} + (2\delta_2 + \delta_1) \left(-\frac{dp}{dx}\right) . \quad (4.4)$$

By measuring the pressure gradient and the mean velocity profiles at different values of x , which lead to known functions $\delta_1(x)$ and $\delta_2(x)$, the value of $\tau_w(x)$ can be calculated from Eq. (4.4). Since we have to differentiate measured quantities to calculate τ_w , this method is not a very accurate one. However, the results can be used as a check on the data obtained with the Preston tubes and on the two-dimensionality of the boundary layer.

2. Measurement of the Mean Velocity and the Longitudinal Velocity Fluctuations

Mean and fluctuating velocities were determined with a hot-wire anemometer, which is today the most widely used instrument for local measurements of flow parameters in turbulent flow. Essentially, it consists of a very thin, electrically heated, metal wire, suspended in the flow and connected to an electronic device measuring the electrical input of the wire, which is a measure of the heat transfer from the wire. The local flow velocity can be determined if the relation between it and the heat transfer is known.

Since a sufficiently fine wire has a very small heat capacity, it will also be able to respond to velocity fluctuations, so that is it suited for turbulence measurements. The response is limited by the thermal inertia of the wire. However, this inertia can be compensated for by electrical means. With modern advances in electronic circuitry the hot-wire anemometer can even measure velocity fluctuations with frequencies as high as 400 kHz.

In the following we shall only consider those features of hot-wire anemometry which are of direct importance for our measurements. A detailed description of all problems and corrections in hot-wire anemometry can be found in references [22, 172-182].

Our turbulence measurements were carried out with Disa 55D00 universal anemometers, using 55A06 correlators to measure root-mean-square values of velocity fluctuations and correlations between them. The Disa anemometer is based on the constant-temperature method. Its principle of operation is shown in Fig. 4.14. The hot wire forms one arm of a Wheatstone bridge which is in exact balance at a certain bridge voltage applied by the servo amplifier. A slight change of probe resistance, e.g. due to a change in local velocity, will produce a small unbalance which, after considerable amplification, is used to adjust the bridge voltage in such a way that the bridge will be kept close to balance. The bridge voltage is now a measure of the velocity. In this way the temperature variations of the hot wire are reduced to a minimum and in consequence the frequency response of the system is greatly improved in comparison with the constant-current method. For our measurements the time constant as determined with a square-wave test of 10 kHz was about 2 μ s, hence sufficiently small for us to neglect the inertia of the measuring system towards velocity fluctuations with a frequency less than, say, 10,000 Hz.



Figure 4.13 Preston tubes used

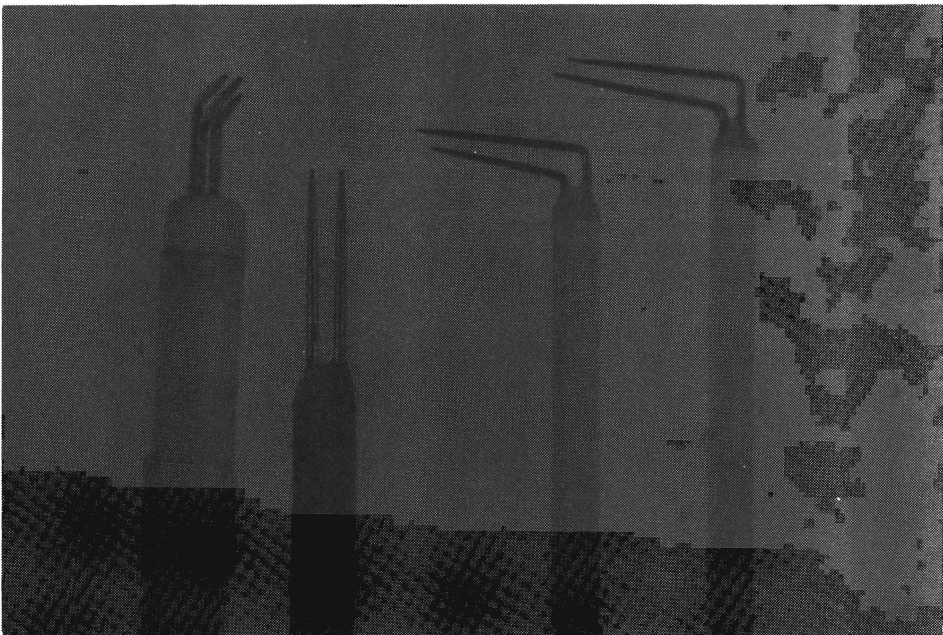


Figure 4.17 Hot-wire probe configurations

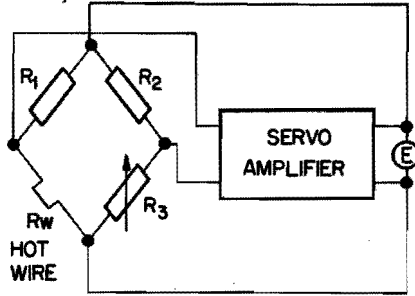


FIG 4.14 PRINCIPLE OF OPERATION OF CONSTANT-TEMPERATURE METHOD

For subsonic flow, without free convection effects, the heat transfer of an infinitely long wire with air as flowing medium can be represented by

$$Nu_d = f(Re_d, T_m/T_o), \quad (4.5)$$

with $T_m = \frac{1}{2}(T_w + T_o)$. Much work has been done to ascertain the form of this relation. An often-used relation is King's law

$$Nu_d = A' + B' Re_d^{0.5}, \quad (4.6)$$

in which A' depends on $(T_w - T_o)$ and B' can be taken as constant. A more accurate relation is given by Collis and Williams [183], which for $Re_d < 44$ (the range of interest for most hot-wire applications) can be written as

$$\left(\frac{T_m}{T_o}\right)^{-0.17} Nu_d = C + D Re_d^{0.45}, \quad (4.7)$$

with C and D being constants.

However, the heat transfer of the rather short wires (length about 1 mm) used for velocity measurements is greatly affected by the heat loss towards its ends, the interference of the prongs of the probe with the flow round the wire and the collection of dirt on the wire. Besides, the relation between bridge voltage and velocity can only be calculated with an accurate knowledge of the characteristics of the wire material, such as resistivity and temperature coefficient of resistance. For these reasons the wire sensitivity in volts per unit change of velocity can only be determined accurately by frequent calibration, making the use of accurate relations for the heat transfer like Eq. (4.7) unnecessary. In fact these heat-transfer formulae must only be regarded as a basis for the calibrations of individual probes.

Within the velocity range of interest the calibration curves of our probes with the wire normal to the flow all conformed to the relation:

$$\frac{I^2 R_w}{R_w - R_o} = A_2 [1 + \gamma (T_w - T_o)] + B_2 \sqrt{U}, \quad (4.8)$$

in which A_2 and B_2 are constants. From measurements with wires of diameters between 3.0 and 11.7 μm and temperature differences $T_w - T_o$ between 40 and 240 $^{\circ}\text{C}$, we have found for γ the value

$$\gamma = 1.7 \pm 0.1 \cdot 10^{-3} \text{ } ^{\circ}\text{C}^{-1},$$

which is in good agreement with the values of 1.64 and $1.68 \cdot 10^{-3} \text{ } ^{\circ}\text{C}^{-1}$, obtained by Collis [184] and Davies [185].

The wires were normally operated with $T_w - T_o$ about 200 $^{\circ}\text{C}$. During the measurements of velocity profiles T_o was kept constant within 0.5 $^{\circ}\text{C}$ and for the measurements in the temperature boundary layer the change of T_o was maximally about 10 $^{\circ}\text{C}$, so that the term $A_2 [1 + \gamma (T_w - T_o)]$ could be treated as a constant, denoted by A_2' .

Equation (4.8) gives for the relation between bridge voltage and velocity (see also Fig. 4.14):

$$E^2 = I^2 (R_w + R_1)^2 = \frac{(R_w + R_1)^2 (R_w - R_o)}{R_w} (A_2' + B_2 \sqrt{U}), \quad (4.9)$$

which for the constant-temperature operation reduces to

$$E^2 = A + B \sqrt{U}. \quad (4.10)$$

The constants A and B must be determined by calibration of the wire.

Differentiation of Eq. (4.10) gives

$$2E \frac{dE}{dU} = \frac{B}{2\sqrt{U}}, \quad (4.11)$$

which, when for $u \ll U$ only the linear terms of the fluctuations are retained, results in

$$e = S_u u, \quad (4.12)$$

with

$$S_u' = \frac{B}{4E\sqrt{U}}, \quad (4.13)$$

giving the relation between velocity and voltage fluctuations.

In practice the root-mean-square values are taken as a measure of the magnitude of the velocity fluctuations. For the longitudinal turbulent intensity, u' , this means:

$$e' = S_u u'. \quad (4.14)$$

(The prime ' denotes a root-mean-square value, so $u' = \sqrt{u^2}$.)

S_u can be calculated from the calibration curve of the wire and the value of E , which was measured by means of a John Fluke D.C. voltmeter (accuracy 0.02 percent).

Calibration consisted in placing the wire normal to the flow in the free stream of the test section and measuring the bridge voltage E at different values of the free stream velocity. These values were obtained by means of a pitot-static tube mounted close by the hot wire. By plotting E^2 against \sqrt{U} a straight line was fitted to the measuring points, from which A and B could be determined. It turned out that at velocities below 2 m/s free-convection effects were present, causing deviations from the linear relation between E^2 and \sqrt{U} . At these low velocities an accurate calibration was attained by using an anemometer developed by TNO [186] (velocity range 0.5 - 200 cm/s) as a standard. In this velocity range the sensitivity S_u was determined by drawing tangents to the calibration curve.

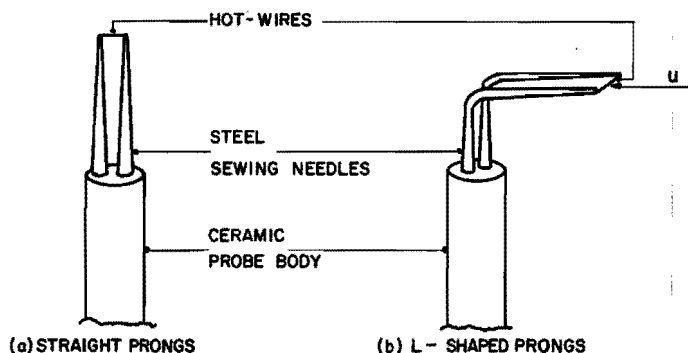


FIGURE 4.15 HOT-WIRE PROBES

Two designs of single-wire probes are illustrated in Fig. 4.15. The prongs of the probe consisted of steel sewing needles, which were fixed with Araldite resin into a ceramic probe body. The wire was spot-welded between the needle points, using a Disa 55A11 micromanipulator. Lengths of copper wire were soldered to the eye ends for connection of the probe to the Wheatstone bridge. After preliminary measurements with platinum and pure tungsten wires we used platinum-plated tungsten wires, available from Disa, with a diameter of about $5 \mu\text{m}$ and a resistance of about 3Ω per mm. The measured temperature coefficient of resistance at 20°C was $3.98 \pm 0.04 \cdot 10^{-3} \text{ }^\circ\text{C}^{-1}$.

For the boundary-layer measurements we initially used probes with straight prongs, depicted in Fig. 4.15^a. However, the mean velocity profiles measured with these probes showed a considerable deviation from the law of the wall. This was caused by the fact that the wire was in the same cross-section of the test section as the probe body and the probe holder of the traversing mechanism, which produced a blockage effect on the boundary layer in this cross-section. No such blockage effects were observed when we used the probes with L-shaped prongs shown in Fig. 4.15^b. They were positioned in the boundary layer with the prongs facing upstream, so that the wire was not in the same cross-section as the probe body and the probe holder. The necessary corrections of the hot-wire results will be discussed in the next chapter together with the measuring results.

3. Measurement of Transverse Velocity Fluctuations and Reynolds Shear Stresses

Fluctuations in transverse velocity can be measured by making use of the dependence of the heat transfer on the angle between the wire and the velocity vector. Assume that the wire is placed in the x-y plane, making an angle ϕ with the mean velocity in the x-direction (see Fig. 4.16).

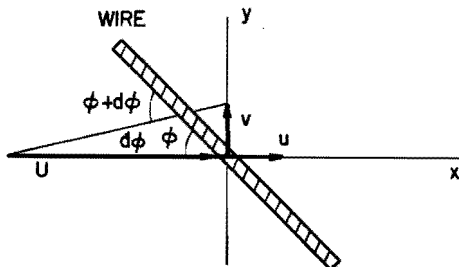


FIG 4.16 POSITION OF THE WIRE IN THE X-O-Y PLANE

For an infinitely long wire the heat transfer is only determined by the velocity component perpendicular to the wire, which for constant-temperature operation leads to

$$E^2 = A + B\sqrt{U \sin \phi} . \quad (4.15)$$

Equation (4.15) is often used to calculate the sensitivity of a hot wire to transverse velocity fluctuations. However, for the short wires used in hot-wire anemometry there are deviations from Eq. (4.15) due to the tangential velocity component, causing an increase in the heat transfer of the wire. This may be expressed as

$$E^2 = A + B\sqrt{U (\sin^2 \phi + k^2 \cos^2 \phi)^{\frac{1}{2}}} . \quad (4.16)$$

The behaviour of k is still imperfectly understood. Hinze [22] reports that k increases with decreasing velocity and ranges from 0.1 to 0.3. Webster found k to be 0.20 ± 0.01 with no systematic dependence of k on the length-to-diameter ratio, l/d , or the velocity. More recently, Champagne et al. [187] found that k depends primarily on l/d , k being approximately 0.20 for $l/d = 200$ and decreasing with increasing l/d till at $l/d = 600$ k becomes effectively zero. However, for hot-wire anemometry the factor $(\sin^2 \phi + k^2 \cos^2 \phi)$ can always be determined by calibration of the wire making angles of ϕ and 90° , respectively, with the flow direction. With a given ϕ value, this leads to a known k -value for the wire used.

In determining the sensitivity of the inclines wire to the velocity fluctuation v , we take it that v causes a change $d\phi$ in the angle between U and the wire (see Fig. 4.16). Assuming that the velocity fluctuations are small compared with U and neglecting the inertia of the anemometer, we may write:

$$v = U \, d\varphi \quad (4.17)$$

and

$$e_{\varphi} = S_{u,\varphi} u + S_{v,\varphi} v, \quad (4.18)$$

with

$$S_{u,\varphi} = \frac{B_{\varphi}}{4 E \sqrt{U}}, \quad (4.19)$$

$$S_{v,\varphi} = \frac{B_{\varphi}}{4 E \sqrt{U}} \frac{(1-k^2) \sin^2 \varphi}{2(\sin^2 \varphi + k^2 \cos^2 \varphi)} \quad (4.20)$$

and

$$B_{\varphi} = B(\sin^2 \varphi + k^2 \cos^2 \varphi)^{\frac{1}{4}}. \quad (4.21)$$

With a given φ value the sensitivities $S_{u,\varphi}$ and $S_{v,\varphi}$ can be established from calibrations described above.

Since the voltage fluctuation e_{φ} depends on both u and v , it is impossible to measure v with one inclined wire. The simplest way to do this, is to use an X-probe with two identical wires, making angles of φ and $-\varphi$, respectively, with the x-direction. This results in

$$\text{angle } +\varphi : e_{\varphi} = S_{u,\varphi} u + S_{v,\varphi} v, \quad (4.22)$$

$$\text{angle } -\varphi : e_{-\varphi} = S_{u,\varphi} u - S_{v,\varphi} v, \quad (4.23)$$

which implies that the turbulent intensities u' and v' can be determined by measuring the sum and the difference of the voltage fluctuations:

$$(e_{\varphi} + e_{-\varphi})' = 2 S_{u,\varphi} u', \quad (4.24)$$

$$(e_{\varphi} - e_{-\varphi})' = 2 S_{v,\varphi} v'. \quad (4.25)$$

In this way the Reynolds shear stress can be measured by forming the product of the voltage fluctuations:

$$\overline{(e_{\varphi} + e_{-\varphi})(e_{\varphi} - e_{-\varphi})} = 4 S_{u,\varphi} S_{v,\varphi} \overline{u'v'}. \quad (4.26)$$

In practice, however, the measurements are not so simple as stated above. The chances of exactly matching the two wires of an X-probe in the required manner are very small, because it is hardly possible to place two identical wires at angles of φ and $-\varphi$, respectively, with the mean velocity. In this context it should be noted that deviations in wire angle of only 3° correspond to a change of nearly 10% in the v' values calculated by means of Eq. (4.23). In fact, it would be extremely difficult to attain a better accuracy than 3° in setting the angle.

These uncertainties imply that we must calibrate the wires individually in their measuring position for their sensitivities to the u and v fluctuations. We calibrated each wire placed at an angle φ as follows: first we measured the calibration curve $E(U)$, giving a linear relation between E^2 and \sqrt{U} , from which B_φ could be deduced. $S_{u,\varphi}$ was then calculated by means of Eq. (4.19). For a wire at a fixed angle φ and assuming k to be independent of U , which is verified by our own measurements and those of Webster [188] and Champagne et al., the ratio $c = S_{v,\varphi}/S_{u,\varphi}$ proved constant, irrespective of wire operating conditions, as can be seen from Eqs. (4.19) and (4.20). By rotating the wire in the x - y plane we measured $E(\varphi)$ at five constant values of U , calculating $S_{v,\varphi}$ according to

$$S_{v,\varphi} = \frac{\partial E}{\partial v} = \frac{1}{U} \frac{\partial E}{\partial \varphi} \quad (4.27)$$

In this way values of c could be determined, which indeed resulted in a constant value with deviations of about 5 percent from the average value.

The voltage fluctuations of the wires can now be written as

$$\text{wire 1 : } e_1 = S_{u,\varphi_1} (u + c_1 v) \quad (4.28)$$

$$\text{wire 2 : } e_2 = S_{u,\varphi_2} (u + c_2 v) \quad (4.29)$$

$$e_1 + e_2 = (S_{u,\varphi_1} + S_{u,\varphi_2})u + (c_1 S_{u,\varphi_1} + c_2 S_{u,\varphi_2})v \quad (4.30)$$

$$e_1 - e_2 = (S_{u,\varphi_1} - S_{u,\varphi_2})u + (c_1 S_{u,\varphi_1} - c_2 S_{u,\varphi_2})v \quad (4.31)$$

Measuring the root-mean-square values of the above voltage fluctuations, we get four equations with three unknown quantities $(u')^2$, $(v')^2$ and \overline{uv} . These equations were solved with the aid of a computer program which determined the values of u' , v' and \overline{uv} giving the best fit to the four equations.

At first we used X-probes shown in Fig. 4.17^a. Four L-shaped sewing needles were stuck with Araldite epoxy resin into a ceramic probe body with an outside diameter of 5 mm in such a way that the needle points formed the angular points of a square with sides of 1 mm in a plane parallel with the probe axis. Two wires were spot-welded diagonally between the needle points making angles of about 45° and -45°, respectively, with the probe axis.

Just as with the single-wire probe with straight prongs, however, the measuring point of the X-probe was in the same cross-section as the probe holder and erroneous measurements had to be expected. For this reason we designed another X-probe, consisting of two separate single-wire probes, whose wires made angles of about +45° and -45°, respectively, with the probe axis. Photographs of these separate probes are presented in Fig. 4.17^{c,d}. The two probes were mounted into a special device which allowed the wires to be positioned very close to each other with the needle points facing upstream. The mounting device could be fixed into the probe holder of the traversing mechanism.

Each wire of the X-probe was connected to a Disa 55D00 universal anemometer. The voltage fluctuations e_1 and e_2 were transferred to the two input channels of the Disa 55A06 correlator, with which e_1' , e_2' , $(e_1+e_2)'$ and $(e_1-e_2)'$ could be measured.

4. Measurement of the Heat Flux Density at the Wall

The local heat flux density at the wall was measured in three ways:

(a) From the Electrical Power Input

The heat flux density at the surface of a main element, q_w , can be obtained by dividing its electrical power input by the area of its surface. As we want to determine the value of the convective heat transfer, the power input must be corrected for the radiation heat transfer and the heat losses due to conduction to the surrounding elements and in the downward direction. Taking $\epsilon = 0.1$ for the emissivity of the aluminium surface and $T_w - T_o = 10$ °C, we calculated the radiation heat loss to be about 0.1 W per main element, which was about two percent of the power input.

The heat loss in the downward direction was evaluated from the measured temperature differences across the Sindanyo plate, assuming a one-dimensional heat flow through it. With $\lambda_s = 0.66$ W m⁻¹ °C⁻¹, a value given by the supplier, this heat loss was about 20 percent of the power input. Assuming an uncertainty of 10% in λ_s , this heat loss gives rise to an inaccuracy of about 2 percent in q_w .

The maximum deviations in T_w were about 0.2 °C. With $\lambda_{al} = 0.23$ W m⁻¹ °C⁻¹ the maximum heat loss to the sides was about 0.1 W per main element, leading to an uncertainty in q_w of about 2 percent.

Thus the heat flux density at the wall could be determined with an accuracy of about 4 percent.

The above considerations are not valid for the two main elements adjoining the unheated parts of the plate, where much larger conduction heat losses took place. These losses could be calculated from the measured temperature distribution within the elements. However, since they amounted to nearly half the power input, the calculated q_w values for the two elements concerned are less accurate.

(b) From Measurements of the Mean Temperature Profile in the Viscous Sublayer

From measurements of the mean temperature profile in the viscous sublayer ($y^+ \leq 5$), which is a linear function of y (see Eq. (3.62)), the value of dT/dy at $y = 0$ can be determined. With this result q_w was calculated, using $q_w = -\lambda(dT/dy)_{y=0}$. The accuracy of this q_w value is about the same as that determined by method (a).

(c) By Application of the Integral Energy Equation

Integration of the energy equation between $y = 0$ and $y = \delta_T$ yields

$$\rho c_p \int_0^{\delta_T} U(T - T_o) dy = q_w(x) \quad (4.32)$$

Introduction of the convection thickness, δ_T^* , defined as

$$\delta_T^* \equiv \int_0^{\delta_T} U(T - T_o) dy \quad (4.33)$$

leads to

$$q_w(x) = \frac{1}{\rho c_p} \frac{d\delta_T^*}{dx} \quad (4.34)$$

By measuring the mean temperature and velocity profiles for various values of x along the heated plate, the function $\delta_T^*(x)$ can be evaluated, after which $q_w(x)$ can be calculated from Eq. (4.34)

Since an experimentally determined $\delta_T^*(x)$ -curve has to be differentiated, this method does not give as accurate results as procedures (a) and (b). However, the data so obtained may serve as an independent check on the results of both other methods.

5. Measurement of Mean Temperature and Temperature Fluctuations

For the temperature measurements a new kind of temperature-sensing element was developed at the Heat-Transfer Laboratory of the Physics Department of the Eindhoven University of Technology. It consists of a quartz wire, diameter about $5 \mu\text{m}$, covered with a thin layer of platinum (thickness about $0.1 \mu\text{m}$). The very thin quartz wires were fabricated by a drawing technique, while the thin layers were applied by sputtering in an argon gas discharge tube, giving a strong adhesion between the platinum and the quartz wire. Generally wires with a length of 1 mm were used, having a resistance of about 500Ω . For each wire the temperature coefficient of resistance was measured in an accurately controlled thermostat. Values of about $2 \cdot 10^{-3} \text{ } ^\circ\text{C}^{-1}$ were found (accuracy 2%), i. e. nearly half the value of bulk platinum.

The temperature-sensing elements were employed as resistance thermometers. Applying a measuring current of 0.4 mA, which was kept constant within 0.05%, we found the temperature sensitivity of the wire to be about $400 \mu\text{V}/^\circ\text{C}$, i. e. about 10 times as high as that of conventional thermocouples. The elements had a response time of less than 1 ms, which makes them very suitable for measuring temperature fluctuations.

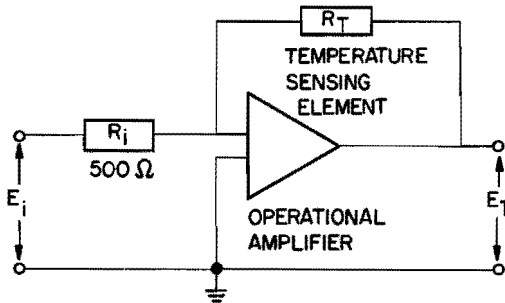


FIG 4.18 ELECTRICAL CIRCUITRY FOR TEMPERATURE MEASUREMENTS

A sketch of the electrical circuitry is shown in Fig. 4.18. The D. C. output voltage of the Philbrick Model SP 656 high-gain, chopper-stabilized operational amplifier is given by

$$E_T = - \frac{R_T}{R_i} E_i . \quad (4.35)$$

The input voltage delivered by a highly stabilized voltage source was set at 200.0 ± 0.1 mV with $R_1 = 500\Omega$. The output voltage was measured with an accuracy of $6 \mu\text{V}$ by means of a John Fluke Model 885A D.C. differential voltmeter, from which $T-T_0$ could be calculated within 0.03°C according to

$$T-T_0 = (E-E_0)/(E_0\beta_0) \quad (4.36)$$

Temperature fluctuations cause resistance fluctuations which result in fluctuations e_T of the output voltage. These voltage fluctuations were amplified by a factor of 10^3 with a P.A.R. Model CR-4 low-noise, high-gain amplifier with differential input, while the root-mean-square value was measured by means of a Disa correlator, accuracy 2%. The intensity of the temperature fluctuations can then be calculated from

$$e_T' = \beta_0 E_0 \theta' \quad (4.37)$$

with an accuracy of about 2%.

The measurements of the mean temperature profiles and the temperature fluctuations were carried out with the same type of probe as the velocity measurements (see Fig. 4.15^b). In this case the temperature-sensing elements were fixed between the prongs with the aid of silver paint.

6. The Measurement of $\overline{v\theta}$

The quantity $\overline{v\theta}$, which is of great importance for the description of turbulent heat transfer, is rather difficult to measure. Up to now - to the author's knowledge - Johnson [17] has been the only one to do so.

We adopted the following procedure: placing an X-probe and a temperature-sensing probe very close to each other (the separate wires being at distances of about 0.3 mm from each other) at the same location in the temperature boundary layer, we could measure the fluctuations v and θ simultaneously. The quantity $\overline{v\theta}$ was then determined electronically, with the help of two Disa correlators, according to a special measuring procedure. The X-probe was the one that consisted of two separate single-wire probes described above; the construction of the temperature probe is shown in Fig. 4.15^b. Fig. 4.19 illustrates the configuration of the wires in the boundary layer, viewed perpendicular to the x-y plane.

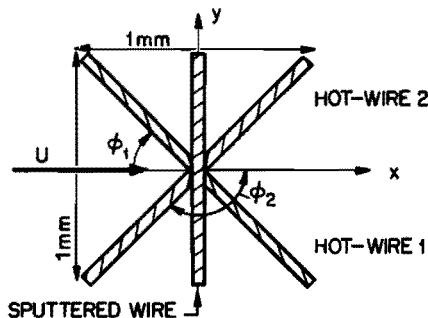


FIG 4.19 CONFIGURATION OF THE WIRES FOR THE MEASUREMENTS OF $\overline{v\theta}$

For the voltage fluctuations across the hot wires 1 and 2 we may write in a non-isothermal turbulent flow:

$$\text{wire 1 : } e_1 = S_{u, \varphi_1} (u + c_1 v) + S_{T_1} \theta , \quad (4.38)$$

$$\text{wire 2 : } e_2 = S_{u, \varphi_2} (u + c_2 v) + S_{T_2} \theta , \quad (4.39)$$

and for that across the sputtered wire:

$$e_T = \beta_0 E_0 \theta , \quad (4.40)$$

where, according to Eq. (4.8),

$$S_T = - \frac{ER_T \beta_T}{2(R_W - R_T)} . \quad (4.41)$$

We used the following measuring procedure: First we carefully calibrated the hot wires in an ambient temperature T_0 outside the boundary layer. The temperature difference between each wire and its surroundings was set at 250 °C ($R_W/R_0 \approx 2$). At this large value the contribution of the temperature fluctuations to the fluctuating voltage across the wire was small in comparison with the contributions of the velocity fluctuations. Besides, the correction of $S_{u, \varphi}$ for changes in the ambient temperature of the wire, being at most 10 °C when traversing the temperature boundary layer, can easily be calculated. In fact, since these temperature changes are small compared with 250 °C, we may take E^2 to be proportional to $R_W - R_T$.

Next we calculated from the calibration curves the ratio $S_{u, \varphi_1}/S_{u, \varphi_2} = k$. It turned out that k can be taken as a constant for the velocity range used. Hence, from Eqs. (4.38) and (4.39) we have

$$e_1 - ke_2 = (c_1 S_{u, \varphi_1} - kc_2 S_{u, \varphi_2}) v + (S_{T_1} - S_{T_2}) \theta . \quad (4.42)$$

Observe that $c_2 < 0$ because $\varphi_2 > 90^\circ$. Since $S_T \ll S_{u, \varphi}$ and the wires were nearly identical, so that $S_{T_1} \approx S_{T_2}$ and $k \approx 1$, the last term in the above equation may be neglected. For these reasons the voltage combination $e_1 - ke_2$ is directly proportional to the velocity fluctuation v :

$$e_1 - ke_2 = (c_1 S_{u, \varphi_1} - kc_2 S_{u, \varphi_2}) v . \quad (4.43)$$

The quantity $\overline{v\theta}$ can now be determined by measuring

$$\overline{(e_1 - ke_2)e_T} = \beta_0 E_0 (c_1 S_{u, \varphi_1} - kc_2 S_{u, \varphi_2}) \overline{v\theta} . \quad (4.44)$$

A block diagram of the electrical set-up is presented in Fig. 4.20.

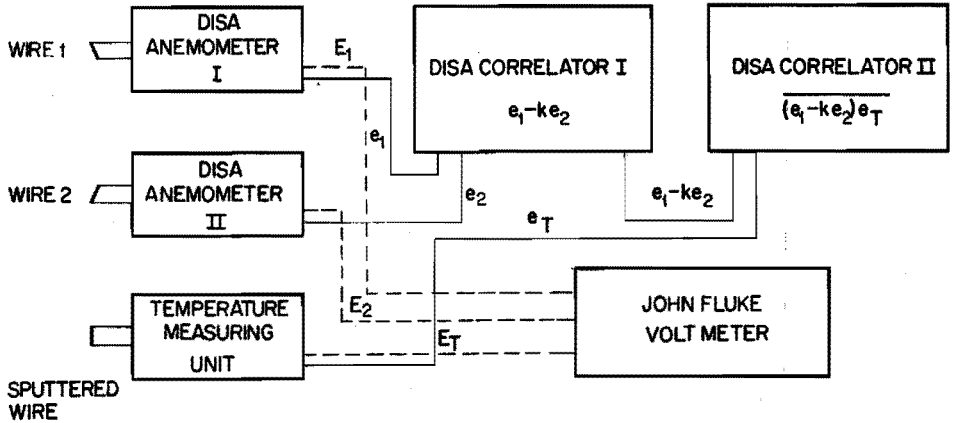


FIG. 4. 20 BLOCK DIAGRAM OF THE SETUP FOR MEASURING $\overline{v\theta}$

The voltage fluctuations e_1 and e_2 were connected to the two input channels of a Disa correlator. This device makes it possible to measure the values A' , B' , $(A+B)'$, $(A-B)'$, $(A/B)'$ and R_{AB} from two input signals A and B , while four output sockets give the amplified quantities pA , qB , $pA+qB$ and $pA-qB$, with amplification factors p and q that are adjustable. With this correlator we formed the voltage combination $e_1 - ke_2$, which was fed together with the voltage fluctuation e_T into a second Disa correlator. With the latter we measured the quantities $(e_1 - ke_2)'$, e_T' and $R_{e_1 - ke_2, e_T}$ from which $(e_1 - ke_2)e_T$ could be calculated.

The John Fluke D.C. voltmeter was used to measure the D.C. voltages E_1 , E_2 and E_T . The sensitivities in the measured point could then be calculated from the calibration curves of the wires.

Measurements conducted in an isothermal turbulent boundary layer with the probe configuration used did not give any voltage fluctuation across the sputtered wire. These experiments clearly demonstrated that the measurement of the temperature fluctuations was not affected by the presence of the hot wires.

V. EXPERIMENTAL RESULTS. COMPARISON WITH THEORY

Our experiments were mainly aimed at determining the distribution of the turbulent Prandtl number within a developing thermal boundary layer. In Chapter I, Section B, we have already mentioned that Pr_t can be determined in two ways, viz. either from the mean quantities, method (b), or from direct measurements of uv and $\overline{v\theta}$, method (a). We shall successively present our measurements of the mean and fluctuating quantities of the velocity and temperature field, followed by the distributions of Pr_t calculated according to both methods.

Measurements were conducted at eight stations along the flat plate, five of which were situated along the heated part. The stations were located at distances of 68.9, 88.9, 108.9, 118.9, 128.9, 148.9, 173.9 and 209.8 cm from the leading edge of the plate. They will be indicated as measuring stations 1-8, respectively (see Fig. 4.4). The leading edge of the heated part was located at a distance of 105.56 cm downstream of the leading edge of the plate.

The measurements of the flow field were carried out with two constant values of the free stream velocity at the entrance of the test section, viz. 6.13 and 10.10 m/s. Those of the temperature field were made under the same flow conditions with a constant value of $T_w - T_o$, being equal to 11.80 °C for the lower and 10.80 °C for the higher velocity.

A. The Mean Velocity Field

1. The Pressure Gradient

The measurements of the static pressure distribution along the flat plate obtained by means of the static pressure holes and those derived from the measurements of $U_o(x)$ by means of a pitot-static tube outside the boundary layer agreed very well. For $x > 30$ cm the pressure gradient was constant, giving $dp/dx = 4.10 \text{ N/m}^3$ for the lower and $dp/dx = -11.9 \text{ N/m}^3$ for the higher velocity.

2. The Skin Friction

The skin friction was measured at the stations 1-3 and 5-8* by means of Preston tubes as a function of the free stream velocity at the entrance of the test section, $U_{o,e}$ (measured by means of a pitot-static tube). The values of τ_w obtained with the various Preston tubes agreed within 3 percent. The experimental data for $\tau_w(x)$ at $U_{o,e} = 6.13$ and 10.10 m/s, respectively, are presented in Fig. 5.1, which also shows the results obtained with the aid of the von Kármán momentum integral equation, Eq. (2.15), and the values calculated from the Ludwig and Tillmann relation, Eq. (2.19). The distributions of $\delta_1(x)$ and $\delta_2(x)$, necessary for obtaining $\tau_w(x)$ from Eqs. (2.14) and 2.19), were determined by integration of the measured mean velocity profiles using Eqs. (2.15) and (2.16) (see also the next section). For the calculation of $d\delta_2/dx$ a smooth curve was drawn through the experimental values of δ_2 at the various measuring stations. The experimental and calculated τ_w values are given in Table 5.1, together with the τ_w values calculated from Eq. (2.99).

* Station 4 was introduced after the measurements of the flow field had been concluded, in order to obtain an additional measuring station close downstream of $x = L$ in the thermal boundary layer.

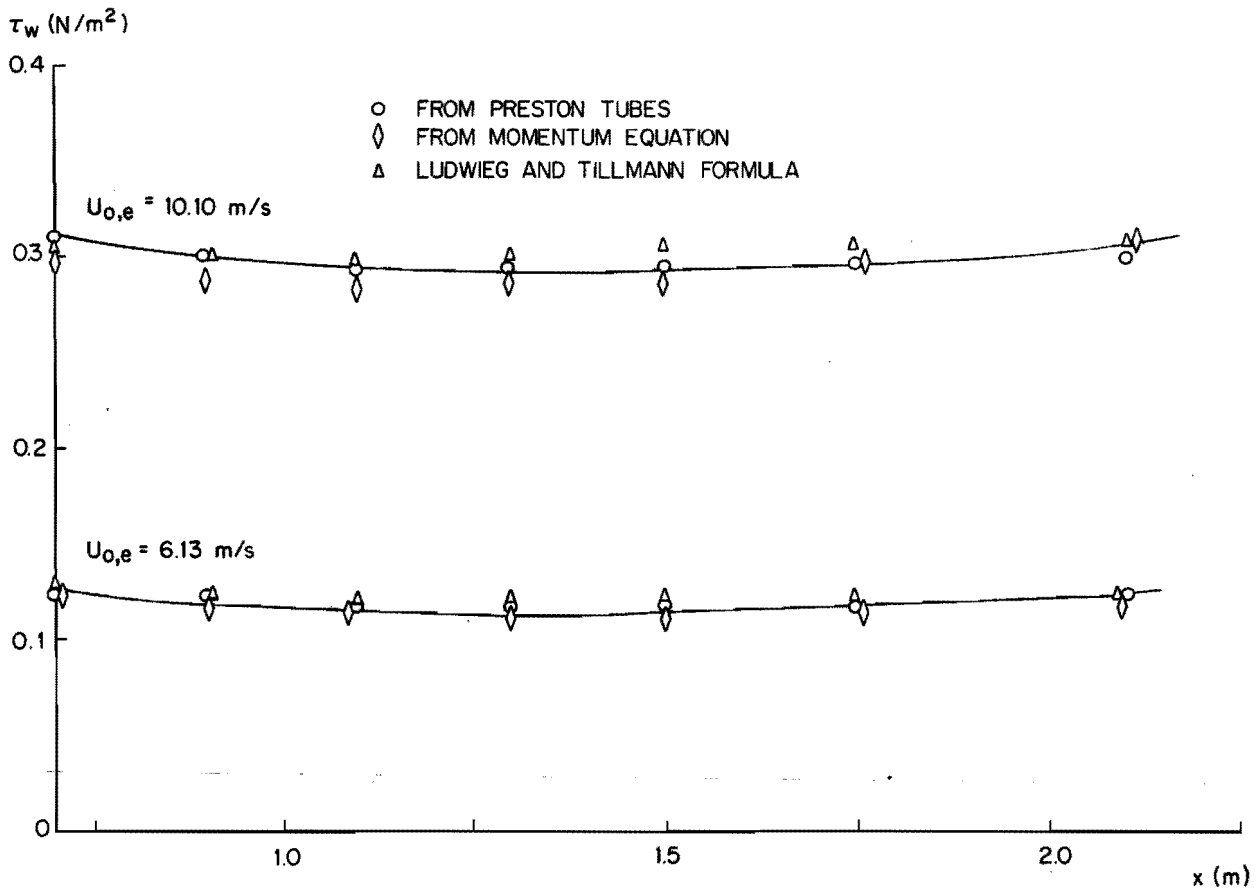


FIGURE 5.1 EXPERIMENTAL AND CALCULATED RESULTS FOR $\tau_w(x)$

Table 5.1.

Survey of τ_w values (N/m^2) at the various measuring stations

Station No.	$U_{o,e} = 6.13 \text{ m/s}$			$U_{o,e} = 10.10 \text{ m/s}$				
	Preston tube	Eq. (2.14)	Eq. (2.19)	Eq. (2.99)	Preston tube	Eq. (2.14)	Eq. (2.19)	Eq. (2.99)
		τ_w	τ_w	τ_w		τ_w	τ_w	τ_w
1	0.126	0.123	0.127	0.124	0.311	0.297	0.306	0.298
2	0.123	0.118	0.124	0.118	0.302	0.290	0.301	0.290
3	0.117	0.115	0.121	0.115	0.295	0.286	0.299	0.286
5	0.118	0.115	0.122	0.115	0.295	0.288	0.303	0.288
6	0.119	0.115	0.123	0.116	0.295	0.289	0.308	0.289
7	0.119	0.117	0.123	0.117	0.297	0.298	0.309	0.298
8	0.124	0.120	0.125	0.120	0.300	0.312	0.310	0.312

From this table and Fig. 5.1 we see that the deviations of the various τ_w values from a mean value are less than 3 per cent, a very satisfactory result for measurements of this kind. Although the application of Eq. (2.14) is less accurate owing to the differentiation of a measured distribution of $\delta_2(x)$, the agreement with the other results is very close. This can be interpreted as an experimental verification of the two-dimensional character of our developing turbulent boundary layer. Figure 5.1 also demonstrates that for both values of $U_{o,e}$ $\tau_w(x)$ is nearly constant along the heated part of the flat plate.

3. The Mean Velocity Profile

The mean velocity profiles $U(y)$ were measured by means of a hot-wire anemometer at stations 1-3 and 5-8 for the two different values of $U_{o,e}$, which were kept constant within one percent. The experimental values of $u^+(y^+)$ at the stations 5, 6 and 7, which may be regarded as representative of all other stations, are presented in Fig. 5.2. For the calculation of $u^+(y^+)$ from the measured distribution $U(y)$ the friction velocity u_τ was determined from the τ_w values obtained by means of the Preston tubes. In the case of very low values of y^+ the hot-wire readings were corrected for the effect of the proximity of the wall, using a correction method given by Wills [189]. These corrections are negligibly small for $y^+ > 10$.

Together with some additional information a complete survey of the measured distributions of $u^+(y^+)$ is presented in Table 1 of Appendix II along with the calculated values of δ_1 , δ_2 and u_τ .

In Fig. 5.2 the experimental results are checked against some frequently used formulae for the law of the wall. We see that for $25 < y^+ < 300$ the results agree very closely with the logarithmic law of the wall, $u^+ = 2.5 \ln y^+ + 5.5$. In the viscous sublayer, $y^+ < 5$, the measured profiles agree very well with the linear velocity distribution, $u^+ = y^+$. In the transition region, $5 < y^+ < 25$, there is a marked difference between our results and the u^+ values obtained from the velocity profile given by Spalding, Eq. (3.35).

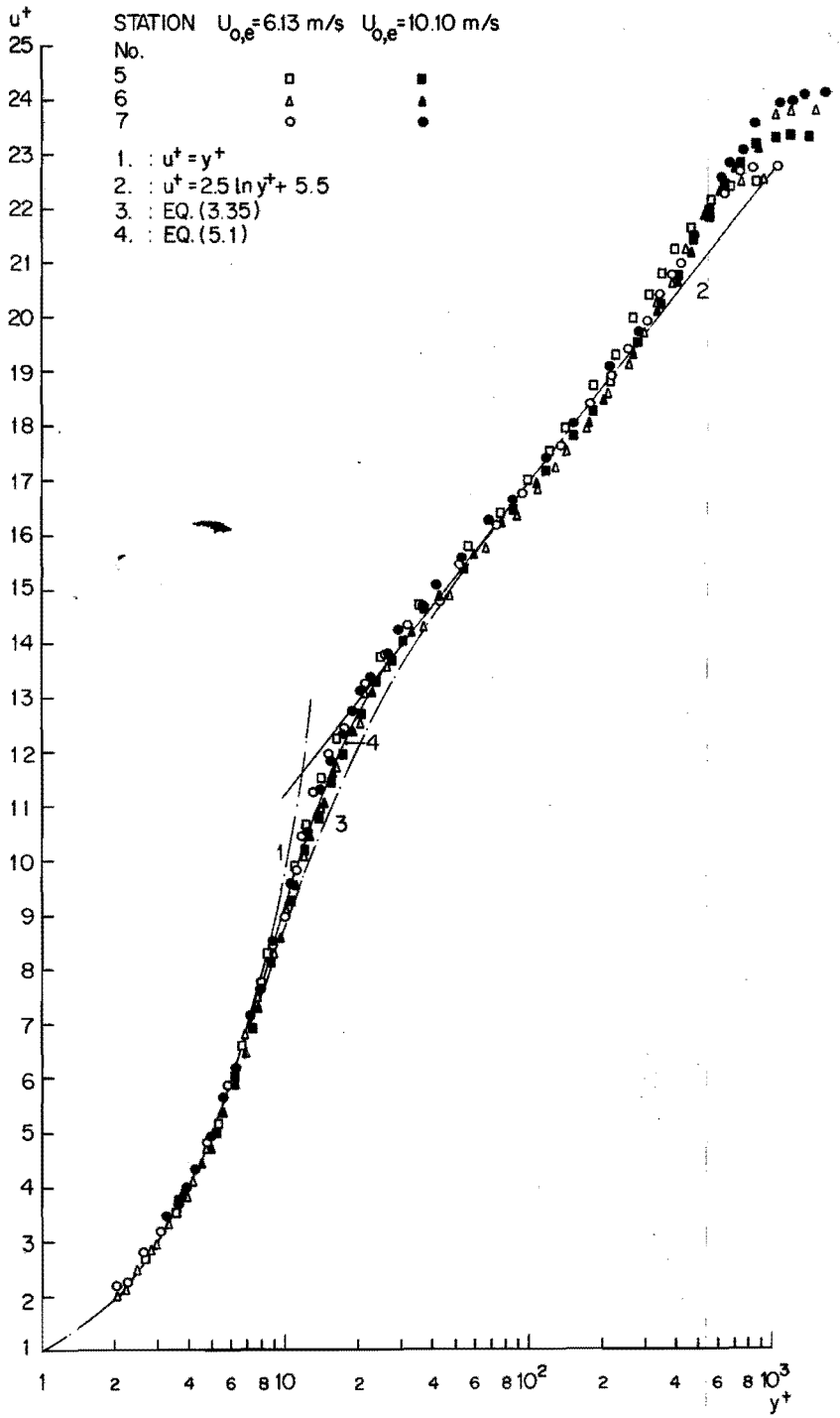


FIGURE 5.2 COMPARISON OF THE LAW OF THE WALL WITH EXPERIMENTAL DATA

But if we introduce an additional term $-(0.4 u^+)^5/5!$ into the form between brackets of Eq. (3.35), excellent agreement between this formula and the experimental data is obtained. Hence, for $0 < y^+ < 25$ we find

$$y^+ = u^+ + 0.1108 \left[e^{(0.4 u^+)} - 1 - (0.4 u^+) - \frac{(0.4 u^+)^2}{2!} - \frac{(0.4 u^+)^3}{3!} - \frac{(0.4 u^+)^4}{4!} - \frac{(0.4 u^+)^5}{5!} \right] \quad (5.1)$$

A good agreement is also obtained if, in analogy with the formulae given by von Kármán (Eq. (2.65)), we take for the velocity profile:

$$0 < y^+ \leq 5 : u^+ = y^+ \quad (5.2^a)$$

$$5 < y^+ \leq 20 : u^+ = 5.78 \ln y^+ - 4.3 \quad (5.2^b)$$

$$20 < y^+ \leq 300 : u^+ = 2.5 \ln y^+ + 5.5 \quad (5.2^c)$$

Comparison of Figs. 5.2 and 2.7 shows that our velocity profiles lie fully within the region of experimental results published by other investigators.

In order to compare our measured velocity profiles in the outer region with the formulae given in Chapter II, Section B, we must determine the value of the boundary layer thickness, δ . This is a rather nebulous quantity, since in principle the boundary layer velocity attains the free stream velocity at an infinite distance from the flat plate. Often the distance at which the velocity is 99 per cent of U_0 is taken as the boundary layer thickness. This definition has no physical meaning, however. Moreover, owing to the small values of $\partial U/\partial y$ in the outer region of the boundary layer, the distance in question is difficult to determine accurately from the experimental data.

To arrive at a more meaningful boundary layer thickness, we have made use of the fact that the velocity profiles can, to a good approximation, be represented by a power-law velocity profile, Eq. (2.90). For this velocity profile the boundary layer thickness δ is related to the displacement thickness, δ_1 , which has real physical meaning, by

$$\delta = (1 + 1/n) \delta_1 \quad (2.91)$$

This displacement thickness δ_1 can be determined quite accurately by integration of the velocity profile, while n can be determined by plotting $\log(U/U_0)$ versus $\log y$. Then, δ may be calculated from Eq. (2.91).

Our experiments yielded a value of $n = 1/6.75$, which implies $\delta = 7.75 \delta_1$ and a power-law velocity profile of the form:

$$\frac{U}{U_0} = \left(\frac{y}{\delta} \right)^{1/6.75} \quad (5.3)$$

Figure 5.3 affords a comparison between Eq. (5.3) and the measured velocity profiles. We see that there is a close agreement for $0.05 < y/\delta < 1$. It turned out that the values of δ calculated by means of Eq. (2.91) are quite close to those of the "99-per cent" boundary layer thickness.

In Fig. 5.4 we have represented the measured velocity profiles at the stations 5, 6 and 7 as velocity defect profiles by plotting $(U_0 - U)/u_\tau$ versus y/δ . We see that for $y/\delta > 0.03$ a universal profile of this kind is obtained. In Chapter II, Section B we have mentioned that in the fully turbulent part of the boundary layer the law of the wall and the velocity defect profile must overlap, resulting in

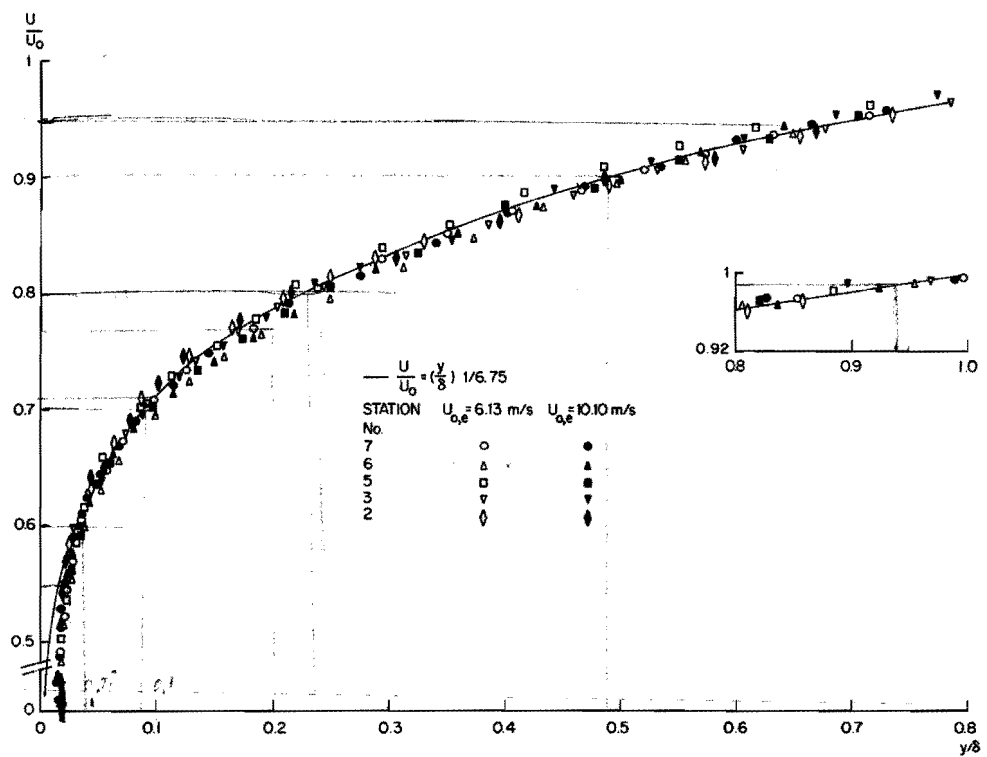


FIGURE 5.3 POWER-LAW REPRESENTATION OF MEASURED VELOCITY PROFILES

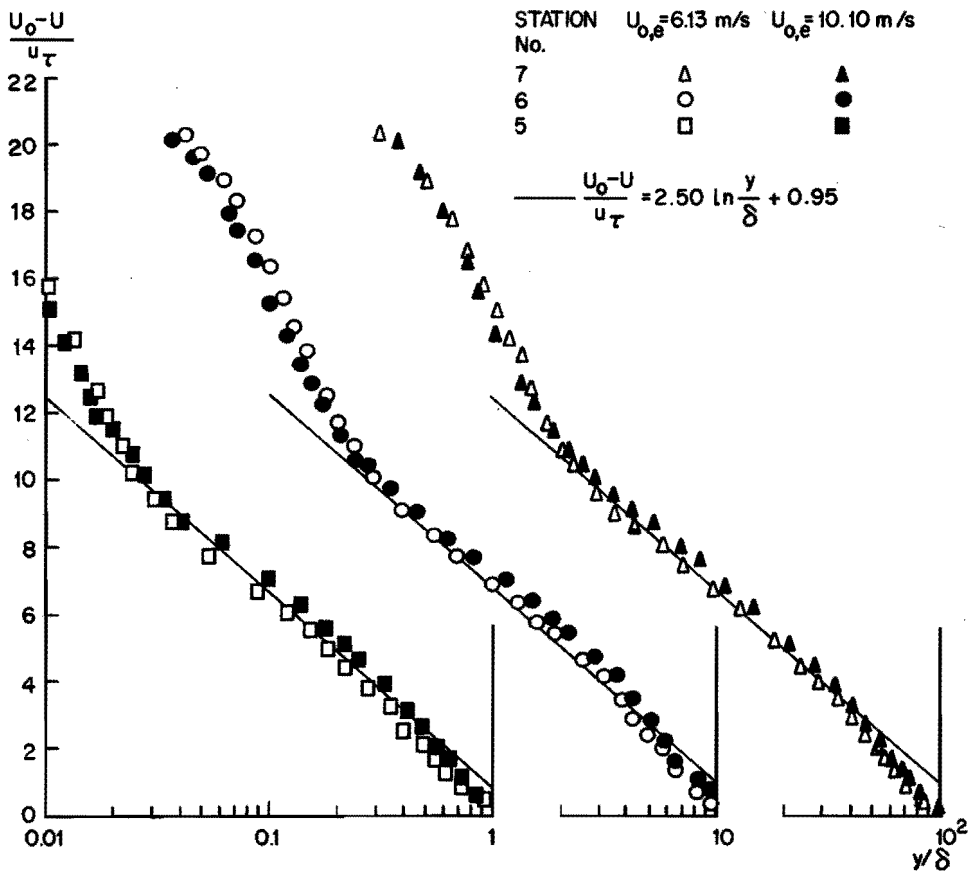


FIGURE 5.4 EXPERIMENTAL RESULTS FOR THE VELOCITY DEFECT PROFILE

$$\frac{U_0 - U}{u_\tau} = -2.5 \ln(y/\delta) + K . \quad (2.94)$$

Combination of Eq. (2.94) with the logarithmic law of the wall, $u^+ = 2.5 \ln y^+ + 5.5$, results in a skin friction law:

$$U_0/u_\tau = 2.5 \ln(\delta u_\tau/\nu) + 5.5 + K . \quad (5.4)$$

Making use of $\delta = 7.75 \delta_1$ and Eq. (2.99), we find for K

$$\begin{aligned} K &= -2.5 \ln(u_\tau/U_0) - 2.5 \ln 7.75 + 3.7 - 5.5 = \\ &= -2.5 \ln(u_\tau/U_0) - 6.9 . \end{aligned} \quad (5.5)$$

Substitution of the values of u_τ/U_0 , obtained from the Preston tube measurements, into Eq. (5.5) yields $K = 1.00 (\pm 0.03)$ for the higher value of $U_{0,e}$ and $K = 0.90 (\pm 0.03)$ for the lower value of $U_{0,e}$. Hence, taking for K a mean value of 0.95, we find

$$\frac{U_0 - U}{u_\tau} = -2.5 \ln\left(\frac{y}{\delta}\right) + 0.95 , \quad (5.6)$$

which, as can be seen from Fig. 5.4, is in close agreement with the measured velocity profiles. Figure 5.4 also illustrates that the values of $(U_0 - U)/u_\tau$ are indeed slightly smaller at the lower than at the higher value of $U_{0,e}$. The close agreement between Eq. (5.6) and our experimental data proves that the latter are consistent with theory.

Finally we have compared our measured velocity profiles with some of the two-parameter velocity profiles presented in Chapter II, Section B. From the measured velocity profiles at the stations 6 and 7 we calculated the values of $\Delta U k / (2u_\tau \Pi)$ as a function of y/δ for both values of $U_{0,e}$. Here ΔU is the difference between the measured velocity U_m and the velocity U_{wall} calculated from the law of the wall, Eq. (5.2^c), implying $k = 0.4$. Π is Cole's profile parameter, defined in Eq. (2.101), which is equal to $0.2 (U_m^+ - U_{wall}^+)_{y=\delta}$. In Fig. 5.5 the results are compared with Cole's law of the wake, $w(y/\delta)$, for which we have taken the expression given by Hinze [22], Eq. (2.103), and also with the calculated values of $\Delta U k / (2u_\tau \Pi)$ from the velocity profile proposed by Sarnecki [117], given by Eqs. (2.112) and (2.113). The wide band round $w(y/\delta)$ represents the uncertainty in the value of $\Delta U k / 2u_\tau \Pi$ calculated from Cole's law of the wake, assuming an experimental uncertainty of one per cent in the measured velocities. From Fig. 5.5 we see that our experimental results agree with Cole's law of the wake within the experimental uncertainty and deviate widely from the profile proposed by Sarnecki. Hence, when applying a two-parameter velocity profile we recommend the use of the velocity profiles given by Eqs. (2.101), (2.103) and Eq. (2.108).

EXPERIMENTAL RESULTS

STATION No. $U_{0,e} = 6.13 \text{ m/s}$ $U_{0,e} = 10.10 \text{ m/s}$

7 \circ \diamond

6 \triangle \square

DISTRIBUTION CALCULATED FOR SARNECKI'S PROFILE, EQ.(2.112)

STATION No. $U_{0,e} = 6.13 \text{ m/s}$ $U_{0,e} = 10.10 \text{ m/s}$

7 \bullet \blacklozenge

6 \blacktriangle \blacksquare

— COLES' LAW OF THE WAKE, EQ.(2.103)

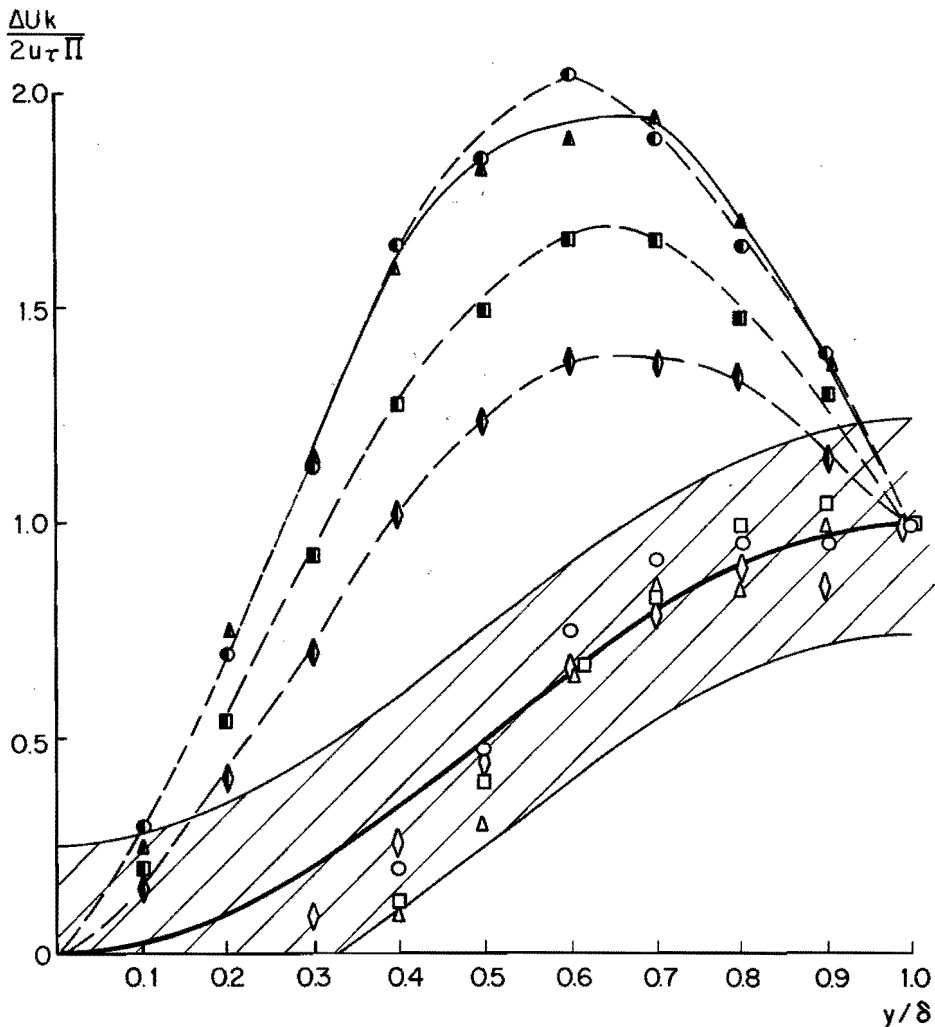


FIGURE 5.5 COMPARISON OF EXPERIMENTAL RESULTS WITH SOME PROPOSED TWO-PARAMETER VELOCITY PROFILES

B. The Mean Temperature Field

1. The Heat Flux Density at the Wall

The experimental values of $q_w(x)$ for both values of $U_{O,e}$ are presented in Fig. 5.6. They were obtained both from the electrical power supply to the main elements (method (a)) and from the measured mean temperature gradients in the viscous sublayer at the stations 3 to 7 (method (b)) (see Chapter IV, Section B.4.). The former q_w values were considered representative of the q_w value at the centre of a main element; those for the main elements 1 and 15 (see Fig. 4.7) have been disregarded because of the large heat losses to the unheated parts.

As the results of both methods showed a very satisfactory agreement, the less accurate method (c) described in Chapter IV, Section B.4. has not been applied.

For comparison, Fig. 5.6 also shows the values of $q_w(x)$ calculated by means of the Spalding method, assuming $Pr_t = 1$, and of Eq. (3.27), adopting for St the formula recommended by Reynolds et al. [129]:

$$St_x Pr^{0.4} [(T_w + T_f)/(T_o + T_f)]^{0.4} = 0.0296 Re_x^{-0.2}, \quad (5.7)$$

where $T_f = 273.15$ K is the Kelvin temperature of freezing water. For the application of the Spalding method, the quantity x^+ was calculated from Eq. (3.30) by assuming u_τ to be constant along the heated plate for both values of $U_{O,e}$. This assumption is justified by our measurements of $\tau_w(x)$ (see Fig. 5.1 and Table 5.1). We have used $u_\tau = 0.314$ m/s for $U_{O,e} = 6.13$ m/s and $u_\tau = 0.492$ m/s for $U_{O,e} = 10.10$ m/s. The corresponding values of $Sp(x^+, 0.71, 1)$ were calculated from the tables given by Gardner and Kestin [139] or for small x^+ values from Eq. (3.44), whereupon q_w was obtained by means of Eqs. (3.38) and (3.32).

The experimental and calculated values of q_w at the stations 3 to 7 are given in Table 5.2 together with the values of T_τ , calculated from the q_w values obtained from the measurements of the mean temperature in the viscous sublayer.

Table 5.2.

Survey of the values of q_w (W/m^2) and T_τ ($^\circ C$)
at the stations 3 to 7

$U_{O,e} = 6.13$ m/s, $T_w - T_o = 11.80$ $^\circ C$

Station No.	x^+	From electrical	From measured	Eqs. (3.27)	Spalding	T_τ
		heat supply	$(\partial T/\partial y)_{y=0}$	and (5.7)	method	
		q_w	q_w	q_w	q_w	
3	698	-	449	370	436	1.180
4	$2.79 \cdot 10^3$	330	343	317	343	0.981
5	$4.87 \cdot 10^3$	309	317	296	317	0.830
6	$9.05 \cdot 10^3$	288	293	277	293	0.765
7	$1.43 \cdot 10^4$	273	275	264	280	0.726

$U_{O,e} = 10.10$ m/s, $T_w - T_o = 10.80$ $^\circ C$

3	$1.102 \cdot 10^3$	-	575	501	575	0.955
4	$4.40 \cdot 10^3$	433	460	430	465	0.761
5	$7.70 \cdot 10^3$	417	412	404	430	0.681
6	$1.43 \cdot 10^3$	383	380	375	401	0.627
7	$2.25 \cdot 10^4$	362	354	357	375	0.588

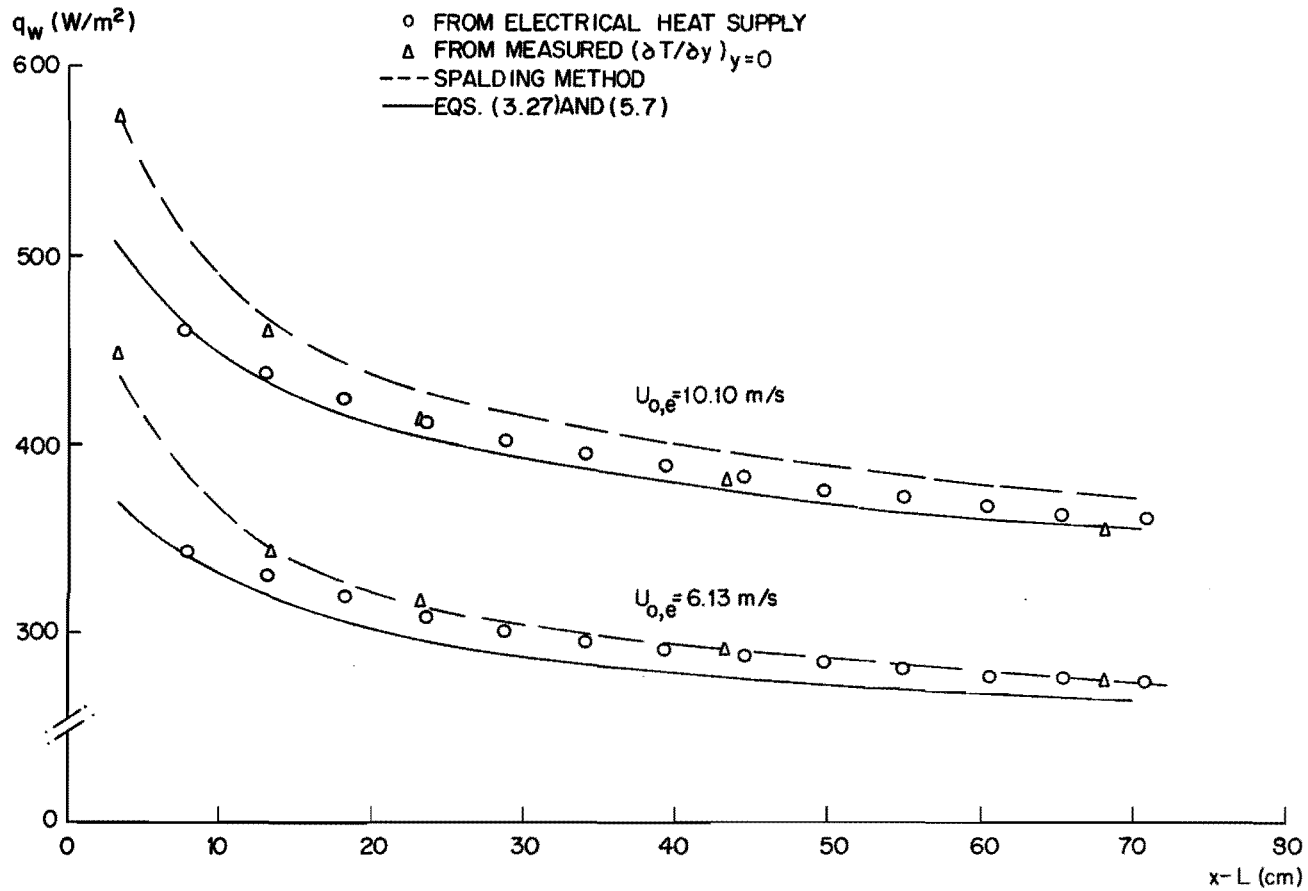


FIGURE 5.6 EXPERIMENTAL AND CALCULATED RESULTS FOR $q_w(x)$

From this table and Fig. 5.6 we see that at the stations 4 to 7 the experimental results of both methods agree within 3 per cent of the mean value, which is a very satisfactory result. For decreasing values of $x-L$ they show an increasing disagreement. We assume that in this region the q_w values obtained from the measurements of $(\partial T/\partial y)_{y=0}$ are the correct ones. This assumption is justified by the fact that the corresponding T_τ values also give rise to a correct behaviour of the measured $T^+(y^+)$ distributions at station 3 (see also the next section). The smaller q_w values obtained from the measured electrical power supply probably result from the heat loss to the unheated part of the plate at $x < L$, for which no correction has been applied.

We further see that the Spalding method gives a very satisfactory prediction of $q_w(x)$, particularly for the smaller values of $x-L$, for which the assumptions underlying the method are best fulfilled. The formula of Reynolds et al. leads to too low values of q_w for small values of $x-L$.

2. The Mean Temperature Profile

Mean temperature profiles $T(y)$ were measured with a temperature-sensing element* (see Chapter IV, Section B.5.) at the stations 3 to 7 for the two different values of $U_{0,e}$. The experimental results for $T^+(y^+)$ at $U_{0,e} = 6.13$ m/s are presented in Fig. 5.7 and those obtained at $U_{0,e} = 10.10$ m/s in Fig. 5.8. For the calculation of $T^+(y^+)$ from the measured profile $T(y)$, we have used the T_τ values given in Table 5.2. A complete survey of the measured distributions of $T^+(y^+)$ can be found in Table 2 of Appendix II.

The temperature profiles in Figs. 5.7 and 5.8 clearly show a developing character. For small values of y^+ all profiles are identical, but with increasing y^+ the mutual differences increase. At higher values of $x-L$ the profiles become identical for a wider range of y^+ values. The maximum value of T^+ , which is equal to $(T_w - T_0)/T_\tau$, becomes higher with increasing $x-L$, since T_τ decreases with $x-L$ (see Table 5.2). As the thickness of the thermal boundary layer increases with $x-L$, the maximum value of T^+ is reached for a lower value of y^+ at a smaller $x-L$ value. Moreover, the temperature profiles at the stations 4 to 7 show a linear relation between T^+ and $\ln y^+$ for a range of y^+ values within the fully turbulent part of the boundary layer.

In Fig. 5.7 we have compared the experimental results with some temperature profiles calculated from our measured velocity profile, Eq. (5.2), for Pr_t values of 1.0, 0.8 and 0.6, respectively. Assuming Pr_t to be constant, substitution of Eq. (5.2) into Eq. (3.9) yields upon integration of Eq. (3.7):

$$0 \leq y^+ \leq 5 : T^+ = Pr_t y^+ \quad (5.8^a)$$

$$5 < y^+ \leq 20 :$$

$$T^+ = 5.78 \ln \left[\frac{5.78 Pr_t^{-1} + Pr_t^{-1} (y^+ - 5.78)}{5.78 Pr_t^{-1} - 0.78 Pr_t^{-1}} \right] + 5 Pr_t \quad (5.8^b)$$

$$20 < y^+ \leq 300 :$$

$$T^+ = 2.5 Pr_t \ln(y^+/20) + (T^+)_{y^+=20} \quad (5.8^c)$$

The last equation was derived with the assumption $v_t \gg v$ and $a_t \gg a$. For the various values of Pr_t Eq. (5.8^c) reduces to

* These elements were developed by Nieuwvelt and coworkers [190].

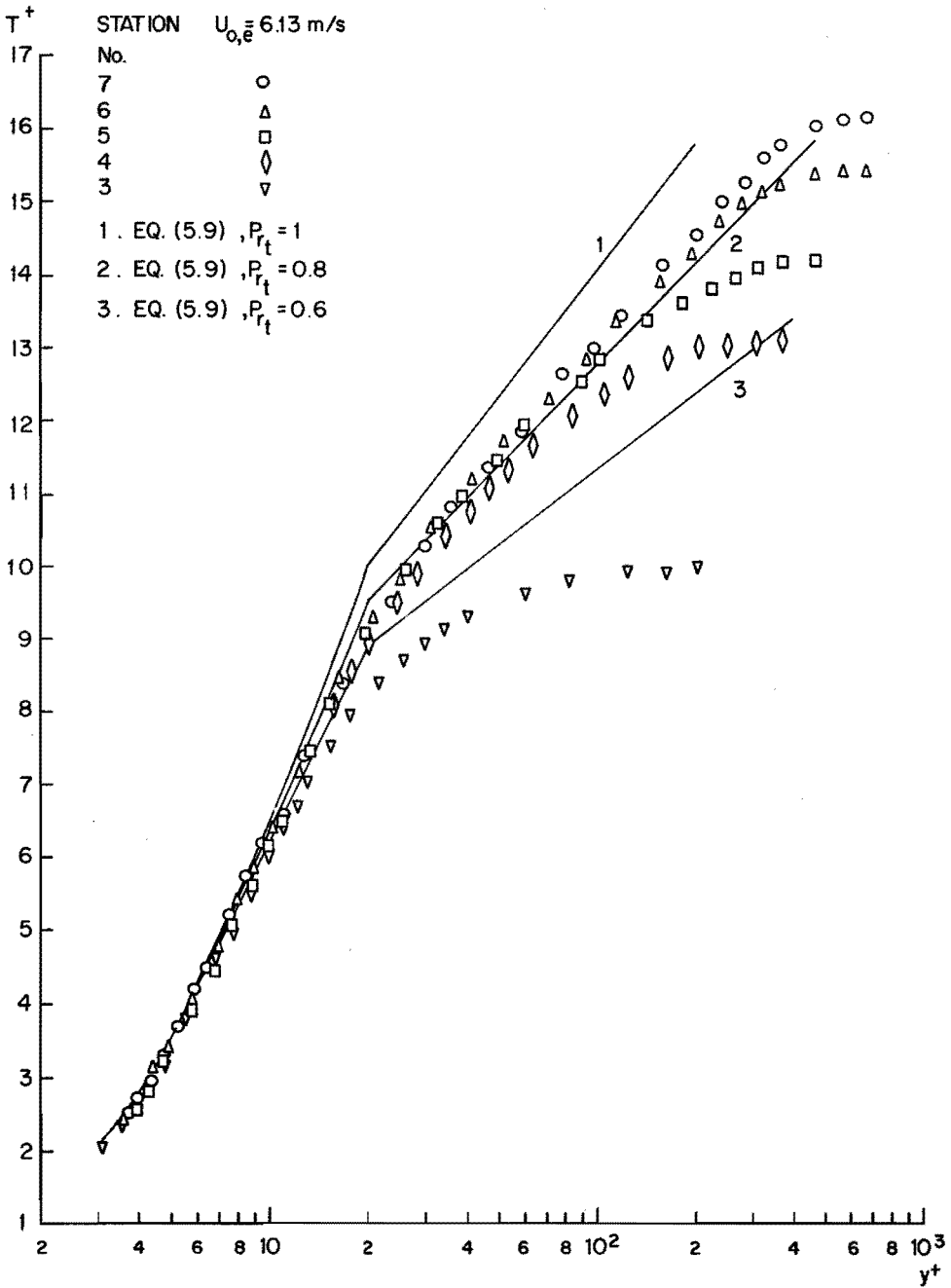


FIGURE 5.7 TEMPERATURE PROFILES FOR THE LOWER VELOCITY

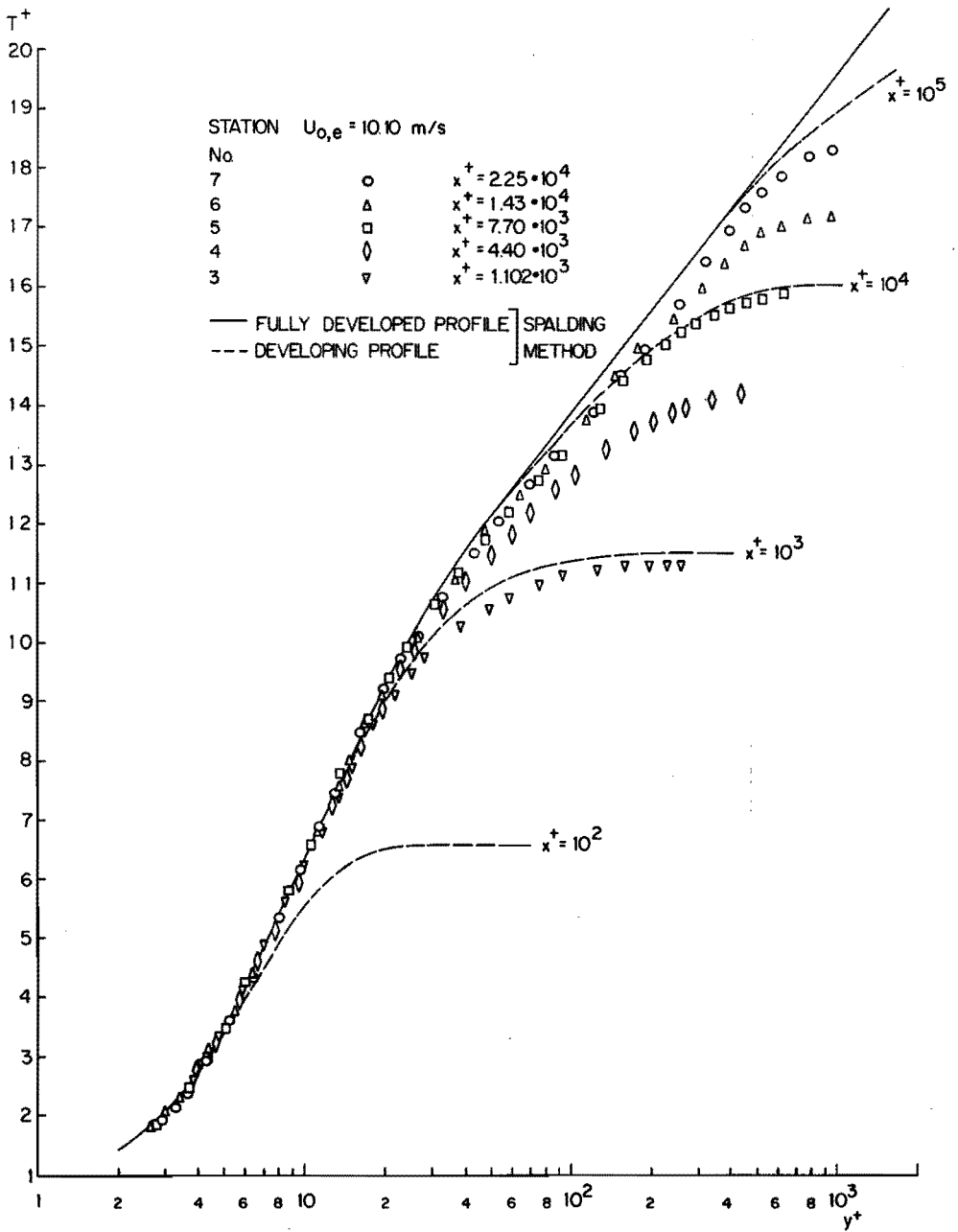


FIGURE 5.8 TEMPERATURE PROFILES FOR THE HIGHER VELOCITY

$$\left. \begin{aligned} \text{Pr}_t = 1 & : T^+ = 2.5 \ln y^+ + 2.46 \\ \text{Pr}_t = 0.8 & : T^+ = 2.0 \ln y^+ + 3.52 \\ \text{Pr}_t = 0.6 & : T^+ = 1.5 \ln y^+ + 4.41 . \end{aligned} \right\} (5.9)$$

From Fig. 5.7 it appears that Eq. (5.8^a) affords correct results for all profiles. For $y^+ > 5$ the assumption of $\text{Pr}_t = 1$ certainly does not lead to correct results. For the profiles at the stations 4 to 7 good agreement is obtained with Eq. (5.8^b) if we take $\text{Pr}_t =$ about 0.7. At these stations and for $y^+ > 30$ the measured profiles given in Figs. 5.7 and 5.8 were approximated by straight lines, yielding relations of the form

$$T^+ = A_T \ln y^+ + B_T . \quad (3.69)$$

From the resulting A_T values Pr_t was determined with the aid of Eq. (5.8^c). The data obtained are presented in Table 5.3 for both values of $U_{o,e}$.

Table 5.3.
Values of Pr_t from Eqs. (3.69) and (5.8^c)

Station No.	$U_{o,e} = 6.13 \text{ m/s}$			$U_{o,e} = 10.10 \text{ m/s}$		
	A_T	B_T	Pr_t	A_T	B_T	Pr_t
4	1.72	4.45	0.69	1.91	3.90	0.76
5	1.91	3.90	0.76	2.17	3.20	0.87
6	2.07	3.45	0.83	2.28	2.90	0.91
7	2.15	3.15	0.86	2.39	2.60	0.96

In Fig. 5.8 our experimental results are compared with the predictions of the Spalding method, which are based on the results published by Gardner and Kestin [139]. For $y^+ < 20$ the agreement between the calculated fully developed temperature profile and the measured ones is almost perfect. The fully developed temperature profile was determined from Eqs. (3.7), (3.8) and (3.35), assuming $\text{Pr}_t = 1$, which implies

$$\frac{a_t}{v} = kA \left\{ e^{ku^+} - 1 - ku^+ - \frac{(ku^+)^2}{2!} - \frac{(ku^+)^3}{3!} \right\} , \quad (5.10)$$

with $k = 0.4$ and $A = 0.1108$. From our measured velocity profiles we can derive, using Eq. (5.1),

$$\frac{v_t}{v} = kA \left\{ e^{ku^+} - 1 - ku^+ - \frac{(ku^+)^2}{2!} - \frac{(ku^+)^3}{3!} - \frac{(ku^+)^4}{4!} \right\} . \quad (5.11)$$

From Eqs. (5.10) and (5.11) we find for Pr_t

$$Pr_t = \frac{e^{ku^+} - 1 - ku^+ - (ku^+)^2/2! - (ku^+)^3/3! - (ku^+)^4/4!}{e^{ku^+} - 1 - ku^+ - (ku^+)^2/2! - (ku^+)^3/3!} \quad (5.12)$$

For y^+ (or u^+) $\rightarrow 0$ this implies

$$Pr_t \rightarrow \frac{k}{5} u^+ = 0.08 y^+ \quad (y^+ < 3) , \quad (5.13)$$

while for large values of y^+ we have $Pr_t \simeq 1$. The implications of Eq. (5.12) will be discussed in more detail in Section D.

Figure 5.8 also depicts some calculated temperature profiles for $x^+ = 10^2, 10^3, 10^4$ and 10^5 . It is seen that experimental and calculated profiles show similar distributions.

For a description of the temperature profiles in the outer region of the thermal boundary layer we have, in analogy with the velocity distribution, tried to find a power-law representation:

$$1 - \Theta = (y/\delta_T)^n \quad (5.14)$$

For the determination of δ_T we initially followed a procedure similar to that adopted to obtain δ (see Section A.3.). Accordingly, we introduced a "thermal displacement" thickness

$$\delta_{T,1} = \int_0^\infty \Theta dy , \quad (5.15)$$

which can easily be determined by integration of the measured temperature profile. From (5.14) and (5.15) it follows that

$$\delta_T = (1 + 1/n)\delta_{T,1} , \quad (5.16)$$

whence δ_T can be calculated from a known value of n . The temperature profiles at the different stations proved to give different values of n , for which to a good approximation a mean value of $n = 1/12$ could be taken. This value of n , however, led to values of δ_T far beyond the region where temperature fluctuations were observed. Therefore we have determined δ_T by plotting straight lines through the curves of θ' versus $\ln y^+$ in the outer region of the thermal boundary layer (see Fig. 5.12). The point of intersection of this line with the $\ln y^+$ axis was taken equal to $\ln(\delta_{T,u_T}/\nu)$. The results for $U_{O,e} = 10.10$ m/s are presented in Fig. 5.9, from which we see that Eq. (5.14) with $n = 1/12$ gives a good approximation of the measured temperature profiles for $y/\delta_T > 0.3$. The same result was obtained for the temperature profiles at $U_{O,e} = 6.13$ m/s. The values obtained for $\delta_{T,1}$ and δ_T are recorded in Table 2 of Appendix II.

We have finally compared our measured temperature profiles with the universal temperature distribution proposed by Persen [143], Eq. (3.59). This comparison is represented in graph form in Fig. 5.10, which clearly shows that Persen's assumption is not correct.

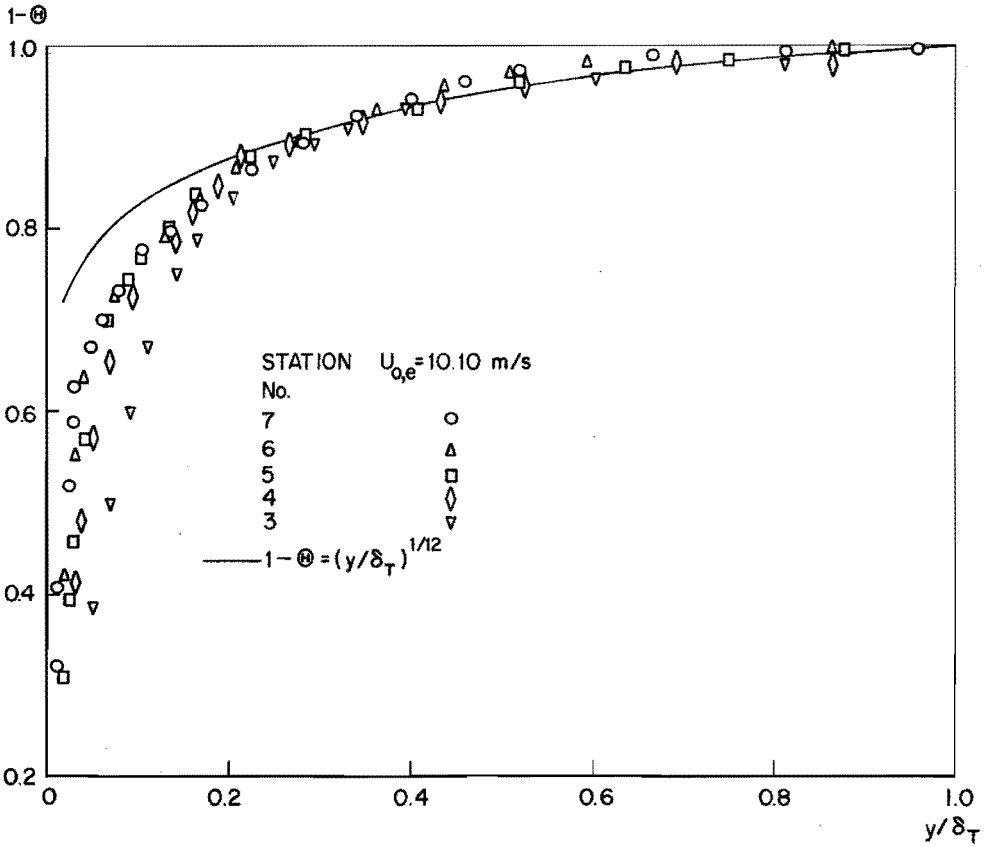


FIGURE 5.9 THE POWER-LAW TEMPERATURE PROFILE

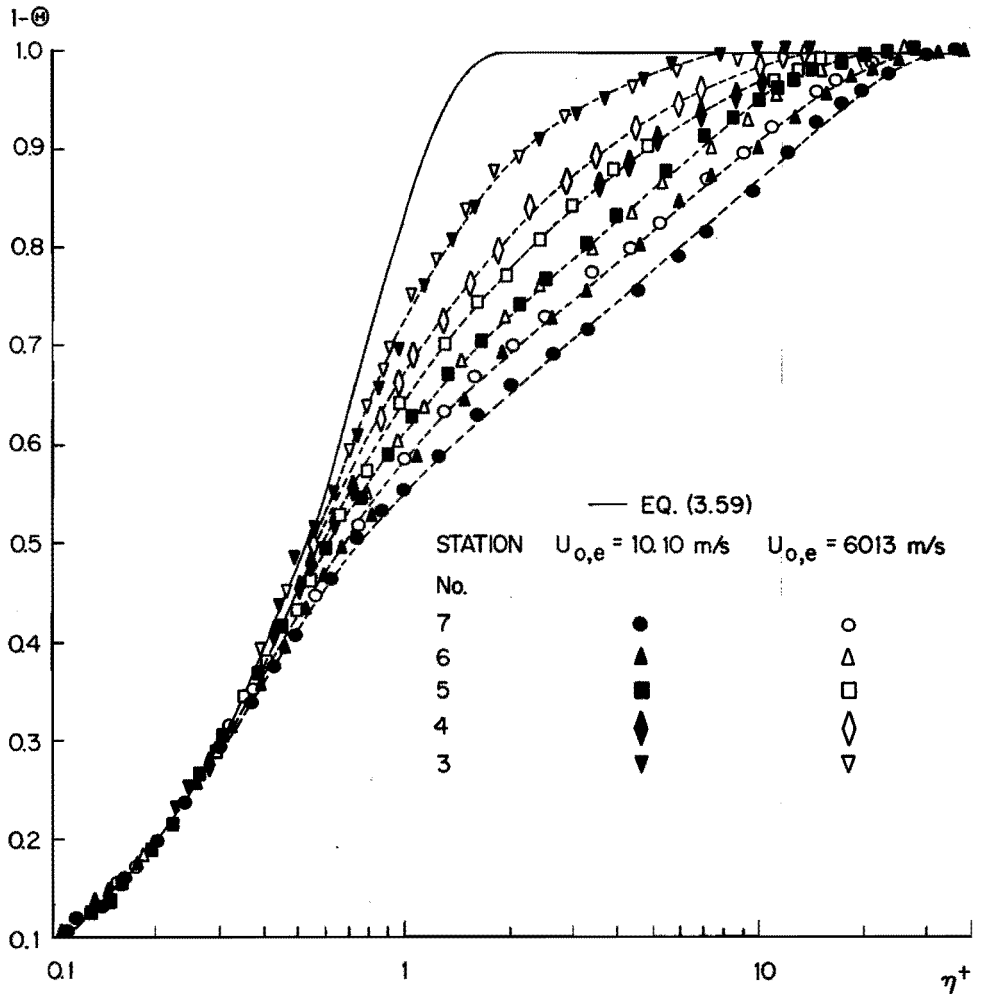


FIGURE 5.10 COMPARISON OF EXPERIMENTAL RESULTS WITH THE UNIVERSAL TEMPERATURE PROFILE OF PERSEN [143]

C. The Turbulent Quantities

1. The Longitudinal Turbulent Intensity

In addition to the measurements of $U(y)$ we have also determined the distributions of $u'(y)$. Figure 5.11 represents the distributions of $u'(y^+)/u_\tau$ at the measuring stations 5, 6 and 7 for both values of $U_{0,e}$. Those at the other stations were of a similar pattern. As can be seen from Fig. 5.11, our experimental results give a universal distribution of $u'(y^+)/u_\tau$ for $y^+ < 100$. This was to be expected since in the wall region, as pointed out by Townsend [40,49], the turbulent boundary layer has a universal structure, also resulting in a universal relation $u^+(y^+)$. A further point is that $u'(y^+)$ reaches a maximum in the region $10 < y^+ < 20$, which happens to be the region where the production of the turbulent kinetic energy reaches a maximum, in conformity with the flow structure emerging from the flow visualization studies by Kline et al. [86] and Corino and Brodkey [95] (see also Chapter II, Section B.1.1.). For larger values of y^+ different distributions of $u'(y^+)/u_\tau$ were found, due to the differences in boundary layer thickness at the various measuring stations.

2. The Intensity of the Turbulent Temperature Fluctuations

In addition to the distributions of $T^+(y^+)$ we have also measured the distributions of $\theta'(y^+)$ at the same places in the thermal boundary layer, using the same temperature-sensing elements. Figure 5.12 represents the experimental values of $\theta'(y^+)$ for all measuring stations along the heated plate at $U_{0,e} = 10.10$ m/s. Those obtained at $U_{0,e} = 6.13$ m/s showed a similar distribution. From Fig. 5.12 we see that the distribution of $\theta'(y^+)$ is analogous to that of $u'(y^+)$, giving a universal relation for small values of y^+ . This is not surprising, since the temperature fluctuations owe their existence entirely to velocity fluctuations, which also showed a universal distribution for small values of y^+ (see Fig. 5.11). The distributions of $\theta'(y^+)$ pass through a maximum in the region $10 < y^+ < 20$, which is also in accordance with the behaviour of $u'(y^+)$. Owing to the differences in δ_T at the various stations different distributions of $\theta'(y^+)$ are obtained in the outer region of the thermal boundary layer. It can be seen from Fig. 5.12 that in this region the $\theta'(y^+)$ distributions can be approximated reasonably well by straight lines, a feature which was used for the determination of δ_T (see Section B.2.).

In conclusion we remark that, in analogy with the experimental results of Johnson [155], we also observed intermittency of the temperature fluctuations in the outer region of the thermal boundary layer. This means that there is a sharp line of demarcation between heated and unheated parcels of air. However, at these places the velocity field was still fully turbulent, which can be interpreted as an experimental proof that in the outer region of a developing thermal boundary layer the distributions of uv and $v\theta$ differ.

3. The Spectra of Temperature and Velocity Fluctuations

In Fig. 5.13 we present some spectra of the velocity and temperature fluctuations, measured at station 7 for $U_{0,e} = 6.13$ m/s and at different values of y^+ . These spectra merely serve as a further illustration of the characteristics of the fluctuating quantities. They were obtained by means of a frequency analyser (Brüel and Kjaer, Type 2107) together with a band-pass filter set (Brüel and Kjaer, Type 1612), equipped with 33 filters ranging from 25 to 40,000 Hz with a band width of 1/3 octave. From our measurements we have calculated the distribution functions $E_u(n)$ and $E_\theta(n)$, defined by the conditions that $E_u(n)dn$ and $E_\theta(n)dn$ are the contributions to $(u')^2$ and $(\theta')^2$, respectively, of the frequencies between n and dn .

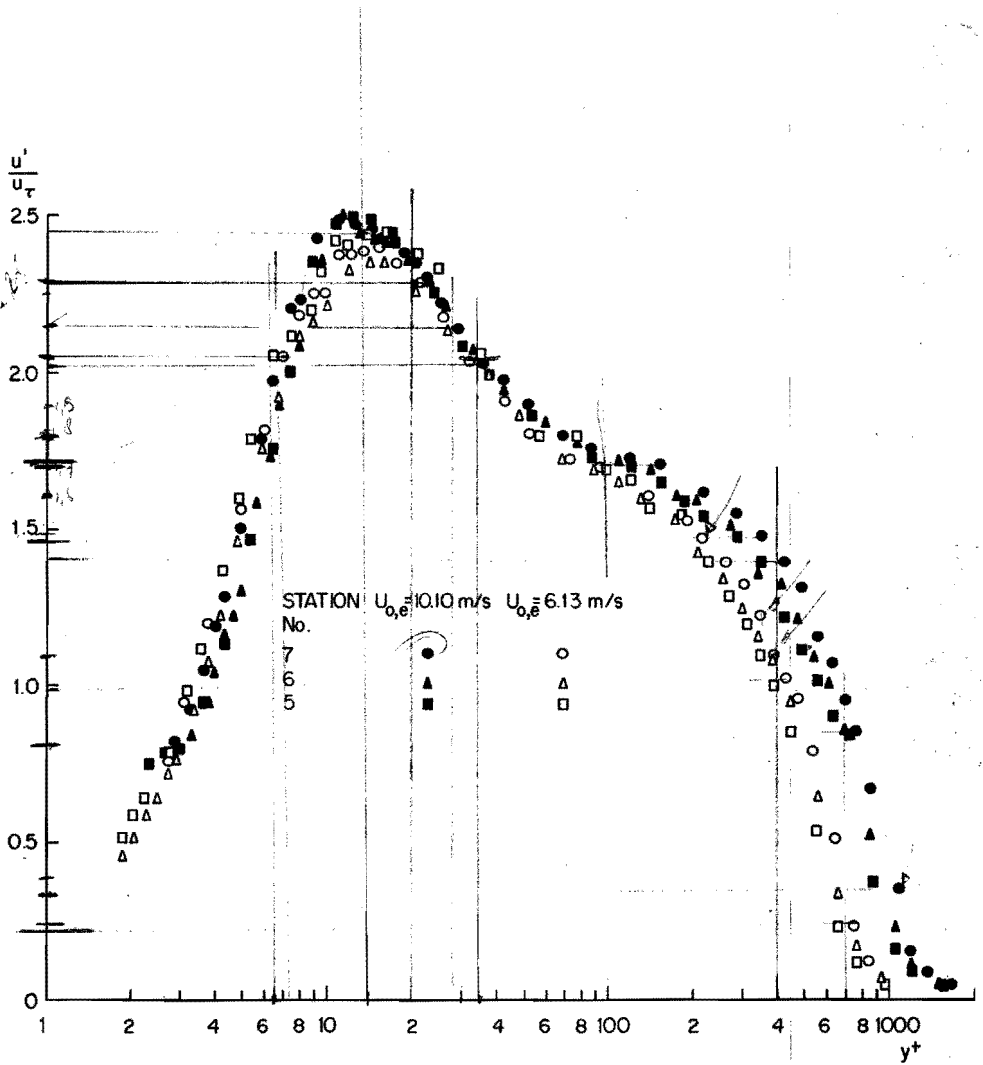


FIGURE 5.11 DISTRIBUTIONS OF THE LONGITUDINAL TURBULENT INTENSITY

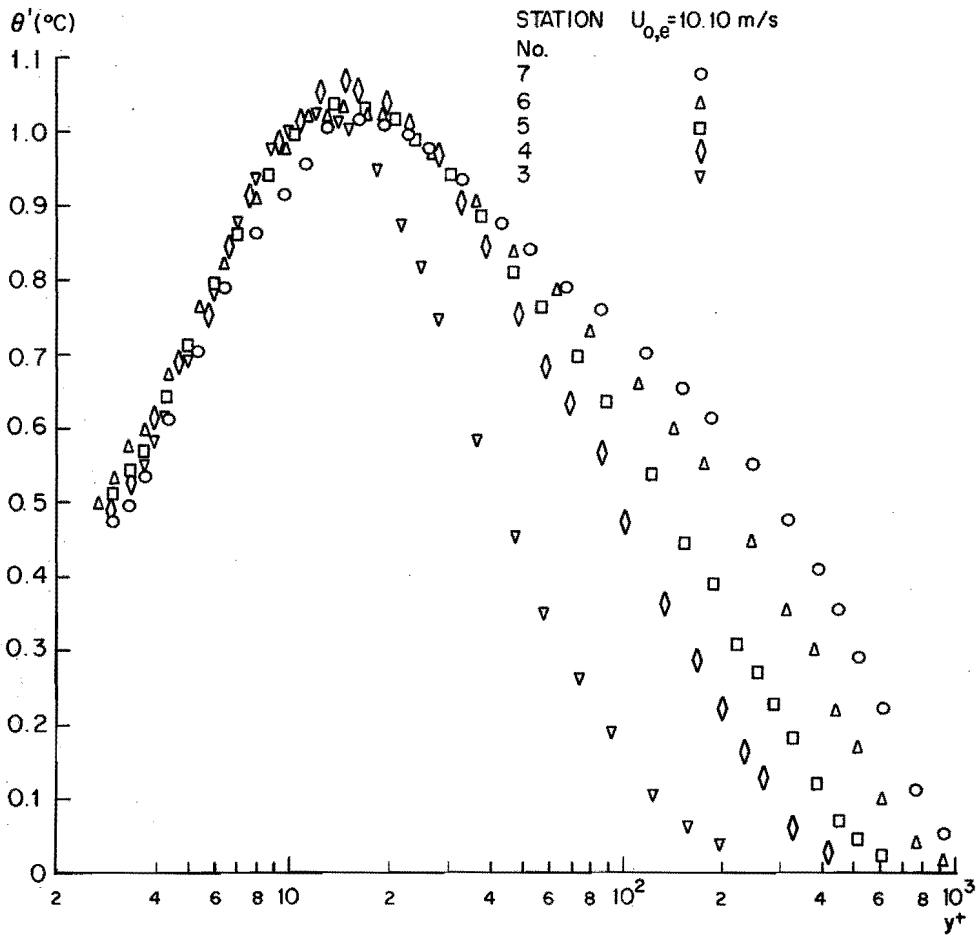


FIGURE 5.12 DISTRIBUTIONS OF THE INTENSITY OF THE TURBULENT TEMPERATURE FLUCTUATIONS

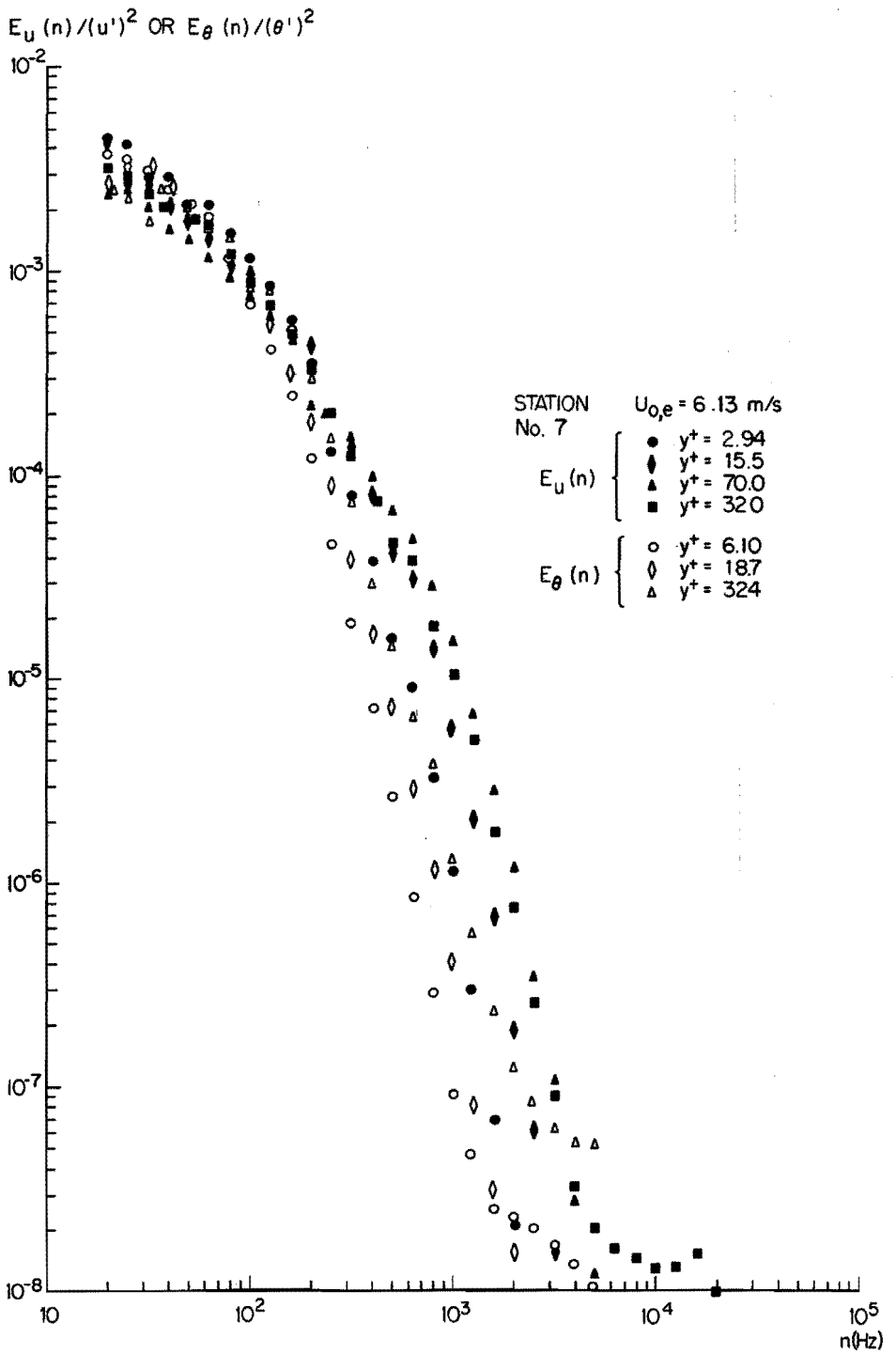


FIGURE 5.13 SPECTRA OF VELOCITY AND TEMPERATURE FLUCTUATIONS

It appears that the distributions of $E_u(n)$ and $E_\theta(n)$ are very similar. The greater deviations between them at higher frequencies are caused by the larger time constant of the temperature measuring system (about 1 ms as compared with about 2 μ s for the hot-wire anemometer). As the spectra were only recorded to provide additional information concerning the fluctuating quantities, no correction has been applied for the inertia of the measuring systems.

4. The Quantities \overline{uv} and $\overline{v\theta}$

The distributions of the quantities \overline{uv} and $\overline{v\theta}$ have been measured at stations 6 and 7 for both values of $U_{0,e}$. A detailed description of the measuring techniques employed can be found in Chapter IV, Sections B.3. and B.6. However, as the wires are in a plane perpendicular to the flat plate, owing to the X-probe configuration, the velocity distribution along the wire is no longer uniform and corrections must be applied for the effect of the wire length. Moreover the wires do not measure the turbulent fluctuations at the same point, since they are at a certain distance (about 0.3 mm) from one another. Because of these two effects, values of \overline{uv} and $\overline{v\theta}$ deduced from the measured voltage fluctuations by means of the equations given in Chapter IV are too low. In general, the magnitude of the effects is determined by the auto- and intercorrelation functions that hold for the fluctuating quantities involved (see also Hinze [22]).

In order to get an impression of the behaviour of the correction functions needed, we have also measured the distributions of u' and θ' at stations 6 and 7 with single-wire probes, having their axis in the y-direction. Comparison of the results with those presented in Sections C.1. and C.2. showed that in this way smaller values of u' and θ' were indeed obtained. However, we also observed that a constant correction factor could be applied to match the results of both methods: the experimental results for u' and θ' had to be multiplied by 1.12 ± 0.02 to obtain agreement with those presented in Sections C.1. and C.2.

We have interpreted this result as a justification for applying a constant correction factor to the experimental results of \overline{uv} and $\overline{v\theta}$. For the quantity \overline{uv} the correction factor was determined by matching the maximum value of $-\overline{uv}$, obtained experimentally, with the one calculated from the measured mean velocity distributions. An analogous procedure was used to find the correction factor for $\overline{v\theta}$.

The correction factors for $-\overline{uv}$ and $\overline{v\theta}$ were only determined at one measuring station at the higher value of $U_{0,e}$, and were taken as constants for the particular probe configuration, in accordance with the results mentioned above for the measurements of u' and θ' with different wire orientations. After correction with these factors, in our case 1.41 and 1.54 respectively, the values of $-\overline{uv}$ and $\overline{v\theta}$ at measuring stations other than the one at which the correction factors were determined, also fitted in with the distributions calculated from the measured mean quantities.

The corrected experimental results of $-\rho\overline{uv}$ and $\rho c_p \overline{v\theta}$ at station 7 for both values of $U_{0,e}$ are presented in Fig. 5.14. Those obtained at station 6 showed a similar distribution. The measured distributions of v' had the same characteristics as those reported by other investigators, for instance those of Klebanoff [36] and Laufer [37]. We also remark that the distributions of u' , v' and \overline{uv} were measured both with the heated plate at a temperature T_0 and at a temperature T_w . Within the experimental accuracy, the measured distributions of u' , v' and \overline{uv} turned out to be identical under both conditions. This can be interpreted as an experimental proof that the temperature difference $T_w - T_0$ applied was small enough to have a velocity field unaffected by the presence of the temperature field.

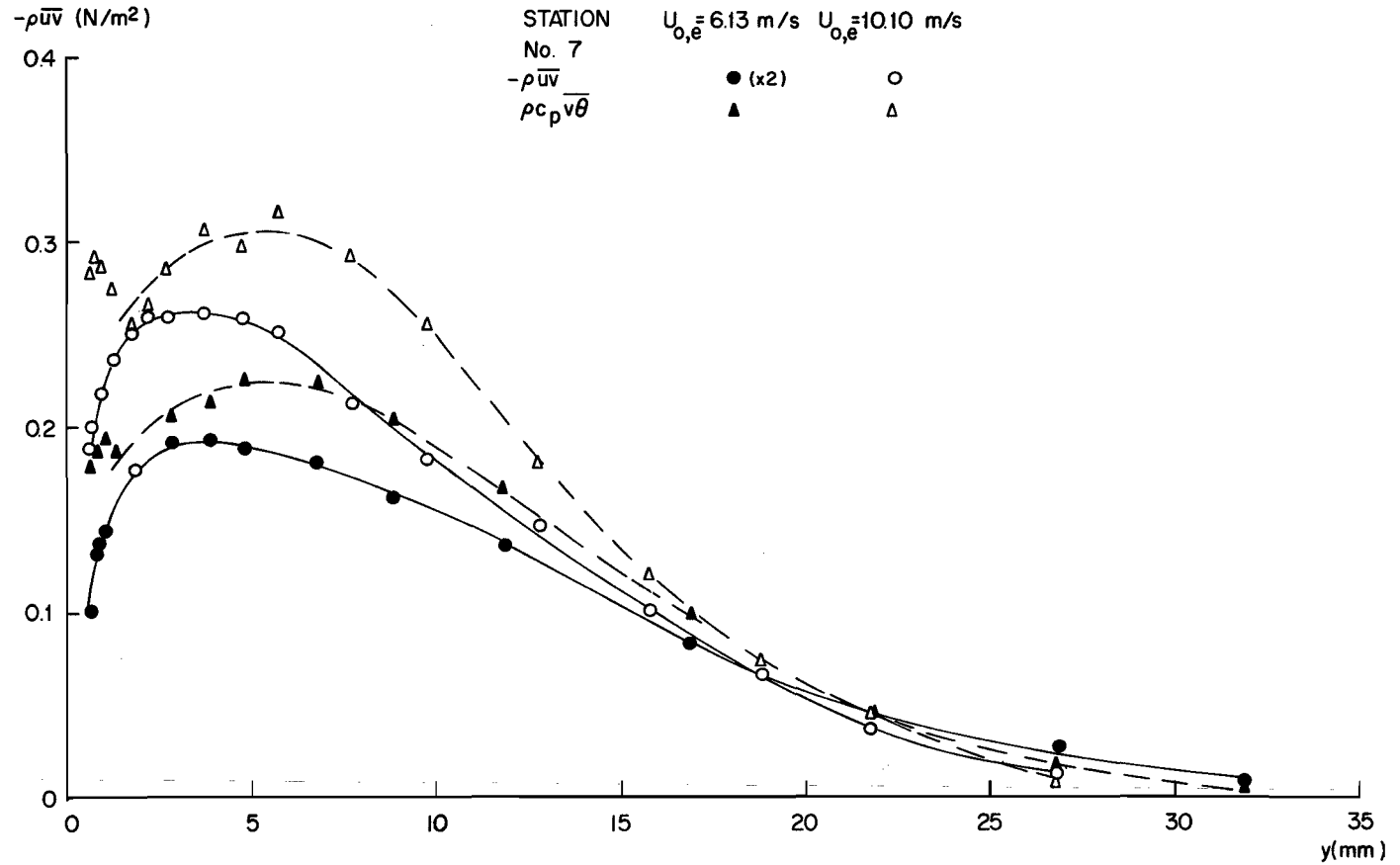


FIGURE 5.14 DISTRIBUTIONS OF THE TURBULENT HEAT AND MOMENTUM TRANSFER AT STATION 7

D. The Distribution of Pr_t

From the experimental results given above we have calculated the distributions of Pr_t, applying both methods mentioned in Chapter I, Section B. To this end we calculated the distributions of du⁺/dy⁺ from the experimentally verified Eq. (2.101). For the inner region of the thermal boundary layer the distributions of ∂T⁺/∂y⁺ were obtained from the analytical approximations of T⁺(y⁺) presented in Section B, while for larger y⁺ values they were determined graphically. For the application of method (b) the distributions of τ(y) and q(y) were computed by integration of Eqs. (1.1) and (1.3), respectively, with substitution of the experimentally determined distributions for U(x, y), T(x, y) and dp/dx.

For the inner regions of the velocity and temperature boundary layers τ(y) and q(y) were determined from the universal distributions u⁺ = f(y⁺) and T⁺ = g(y⁺). With the application of the boundary conditions τ = τ_w for y⁺ = 0 and q = q_w for y⁺ = 0, respectively, we obtain

$$\tau = \tau_w + y \frac{dp}{dx} + \frac{\nu}{u_\tau} \frac{du_\tau}{dx} \int_0^{y^+} [f(y^+)]^2 dy^+ \quad (5.17)$$

and

$$q = q_w + \nu \frac{d(q_w/u_\tau)}{dx} \int_0^{y^+} f(y^+)g(y^+)dy^+ . \quad (5.18)$$

For the outer regions of both layers the power-law representations of T(y) and U(y) were used, cf. Eqs. (5.3) and (5.14) respectively. Upon integration of Eqs. (1.1) and (1.3), with the boundary conditions τ = 0 for y = δ and q = 0 for y = δ_T, we find

$$\tau = \frac{U_o m^2 \rho A_1}{(m+1)(m+2)} \left[y \left(\frac{y}{\delta} \right)^{2/m} - \delta \right] + \frac{dp}{dx} (y - \delta) , \quad (5.19)$$

with m = 6.75 and

$$A_1 = \frac{dU_o}{dx} - \frac{U_o}{m\delta} \frac{d\delta}{dx} , \quad (5.19^a)$$

and

$$q = \frac{\rho c_p S n m}{n+m} \left(\frac{\delta_T}{\delta} \right)^{1/n} \left[1 - \left(\frac{y}{\delta_T} \right)^{1+n^{-1}+m^{-1}} \right] , \quad (5.20)$$

with n = 12 and

$$S = \frac{U_o}{\delta_T} \frac{d\delta_T}{dx} + A_1 \frac{n}{n+1} . \quad (5.20^a)$$

In these equations the quantities A₁ and S were determined from the measured distributions of δ(x) and δ_T(x).

Figure 5.15 gives the results of method (b) for U_{o, e} = 10.10 m/s. We have only represented the Pr_t values for those y values for which the uncertainty of Pr_t is less than 10 per cent. Consequently, Pr_t values for y/δ_T > about 0.7 are not represented, since for these larger distances from the wall the calculated values of ∂T⁺/∂y⁺ are too inaccurate. Besides, for the calculation

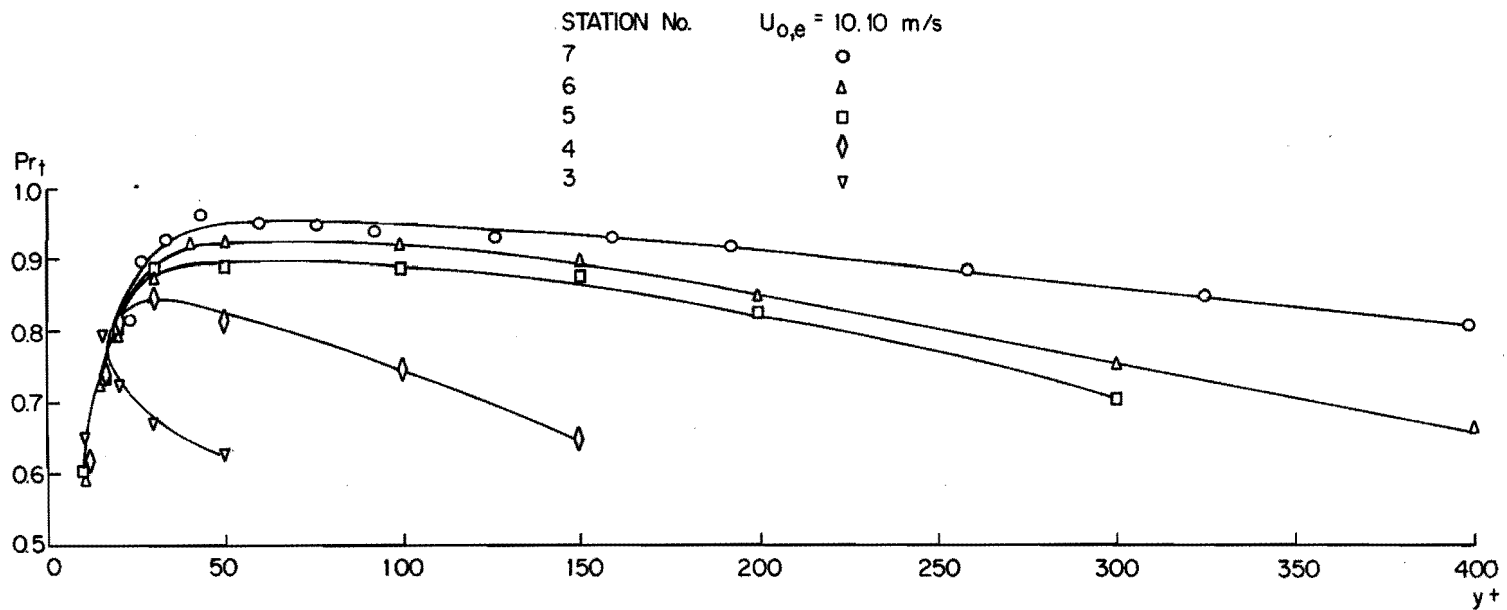


FIGURE 5.15 DISTRIBUTIONS OF Pr_t CALCULATED FROM THE MEASURED MEAN QUANTITIES

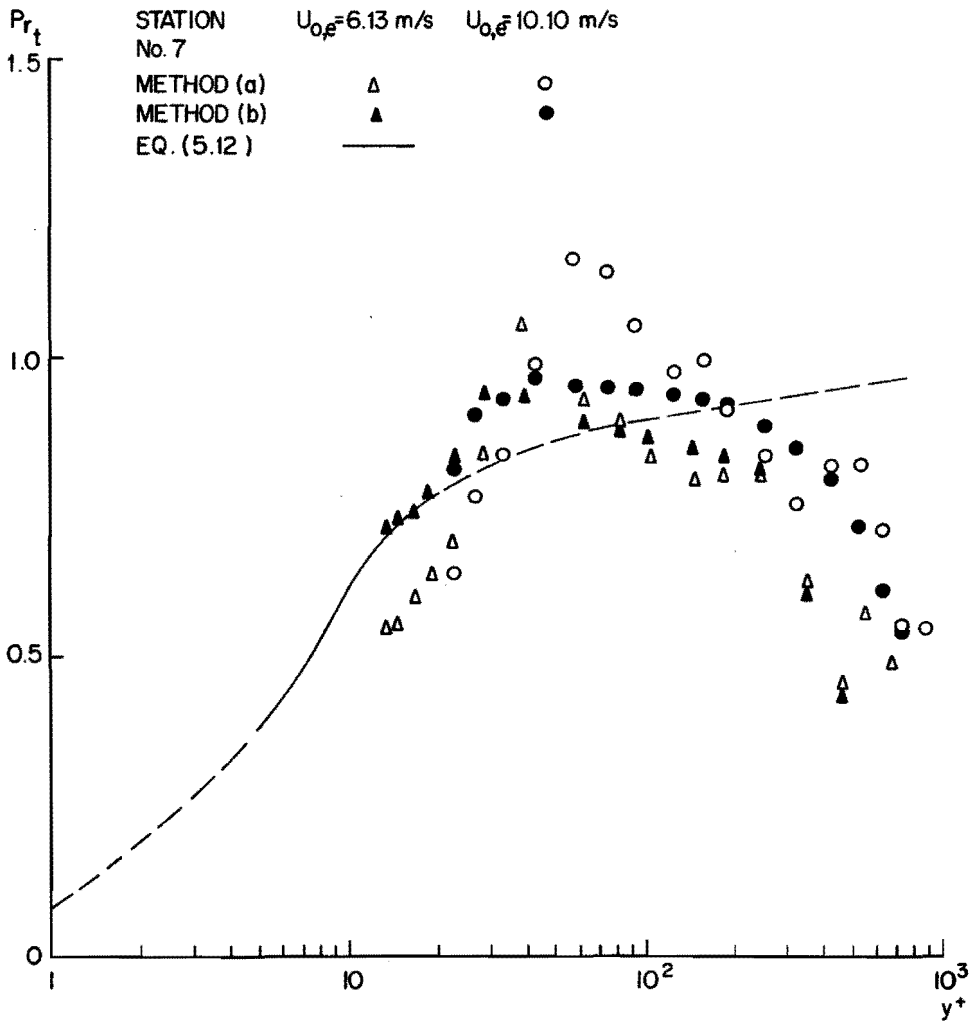


FIGURE 5.16 COMPARISON OF Pr_t VALUES CALCULATED FROM THE MEASURED MEAN AND TURBULENT QUANTITIES

of heat transfer the distribution of Pr_t in the outer region of the thermal boundary layer is of secondary importance, because the largest resistance to heat transfer is concentrated in the inner region (except for very small values of Pr). From Fig. 5.15 we see that the distributions of Pr_t , like those of $T^+(y^+)$, are of a developing character. For small values of y^+ there is a close agreement between the Pr_t values at the various measuring stations. In general, Pr_t increases with increasing y^+ for small y^+ values, is nearly constant for a certain range of intermediate y^+ values, and decreases again in the outer region of the thermal boundary layer. The above-mentioned constant values of Pr_t are in close agreement with those of Pr_t presented in Table 5.3. The distributions of Pr_t for $U_{0,e} = 6.13 \text{ m/s}$ showed the same characteristics.

Figure 5.16, finally, depicts the distributions of Pr_t calculated from the experimental results of \overline{uv} and $\overline{v\theta}$ at station 7 for both values of $U_{0,e}$. In order to get an impression of the reliability and accuracy of the results, we have included the values of Pr_t , calculated by means of method (b). Considering that the uncertainty in the determined Pr_t values is about 10 per cent, the agreement between the results of the two methods is satisfactory.

In Fig. 5.16 we have also represented the distribution of Pr_t according to Eq. (5.12). For increasing values of y^+ this relation shows a good link with the other Pr_t values given. One must bear in mind that Eq. (5.12) only presents an experimental relation between the measured mean velocity and temperature profiles which holds in particular for the interval $5 < y^+ < 20$. For larger y^+ values, it may be assumed to hold only when the temperature field is fully developed, a situation which was not attained in the present investigation.

E. Concluding Remarks and Suggestions for Future Research

The experimental results presented above have clearly shown that Pr_t is not a constant across the thermal boundary layer but a function of the distance from the wall. For a developing thermal boundary layer it is also a function of the distance from the origin of the thermal boundary layer. However, in the developing thermal boundary layer we can distinguish a region adjacent to the wall where the mean temperature profile is identical with that of the fully developed thermal boundary layer (see Figs. 5.7 and 5.8). In this region the temperature field can be considered to be fully adapted to the local heat transfer situation, while outside this region - let us call it the adapted region - the thermal boundary layer is greatly influenced by upstream heat transfer conditions.

As in the inner region of the velocity boundary layer the turbulent flow field has a universal structure (see, for instance, the distributions of $u'(y^+)$ given in Fig. 5.11), and since the temperature fluctuations owe their existence to the presence of the turbulent flow field, we must expect that in the adapted region of the thermal boundary layer the turbulent temperature field also has a universal structure. This is indeed confirmed by our measurements of the turbulent temperature fluctuations (see Fig. 5.12). In consequence, a universal distribution of a_t and hence of Pr_t can exist only in the adapted layer, which is again confirmed by our experimental values of Pr_t (see Fig. 5.15).

Recapitulating, the turbulent Prandtl number can only be expected to have a universal distribution in the inner region of a fully developed thermal boundary layer and for a developing thermal boundary layer only in those parts of the inner region which are already fully adapted to the local heat transfer situation. For the calculation of heat transfer the distribution of Pr_t in the inner region is also of primary importance, since this region is the seat of the main resistance for heat transfer (provided that Pr is not much smaller than unity).

No universal distribution of a_t can be expected in the outer region of the thermal boundary layer, where the temperature field is greatly dependent on upstream heat transfer conditions. In this region, therefore, Pr_t is not a physically meaningful quantity and the experimental values represent only an experimental relation between the heat and momentum transfer.

With regard to the universal Pr_t distribution in the inner region of the thermal boundary layer, for which Eq. (5.12) can be taken as a first approximation, it can be explained why in general $Pr_t < 1$. If we take a closer look at the equations describing the distributions of the turbulent quantities of the velocity and temperature fields, Eqs. (2.9) and (3.60), we distinguish a mechanism for turbulent momentum transfer, which is lacking for turbulent heat transfer, namely the action of pressure fluctuations, represented by the term $\bar{p}'v'$. By the action of pressure fluctuations in a turbulent flow field, turbulent kinetic energy is transferred from the larger velocity fluctuation components to the smaller ones, thus giving the flow a tendency to isotropy (see also Rotta [27]). Since in a turbulent boundary layer u' is larger than the other fluctuating velocity components v' and w' , it follows that there is a loss of the x-component of momentum due to the influence of the pressure fluctuations. Consequently, thinking in terms of mixing lengths, we might expect the mixing length for heat transfer to be larger than that for momentum transfer, which leads to $Pr_t < 1$. In this way the variation of Pr_t across the boundary layer can be explained by a variation of the action of the pressure fluctuations across the boundary layer. Future research on the distribution of the pressure fluctuations and their correlation with velocity fluctuations will thus be very valuable for a better insight into the mechanism of momentum transfer.

To verify the hypothesis of a universal distribution of Pr_t in the inner region of a thermal boundary layer, further research is needed with regard to the turbulent structure of the thermal boundary layer under various flow conditions. In this connexion measurements of Pr_t for the thermal boundary layer, both fully developed and developing, in severely accelerating and decelerating velocity boundary layers are of great value.

Finally, instead of introducing a turbulent conductivity relating a mean quantity to a turbulent one (Eq. (1.8)), we might expect to obtain more universally valid relations by connecting a turbulent quantity to another turbulent one. This has been proposed by Bradshaw [52] (see Eqs. (3.61^{a,b,c})). From considerations of this kind it follows that further experiments concerning correlation between turbulent velocity and temperature fluctuations are needed, for instance the determination of $\overline{\theta^2 v}$.

SUMMARY AND CONCLUSIONS

The present thesis deals with the heat transfer in a turbulent boundary layer. Experiments have been carried out in a wind tunnel with air flowing over a partially heated, aerodynamically smooth, flat plate.

As convective heat transfer can only be described if the velocity field is known, we have given in Chapter II a survey of the existing theories concerning the velocity field together with the momentum transfer implied. Special attention is given to new developments which have become possible by the application of large computers for solving the equations of motion. Among the solution methods discussed the so-called differential methods are to be preferred, in particular that given by Bradshaw, which starts from a universal relation between the turbulent momentum transfer and the other turbulent quantities.

Chapter III deals with the existing theories concerning the temperature field and the heat transfer implied. Essentially, these theories are based on a known solution of the velocity field, and the energy equation can be solved via the introduction of an assumption concerning the value of Pr_t . Usually one assumes $Pr_t = 1$ or $Pr_t = \text{constant}$. A review of published experimental values of Pr_t , however, demonstrates that these assumptions for Pr_t are incorrect. The various experimental results, besides being few in number, show a large scatter. Hence, there is a distinct need for an accurate determination of the distribution of Pr_t within a thermal boundary layer. This has led to our experimental investigation, in which we have tried to determine the distribution of Pr_t as accurately as possible. We have made extensive measurements of all quantities that are necessary for a full description of the velocity and the temperature field. In this way it is possible to determine the distribution of Pr_t from the experimental results by means of two independent methods.

The experimental set-up and the measuring techniques are described in Chapter IV. In order to get an impression of the reliability and accuracy of the measurements, various quantities have been determined with different, mutually independent methods. For the measurements of the flow field we employed the well-known hot-wire techniques, paying special attention to the accurate determination of the various turbulent quantities. Mean and fluctuating temperatures were measured with the aid of new temperature-sensing elements, developed in the laboratory where the present investigation was performed. In our experiments the applicability of these elements was investigated.

In a wind tunnel measurements were carried out on the velocity and the temperature field for the flow of air along a flat plate, part of which was heated to a uniform temperature, T_w , being higher than that of the free stream, T_0 . The free stream velocity at the entrance of the test section was maintained at constant values of 6.13 m/s and 10.10 m/s, respectively, with corresponding temperature differences, $T_w - T_0$, of 11.80 °C and 10.80 °C. In Appendix II and Chapter V the experimental results are presented in tables and in graphical form, and compared with existing theories.

The experimental values for the distribution of the skin friction agree within three per cent for the different methods applied. The mean velocity profiles of the velocity field are in good agreement with the existing theories, while the distribution of the turbulent velocity fluctuations confirms the existence of a universal structure of the turbulent flow field for the inner region of the boundary layer.

In the outer region of the velocity boundary layer, the experimental results show a close agreement with the velocity profile put forward by Coles, while large discrepancies occur with the two-parameter velocity profile given by Sarnecki. Within the transition region, $5 < y^+ < 25$, the measured velocity profiles are excellently described by Spalding's velocity profile, provided a small correction is applied, as indicated in Eq. (5.1).

Except for the measuring station close behind the origin of the thermal boundary layer, the measured distributions of the heat flux at the wall, obtained by means of different measuring techniques, agree mutually within three per cent. The measured heat flux proves to accord well with Spalding's theory, in particular close behind the step-wise discontinuity in wall temperature.

The new temperature-sensing elements have given a very satisfactory performance and the measured differences between the mean temperatures, $T-T_0$, are accurate within 0.03 °C. Because of the very small dimensions of the elements it was also possible to carry out accurate measurements within the viscous sublayer, without any corrections for the effects of conduction or radiation being necessary.

The measured mean temperature profiles clearly show the development of the thermal boundary layer with increasing distance from its origin. Adjacent to the wall a so-called adapted layer can be distinguished, in which the distributions of $T^+(y^+)$ and $\theta^+(y^+)$ have a universal character. The temperature profile of this adapted layer is in excellent agreement with the fully developed temperature profile of Spalding with the assumption $Pr_t = 1$. From this distribution of the mean temperature profile and the corrected velocity profile mentioned above, we have derived the following approximate expression for the distribution of Pr_t in the transition region:

$$Pr_t = \frac{e^{ku^+} - 1 - ku^+ - (ku^+)^2/2! - (ku^+)^3/3! - (ku^+)^4/4!}{e^{ku^+} - 1 - ku^+ - (ku^+)^2/2! - (ku^+)^3/3!} \quad (5.12)$$

If we assume this equation also to be valid within the viscous sublayer, we find for $y^+ < 4$: $Pr_t = 0.08 y^+$. Substitution of this relation into the heat transfer theories of Spalding and Jayatilke, instead of the assumption $Pr_t = 1$ used by them, results for large values of Pr in the relation $Nu \propto Pr^{1/3}$ instead of $Nu \propto Pr^{1/4}$, which accords better with the experimental heat and mass transfer results.

The distributions of Pr_t in the thermal boundary layer were determined both from the measurements of the mean quantities and from those of uv and $v\theta$. The results of both methods agree well within the experimental uncertainty (10%). The experimental values of Pr_t clearly show that Pr_t is not a constant, but a function of the distance from the wall. Also, for the developing thermal boundary layer the distribution of Pr_t shows a developing character.

The implications of these results are extensively discussed in Chapter V, Section E. Recapitulating, we can state that the distribution of Pr_t can only be universal for the inner region of a fully developed thermal boundary layer, in which region the turbulent flow field also has a universal structure. For a developing thermal boundary layer, this is only the case in that part of the inner region of the thermal boundary layer where the turbulent temperature field is fully adapted to the local heat transfer situation. For this universal distribution one can take, as a first approximation, the experimentally determined distribution or the one given by Eq. (5.12). The fact that in general Pr_t will be smaller than unity can be ascribed to the transfer of momentum due to the turbulent pressure fluctuations; a corresponding mechanism for the case of heat transfer is lacking.

From a physical point of view, Pr_t is hardly a meaningful quantity in the outer region of the thermal boundary layer, where the local heat and momentum transfer are greatly influenced by upstream conditions. In this case Pr_t must only be interpreted as an expression for the empirical relation between momentum and heat transfer. However, for the calculation of heat transfer, the distribution of Pr_t in the outer region is of minor importance, since the largest resistance for the heat transfer is localized in the inner region (provided Pr is not much smaller than unity).

Finally, we must expect that the heat transfer theory of Spalding, which has up to now presented the best approximation of reality, can be improved if the distribution of $Pr_t(y^+)$ resulting from our measurements, is incorporated in the existing computer program. Moreover, the experimental results for the flow and temperature field, which form a consistent whole, might be used as a test case for future, new heat transfer theories.

SAMENVATTING EN CONCLUSIES

Dit proefschrift houdt zich bezig met het warmtetransport in een turbulente grenslaag. In een windtunnel zijn metingen verricht bij stroming van lucht over een gedeeltelijk verwarmde, aerodynamisch gladde, vlakke plaat.

Aangezien convectief warmtetransport alleen te beschrijven is, indien men het stromingsveld kent, hebben we in Hoofdstuk II een overzicht gegeven van de bestaande theorieën betreffende het stromingsveld en het daarmee samenhangende impulstransport. Hierbij is speciale aandacht geschonken aan nieuwe ontwikkelingen, welke mogelijk zijn geworden door het toepassen van grote computers voor het oplossen van de bewegingsvergelijkingen. Van de behandelde oplossingsmethoden verdienen de zogenaamde differentieële methoden de voorkeur, in het bijzonder die van Bradshaw, welke uitgaat van een universele relatie tussen het turbulente impulstransport en de overige turbulente grootheden.

Hoofdstuk III behandelt de bestaande theorieën betreffende het temperatuurveld en het daarmee samenhangende warmtetransport. In essentie berusten deze theorieën op een bekende oplossing voor het stromingsveld en kan men de energievergelijking oplossen via de invoering van een veronderstelling betreffende de waarde van Pr_t . Meestal gaat men uit van $Pr_t = 1$ of van $Pr_t = \text{konstant}$. Een overzicht van de gepubliceerde experimentele waarden van Pr_t toont echter duidelijk dat deze veronderstellingen voor Pr_t niet juist zijn. De verschillende experimentele resultaten zijn gering in aantal en vertonen bovendien een zeer grote spreiding. Hieruit blijkt duidelijk hoezeer er behoefte bestaat aan een nauwkeuriger meting van het verloop van Pr_t in een thermische grenslaag. Dit heeft geleid tot ons experimenteel onderzoek, waarbij wij hebben getracht de verdeling van Pr_t zo nauwkeurig mogelijk te bepalen. Hiertoe zijn uitgebreide metingen verricht van alle grootheden die nodig zijn voor een volledige beschrijving van het stromings- en temperatuurveld. Het is dan mogelijk de verdeling van Pr_t door middel van twee verschillende methoden uit de experimentele gegevens te bepalen.

De proefopstelling en de experimentele methoden zijn beschreven in Hoofdstuk IV. Teneinde een indruk te krijgen van de betrouwbaarheid en nauwkeurigheid van de metingen, zijn diverse grootheden op verschillende, onderling onafhankelijke manieren bepaald. Voor de meting van het snelheidsveld werd gebruik gemaakt van de bekende hetdraad-techniek, waarbij speciale aandacht werd geschonken aan een nauwkeurige bepaling van de verschillende turbulente grootheden. Voor het meten van gemiddelde temperaturen en temperatuurfluctuaties is gebruik gemaakt van nieuwe meetelementen, die ontwikkeld zijn op het laboratorium waar dit onderzoek werd verricht. In onze experimenten is de toepasbaarheid hiervan onderzocht.

In een windtunnel werden metingen verricht aan het stromings- en temperatuurveld bij stroming van lucht over een vlakke plaat, waarvan een gedeelte werd verhit op een uniforme temperatuur T_w die boven de omgevingstemperatuur T_0 lag. De metingen vonden plaats bij twee constante waarden van de hoofdstroomsnelheid aan de voorkant van de vlakke plaat, respectievelijk 6,13 m/s en 10,10 m/s, waarvoor de bijbehorende temperatuurverschillen $T_w - T_0$ gelijk waren aan 11,80 °C en 10,80 °C. In Appendix II en Hoofdstuk V zijn de meetresultaten in tabelvorm en grafisch weergegeven en met bestaande theorieën vergeleken.

De meetresultaten voor het verloop van de schuifspanning aan de wand stemmen voor de verschillende methoden binnen drie procent met elkaar overeen. Voor het snelheidsveld zijn de gemiddelde snelheidsprofielen in goede overeenstemming met de bestaande theorieën, terwijl het verloop van de turbulente snelheidsfluctuaties het bestaan van een universele structuur van het turbulente snelheidsveld in het binnenste deel van de grenslaag bevestigt.

In het buitenste deel van de stromingsgrenslaag stemmen de metingen zeer goed overeen met het door Coles voorgestelde snelheidsprofiel, terwijl grote verschillen optreden met het door Sarnecki gegeven twee-parameter-snelheidsprofiel. In het overgangsgebied, $5 < y^+ < 25$, laten de gemeten snelheidsverdelingen zich uitstekend met het snelheidsprofiel van Spalding beschrijven, mits we een kleine correctieterm aanbrengen, zoals is aangegeven in vergelijking (5.1).

Behalve voor de meetplaats onmiddellijk na de oorsprong van de thermische grenslaag, stemmen de verdelingen van de warmtestroomdichtheid, gemeten volgens de verschillende meetmethoden, binnen drie procent met elkaar overeen. De gemeten warmteoverdracht blijkt in goede overeenstemming te zijn met de theorie van Spalding, in het bijzonder vlak na de sprong in oppervlakte-temperatuur van de plaat.

De nieuwe temperatuurmeetelementen blijken zeer goed te voldoen en de gemeten verschillen in de gemiddelde temperaturen, $T-T_0$, zijn tot op 0.03 °C nauwkeurig. Door de geringe afmetingen van de elementen was het ook mogelijk nauwkeurige metingen binnen de viskeuze sublaag te verrichten, zonder dat er correcties voor geleidings- of stralingseffecten behoeften te worden aangebracht.

De gemeten gemiddelde temperatuurprofielen vertonen duidelijk de ontwikkeling van de temperatuurgrenslaag met toenemende afstand tot de plaats van de temperatuursprong. Aansluitend aan de wand kan men echter een zogenaamde aangepaste laag onderscheiden, waarin de verdelingen van $T^+(y^+)$ en $\theta^+(y^+)$ een universeel verloop hebben. Het temperatuurprofiel van deze aangepaste laag komt uitstekend overeen met het volledig ontwikkelde temperatuurprofiel berekend uit het ongecorrigeerde snelheidsprofiel volgens Spalding als men aanneemt dat $Pr_t = 1$. Uit dit verloop van het gemiddelde temperatuurprofiel en het bovengenoemde gecorrigeerde snelheidsprofiel is de volgende benaderende uitdrukking voor het verloop van Pr_t in de overgangslaag afgeleid:

$$Pr_t = \frac{e^{ku^+} - 1 - ku^+ - (ku^+)^2/2! - (ku^+)^3/3! - (ku^+)^4/4!}{e^{ku^+} - 1 - ku^+ - (ku^+)^2/2! - (ku^+)^3/3!} \quad (5.12)$$

Veronderstellen we dat deze vergelijking ook in de viskeuze sublaag geldig is, dan vinden we voor $y^+ < 4$: $Pr_t = 0.08 y^+$. Substitutie van deze relatie in de warmteoverdrachtstheorieën van Spalding en Jayatilke, in plaats van de door hen gebruikte veronderstelling $Pr_t = 1$, leidt voor grote waarden van Pr tot de relatie $Nu \propto Pr^{1/3}$ in plaats van $Nu \propto Pr^{1/4}$, hetgeen beter met de experimentele warmte- en materieoverdrachtmetingen overeenstemt.

Zowel uit de metingen van de gemiddelde grootheden als uit die van u_v en v_θ zijn de verdelingen van Pr_t in de thermische grenslaag bepaald. De resultaten van beide methoden stemmen binnen de meetnauwkeurigheid (10%) goed met elkaar overeen. Uit de experimentele waarden van Pr_t blijkt duidelijk dat Pr_t niet een constante is, doch een functie van de afstand tot de wand. Voor het zich ontwikkelende temperatuurveld vertoont het verloop van Pr_t bovendien een ontwikkelend karakter.

De gevolgtrekkingen uit deze resultaten zijn uitvoerig besproken in Hoofdstuk V, Sectie E. Resumerend kunnen we stellen dat het verloop van Pr_t alleen universeel kan zijn voor het binnenste deel van een volledig ontwikkelde thermische grenslaag, waar ook het turbulente snelheidsveld een universele structuur heeft. Voor een zich ontwikkelende thermische grenslaag is dit alleen het geval in dat deel nabij de wand van de thermische grenslaag waar het turbulente temperatuurveld zich volledig heeft aangepast aan de plaatselijke warmteoverdrachtssituatie. Voor deze universele verdeling kan men in eerste benadering de hier experimenteel gevonden verdeling aannemen of die volgens vergelijking (5.12). Het feit dat in het algemeen Pr_t kleiner is dan 1 kan worden toegeschreven aan de impulsoverdracht tengevolge van de turbulente drukfluctuaties, waarvoor in het geval van warmteoverdracht geen overeenkomstig transportmechanisme bestaat.

In het buitenste deel van de thermische grenslaag is Pr_t een fysisch weinig zinvolle grootte, daar hier de lokale warmte- en impulsoverdracht niet alleen door de plaatselijke maar ook door de stroomopwaartse situaties wordt bepaald. In dit geval moet men Pr_t alleen opvatten als een uitdrukking van de

empirische relatie tussen impuls- en warmteoverdracht. Voor de berekening van de warmteoverdracht is de verdeling van Pr_t in het buitenste deel van ondergeschikte betekenis, daar de grootste weerstand voor de warmteoverdracht in het binnenste deel is gelokaliseerd (mits Pr niet veel kleiner is dan één).

Tenslotte moeten we verwachten dat de warmteoverdrachtstheorie van Spalding, welke tot nu toe de beste benadering van de werkelijkheid geeft, wordt verbeterd indien de door ons gevonden verdelingen van $Pr_t(y^+)$ in het bestaande computerprogramma worden opgenomen. Het hier gepresenteerde consistente geheel van metingen aan het stromings- en temperatuurveld kan bovendien worden gebruikt als een toets voor de geldigheid van toekomstige, nieuwe warmteoverdrachtstheorieën

Appendix I

Procedure for Setting a Uniform Surface Temperature of the Heated Plate

The adjustment procedure required the following programme on the multiple switch:

- positions 1-15 : temperature differences between a surface thermocouple of the main elements and the reference thermocouple,
- positions 16, 17, 18 : short-circuited, to indicate the zero deflection of the recorder,
- positions 19-48 : temperature differences between the fifteen main elements and the associated small elements,
- positions 49-62 : temperature differences between the main elements,
- positions 63, 64 : temperature differences in x-direction over the first element,
- positions 65, 66 : temperature differences in x-direction over the fifteenth element,
- positions 67-81 : temperature differences over the Sindanyo plate to calculate the heat losses of the main elements to the lower side,
- positions 82-96 : temperature differences between the other surface thermocouples of the main elements and the reference thermocouple,
- positions 97-101 : temperature differences between some thermocouples at the inner side of the Sindanyo plate and the reference thermocouple,
- position 102 : short-circuited.

In fact, only the positions 1-48 were used for the adjustment of a uniform surface temperature. The other positions mainly served for the calculation of corrections to the heat transfer and as an extra check on the adjustment.

First of all, the desired velocity was established in the test section and the cooling of the corner blades was switched on. When all the potentiometers on the front panel of the power supply cabinet had been placed in a midway position, the Delta power supplies were switched on. With the help of the controlling potentiometers the surface temperatures of the main elements belonging to the same power supply were made equal, after which all surface temperatures were equalized by regulating the output of the power supplies. The positions 1-15 now gave an identical deflection on the recorder.

Finally the power supply of the small elements was adjusted till all the positions 19-48 gave a zero deflection on the recorder. With this procedure it proved possible to set a uniform surface temperature with deviations less than 0.2 °C within one hour.

To calculate the heat transfer of the main elements 2-15, only the heat loss to the lower sides, determinable from the positions 67-81, must be subtracted from the power input of the main elements. For the main elements 1 and 15 the heat loss to the unheated parts of the plate must also be accounted for.

Survey of measured distributions of $u^+(y^+)$ and $T^+(y^+)$

Table 1
Distributions of $u^+(y^+)$

Station 1				Station 2			
$U_{0,e} = 6.10$ m/s		$U_{0,e} = 10.10$ m/s		$U_{0,e} = 6.13$ m/s		$U_{0,e} = 10.10$ m/s	
$U_0 = 6.69$ m/s		$U_0 = 11.00$ m/s		$U_0 = 6.95$ m/s		$U_0 = 11.23$ m/s	
$\delta_1 = 2.97$ mm		$\delta_1 = 2.63$ mm		$\delta_1 = 3.39$ mm		$\delta_1 = 3.00$ mm	
$\delta_2 = 2.18$ mm		$\delta_2 = 1.89$ mm		$\delta_2 = 2.49$ mm		$\delta_2 = 2.18$ mm	
$u_T = 32.3$ cm/s		$u_T = 50.8$ cm/s		$u_T = 32.0$ cm/s		$u_T = 50.0$ cm/s	
y^+	u^+	y^+	u^+	y^+	u^+	y^+	u^+
597	20.7	938	21.65	876	21.7	1090	22.5
489	20.55	769	21.6	663	21.65	923	22.42
424	20.35	599	21.1	556	21.6	756	22.22
359	19.9	531	20.8	450	21.2	590	21.7
316	19.6	463	20.45	387	20.7	490	21.1
273	19.15	395	19.9	344	20.3	424	20.6
230	18.6	327	19.2	301	19.9	358	20.0
187	18.1	259	18.75	259	19.4	291	19.3
144	17.4	225	18.45	216	18.8	224	18.65
122	16.9	191	18.15	174	18.3	158	17.75
101	16.4	157	17.8	153	18.0	124	17.3
74.0	15.85	124	17.4	132	17.6	91.0	16.75
57.4	15.15	89.9	16.7	110	17.2	74.3	16.2
46.6	14.7	72.8	16.3	89.0	16.8	57.6	15.5
35.8	14.1	55.7	15.6	67.8	16.2	41.0	14.8
25.0	13.1	38.8	14.7	46.5	15.35	31.0	14.4
18.6	12.05	28.6	13.9	35.8	14.75	24.3	13.2
14.2	10.7	21.8	12.9	25.2	13.6	21.0	12.8
12.1	10.1	18.5	12.2	18.8	12.7	17.7	12.0
9.93	8.87	15.1	11.2	16.7	12.25	14.3	11.1
8.85	8.07	13.4	10.55	14.6	11.65	11.0	9.42
7.76	7.23	11.7	9.77	12.4	10.8	9.32	8.23
6.67	6.40	10.0	8.82	10.3	9.70	7.65	6.98
5.61	5.40	8.30	7.64	9.25	8.91	6.56	6.12
4.47	4.58	6.61	6.15	8.19	8.10	5.66	5.29
3.82	3.66	5.60	5.21	7.12	7.03	4.99	4.72
3.39	3.30	4.91	4.68	6.06	5.94	4.33	4.09
2.96	2.84	4.23	4.12	5.42	5.29	3.66	3.52
2.52	2.54	3.90	3.81	5.00	4.77	3.00	2.94
2.09	2.22	3.56	3.43	4.57	4.47	2.66	2.66
		3.22	3.21	4.15	4.03		
		2.88	2.89	3.72	3.74		
		2.54	2.72	3.51	3.51		

Table 1 (continued)

Station 3				Station 5			
$U_{0,e} = 6.08$ m/s		$U_{0,e} = 10.11$ m/s		$U_{0,e} = 6.12$ m/s		$U_{0,e} = 10.08$ m/s	
$U_0 = 6.84$ m/s		$U_0 = 11.40$ m/s		$U_0 = 7.02$ m/s		$U_0 = 11.55$ m/s	
$\delta_1 = 3.78$ mm		$\delta_1 = 3.32$ mm		$\delta_1 = 4.14$ mm		$\delta_1 = 3.62$ mm	
$\delta_2 = 2.77$ mm		$\delta_2 = 2.42$ mm		$\delta_2 = 3.05$ mm		$\delta_2 = 2.64$ mm	
$u_T = 31.2$ cm/s		$u_T = 49.6$ cm/s		$u_T = 31.2$ cm/s		$u_T = 49.4$ cm/s	
y^+	u^+	y^+	u^+	y^+	u^+	y^+	u^+
968	21.9	1205	23.0	972	22.48	1544	23.37
760	21.88	1041	22.95	764	22.45	1205	23.33
657	21.85	877	22.9	659	22.4	1041	23.3
554	21.7	713	22.75	555	22.1	876	23.15
440	21.1	625	22.3	451	21.7	712	22.8
388	20.6	549	22.15	389	21.2	613	22.3
346	20.2	483	21.45	347	20.9	547	21.8
305	19.9	418	21.0	305	20.5	482	21.4
264	19.4	352	20.5	264	20.0	416	20.8
222	18.8	286	19.48	222	19.3	350	20.2
181	18.3	221	18.9	180	18.8	284	19.55
139	17.7	188	18.5	139	18.0	218	18.8
119	17.25	155	17.9	118	17.5	184	18.3
97.7	16.75	123	17.35	97.1	17.0	152	17.8
77.0	16.25	89.9	16.6	76.2	16.4	119	17.15
56.2	15.6	57.1	15.6	55.4	15.8	86.0	16.4
35.5	14.6	50.5	15.35	34.6	14.8	53.2	15.35
31.4	14.2	43.9	15.0	24.2	13.8	36.8	14.6
27.2	13.8	37.4	14.6	20.2	13.1	30.2	14.05
23.1	13.4	30.8	14.2	15.8	12.3	23.6	13.3
18.95	12.7	24.3	13.5	13.7	11.5	20.3	12.7
14.8	11.65	21.0	12.9	11.7	10.65	17.1	12.0
12.7	10.75	19.3	12.65	10.6	9.90	15.4	11.45
11.7	10.2	17.7	12.3	9.58	9.21	13.8	10.85
10.7	9.60	16.1	11.65	8.54	8.29	12.1	10.14
9.62	8.85	14.4	11.33	7.50	7.65	10.5	9.25
8.60	8.02	12.8	10.75	6.46	6.60	8.88	8.16
7.55	7.21	11.1	9.98	5.42	5.44	7.23	6.90
6.52	6.35	9.51	9.08	4.79	4.76	6.25	5.97
5.49	5.66	8.53	8.38	4.17	4.18	5.26	5.02
4.86	4.69	7.54	7.52	3.54	3.54	4.28	4.25
4.25	4.03	6.56	6.53	3.12	3.12	3.62	3.78
3.62	3.40	5.57	5.56	2.71	2.70		
3.00	2.86	4.92	4.88	2.29	2.35		
2.59	2.50	4.26	4.30	2.08	2.22		
2.18	2.31	3.61	3.54				
1.97	2.20	3.28	3.28				

Table 1 (continued)

Station 6				Station 7			
$U_{O,e} = 6.12 \text{ m/s}$		$U_{O,e} = 10.10 \text{ m/s}$		$U_{O,e} = 6.16 \text{ m/s}$		$U_{O,e} = 10.15 \text{ m/s}$	
$U_O = 7.10 \text{ m/s}$		$U_O = 11.70 \text{ m/s}$		$U_O = 7.19 \text{ m/s}$		$U_O = 12.00 \text{ m/s}$	
$\delta_1 = 4.48 \text{ mm}$		$\delta_1 = 3.91 \text{ mm}$		$\delta_1 = 4.88 \text{ mm}$		$\delta_1 = 4.24 \text{ mm}$	
$\delta_2 = 3.30 \text{ mm}$		$\delta_2 = 2.85 \text{ mm}$		$\delta_2 = 3.59 \text{ mm}$		$\delta_2 = 3.11 \text{ mm}$	
$u_T = 31.4 \text{ cm/s}$		$u_T = 49.5 \text{ cm/s}$		$u_T = 31.5 \text{ cm/s}$		$u_T = 49.7 \text{ cm/s}$	
y^+	u^+	y^+	u^+	y^+	u^+	y^+	u^+
965	22.6	1525	23.82	1050	22.8	1670	24.15
755	22.5	1195	23.81	840	22.75	1340	24.1
651	22.3	1030	23.79	736	22.7	1173	24.05
548	21.95	965	23.13	633	22.3	1008	23.95
444	21.2	700	22.7	529	21.8	843	23.6
380	20.65	602	22.3	466	21.35	745	23.1
339	20.2	536	21.7	425	21.0	679	22.85
297	19.65	470	21.2	384	20.75	613	22.6
256	19.1	404	20.6	343	20.3	547	22.0
214	18.55	338	20.1	302	19.9	481	21.5
173	17.9	273	19.3	260	19.4	415	21.0
131	17.2	207	18.5	218	18.9	349	20.4
110	16.85	174	18.0	177	18.4	283	19.7
89.2	16.3	141	17.5	135	17.6	217	19.1
68.3	15.7	108	16.9	94.0	16.7	151	18.05
47.5	14.85	75.4	16.2	73.1	16.15	118	17.4
37.1	14.25	59.0	15.6	52.5	15.4	84.9	16.65
26.7	13.53	42.5	14.8	42.1	14.8	68.4	16.25
20.4	12.5	32.6	14.2	31.7	14.3	51.8	15.56
16.25	11.7	26.0	13.55	25.5	13.8	41.9	15.1
14.15	10.9	22.7	13.1	21.3	13.3	35.3	14.7
12.1	10.1	19.4	12.37	17.2	12.4	28.7	14.25
10.0	9.01	16.1	11.65	15.1	11.9	25.4	13.8
8.96	8.31	14.5	11.0	13.1	11.2	22.1	13.35
7.91	7.61	12.8	10.45	12.0	10.4	20.5	13.1
6.87	6.81	11.2	9.54	10.95	9.83	18.8	12.75
5.83	5.82	9.55	8.59	9.95	8.95	17.15	12.35
4.79	4.75	7.90	7.31	8.90	8.41	15.5	11.8
4.17	4.10	6.91	6.43	7.88	7.73	13.85	11.25
3.75	3.71	6.25	5.88	6.95	6.80	12.2	10.5
3.33	3.30	5.59	5.35	5.80	5.84	10.55	9.53
2.92	2.92	4.93	4.70	4.76	4.82	8.90	8.50
2.71	2.76	4.61	4.42	3.73	3.71	7.92	7.58
2.50	2.62	4.28	4.23	3.11	3.16	7.25	7.14
		3.95	3.98	2.69	2.77	6.27	6.15
				2.28	2.23	5.61	5.58
				2.07	2.17	4.95	4.90
						4.29	4.28
						3.96	3.99
						3.67	3.67

Table 1 (continued)

Station 8			
$U_{o,e} = 6.20 \text{ m/s}$		$U_{o,e} = 10.10 \text{ m/s}$	
$U_o = 7.35 \text{ m/s}$		$U_o = 12.05 \text{ m/s}$	
$\delta_1 = 5.37 \text{ mm}$		$\delta_1 = 4.71 \text{ mm}$	
$\delta_2 = 3.95 \text{ mm}$		$\delta_2 = 3.44 \text{ mm}$	
$u_T = 32.4 \text{ cm/s}$		$u_T = 50.0 \text{ cm/s}$	
y^+	u^+	y^+	u^+
880	22.45	1361	24.10
773	22.25	1195	24.05
666	22.0	1029	23.85
559	21.5	863	23.3
451	20.6	679	22.5
387	20.0	596	21.8
344	19.6	530	21.4
301	19.3	463	20.9
258	18.95	397	20.25
215	18.6	331	19.7
172	17.85	264	18.9
150	17.5	231	18.45
128	17.1	198	18.05
115	16.7	165	17.6
85.5	16.35	132	17.0
63.9	15.65	98.2	16.3
42.4	14.8	65.0	15.45
31.6	14.05	48.3	14.85
25.2	13.4	38.4	14.35
20.9	12.75	31.8	13.8
18.7	12.15	28.5	13.5
16.6	11.6	25.2	13.2
14.4	11.0	21.8	12.6
12.3	10.5	18.5	12.05
10.1	9.27	15.2	11.15
9.03	8.52	13.5	10.5
7.95	7.50	11.85	9.74
6.89	6.79	10.2	8.98
5.81	5.82	8.54	8.06
4.73	4.71	6.87	6.68
3.66	3.64	5.91	5.90
3.01	3.10	5.21	5.34
2.58	2.75	4.55	4.33
2.37	2.42	3.88	3.88
2.15	2.37	3.22	3.44
		2.89	3.08

Table 2

Distribution of T^+ (y^+). Lower velocity, $U_{0,e} = 6.13$ m/s

Station 3		Station 4		Station 5		Station 6		Station 7	
$\delta_{T,1} = 0.642$ mm		$\delta_{T,1} = 1.249$ mm		$\delta_{T,1} = 1.691$ mm		$\delta_{T,1} = 2.286$ mm		$\delta_{T,1} = 3.166$ mm	
$\delta_T = 4.8$ mm		$\delta_T = 11.5$ mm		$\delta_T = 16.9$ mm		$\delta_T = 26.0$ mm		$\delta_T = 35.4$ mm	
y^+	T^+	y^+	T^+	y^+	T^+	y^+	T^+	y^+	T^+
248	10.00	377	13.08	477	14.18	575	15.40	683	16.19
206	9.96	314	13.07	372	14.14	471	15.35	578	16.11
164	9.91	252	13.01	310	14.08	366	15.18	447	16.03
123	9.87	210	12.95	268	13.93	324	15.09	370	15.75
81.8	9.78	168	12.82	226	13.78	282	14.95	328	15.59
60.9	9.62	126	12.56	184	13.61	240	14.70	286	15.23
40.1	9.30	106	12.33	143	13.37	199	14.27	244	14.96
33.9	9.12	84.4	12.01	101	12.81	157	13.86	203	14.52
29.7	8.93	63.5	11.63	79.9	12.49	115	13.33	161	14.09
25.6	8.72	53.1	11.29	59.0	11.92	93.8	12.81	119	13.41
21.4	8.37	46.8	11.04	48.5	11.43	72.9	12.24	77.5	12.58
17.3	7.95	40.6	10.75	38.1	10.93	51.9	11.70	56.6	11.83
15.2	7.53	34.3	10.4	31.8	10.57	41.5	11.19	46.1	11.36
13.1	7.00	28.0	9.92	25.6	9.96	31.0	10.51	35.7	10.86
12.0	6.20	23.9	9.47	19.3	9.11	24.7	9.81	29.4	10.24
11.0	6.37	19.7	8.94	15.1	8.09	20.5	9.30	23.2	9.51
9.94	6.00	17.6	8.56	13.1	7.46	16.3	8.47	16.9	8.39
8.90	5.53	15.5	8.11	11.0	6.49	12.2	7.17	12.7	7.43
7.86	5.00	13.4	7.51	9.92	6.16	10.1	6.39	10.7	6.60
6.82	4.56	11.7	6.78	8.87	5.59	9.00	5.85	9.61	6.18
5.78	3.88	10.3	6.31	7.83	5.05	7.96	5.42	8.56	5.72
4.74	3.22	9.26	5.85	6.79	4.47	6.91	4.78	7.52	5.20
3.60	2.43	8.22	5.34	5.74	3.94	5.86	4.07	6.47	4.50
3.08	2.03	7.18	4.87	4.70	3.26	4.82	3.36	5.85	4.21
2.48	1.68	6.11	4.22	4.28	2.80	4.40	3.13	5.22	3.70
2.00	1.35	5.10	3.49	3.86	2.56	3.98	2.73	4.80	3.35
		4.47	3.04	3.65	2.39	3.56	2.45	4.39	2.96
								4.18	2.89

Table 2

Distribution of $T^+(y^+)$. Higher velocity, $U_{o,e} = 10.10$ m/s

Station 3		Station 4		Station 5		Station 6		Station 7	
$\delta_{T,1} = 0.462$ mm		$\delta_{T,1} = 1.05$ mm		$\delta_{T,1} = 1.467$ mm		$\delta_{T,1} = 2.22$ mm		$\delta_{T,1} = 2.99$ mm	
$\delta_T = 3.71$ mm		$\delta_T = 10.3$ mm		$\delta_T = 15.2$ mm		$\delta_T = 23.7$ mm		$\delta_T = 31.4$ mm	
y^+	T^+	y^+	T^+	y^+	T^+	y^+	T^+	y^+	T^+
256	11.29	432	14.17	520	15.81	774	16.80	940	18.33
223	11.29	333	14.09	454	15.76	609	16.66	776	18.22
190	11.30	267	13.99	388	15.65	510	16.53	611	17.89
157	11.28	234	13.87	322	15.52	443	16.34	513	17.60
124	11.23	201	13.73	289	15.39	377	16.06	447	17.34
90.7	11.12	168	13.56	255	15.24	311	15.67	381	16.96
74.2	10.98	135	13.26	222	15.03	245	15.11	315	16.42
57.7	10.74	102	12.87	189	14.77	178	14.66	250	15.72
47.8	10.56	85.3	12.57	156	14.44	145	14.24	184	14.95
37.9	10.27	68.8	12.20	123	13.95	112	13.48	118	13.89
28.0	9.74	58.8	11.83	89.8	13.17	79.1	12.70	85.2	13.15
24.7	9.50	48.9	11.47	73.2	12.73	62.6	12.22	68.7	12.66
21.4	9.10	39.0	11.01	56.7	12.17	46.6	11.63	52.3	12.05
18.1	8.60	32.4	10.55	46.7	11.76	36.1	10.83	42.4	11.52
14.9	7.88	25.8	9.87	36.8	11.17	26.2	9.89	32.6	10.76
13.2	7.43	19.2	8.97	30.1	10.63	19.5	8.90	26.0	10.12
11.5	6.83	15.9	8.18	23.5	9.93	16.2	8.27	22.7	9.74
9.89	6.22	14.2	7.81	20.2	9.38	14.6	7.84	19.4	9.22
8.90	5.81	12.6	7.36	16.9	8.67	12.9	7.31	16.1	8.49
7.91	5.34	10.9	6.72	13.5	7.82	11.3	6.67	12.8	7.46
6.92	4.94	9.26	6.05	10.3	6.59	9.60	6.00	11.2	6.89
5.93	4.15	7.60	5.23	8.61	5.86	7.95	5.29	9.54	6.19
4.95	3.48	6.61	4.56	6.96	4.87	6.29	4.33	7.89	5.35
4.29	2.96	5.62	3.89	5.96	4.25	5.30	3.71	6.25	4.34
3.96	2.77	4.63	3.22	4.97	3.49	4.30	3.07	5.26	3.64
3.63	2.59	3.97	2.74	4.31	3.02	3.64	2.44	4.28	2.96
		3.31	2.26	3.64	2.57	3.31	2.29	3.62	2.41
		2.98	2.04	3.31	2.16	2.98	2.04	3.29	2.17

LIST OF SYMBOLS

a	= $\lambda/(\rho c_p)$, thermal diffusivity
c	concentration of mass
c_D	dissipation coefficient, Eq. (2.44)
c_f	friction coefficient, Eq. (2.18)
c_p	specific heat at constant pressure
d	diameter of hot-wire
D	molecular diffusivity for mass transfer
E	anemometer D.C. voltage
e	anemometer A.C. voltage
H	= δ_1/δ_2 form parameter of mean velocity profile
I	electrical current through hot-wire
L	x-coordinate of discontinuity in surface temperature
l	mixing length
Nu	= $q_w x / (T_w - T_o) \lambda$, Nusselt number
Nu_d	= $q_w d / (T_w - T_o) \lambda$, Nusselt number
p	static pressure
p'	fluctuating static pressure
P_s	heat transfer resistance, Eq. (3.13)
Pr	= ν/a , Prandtl number
q	heat flux
q_m	mass flux
$\frac{1}{2} \rho q^2$	turbulent kinetic energy per volume
R_o	resistance of hot-wire at temperature T_o
R_T	resistance of temperature-sensing element
R_w	resistance of hot-wire at temperature T_w
Re	$U_o x / \nu$, Reynolds number
Re_2	$U_o \delta_2 / \nu$, Reynolds number
Re_δ	$U_o \delta / \nu$, Reynolds number
Re_d	$U_o d / \nu$, Reynolds number
Sc	= ν/D , Schmidt number
Sh	= $q_m x / (c_w - c_o) D$, Sherwood number
$Sp(x^+, Pr, Pr_t)$	Spalding function, Eq. (3.38)
St	= $Nu / (RePr)$, Stanton number
T	mean temperature
T_τ	= $q_w / (\rho c_p u_\tau)$, friction temperature
T^+	= $(T_w - T) / T_\tau$, dimensionless temperature difference

U, V, W	mean velocity components in x-, y- and z-directions
$U_{0,e}$	free stream velocity at entrance of test section
u, v, w	fluctuating velocity components in x-, y- and z-directions
u_{τ}	$= \sqrt{\tau_w/\rho}$, friction velocity
u^+	$= U/u_{\tau}$, dimensionless velocity
x	coordinate in direction of main stream
y	coordinate perpendicular to wall
z	coordinate along wall, perpendicular to x
x^+	dimensionless x-coordinate, Eq. (3.30)
y^+	$= yu_{\tau}/\nu$, dimensionless y-coordinate
β_0	temperature coefficient of resistance
δ	boundary layer thickness
δ_1	displacement thickness, Eq. (2.15)
δ_2	momentum thickness, Eq. (2.16)
δ_3	kinetic energy thickness, Eq. (2.41)
δ_T	thickness of thermal boundary layer
δ_T^*	convection thickness, Eq. (4.33)
$\delta_{T,1}$	thermal "displacement thickness", Eq. (5.15)
η	dynamic viscosity
Θ	$(T-T_0)/(T_w-T_0)$, dimensionless temperature difference
θ	fluctuating temperature
λ	thermal conductivity
ν	kinematic viscosity
ρ	density
τ	shear stress

Notation

$()_0$	free stream value
$()_w$	value at the wall
$()_e$	effective value
$()_t$	turbulent value
$()'$	$\sqrt{()^2}$, root-mean-square value
$()$	time average value

ERRATA

Eq. (2.31) : δ_2 instead of δ

Eq. (2.49) : V_e/U_o instead of $V_e U_o$

p. 21, 4th line below Fig. 2.6: $\varphi_{max} = y_{max}/\delta$

Eq. (3.13) : $P_s = \int_0^{u_o^+} [(Pr_e - Pr_t)/Pr_t] du^+$

pp. 15 and 16 : Re_2 instead of R_2

p. 37, first word : if instead of is

Eq. (2.126) : A square bracket between 0.04432 and $\exp(0.4 u^+)$ and one at the end of the formula

Eqs. (3.2) and (3.3) : c_p instead of cp

p. 66, fourth line : Δp_p instead of p_p

p. 78, A.1, fifth line : $dp/dx = -4.10 \text{ N/m}^3$

Fig. 5.4 : For the stations 6 and 7 the figures 10 and 10^2 on the y/δ -axis must both be replaced by 1

Fig. 5.13 : Unit belonging to the vertical axis is s

Fig. 5.14 : The linear scale for $\rho c_p \bar{v}\theta$ is missing. The value of 0.1 N/m^2 on the $-\rho uv$ -axis corresponds with 100 W/m^2 for the $\rho c_p \bar{v}\theta$ -axis

Eq. (5.17), last term : v/u_τ^2 must be replaced by η

Eq. (5.20) : The correct coefficient for the time between square brackets is

$$\frac{\rho c_p S m}{m + n + mn} \left(\frac{\delta_T}{\delta} \right)^{1/m} \delta_T (T_w - T_o)$$

Eq. (5.20^a) : n must be replaced by m

REFERENCES

1. D.B. Spalding, Heat transfer to a turbulent stream from a surface with stepwise discontinuity in wall temperature, Intern. Developments in Heat Transfer, ASME/Inst. Mech. Engrs. II, 439 (1961).
2. A.G. Smith and V.L. Shah, The calculation of wall and fluid temperatures for the incompressible turbulent boundary layer, with arbitrary distribution of wall heat flux, Intern. J. Heat Mass Transfer 5, 1179 - 1189 (1962).
3. D.B. Spalding, Contribution to the theory of heat transfer across a turbulent boundary layer, Intern. J. Heat Mass Transfer 7, 743 - 761 (1964).
4. A.P. Hatton, Heat transfer through the turbulent, incompressible boundary layer on a flat plate, Intern. J. Heat Mass Transfer 7, 875 - 896 (1967).
5. L.M. Back and R.A. Seban, On constant property turbulent boundary layers with variable temperature or heat flux at the wall, Trans. ASME, J. Heat Transfer 151 - 156 (1965).
6. E. Baker, Series solution for heat transfer through a turbulent boundary layer, Intern. J. Heat Transfer 9, 417 - 426 (1966).
7. S.V. Patankar and D.B. Spalding, A calculation procedure for heat transfer by forced convection through two-dimensional, uniform-property turbulent boundary layers on smooth impermeable walls, Proc. of Third Intern. Heat Transfer Conference, Chicago, Vol. II, 50 - 63 (1966).
8. S.V. Patankar, Heat transfer across a turbulent boundary layer: application of a profile method to the step-wall-temperature problem, Intern. J. Heat Mass Transfer 9, 829 - 834 (1966).
9. F.A. Dvorak and M.R. Head, Heat transfer in the constant property turbulent boundary layer, Intern. J. Heat Mass Transfer 10, 61 - 81 (1967).
10. R.D. Haberstroh and L.V. Baldwin, Application of a simplified velocity profile to the prediction of pipe-flow heat transfer, Trans. ASME, J. Heat Transfer 191 - 200 (1968).
11. W.H. Corcoran et al., Temperature gradients in turbulent gas streams, Ind. Eng. Chem. 44, 410 - 430 (1952).
12. C.A. Sleicher, Experimental velocity and temperature profiles for air in turbulent pipe flow, Trans. ASME 80, 693 - 704 (1958).
13. B.H. Sage and E. Venezian, Temperature gradients in turbulent gas streams: effect of viscous dissipation on the evaluation of total conductivity, AIChE J. 7, 688 - 692 (1961).
14. S.E. Isakoff and T.B. Drew, Heat and momentum transfer in turbulent flow of mercury. General discussion on heat transfer, Inst. Mech. Engrs. and ASME, 405 - 449 (1951).
15. H.E. Brown et al., The transfer of heat and momentum in a turbulent stream of mercury, Trans. ASME 79, 279 - 285 (1957).
16. H. Ludwig, Bestimmung des Verhältnisses der Austauschkoefizienten für Wärme und Impuls bei turbulenten Grenzschichten, Z. Flugwissenschaften 4, 73 - 81 (1956).
17. D.S. Johnson, Velocity and temperature fluctuation measurements in a turbulent boundary layer downstream of a stepwise discontinuity in wall temperature, Trans. ASME, J. Appl. Mech. 325 - 336 (1959).
18. R.E. Johnk and T.J. Hanratty, Temperature profiles for turbulent flow of air in a pipe, parts I and II, Chem. Eng. Sci. 17, 867 - 892 (1962).
19. A. Sesonki et al., Eddy diffusivity ratios for mercury flowing in a tube, Chem. Eng. Progress, Symposium Series, Vol. 61, No. 57, 101 - 107 (1965).
20. R.A. Gowen and J.W. Smith, Turbulent heat transfer from smooth and rough surfaces, Intern. J. Heat Mass Transfer 11, 1657 - 1673 (1968).
21. E.M. Sparrow and W.J. Minkowycz, Buoyancy effects on horizontal boundary-layer flow and heat transfer, Intern. J. Heat Mass Transfer 5, 505 - 511 (1962).

22. J.O. Hinze, *Turbulence, an Introduction to Its Mechanism and Theory*, McGraw-Hill Book Company, Inc., New York (1959).
23. A. A. Townsend, *The Structure of Turbulent Shear Flow*, Cambridge University Press, New York (1956).
24. G.K. Batchelor, *An Introduction to Fluid Dynamics*, Cambridge University Press, New York (1967).
25. H. Schlichting, *Boundary Layer Theory*, Pergamon Press Ltd., London (1955).
26. J.L. Lumley and H. A. Panofsky, *The Structure of Atmospheric Turbulence*, Interscience Monographs and Texts in Physics and Astronomy, Vol. 12, John Wiley and Sons, New York (1964).
27. J. C. Rotta, *Turbulent Boundary Layers in Incompressible Flow*, Progress in Aeronautical Sciences, Vol. 2, 2 - 220, Pergamon Press Ltd., London (1962).
28. L. Prandtl, Bericht über Untersuchungen zur ausgebildeten Turbulenz, *Z. Angew. Math. and Mech.* 5, 136 (1925).
29. G.I. Taylor, *Phil. Trans. Soc. London* 215A, 1 (1915); *Proc. Roy. Soc. London* 135A, 685 (1932).
30. Th. von Kármán, *Turbulence and skin friction*, *J. Aeronaut. Sci.* 1, 1 (1934).
31. G.L. Mellor, *The effects of pressure gradients on turbulent flow near a smooth wall*, *J. Fluid Mech.* 24, 255 - 274 (1966).
32. N. Stevenson, *The mean flow in the outer region of turbulent boundary layers*, AGARDograph 97, 281 - 314 (1965).
33. F.H. Clauser, *The turbulent boundary layer*, *Adv. in Appl. Mech.* IV, 1 - 51 (1956).
34. J. C. Rotta, *Introduction to turbulent boundary layer calculation*, von Kármán Institute for Fluid Dynamics, Lecture Series 5, 1 - 67 (1968).
35. P. Bradshaw, *The turbulence structure of equilibrium boundary layers*, *J. Fluid Mech.* 29, 625 - 645 (1967).
36. P.S. Klebanoff, *Characteristics of turbulence in a boundary layer with zero pressure gradient*, NACA Tech. Note 3178 (1954).
37. J. Laufer, *The structure of turbulence in fully developed pipe flow*, NACA Tech. Rep. 1174 (1955).
38. H. Reichardt, *Die Grundlagen des turbulenten Wärmeüberganges*, *Archiv für die gesamte Wärme-technik*, Nr. 6/7, 129 - 142 (1951).
39. R.G. Deissler, *Analysis of turbulent heat transfer, mass transfer and friction in smooth tubes at high Prandtl and Schmidt numbers*, NACA Tech. Rep. 1210 (1955).
40. A.A. Townsend, *Equilibrium layers and wall turbulence*, *J. Fluid Mech.* 11, 97 - 120 (1961).
41. A.A. Townsend, *The behaviour of a turbulent boundary layer near separation*, *J. Fluid Mech.* 12, 536 - 554 (1962).
42. G.L. Mellor and D.M. Gibson, *Equilibrium turbulent boundary layers*, *J. Fluid Mech.* 24, 225 - 253 (1966).
43. A.E. Perry, J.B. Bell and P.N. Joubert, *Velocity and temperature profiles in adverse pressure gradient in turbulent boundary layers*, *J. Fluid Mech.* 25, 299 - 320 (1966).
44. A.E. Perry, *Turbulent boundary layers in decreasing adverse pressure gradients*, *J. Fluid Mech.* 26, 481 - 506 (1966).
45. H. McDonald, *The effect of pressure gradient on the law of the wall in turbulent flow*, *J. Fluid Mech.* 35, 311 - 336 (1969).
46. R.S. Brand and L.N. Persen, *Implication of the law of the wall for turbulent boundary layers*, *Acta Polytech. Scand.*, Ph. 30, NTVA Serie 1, Nr. 23 (1964).

47. D.B. Spalding, A single formula for the law of the wall, *J. Appl. Mech.* 28, 455 - 457 (1961).
48. P. Bradshaw, D.H. Ferriss and N.P. Atwell, Calculation of boundary-layer development using the turbulent energy equation, *J. Fluid Mech.* 28, 593 - 616 (1967).
49. A.A. Townsend, Self-preserving flow inside a turbulent boundary layer, *J. Fluid Mech.* 22, 773 - 797 (1965).
50. P.S. Klebanoff, Characteristics of turbulence in a boundary layer with zero pressure gradient, NACA Tech. Rep. 1247 (1955).
51. P. Bradshaw, The turbulence structure of equilibrium boundary layers, *J. Fluid Mech.* 29, 625 - 645 (1967).
52. P. Bradshaw, Calculation of boundary layer development using the turbulent energy equation, von Kármán Institute for Fluid Dynamics, Lecture Series 5, part 2, March (1968).
53. J.F. Nash, The calculation of three-dimensional turbulent boundary layers in incompressible flow, *J. Fluid Mech.* 37, 625 - 642 (1969).
54. B.G. Newman, Some contributions to the study of the turbulent boundary layer, Australian Dept. Supply Rep. ACA - 53 (1951).
55. V.A. Sandborn and R.J. Slogar, Study of the momentum distribution of turbulent boundary layers in adverse pressure gradients, NACA Tech. Note 3264 (1955).
56. G.B. Schubauer and P.S. Klebanoff, Investigation of separation of the turbulent boundary layer, NACA Tech. Rep. 1030 (1951).
57. D. Ross, Evaluation of the momentum integral equation for turbulent boundary layers, *J. Aeronaut. Sci.* 20, 502 (1953).
58. H. Ludwig and W. Tillmann, Investigation of the wall shearing stress in turbulent boundary layers, NACA Tech. Mem. 1285 (1950).
59. B.G.J. Thompson, A critical review of existing methods of calculating the turbulent boundary layer, Aero. Res. Council, R and M 3447, August (1964).
60. J.F. Nash, Turbulent-boundary-layer behaviour and the auxiliary equation, AGARDograph 97, 245 - 280 (1965).
61. A. Buri, Eine Berechnungsgrundlage für die turbulente Grenzschicht bei beschleunigter und verzögerter Grundströmung, Diss. Eidgen. Techn. Hochschule Zürich (1931).
62. D.A. Spence, The development of turbulent boundary layers, *J. Aeronaut. Sci.* 23, 3 - 15 (1956).
63. F.H. Clauser, Turbulent boundary layers in adverse pressure gradients, *J. Aeronaut. Sci.* 21,
64. M.R. Head, Entrainment in the turbulent boundary layer, Aero. Res. Council, R and M 3152 (1958).
65. E.C. Maskell, Approximate calculation of the turbulent boundary layer in two-dimensional incompressible flow, RAE Rep. Aero. 2443 (1951).
66. W.J. Duncan, A.S. Thom and A.D. Young, An Elementary Treatise on the Mechanics of Fluids, Edward Arnold, London (1959).
67. B.G.J. Thompson, Calculations of the turbulent boundary layer, *AIAA Journal* 3, 746 - 747 (1965).
68. B.G.J. Thompson, The calculation of shape-factor development in incompressible turbulent boundary layers with or without transpiration, AGARDograph 97, 159 - 190 (1965).
69. M.R. Head, Entrainment approach, von Kármán Institute for Fluid Dynamics, Lecture Series 5, part 3, March (1968).
70. M.P. Escudier and W.B. Nicoll, The entrainment function in turbulent boundary-layer and wall-jet calculation, *J. Fluid Mech.* 25, 337 - 366 (1966).

71. A. A. Townsend, The development of turbulent boundary layers with negligible wall stress, *J. Fluid Mech.* 8, 143 (1960).
72. D. W. Smith and J. H. Walker, Skin-friction measurements in incompressible flow, NACA TR-R-26 (1959).
73. H. J. Herring and J. F. Norbury, Some experiments on equilibrium turbulent boundary layers in favourable pressure gradients, *J. Fluid Mech.* 27, 541 - 549 (1967).
74. J. Rotta, Über die Theorie der turbulenten Grenzschichten, *Strömungs-Forschung* Nr. 1 (1950). Translated as On the theory of the turbulent boundary layer, NACA Tech. Mem. 1344 (1953).
75. E. Truckenbrodt, Ein Quadraturverfahren zur Berechnung der laminaren und turbulenten Reibungsschicht bei ebener und rotationssymmetrischer Strömung, *Ing. Arch.* 20, 211 (1952).
76. N. Tetervin and C. C. Lin, A general integral form of the boundary layer equation for incompressible flow with an application to the calculation of the separation point of turbulent boundary layers, NACA Rep. 1046 (1951).
77. K. F. Rubert and J. Persh, A procedure for calculating the development of turbulent boundary layers, under the influence of adverse pressure gradients, NACA Tech. Note 2478 (1951).
78. D. B. Spalding, The kinetic-energy-deficit equation of the turbulent boundary layer, *AGARDograph* 97, 199 - 244 (1965).
79. D. B. Spalding, A unified theory of friction, heat transfer and mass transfer in the turbulent boundary layer and wall jet, Mech. Eng. Dept. Imperial College and Aeronautical Research Council 25925 (1964).
80. H. McDonald and J. A. P. Stoddart, On the development of the incompressible turbulent boundary layer, Aero. Res. Council, R and M No. 3484 (1967).
81. T. J. Mueller and J. M. Robertson, A study of the mean motion and turbulence downstream of a roughness element, *Modern Dev. Theor. and Appl. Mech.*, 1, 326 - 340, Plenum Press (1963).
82. H. W. Liepmann and J. Laufer, Investigations of free turbulent mixing, NACA Tech. Note 1257 (1947).
83. S. J. Kline, H. K. Moffatt and M. V. Morkovin, Report on the AFOSR-IFP-Stanford conference on computation of turbulent boundary layers, *J. Fluid Mech.* 36, 481 - 484 (1969).
84. R. G. Deissler, Analytical and experimental investigation of adiabatic flow in smooth tubes, NACA Tech. Note 2138 (1950).
85. A. T. Popovich and R. L. Hummel, Experimental study of the viscous sublayer in turbulent pipe flow, *AIChE J.*, 13, 854 - 860 (1967).
86. S. J. Kline, W. C. Reynolds, F. A. Schraub and P. W. Rundstadler, The structure of turbulent boundary layers, *J. Fluid Mech.* 30, 741 - 773 (1967).
87. T. K. Sherwood, K. A. Smith and P. E. Fowles, The velocity and eddy viscosity distribution in the wall region of turbulent pipe flow, *Chem. Eng. Sci.* 23, 1225 - 1236 (1968).
88. E. R. Lindgren and J. Chao, Average velocity distribution of turbulent pipe flow with emphasis on the viscous sublayer, *Phys. of Fluids* 12, 1364 - 1371 (1969).
89. J. A. Clark, A study of incompressible turbulent boundary layers in channel flow, *Trans. ASME, J. of Basic Eng.* 90, 455 - 468 (1968).
90. R. M. Nedderman, The measurements of velocities in the wall region of turbulent liquid pipe flow, *Chem. Eng. Sci.* 16, 120 - 126 (1961).
91. L. P. Reiss and T. J. Hanratty, An experimental study of the unsteady nature of the viscous sublayer, *AIChE J.* 9, 154 - 160 (1963).
92. J. E. Mitchell and T. J. Hanratty, A study of turbulence at a wall using an electrochemical wall-shear-stress meter, *J. Fluid Mech.* 26, 199 - 221 (1966).

93. P.W. Rundstadler, S.J. Kline and W.C. Reynolds, An experimental investigation of the flow structure of the turbulent boundary layer, Rept. MD-8, Dept. of Mech. Eng., Stanford University (1963).
94. R.A. Armistead and J.J. Keyes, A study of wall-turbulence phenomena using hot-film sensors, Trans. ASME, J. Heat Transfer 90, 13 - 21 (1968).
95. E.R. Corino and R.S. Brodkey, A visual investigation of the wall region in turbulent flow, J. Fluid Mech. 37, 1 - 30 (1969).
96. P.V. Danckwerts, Significance of liquid-film coefficients in gas absorption, Ind. Eng. Chem. 43, 1460 - 1467 (1951).
97. H.A. Einstein and H. Li, The viscous sublayer along a smooth boundary, Proc. Am. Soc. Civil Engrs. 82, paper 945 (1956).
98. T.J. Hanratty, Heat transfer through a homogeneous isotropic turbulent field, AIChE J. 2, 42 - 45 (1956).
99. T.J. Black, Some practical applications of a new theory of wall turbulence, Proc. of the 1966 Heat Transfer and Fluid Mech. Inst., Stanford Univ. Press, 366 - 386 (1966).
100. J. Sternberg, A theory for the viscous sublayer of a turbulent flow, J. Fluid Mech. 13, 241 - 271 (1962).
101. J. Sternberg, The three-dimensional structure of the viscous sublayer, AGARDograph 97, 1 - 33 (1965).
102. Th. von Kármán, The analogy between fluid friction and heat transfer, Trans. ASME 61, 705 - 710 (1939).
103. H. Reichardt, Vollständige Darstellung der turbulenten Geschwindigkeitsverteilungen in glatten Leitungen, Z. angew. Math. Mech. 31, 208 - 219 (1951).
104. E.R. van Driest, On turbulent flow near a wall, J. Aeronaut. Sci. 23, 1007 - 1011 (1956).
105. W.D. Rannie, Heat transfer in turbulent shear flow, J. Aeronaut. Sci. 23, 485 - 489 (1956).
106. R.A. Burton, A simple universal velocity profile equation, AIAA Journal 3, 784 - 785 (1965).
107. H.G. Elrod, Note on the turbulent shear stress near a wall, J. Aeronaut. Sci. 24, 468 - 469 (1957), and: Erratum, J. Aeronaut. Sci. 27, 145 (1960).
108. J. Nikuradse, Strömungsgesetze in rauhen Röhren, Forschung auf dem Gebiet des Ingenieurwesens, Forschungsheft 361, VDI Verlag, Berlin (1933).
109. G. Skinner, Thesis, California Institute of Technology (1950).
110. R.A. Dutton, The velocity distribution in a turbulent boundary layer on a flat plate, Aero. Res. Council, Current Papers, No. 453 (1959).
111. W.G. Spangenberg, W.R. Rowland and N.E. Mease, Fluid Mechanics of Internal Flow, ed. Gino Sovran, Elsevier Amsterdam (1967).
112. B.S. Stratford, An experimental flow with zero skin friction throughout its region of pressure rise, J. Fluid Mech. 5, 17 (1959).
113. C.L. Mellor, The effects of pressure gradients on turbulent flow near a smooth wall, J. Fluid Mech. 24, 255 - 274 (1966).
114. A.E. von Doenhoff and N. Tetervin, Determination of general relations for the behaviour of turbulent boundary layers, NACA Rep. No. 772 (1943).
115. F.R. Hama, Boundary-layer characteristics for smooth and rough surfaces, Trans. Soc. Naval Architects Marine Engrs. 62, 333 - 358 (1954).
116. D. Coles, The law of the wake in the turbulent boundary layer, J. Fluid Mech. 1, 191 - 226 (1956).

117. A.J. Samecki, Ph. D. Dissertation, Cambridge University (1959).
118. C.L.V. Jayatilke, The Influence of Prandtl Number and Surface Roughness on the Resistance of the Laminar Sublayer to Momentum and Heat Transfer, Progress in Heat and Mass Transfer, Vol. 1, 193 - 330, Pergamon Press Ltd., London (1969).
119. J.S. Son and T.J. Hanratty, Limiting relation for the eddy diffusivity close to a wall, AICHE J. 13, 689 - 696 (1967).
120. P. Harriott and R.M. Hamilton, Solid-liquid mass transfer in turbulent pipe flow, Chem. Eng. Sci. 20, 1073 - 1078 (1965).
121. G.A. Hughmark, Eddy diffusivity close to a wall, AICHE J. 14, 352 (1968).
122. A.A. Gukhman and B.A. Kader, Mass transfer from tube walls to turbulent liquid streams at high Schmidt numbers, Theor. Found. of Chem. Eng. 3, 178 - 184 (1969).
123. O. Reynolds, On the extent and action of the heating surface for steam boilers, Proceedings of the Manchester Literary and Philosophical Society 14, 7 (1874). Also: Papers on Mechanical and Physical Subjects, Vol. 1, 81, Cambridge (1890).
124. L. Prandtl, Bemerkung über den Wärmeübergang im Rohr, Physik. Zeitschrift 29, 487 (1928).
125. G.I. Taylor, Conditions at the surface of a hot body exposed to the wind, Technical Report of the Advisory Committee for Aeronautics, 2, Reports and Memoranda No. 272, 423 (1916).
126. S.S. Kutateladze, Fundamentals of Heat Transfer, M.L. Mashgiz (1962). (Engl. translation published by Pergamon Press, 1965).
127. D.T. Wasan and C.R. Wilke, Turbulent exchange of momentum, mass and heat between fluid streams and pipe walls, Intern. J. Heat Mass Transfer 7, 87 - 94 (1964).
128. H.W. Kropholler and A.D. Carr, The prediction of heat and mass transfer coefficients for turbulent flow in pipes at all values of the Prandtl or Schmidt number, Intern. J. Heat Mass Transfer 5, 1191 - 1205 (1962).
129. W.C. Reynolds, W.M. Kays and S.J. Kline, Heat transfer in the turbulent incompressible boundary layer
 - I. Constant wall temperature, NACA Memo 12-1-58 W,
 - II. Step-wall-temperature distribution, NACA Memo 12-2-58 W,
 - III. Arbitrary wall temperature and heat flux, NACA Memo 12-3-58 W,
 - IV. Effect of location of transition and prediction of heat transfer in a known transition region, NACA Memo 12-4-58 W (1958).
130. M.W. Rubesin, The effect of an arbitrary surface-temperature variation along a flat plate on the boundary layer, NACA Tech. Note 2345 (1951).
131. S. Scesa, Experimental investigation of the convective heat transfer to air from a flat plate with a stepwise discontinuous surface temperature, M.S. Thesis, Univ. of California (1951).
132. J. Klein and M. Tribus, Forced convection from nonisothermal surfaces, Eng. Res. Inst., Univ. Michigan (1952) (Contract AF 18 (600)-51).
133. M. Jacob and W.M. Dow, Heat transfer from a cylindrical surface to air in parallel flow with and without unheated starting sections, Trans. ASME 68, 123 - 134 (1946).
134. J. Kestin and R.O. Richardson, Heat transfer across turbulent, incompressible boundary layers, Intern. J. Heat Mass Transfer 6, 147 - 189 (1963).
135. D.B. Spalding, A new analytical expression for the drag of a flat plate valid for both the turbulent and laminar regimes, Intern. J. Heat Mass Transfer 5, 1133 - 1138 (1962).
136. R. Murali Dharan, see Ref. 1.

137. J. Kestin and L.N. Persen, Application of Schmidt's method to the calculation of Spalding's function and of the skin-friction coefficient in turbulent flow, Intern. J. Heat Mass Transfer 5, 143 - 152 (1962).
138. J. Kestin and L.N. Persen, The transfer of heat across a turbulent boundary layer at very high Prandtl numbers, Intern. J. Heat Mass Transfer 5, 355 - 371 (1962).
139. G.O. Gardner and J. Kestin, Calculation of the Spalding function over a range of Prandtl numbers, Intern. J. Heat Mass Transfer 6, 289 - 299 (1963).
140. A.G. Smith and V.L. Shah, Study of heat and mass transfer from non-isothermal surfaces, The College of Aeronautics, Note No. 135 (1962).
141. M.R. Strunk and F.T. Tao, A numerical method for the solution of the energy equation for steady turbulent heat transfer, AIChE J. 10, 269 - 273 (1964).
142. L.N. Persen, Heat transfer through turbulent boundary layers at arbitrary Prandtl number, Acta Polytech. Scand. NTVA Serie 1, Nr. 27 (1965).
143. P.M. Moretti and W.M. Kays, Heat transfer through an incompressible turbulent boundary layer with varying free-stream velocity and varying surface temperature, Rept. PG-1, Dept. of Mech. Eng., Stanford University (1964).
144. J.P. Hartnett, R.C. Birkebak and E.R.G. Eckert, Velocity distribution, temperature distributions and heat transfer for air injected through a tangential slot into a turbulent boundary layer, J. Heat Transfer C83, 293 (1961).
145. J.P. Hartnett, R.C. Birkebak and E.R.G. Eckert, Velocity distributions, temperature distributions, effectiveness and heat transfer in cooling of a surface with a pressure gradient, Int. Developments in Heat Transfer, Part IV, 682 (1961).
146. R.A. Seban and D.L. Doughty, Heat transfer to turbulent boundary layers with variable free-stream velocity, Trans. ASME 78, 217 (1956).
147. R.A. Seban and L.M. Back, Effectiveness and heat transfer for a boundary layer with tangential injection and variable free-stream velocity, ASME paper No. 61-WA-156 (1961).
148. J.C. Rotta, Temperaturverteilungen in der turbulenten Grenzschicht an der ebenen Platte, Intern. J. Heat Mass Transfer 7, 215 - 228 (1964).
149. L.S. Kokorev and V.N. Ryapovor, Turbulent heat transfer during the flow of a heating medium of small Prandtl number along a tube, Intern. Chem. Eng. 2, 514 - 519 (1962).
150. W.F. Beckwith and R. Fahien, U.S. At. Energy Comm. Report IS 734 (1963).
151. R.A. Gowen and J.W. Smith, The effect of the Prandtl number on temperature profiles for heat transfer in turbulent pipe flow, Chem. Eng. Sci. 22, 1701 - 1711 (1967).
152. L. Taccoen, Contribution à l'étude des échanges thermiques en écoulement turbulent dans un tube lisse, Intern. J. Heat Mass Transfer 10, 1649 - 1660 (1967).
153. E. Brundrett and P.R. Burroughs, The temperature inner-law and heat transfer for turbulent air flow in a vertical square duct, Intern. J. Heat Mass Transfer 10, 1133 - 1142 (1967).
154. Che Pen Chen, Etude expérimentale de la couche limite thermique turbulente dans l'eau, Intern. J. Heat Mass Transfer 12, 61 - 70 (1969).
155. D.S. Johnson, Turbulent heat transfer in a boundary layer with discontinuous wall temperature, Thesis, The Johns Hopkins University, Baltimore (1955).
156. J. Blom and D.A. de Vries, On the values of the turbulent Prandtl number, Third All-Union Heat and Mass Transfer Conference, Minsk, paper No. 1.8 (1968).
157. V.I. Subbottin, M.K. Ibragimov, M.N. Ivanofsky, M.N. Arnoldov and E.V. Nomofilov, Turbulent heat transfer in a flow of liquid metals, Intern. J. Heat Mass Transfer 4, 79 - 87 (1961).

158. H.O. Buhr, A.D. Carr and R.E. Balzhiser, Temperature profiles in liquid metals and the effect of superimposed free convection in turbulent flow, Intern. J. Heat Mass Transfer 11, 641 - 654 (1968).
159. C.H.B. Priestley, Turbulent transfer in the lower atmosphere, Univ. Chicago Press (1959).
160. H. Chuang and R.B. Renda, Turbulent Prandtl number in thermally stratified shear flows of air, Intern. J. Heat Mass Transfer 12, 1585 - 1594 (1969).
161. A. Quarmby and R.K. Anand, Axisymmetric turbulent mass transfer in a circular tube, J. Fluid Mech. 38, 433 - 455 (1969).
162. A. Quarmby and R.K. Anand, Non-axisymmetric turbulent mass transfer in a circular tube, J. Fluid Mech. 38, 457 - 472 (1969).
163. I.B. Goldman and J.M. Marchello, Turbulent Schmidt numbers, Intern. J. Heat Mass Transfer 12, 797 - 802 (1969).
164. R. Jenkins, Variation of eddy conductivity with Prandtl modulus and its use in prediction of turbulent heat transfer coefficients, Heat Transfer and Fluid Mech. Inst., Stanford Univ. Press (1951), pp. 147 - 158.
165. N.Z. Azer and B.T. Chao, A mechanism of turbulent heat transfer in liquid metals, Intern. J. Heat Mass Transfer 1, 121 - 138 (1960).
166. J.R. Tyldesley and R.S. Silver, The prediction of the transport properties of a turbulent fluid, Intern. J. Heat Mass Transfer 11, 1325 - 1340 (1968).
167. J.R. Tyldesley, Transport phenomena in free turbulent flows, Intern. J. Heat Mass Transfer 12, 489 - 496 (1969).
168. J.H. Preston, The minimum Reynolds number for a turbulent boundary layer and the selection of a transition device, J. Fluid Mech. 3, 373 - 384 (1957).
169. J.C. Ascough, The development of a nozzle for absolute air flow measurements by pitot-static traverse, Ministry of Aviation, Aero. Res. Council, R and M No. 3384 (1964).
170. J.H. Preston, The determination of turbulent skin friction by means of pitot tubes, J. Roy. Aeron. Soc. 58, 109 - 121 (1954).
171. V.C. Patel, Calibration of the Preston tube and limitations on its use in pressure gradients, J. Fluid Mech. 23, 185 - 208 (1965).
172. L. S.G. Kovaszny, Development of turbulence-measuring equipment, NACA Tech. Note 2839 (1953).
173. R.D. Cooper and M.P. Tulin, Turbulence measurements with the hot-wire anemometer, AGARDograph
174. H.P. Grant and R.E. Kronauer, Fundamentals of hot wire anemometry, Symposium on Measurements in Unsteady Flow, ASME, Worcester, Mass., 44 - 53 (1962).
175. F.N. Frenkiel, Effects of wire length in turbulence investigations with a hot-wire anemometer, The Aeronautical Quarterly 5, 1 - 24 (1954).
176. P. Freymuth, Grundlagen der selbsttätigen Regelung auf konstante Temperatur bei Hitzdrahtanemometern, Deutsche Luft- und Raumfahrt, Mitteilung 64-04, 40 - 51 (1964).
177. H. Fiedler and J. Sakagami, Methoden zur Richtungsmessung mittels Hitzdrahtmesstechnik mit X- und V-Sonden, Deutsche Luft- und Raumfahrt, Mitteilung 64-04, 98 - 112 (1964).
178. K. Wieghardt and J. Kux, Experimental methods in wind tunnels, with special emphasis on the hot-wire anemometer, AGARD Rep. 558 (1967).
179. S. Cousin, Extended applications of the hot-wire anemometer, NACA Tech. Note No. 1864 (1947).
180. P. Bradshaw and R.F. Johnson, Turbulence measurements with hot-wire anemometers, N.P.L. Notes on Applied Science No. 33 (1963).

181. H. Fujita and L.S.G. Kovaszny, Measurements of Reynolds stress by a single rotated hot-wire anemometer, Rev. Sci. Instr. 39, 1351 - 1355 (1968).
182. W.G. Rose, Some corrections to the linearized response of a constant-temperature hot-wire anemometer operated in a low speed flow, Trans. ASME, J. Appl. Mech. 554 - 558 (1962).
183. D.C. Collis and M.J. Williams, Two-dimensional convection from heated wires at low Reynolds numbers, J. Fluid Mech. 6, 357 - 384 (1959).
184. D.C. Collis, Forced convection of heat from cylinders at low Reynolds numbers, J. Aeron. Sci. 23, 697 - 698 (1956).
185. P.O.A.L. Davies and M.J. Fisher, Heat transfer from electrically heated cylinders, Proc. Roy. Soc., Ser. A 280, 486 - 527 (1964).
186. Instituut voor Gezondheidstechniek TNO, Afdeling Binnenklimaat, Delft, The Netherlands.
187. F.H. Champagne, C.A. Sleicher and O.H. Wehrmann, Turbulence measurements with inclined hot-wires, Part I. Heat transfer experiments with inclined hot-wire; Part II. Hot-wire response equations, J. Fluid Mech. 28, 153 - 182 (1967).
188. C.A.G. Webster, A note on the sensitivity to yaw of a hot-wire anemometer, J. Fluid Mech. 13, 307 - 312 (1962).
189. J.A.B. Wills, The correction of hot-wire readings for proximity to a solid boundary, J. Fluid Mech. 12, 388 - 396 (1962).
190. C. Nieuwvelt, Ontwikkeling van een systeem voor het meten van snelle temperatuurvariaties (in Dutch). Thesis for obtaining the degree of "Ingenieur", Technological University, Eindhoven (1968).

ACKNOWLEDGEMENTS

I wish to thank the members of the Heat Transfer Section, Department of Physics, Technological University, Eindhoven, in particular Ir. C. Nieuwvelt, Mr. J.M. Bessem, Mr. L.C. de Folter and Mr. G.R.M. Trines for their pleasant collaboration and helpful discussions in the course of this investigation.

Among the students who have carried out parts of the measuring programme, I specially want to thank Mr. H. Hasenack who has been an indispensable stand-by, particularly in the last phase of the experimental work. I would like to wish him a successful completion of his studies.

Finally, I wish to express my gratitude to the directors of the Koninklijke/Shell-Laboratorium, Amsterdam for making part of the present investigation possible and for the facilities offered in the preparation of the manuscript. Concerning the latter I have really been impressed by the fast and excellent way in which the people involved have performed their work. I am fully convinced that without the enthusiastic cooperation of Miss D. Zwaan, Mrs. P. Bernsen, Miss M.F. Koch, Miss P.J. Jansen, Mr. R.A. Belder, Mr. G.J. Bouma and Mr. W.F. Kempff it would never have been possible to prepare the manuscript in such a short time, for which I am very grateful to them.

CURRICULUM VITAE

Op aanbeveling van de Senaat volgt hier een kort levensbericht van de schrijver van dit proefschrift. Hij werd geboren te 's-Hertogenbosch op 14 februari 1943. Na de lagere school bezocht hij de Rijks-H. B. S. te 's-Hertogenbosch, waar het eindexamen H. B. S. -b werd afgelegd in 1959. Aansluitend studeerde hij één jaar electrotechniek, waarna hij in 1960 met de natuurkundestudie begon, beide aan de Technische Hogeschool te Eindhoven. Zijn afstudeerwerk voerde hij uit onder leiding van Prof. Dr. D. A. de Vries in de sectie warmte-overdracht van de afdeling der technische natuurkunde. Het ingenieursexamen werd afgelegd in december 1964.

Hierna trad hij als wetenschappelijk medewerker in dienst van de T. H., waarbij onder leiding van bovengenoemde hoogleraar werd begonnen met een onderzoek dat tot dit proefschrift leidde. In september 1966 trad hij in dienst van het Koninklijke/Shell-Laboratorium te Amsterdam, waarbij hij tot september 1968 op de T. H. Eindhoven gedetacheerd bleef. Sindsdien is hij op het laboratorium te Amsterdam werkzaam.

C O N T E N T S

	page:
I. INTRODUCTION AND DESCRIPTION OF THE PROBLEM INVESTIGATED	1
A. Introduction	1
B. Problem Investigated	2
II. THE TURBULENT BOUNDARY LAYER	5
A. Review of Recent Calculation Methods	5
1. Differential Methods	6
2. Integral Methods	11
B. The Distribution of Mean Quantities in a Turbulent Boundary Layer	23
1. The Mean Velocity Profile	23
2. The Distribution of Eddy Viscosity	34
III. TURBULENT HEAT TRANSFER	39
A. The Calculation of Turbulent Heat Transfer	39
B. The Mean Temperature Profile	52
C. The Distribution of the Turbulent Prandtl Number	56
IV. EXPERIMENTAL EQUIPMENT AND MEASURING TECHNIQUES	59
A. Experimental Equipment	59
1. Wind Tunnel	59
2. Traversing Mechanism	59
3. Test Plate	60
B. Measuring Techniques	65
1. Measurement of the Skin Friction	65
2. Measurement of the Mean Velocity and the Longitudinal Velocity Fluctuations	66
3. Measurement of Transverse Velocity Fluctuations and Reynolds Shear Stresses	70
4. Measurement of the Heat Flux Density at the Wall	73
5. Measurement of Mean Temperature and Temperature Fluctuations	74
6. The Measurement of $\overline{v\theta}$	75
V. EXPERIMENTAL RESULTS. COMPARISON WITH THEORY	78
A. The Mean Velocity Field	78
1. The Pressure Gradient	78
2. The Skin Friction	78
3. The Mean Velocity Profile	79
B. The Mean Temperature Field	82
1. The Heat Flux Density at the Wall	82
2. The Mean Temperature Profile	83

C. The Turbulent Quantities	86
1. The Longitudinal Turbulent Intensity	86
2. The Intensity of the Turbulent Temperature Fluctuations	86
3. The Spectra of Temperature and Velocity Fluctuations	86
4. The Quantities \overline{uv} and $\overline{v\theta}$	87
D. The Distribution of Pr_t	88
E. Concluding Remarks and Suggestions for Future Research	89
SUMMARY AND CONCLUSIONS	91
SAMENVATTING EN CONCLUSIES	94
APPENDIX I	97
APPENDIX II	98
LIST OF SYMBOLS	104
ERRATA	106
REFERENCES	107
ACKNOWLEDGEMENTS	116
CURRICULUM VITAE	117

STELLINGEN

1. Zolang verschillende meetmethoden voor het bepalen van de dikte van de microlaag onder een groeiende dampbel in kernkoken zeer uiteenlopende resultaten geven, kan niet worden vastgesteld welk model het groeimechanisme correct beschrijft.

H.H. Jawurek, Int. J. Heat Mass Transfer, 12, 843 - 848 (1969).

M.G. Cooper en A.J.P. Lloyd, Int. J. Heat Mass Transfer, 12, 895 - 913 (1969).

2. Het begrip "self-preserving flow" kan in het nederlands het best worden vertaald met conformistische stroming.

A.A. Townsend, The Structure of Turbulent Shear Flow, Cambridge University Press, New York (1956).

3. Bij turbulente stroming over een oppervlak waarvan de ruwheid abrupt verandert, zal stroomafwaarts van deze ruwheidsverandering het snelheidsprofiel van de turbulente grenslaag geleidelijk moeten veranderen in een aan de nieuwe ruwheid aangepast profiel. De door Townsend voor het snelheidsprofiel afgeleide formules voldoen niet aan de aan het oppervlak geldende randvoorwaarde. Hieraan kan wel worden voldaan indien een gemodificeerde snelheidsschaal wordt ingevoerd.

A.A. Townsend, J. Fluid Mech. 22, 773 - 797 en 799 - 822 (1965).

J. Blom en L. Wartena, J. of the Atmospheric Sciences, 26, 255 - 265 (1969).

4. Bij de bepaling van de ruwheidshoogte van een oppervlak uit het gemeten snelheidsprofiel wordt vaak onvoldoende rekening gehouden met stroomopwaartse veranderingen in deze ruwheidshoogte. Als vuistregel kan men stellen dat de snelheidsverdeling voor een hoogte kleiner dan 0,1 L gelijk is aan het aan de lokale ruwheid aangepaste snelheidsprofiel. Hierbij is L de afstand van de meetplaats tot de dichtstbijzijnde stroomopwaartse verandering in ruwheid.

J. Blom en L. Wartena, J. of the Atmospheric Sciences, 26, 255 - 265 (1969).

5. De berekeningen van Joseph en Tao van de weerstand van een poreuse bol die langzaam door een incompressibel fluïdum beweegt, gaan uit van een incorrecte bewegingsvergelijking voor de stroming in een poreus medium. Hun oplossing is bovendien in strijd met de wet van behoud van impuls.

D.D. Joseph en L.N. Tao, Z. angew. Math. und Mech., 44, 361 - 364 (1964).

6. In het algemeen kan men stellen dat het aanleggen van groenzones slechts een zeer lokale invloed heeft op de concentratie van de in de lucht aanwezige stoffen.

7. Het verdient aanbeveling dat men, voorafgaande aan de realisatie van nieuwe woonwijken, een deskundig milieufysisch, bijvoorbeeld een hydrologisch en aerodynamisch, onderzoek laat verrichten.

8. De verdeling van de turbulente viscositeit in een grenslaag dicht bij de wand kan alleen uit de warmte- of stofoverdrachtsmetingen voor hoge waarden van Pr of Sc worden afgeleid, indien men een veronderstelling invoert betreffende het turbulente getal van Prandtl. De tot nu toe gepubliceerde resultaten zijn alle afgeleid met de veronderstelling $Pr_t = 1$, hetgeen in het algemeen incorrecte resultaten oplevert.

Dit proefschrift.

9. Er bestaat geen universeel temperatuurprofiel zoals door Persen is aangegeven. Dit wordt door de in dit proefschrift gegeven meetresultaten duidelijk aangetoond.

Dit proefschrift.

10. Het gebruik van een turbulent getal van Prandtl is fysisch gezien alleen zinvol voor die gebieden, waarin het turbulente temperatuurveld een universeel karakter heeft. Dit betekent ook dat in het buitenste deel van de thermische grenslaag het turbulente getal van Prandtl niet meer is dan een empirische relatie tussen het impuls- en warmtetransport en een waarde aanneemt die geheel afhangt van de situatie stroomopwaarts.

Dit proefschrift.

11. Evenals de sociale voorzieningen dat zijn, is de gezondheidszorg een nationale zaak. Het invoeren van een nationale gezondheidsdienst zou iedereen kunnen verzekeren van een volledige en zo goed mogelijke medische behandeling, terwijl bovendien vele misstanden in de medische wereld uit de weg zouden worden geruimd.

12. Het uitzenden van interviews met vooraanstaande politici na afloop van een verkiezing kan als nieuwsgaring volkomen achterwege blijven. Deze interviews kunnen hoogstens als onderdeel van een amusementsprogramma worden gebruikt.

13. Het protocol van een promotie aan deze Technische Hogeschool schrijft aan een vrouwelijke promovendus of paranimf óf het dragen van een rok met wit vest en witte das voor óf schenkt in het geheel geen aandacht aan het bestaan van vrouwelijke promovendi of paranimfen. Beide mogelijkheden vormen een bevestiging van het bestaansrecht van de actie "Dolle Mina".